# Grant ARO DAAH04-95-1-0246: Wireless Distributed Multimedia Communications Networks for the Digital Battlefield –Final Progress Report, 31 December 1998

*Purdue University: E. Chong, J. Lehnert, M. Zoltowski*
*University of Illinois: B. Hajek, U. Madhow, D. Sarwate*
*University of Michigan: W. Stark*
*Raytheon Systems Company (formerly Hughes Defense Communications, and formerly Magnavox) : R. Bergstedt, A. Brothers, J. Ginther, A. McDowell, D. Peterson, K. Warren, J. Young*
*Hughes Network Systems: R. Hammons, L. Lee*

*Principal Investigator: James S. Lehnert*
*1285 Electrical Engineering Building*
*West Lafayette, IN 47907-1285*
*(765) 494-2362*
*lehnert@purdue.edu*

VOLUME 1

# REPORT DOCUMENTATION PAGE

Form Approved
OMB NO. 0704-0188



| 1. AGENCY USE ONLY *(Leave blank)* | 2. REPORT DATE | 3. REPORT TYPE AND DATES COVERED |
|---|---|---|
| | | Final Progress 7 Jul 95-31 Dec. 98 |

**4. TITLE AND SUBTITLE**
Wireless Distributed Multimedia Communications Networks for the Digital Battlefield

**5. FUNDING NUMBERS**
DAAH04-95-1-0246

**6. AUTHOR(S)**
Brothers, Chong, Hajek, Hammons, Lee, Lehnert, Madhow, McDowell, Sarwate, Stark, Warren, Zoltowski

**7. PERFORMING ORGANIZATION NAMES(S) AND ADDRESS(ES)**
Purdue University, West Lafayette, IN
University of Illinois, Urbana, IL
University of Michigan, Ann Arbor, MI
Hughes Defense Communications, Fort Wayne, IN
Hughes Network Systems, Germantown, MD

**8. PERFORMING ORGANIZATION REPORT NUMBER**

**9. SPONSORING / MONITORING AGENCY NAME(S) AND ADDRESS(ES)**
U.S. Army Research Office
P.O. Box 12211
Research Triangle Park, NC 27709-2211

**10. SPONSORING / MONITORING AGENCY REPORT NUMBER**
AMXRO-PR
P-33988-EL-FRI

**11. SUPPLEMENTARY NOTES**
The views, opinions and/or findings contained in this report are those of the author(s) and should not be construed as an official Department of the Army position, policy or decision, unless so designated by other documentation.

**12a. DISTRIBUTION / AVAILABILITY STATEMENT**
Approved for public release; distribution unlimited.

**12 b. DISTRIBUTION CODE**

**13. ABSTRACT** *(Maximum 200 words)*

The Focused Research Initiative (FRI) group from Purdue University, the University of Illinois, the University of Michigan, Hughes Defense Communications (formerly Magnavox), and Hughes Network Systems (HNS) began work in July of 1995. Technical efforts are concentrated on multimedia wireless communication links, routing and congestion control, adaptive channel coding, adaptive antenna arrays, and the interface to and use of high speed networks. The FRI Group is uniquely integrating several Department of Defense Programs and the research and educational programs at three major universities, while achieving the benefits of collaboration with industry and the military. The FRI program has fostered and encouraged collaboration and technology exchange among the universities, industrial research groups, and the Army laboratories. Progress has occurred in the area of determining military requirements and using those requirements to guide basic research. Progress in the five areas of concentration is outined in this Interim Progress Report.

| 14. SUBJECT TERMS | 15. NUMBER IF PAGES |
|---|---|
| Wireless Communications; Networking; Multimedia; Digital Battlefield; CDMA; Coding; TCP/IP | 16. PRICE CODE |

| 17. SECURITY CLASSIFICATION OR REPORT | 18. SECURITY CLASSIFICATION OF THIS PAGE | 19. SECURITY CLASSIFICATION OF ABSTRACT | 20. LIMITATION OF ABSTRACT |
|---|---|---|---|
| UNCLASSIFIED | UNCLASSIFIED | UNCLASSIFIED | UL |

# Grant ARO DAAH04-95-1-0246: Wireless Distributed Multimedia Communications Networks for the Digital Battlefield –Final Progress Report, 31 December 1998

*Purdue University: E. Chong, J. Lehnert, M. Zoltowski*
*University of Illinois: B. Hajek, U. Madhow, D. Sarwate*
*University of Michigan: W. Stark*
*Raytheon Systems Company (formerly Hughes Defense Communications, and formerly Magnavox) : R. Bergstedt, A. Brothers, J. Ginther, A. McDowell, D. Peterson, K. Warren, J. Young*
*Hughes Network Systems: R. Hammons, L. Lee*

*Principal Investigator: James S. Lehnert*
*1285 Electrical Engineering Building*
*West Lafayette, IN 47907-1285*
*(765) 494-2362*
*lehnert@purdue.edu*

**VOLUME 1**

# Abstract

The Focused Research Initiative (FRI) group from Purdue University, the University of Illinois, the University of Michigan, Raytheon Systems Company (formerly Hughes Defense Communications and formerly Magnavox), and Hughes Network Systems (HNS) began work in July of 1995. Technical efforts are concentrated on multimedia wireless communication links, routing and congestion control, adaptive channel coding, adaptive antenna arrays, and the interface to and use of high speed networks. The FRI Group has integrated several Department of Defense Programs and the research and educational programs at three major universities, while achieving the benefits of collaboration with industry and the military. The FRI program has fostered and encouraged collaboration and technology exchange among the universities, industrial research groups, and the Army laboratories. Progress has occurred in the area of determining military requirements and using those requirements to guide basic research. Progress in the five areas of concentration is outlined in this Final Progress Report. Detailed research is reported in the research papers referenced by this document.

# 1 List of Manuscripts Submitted or Published under ARO Sponsorship

1. T. T. Chen and J. S. Lehnert, "TCM/SSMA communication systems with cascaded sequences and PAM/QAM signal sets," *Proceedings of the Thirty-Third Annual Allerton Conference on Communication, Control, and Computing*, pp. 225–234, October 4-6, 1995.

2. D. L. Goeckel and W. E. Stark, "Throughput optimization in faded multicarrier systems," *Proceedings of the Thirty-Third Annual Allerton Conference on Communication, Control, and Computing*, pages 815–824, October 4-6, 1995.

3. A. Hafeez and W. Stark, "Combined decision-feedback multiuser detection/soft-decision decoding for CDMA channels," In *Proc. IEEE Vehicular Technology Conf.*, pp. 382-386, April 1996.

4. T. M. Lok and J. S. Lehnert, "Limits on performance with random polyphase sequences in DS/SSMA systems," *Proceedings of the Thirty-Third Annual Allerton Conference on Communication, Control, and Computing*, pp. 805–814, October 4-6, 1995.

5. M. D. Zoltowski and J. Ramos, "Blind multi-user access interference cancellation for CDMA based PCS/cellular using antenna arrays," in *Proceedings of the 1996 IEEE Int'l Conference on Acoustics, Speech, and Signal Processing*, pp. 2730-2733, May 1996.

6. M. D. Zoltowski and J. Ramos, "Reduced complexity blind 2D RAKE receiver for CDMA," in *8th IEEE Signal Processing Workshop on Statistical and Array Processing*, Corfu, Greece, pp. 502-505, June 24-26, 1996.

7. K. Wong and M. Zoltowski, "High accuracy 2D angle estimation with extended aperture vector sensor arrays," in *Proceedings of the 1996 IEEE Int'l Conference on Acoustics, Speech, and Signal Processing*, pp. 2789-2792, May 1996.

8. M. D. Zoltowski, "Blind adaptive beamforming for CDMA based PCS/cellular," *Conference Record of the 29th Asilomar IEEE Conference on Signals, Systems, and Computers*, pp. 378-382, Oct. 30 - Nov. 1, 1995.

9. H. Chaskar, T. V. Lakshman, U. Madhow, "On the design of interfaces for TCP/IP over wireless," *Proc. IEEE Milcom '96,* October 1996.

10. B. Hajek, A. Krishna, R.O. LaMaire, "On the capture probability for a large number of stations," *IEEE Transactions on Communications*, vol. 42, pp. 254-260, February 1997.

11. L. He and U. Madhow, "Pipelined MMSE equalizers for direct-sequence spread-spectrum CDMA channels," *Proc. International Conf. Univ. Personal Commun. (ICUPC'96),* Boston, MA, September 29-October 2, 1996.

12. T. V. Lakshman and U. Madhow, "The performance of TCP/IP for networks with high bandwidth-delay products and random loss," *IEEE/ACM Transactions on Networking,* June 1997.

13. K. Mitzel, *Iterative Optimization of Registration and Paging Policies in Cellular Networks,* M.S. Thesis and CSL Technical Report, B. Hajek, advisor. January 1997.

14. D. V. Sarwate and D. A. Losada, "A new class of frequency-hop patterns," presented at the *1997 IEEE International Symposium on Information Theory,* Ulm, Germany, p. 125, June 29 - July 5, 1997.

15. V. Subramaniam and U. Madhow, "Blind Demodulation of Direct-Sequence CDMA Signals Using an Antenna Array," *Proc. Conf. Inform. Sci. Sys. (CISS'96),* Princeton, NJ, March 1996.

16. J. Waldby and U. Madhow, "Dynamic window-based flow control with end-to-end selective acknowledgments," *Proc. 3rd International Workshop on Mobile Multimedia Communications (MoMuC-3),* Princeton, NJ, September 25-27, 1996.

17. H. Liu and M. D. Zoltowski, "Blind equalization in antenna array CDMA systems," *IEEE Trans. on Signal Processing, Special Issue on Signal Processing for Advanced Digital Communications,* pp. 161-172, Jan. 1997.

18. C. Chatterjee, V. Roychowdhury, J. Ramos, and M. D. Zoltowski, "Self-organizing and adaptive algorithms for generalized eigen-decomposition," *IEEE Trans. on Neural Networks,* vol. 8, no. 6, pp. 1518-1530, Nov. 1997.

19. M. D. Zoltowski, J. Ramos, C. Chatterjee, and V. Roychowdhury, "Blind adaptive 2D RAKE receiver for DS-CDMA based on space frequency MVDR processing," accepted subject to revisions, *IEEE Trans. on Signal Processing.*

20. M. D. Zoltowski and J. Ramos, "Blind 2D RAKE receivers based on space-time MVDR processing," *Proc. IRSS '96: Interference Rejection and Signal Separation in Wireless Communications Symposium,* New Jersey Institute of Technology, Newark, NJ, 19 Mar. 1996, pp. 217-239.

21. J. Ramos and M. Zoltowski, "Optimum filter for blind adaptive beamformers based on baud rate knowledge," (Invited Paper) *Proc. of the 1996 Int'l. Conference on Telecommunications,* (co-sponsored by IEEE and IEE), 13-17 April 1996, Istanbul, Turkey, pp. 423-426.

22. M. D. Zoltowski, Y.-F. Chen, and J. Ramos, "Blind 2D RAKE receivers based on space-time adaptive MVDR processing for the IS-95 CDMA system," *Milcom '96,* McLean, VA, 21-24 Oct. 1996, pp. 618-622.

23. T. A. Thomas and M. D. Zoltowski, "Novel receiver signal processing for interference cancellation and equalization in cellular TDMA communications," in *Proc. of the 1997 IEEE Int'l Conf. on Acoustics, Speech, and Signal Processing,* Munich, Germany, pp. 3881-3884, 21-24 April 1997.

24. J. Ramos and M. D. Zoltowski, "Blind 2D RAKE receiver for CDMA incorporating code synchronization and multipath time delay estimation," in *Proc. of the 1997 IEEE Int'l Conf. on Acoustics, Speech, and Signal Processing,* Munich, Germany, pp. 4025-4029, 21-24 April 1997.

25. K. T. Wong and M. D. Zoltowski, "Closed-form multiple invariance ESPRIT," in *Proc. of the 1997 IEEE Int'l Conf. on Acoustics, Speech, and Signal Processing,* Munich, Germany, pp. 3489-3492, 21-24 April 1997.

26. T. A. Thomas and M. D. Zoltowski, "Novel receiver space-time processing for interference cancellation and equalization in narrowband TDMA communications," in *Proc. of IEEE Vehicular Technology Conference (VTC) '97,* Phoenix, AZ, 4-7 May 1997.

27. K. T. Wong and M. D. Zoltowski, "Extended aperture spatial diversity & polarization diversity using a sparse array of electric dipoles or magnetic loops," in *Proc. of IEEE Vehicular Technology Conference (VTC) '97,* Phoenix, AZ, pp. 160-164, 4-7 May 1997.

28. T. A. Thomas and M. D. Zoltowski, "Space-time processing for interference cancellation and equalization in narrowband digital communications," in *IEEE Signal Processing Advances in Wireless Communications Workshop - SPAWC '97,* Paris, France, pp. 185-188, 16-18 April 1997.

29. J. Ramos and M. D. Zoltowski, "Blind space-time processor for CDMA cellular systems for SINR maximization," in *IEEE Signal Processing Advances in Wireless Communications Workshop - SPAWC '97,* Paris, France, pp. 273-276, 16-18 April 1997.

30. M. D. Zoltowski and T.A. Thomas, "Nonparametric channel identification, interference cancellation, and multichannel equalization for narrowband digital communications," (Invited Paper) *MILCOM '97,* Monterey, CA, pp. 1082-1086, 2-5 Nov. 1997.

31. J. Li, N. Shroff, and E. K. P. Chong, "Channel carrying: A novel handoff scheme for mobile cellular networks," in *Proceedings of the IEEE INFOCOM '97* (16th Annual Joint Conference of the IEEE Computer and Communication Societies), Kobe, Japan, pp. 909-917, April 9–11, 1997.

32. Victor W. Cheng and Wayne E. Stark, "Performance of trellis coded direct-sequence spread-spectrum with noncoherent reception in a fading environment," *Proceedings of the 1997 IEEE Personal, Indoor and Mobile Radio Communications Conference*, pages 1125–1130, October 1996.

33. Victor W. Cheng and Wayne E. Stark, "Performance of trellis coded direct-sequence spread-spectrum with noncoherent reception in a fading environment," *IEEE Transactions on Vehicular Technology*, 1998.

34. Victor Wen-Kai Cheng and Wayne E. Stark, "Adaptive coding and modulation for spread-spectrum signals," *Proceedings of the 1997 IEEE Vehicular Technology Conference*, pages 1987–1991, May 1997.

35. Dennis Goeckel and Wayne Stark, "Optimal diversity allocation in coherent multiuser systems," *1996 Tactical Communications Conference*, Fort Wayne, IN, pages 1–10, April 30- May 2, 1996.

36. Dennis Goeckel and Wayne Stark, "Throughput optimization in multiple-access communication systems with decorrelator reception," *1996 IEEE International Symposium on Information Theory and Its Applications*, pages 653–656, September 1996.

37. Dennis Goeckel and Wayne E. Stark, "A coded multicarrier framework for the optimization of coherent multi-user communication systems over fading channels," *Proceedings of the 1997 IEEE Vehicular Technology Conference*, pages 2075–2079, May 1997.

38. Dennis L. Goeckel and Wayne E. Stark, "A multicarrier framework for coherent multiuser systems," *IEEE Transactions on Communications*, Submitted for Publication.

39. Dennis L. Goeckel and Wayne E. Stark, "Optimal diversity allocation in coherent multiuser communication systems," *IEEE Transactions on Communications*, Submitted for Publication.

40. Abdulrauf Hafeez and Wayne E. Stark, "Soft-output multiuser estimation for asynchronous CDMA channels," *Proceedings of the 1997 IEEE Vehicular Technology Conference*, pages 465–469, May 1997.

41. T. M. Lok and J. S. Lehnert, "An asymptotic analysis of DS/SSMA communication systems with random polyphase signature sequences," *IEEE Transactions on Information Theory*, vol. 42, pp. 129-136, January 1996.

42. T. M. Lok and J. S. Lehnert, "Error probabilities for generalized quadriphase DS/SSMA communication systems with random signature sequences," *IEEE Transactions on Communications*, vol. 44, pp. 876-885, July 1996.

43. T. M. Lok and J. S. Lehnert, "Efficient approximations in DS/SSMA communication systems with general linear modulation and error control coding," *1996 Tactical Communications Conference*, Fort Wayne, IN, pp. 469-478, April 30-May 2, 1996.

44. A. Brothers, J. Ginther, and J. S. Lehnert, "Wireless distributed multimedia communications networks for the digital battlefield," *1996 Tactical Communications Conference*, Fort Wayne, IN, pp. 349-356, April 30-May 2, 1996.

45. T. F. Wong, T. M. Lok, J. S. Lehnert, and M. D. Zoltowski, "Spread-Spectrum Signaling Techniques With Antenna Arrays and Blind Adaptation," *IEEE Military Communications Conference (MILCOM '96)*, McLean, VA, 21-24 Oct. 1996, pp. 194-198.

46. T. F. Wong, T. M. Lok, and J. S. Lehnert, "Performance Evaluation of a Blind Adaptive Linear Receiver for Cellular DS/CDMA Systems," *Thirty-Fourth Annual Allerton Conference on Communication, Control, and Computing, Allerton House, Monticello, Illinois*, (Invited Paper), pp. 642-651, October 2-4, 1996.

47. Q. Zhang and J. S. Lehnert, "Adaptive coding for slotted DS-SSMA packet radio systems," *IEEE Military Communications Conference (MILCOM '97)*, Monterey, California, pp. 291-295, November 3-7, 1997.

48. Bruce Hajek and Pierre Seri, "On Causal Scheduling of Multiclass Traffic with Deadlines", Technical Report, Coordinated Science Laboratory, UILU-ENG-97-2220, August 1997 (and presented at the IEEE International Symposium on Information Theory, Boston, MA, August 1998).

49. J. Li, N. Shroff, and E. K. P. Chong, "A channel sharing scheme to improve system capacity and quality of service in wireless cellular networks," in the third IEEE Symposium on Computers and Communications (ISCC'98), Athens, Greece, pp. 700-704, June 30- July 2, 1998.

50. Sang W. Kim and Wayne E. Stark, "Performance limits of Reed-Solomon coded CDMA with orthogonal signaling in a Rayleigh fading channel," *IEEE Transactions on Communications*, 1998.

51. Joseph H. Kang and Wayne E. Stark, "Turbo codes for noncoherent FH-SS with partial band interference," submitted to the *IEEE Transactions on Communications.*

52. T. T. Chen and J. S. Lehnert, "TCM/SSMA communication systems with cascaded-sequences and PAM/QAM signal sets," *IEEE Transactions on Communications*, vol. 46, no. 7, pp. 950-956, July 1998.

53. T. M. Lok and J. S. Lehnert, "Asymptotic analysis of DS/SSMA communication systems with general linear modulation and error control coding," *IEEE Transactions on Information Theory*, vol. 44, pp. 870-881, March 1998.

54. T. F. Wong, T. M. Lok, J. S. Lehnert, and M. D. Zoltowski, "A Linear Receiver for direct-sequence spread-spectrum multiple-access systems with antenna arrays and blind adaptation," *IEEE Transactions on Information Theory* , vol. 44, pp. 659-676, March 1998.

55. T. T. Chen and J. S. Lehnert, "Bounds on the pairwise error probability of coded DS/SSMA communications systems in Rayleigh fading channels," *IEEE Transactions on Communications*, vol. 46, no. 12, pp. 1685-1692, December 1998.

56. T. F. Wong, T. M. Lok, and J. S. Lehnert, "Asynchronous Multiple-Access Interference Suppression and Chip Waveform Selection with Aperiodic Random Sequences," *IEEE Transactions on Communications*, vol. 47, no. 1, pp. 103-144, January 1999.

57. Q. Zhang, T. F. Wong, and J. S. Lehnert, "Performance of a type-II hybrid ARQ protocol in slotted DS-SSMA packet radio systems," *IEEE Transactions on Communications* , vol. 47, no. 2, pp. 281-290, February 1999.

58. Q. Zhang, T. F. Wong, and J. S. Lehnert, "Buffered type-II hybrid ARQ protocol for DS-SSMA packet radio systems, *International Journal on Wireless Information Networks*, vol. 5, no. 3, pp. 203-217, July 1998.

59. T. M. Lok, T. F. Wong, and J. S. Lehnert, "Blind adaptive signal reception for MC-CDMA systems in Rayleigh fading channels," *IEEE Transactions on Communications*, vol. 47, no. 3, pp. 464-471, March 1999.

60. T. T. Chen and J. S. Lehnert, "Multiuser decision-feedback receivers for asynchronous CDMA systems over a mismatched Rayleigh fading channel," *IEEE Transactions on Communications*, Submitted.

61. T. F. Wong, T. M. Lok, and J. S. Lehnert, "Chip waveform selection in asynchronous DS-CDMA systems with interference suppression," *IEEE International Conference on Universal Personal Communications*, pp. 208-212, October 12-16, 1997.

62. T. T. Chen and J. S. Lehnert, "Bounds on the pairwise error probability of coded DS/SSMA communication systems in Rayleigh fading channels," *IEEE International Conference on Universal Personal Communications*, pp. 337-341, October 12-16, 1997.

63. T. M. Lok, T. F. Wong, and J. S. Lehnert, "Blind adaptive signal reception for MC-CDMA systems with interference suppression," *IEEE Military Communications Conference (MILCOM '98)*, Boston, Massachusetts, pp. 752-756, October 18-21, 1998.

64. T. T. Chen and J. S. Lehnert, "Multiuser decision-feedback receivers for asynchronous CDMA systems over a mismatched Rayleigh fading channel," *Thirty-Fifth Annual Allerton Conference on Communication, Control, and Computing*, Allerton House, Monticello, Illinois, pp. 311-320, September 29-October 1, 1997.

65. Q. Zhang, T. F. Wong, and J. S. Lehnert, "Stability of a type-II hybrid ARQ protocol for DS-SSMA packet radio systems," *IEEE INFOCOM'98* , San Francisco, California, pp. 1301-1308, March 29-April 2, 1998.

66. S. H. Tsai, T. T. Chen, and J. S. Lehnert,"Implementation of fixed delay soft-output algorithms," *IEEE Military Communications Conference (MILCOM'98)*, Boston, Massachusetts, pp. 993-997, October 18-21, 1998.

67. Yung-Fang Chen and Michael D. Zoltowski, "Convergence analysis and tracking capability of reduced dimension blind space-time RAKE receivers," *IEEE Vehicular Technology Conference (VTC) '98,* Ottawa, Ontario, Canada, pp. 2333-2337, 18-21 May 1998.

68. Yung-Fang Chen and M. D. Zoltowski,"Blind 2-D RAKE Receivers Based on RLS-Type Space-Time Adaptive Filtering for DS-CDMA System," in *Proc. of the 1998 IEEE Int'l Conf. on Acoustics, Speech, and Signal Processing,* Seattle, WA, May 1998.

69. Yung-Fang Chen and Michael D. Zoltowski, "Joint angle and delay estimation for reduced dimension space-time RAKE receiver with application to IS-95 CDMA uplink," accepted for *IEEE Fifth International Symposium on Spread Spectrum Techniques and Applications (ISSSTA) '98,* Sun City, South Africa, pp. 606-610, 2-4 September 1998.

70. K. T. Wong and M. D. Zoltowski, "ESPRIT-Based Direction Finding Using A Sparse Rectangular Array with Dual-Size Spatial Invariances," *IEEE Transactions on Aerospace and Electronic Systems,* pp. 1320-1336, Oct. 98.

71. M. D. Zoltowski and D. Tseng, "Blind Channel Identification for Narrowband Digital Communications Based on Parametric Modelling of the Channel Impulse Response," (*Invited Paper*) *Proceedings 35th Annual Allerton Conference on Communications, Systems, and Computing,* pp. 503-512, 29 Sept.-1 Oct., 1997.

72. M. D. Zoltowski and D. Tseng, "On The Use of Basis Functions in Blind Equalization Based on Deterministic Least Squares," *Invited Paper, Conf. Record of the 31st Asilomar IEEE Conference on Signals, Systems, and Computers,* pp. 816-822, 30 Oct.-1 Nov. 1997.

73. M. D. Zoltowski and D. Tseng,"Blind Multichannel Identification for High-Speed TDMA," *IEEE Military Communications Conference (MILCOM'98)*, Boston, Massachusetts, pp. 176-181, October 18-21, 1998.

74. D. V. Sarwate, "Meeting the Welch bound with equality," *International Conference on Sequences and Their Applications*, December 14 – 17, 1998, Singapore (to appear in Discrete Math/Theoretical Computer Science series volume to be published later by Springer-Verlag).

75. H. Chaskar, T. V. Lakshman, U. Madhow, "TCP over wireless with link level error control: analysis and design methodology," Accepted for publication, *IEEE/ACM Trans. Networking.*

76. H. Chaskar and U. Madhow, "Traffic multiplexing and service guarantees on wireless downlinks," submitted for publication.

77. U. Madhow, L. J. Zhu and L. Galup, "Differential MMSE: new adaptive algorithms for equalization, interference suppression, and beamforming," *Invited Paper, Proc. 32nd Asilomar Conf. Signals, Systems and Computers (Asilomar'98),* Pacific Grove, CA, October 1998.

78. L. Galup and U. Madhow, "Blind spatial interference suppression of DS-CDMA with long spreading sequences," *Proc. 1998 International Symposium on Information Theory (ISIT'98),* Cambridge, MA, June 1998.

79. H. Chaskar and U. Madhow, "Wireless link shaping for service guarantees," *Proc. 1998 International Symposium on Information Theory (ISIT'98),* Cambridge, MA, June 1998.

80. J. Waldby, U. Madhow, T. V. Lakshman, "Total acknowledgements: A robust feedback mechanism for end-to-end congestion control," *Proc. ACM Sigmetrics'98.*

81. U. Madhow, "Dynamic congestion control and error recovery over a heterogeneous Internet," *Invited Paper, Proc. 36th IEEE Conference on Decision and Control (CDC'97),* San Diego, CA, December 1997.

82. B. Hajek and P. Seri, "On causal scheduling of multiclass traffic with deadlines," *Proceedings 1998 IEEE International Symposium on Information Theory,* Cambridge, MA, p. 166, August 1998.

83. P. Seri, "Causal Scheduling of Multiclass Traffic with Deadlines and Priorities," MS Thesis, CSL Technical Report UILU-ENG-98-2211, June 1998.

84. Vijay G. Subramanian and B. Hajek, "Capacity and reliability functions per unit cost for WSSUS fading channels," To appear, *Proc. 33rd Annual Conference on Information Sciences and Systems,* Johns Hopkins University, March 1999.

85. Vijay G. Subramanian and B. Hajek, "Capacity and Reliability Function per Fourth Moment Cost for WSSUS Fading Channels," To appear, *Proc. IEEE Information Theory and Communications Workshop,* Kruger National Park, South Africa, June 1999.

86. P. Bruneteau, "One-success random access without feedback for a bounded number of active stations," MS Thesis, CSL Technical Report UILU-ENG-98-2214, June 1998.

87. J. Li, N. B. Shroff, and E. K. P. Chong, "Channel carrying: A novel handoff scheme for mobile cellular networks," To appear in *IEEE/ACM Transactions on Networking.*

88. J. Li, N. B. Shroff, and E. K. P. Chong, "The study of a channel sharing scheme in wireless cellular networks including handoffs," in *Proceedings of the 1999 IEEE INFOCOM*, New York, New York, March 21–25, 1999.

89. J. Li, N. B. Shroff, and E. K. P. Chong, "A new localized channel sharing scheme for cellular networks," to appear in *Wireless Networks.*

90. S. Kalyanasundaram, E. K. P. Chong, and N. B. Shroff, "An efficient scheme to reduce handoff dropping in LEO satellite systems," in *Proceedings of the 17th IEEE Symposium on Reliable Distributed Systems*, Purdue University, West Lafayette, Indiana, October 20–23, 1998.

91. S. Kalyanasundaram, J. Li, E. K. P. Chong, and N. B. Shroff, "Channel sharing scheme for packet-switched cellular networks," in *Proceedings of the 1999 IEEE INFOCOM*, New York, New York, March 21–25, 1999.

92. J. Li, N. B. Shroff, and E. K. P. Chong, "A static power control scheme for wireless cellular networks," in *Proceedings of the 1999 IEEE INFOCOM*, New York, New York, March 21–25, 1999.

93. J. Zhang and E. K. P. Chong, "Admissibility and network capacity of power-controlled CDMA systems in fading channels," in *Proceedings of the 36th Annual Allerton Conference on Communication, Control and Computing*, Monticello, Illinois, September 23–25, 1998.

94. J. Zhang and E. K. P. Chong, "CDMA systems with random spreading in fading channels: network capacity and power control," in *Proceedings of the 1999 IEEE INFOCOM*, New York, New York, March 21–25, 1999.

95. J. Zhang and E. K. P. Chong, "CDMA systems in fading channels: admissibility, network capacity, and power-control," submitted to *IEEE Transactions on Information Theory.*

96. J. Li, N. B. Shroff, and E. K. P. Chong, "A static power control scheme for wireless cellular networks," submitted to *IEEE/ACM Transactions on Networking.*

97. J. Herdtner and E. K. P. Chong, "Analysis of a simple distributed power control algorithm," in *Proceedings of the 36th Annual Allerton Conference on Communication, Control and Computing*, Monticello, Illinois, September 23–25, 1998.

98. A. Hafeez and W. E. Stark, "Decision feedback sequence estimation for unwhitened ISI channels," *Annual Allerton Conference on Communication, Control and Computing*, pp. 493–502, September 1997.

99. A. Hafeez and W. E. Stark, "A family of soft-output multiuser demodulators for coded asynchronous CDMA channels," *Proceedings of Interference Rejection and Signal Separation in Wireless Communications*, March 1997.

100. A. Hafeez and W. E. Stark, "Decision feedback sequence estimation," *IEEE International Symposium on Information Theory*, page 124, August 1998.

101. A. Hafeez and W. E. Stark, "Decision feedback sequence estimation for unwhitened ISI and multiuser CDMA channels," *IEEE Vehicular Technology Conference*, pages 424–429, May 1998.

102. A. Hafeez and W. E. Stark, "Decision feedback sequence estimation for unwhitened ISI channels with applications to multiuser detection," *IEEE Journal on Selected Areas in Communications*, pp. 1785–1795, December 1998.

103. A. Hafeez and W. E. Stark, "A new fractional MLSE receiver for time-varying channels," *IEEE Transactions on Communications*, 1999. To be submitted.

104. A. Hafeez and W. E. Stark, "Reduced trellis and tree search algorithms: the effect of the receive filter and the branch metric," *IEEE Transactions on Information Theory*, March 1999. Submitted.

# 2 Scientific Personnel and Honors/Awards/Degrees

**SENIOR INVESTIGATORS**
Alfred Brothers
Edwin Chong
Jack Ginther
Bruce Hajek, elected to National Academy of Engineering, 1998
Roger Hammons
Lin-Nan Lee
James Lehnert
Upamanyu Madhow
Anthony McDowell
Dilip Sarwate
Wayne Stark, IEEE Fellow, 1997
Kevin Warren
Jeff Young
Michael Zoltowski, IEEE Fellow, 1999

**STUDENTS**
Hemant Chaskar, Ph.D. received, May 1999
Vijay Subramanian, Ph.D., anticipated August 1999
Kevin Mitzel, MS received, February 1997
T. Wong, Ph. D. received, December 1997
Qian Zhang, Ph.D. received, August 1998
T. Chen, Ph.D. received, December 1997
Y. Chen, Ph.D. received, December 1998
D. Tseng, December 1998
Victor Cheng, Ph.D., anticipated August 1999
A. Hafeez, Ph.D. received, April 1999
Jefferey Herdtner
J. Li, Ph.D. received, May 1998
Julian Waldby, Ph.D., anticipated December 1999
Linhai He, MS received, May 1996
Kevin Mitzel, MS received, February 1997
Pierre Seri, Ph.D., anticipated August 1999
Luis Galup, Postdoctoral Researcher with Ph.D. in Mathematics

# 3 Determination of Military Requirements, Scientific Progress, and Accomplishments

The Focused Research Initiative (FRI) group from Purdue University, the University of Illinois, the University of Michigan, Raytheon Systems Company (formerly Hughes Defense Communications and formerly Magnavox), and Hughes Network Systems (HNS) began work in July of 1995. Technical efforts are concentrated on multimedia wireless communication links, routing and congestion control, the interface to and use of high speed networks, adaptive coded modulation for spread-spectrum communication systems, and adaptive antenna arrays. Our industrial partners have completed a requirements analysis stage with the purpose of guiding our work and making it relevant.

Communications requirements and goals have been obtained through interview and discussion with various Army organizations. These requirements and goals are those that were specifically identified as important to the organization and its objectives. We summarize information obtained in an updated requirements matrix that is shown in vol. 2 of this report. The requirements matrix is divided into six segments depending on the specific application: the Task Force XXI Brigade (force level communication exercise), Untethered Node Operation, Future Digital Radio, High Capacity Trunk Radio, Information Management, and General Communication Requirements. The requirement or goal is identified in a statement, and a key is provided to identify the source of the requirement or goal. Universities with projects that address these requirements and goals have now been identified in our updated requirements matrix.

Some details follow which describe our interactions among the universities and industry. Brief descriptions of accomplishments are given with details and graphics provided in the appended selection of research papers and reports.

## 3.1 Wireless Multimedia Networks, Routing and Congestion Control, Interface of Wireless Networks to High-Speed Wide-Area Wireline Networks (Bruce Hajek, Univ. of IL; U. Madhow, Univ. of IL; E. Chong, Purdue Univ.)

### 3.1.1 Capture Probability for a Large Number of Stations

The probability of capture under a model based on the ratio of largest received power to sum of interference powers is examined in [20] in the limit of a large number of transmitting mobiles. Specifically, if $n$ transmitters are present, the transmission of a given mobile $j$ is captured if the power received from that mobile exceeds a threshold $z$ times the sum of the powers received from the other mobiles and the thermal noise. The parameter $z$ is the minimum carrier-to-interference ratio needed for successful reception, and is determined by such factors as the type of modulation and the receiver sensitivity. In a land mobile radio system, the received power from a remote mobile at distance $r$ can be reasonably modeled as the product of the transmitted power, a Rician or Rayleigh distributed random variable to account for multipath fading, an exponential of a Gaussian random variable to account for shadowing, and a power-law term to account for the near-far effect.

The paper [20] makes two points: (1) In the limit of a large number of transmitters, the probability of capture is a simple function depending only on $z$ and the roll-off parameter of the distribution of power received from a typical mobile, and (2) under broad conditions the roll-off parameter is determined by the near-far effect (through the power roll-off with distance and the spatial distribution of mobiles), and is insensitive to many typical channel effects such as Rayleigh or Rician fading and log-normal shadowing.

### 3.1.2 Packet Scheduling with Deadlines and Priorities

Causal scheduling-dropping policies for multiclass traffic with deadlines have been developed. Packets with deadlines and class labels arrive in discrete time and are either scheduled by their deadlines, or dropped on, or possibly before, their deadlines. This work is motivated by the problem of scheduling packet transmissions in a radio network. Typically, only limited bandwidth is available. It is therefore crucial that the nodes carefully determine the order in which they transmit packets over their outgoing links. There is a tradeoff between respecting the priority class of a packet, and excessively delaying lower priority traffic. Our work has addressed this tradeoff in a principled way.

Initially, our research focused on the case in which there are two classes of traffic, and on causal policies which at any given time base decisions on arrivals up to that time. These results were written up in [38] and presented in [39]. First, the causal scheduling-dropping policies that maximize total throughput are identified. Then, those scheduling-dropping policies with the greatest throughput for the high priority class, subject to being causal and maximizing total throughput, are identified.

In late 1997 and early 1998 our attention turned to improving our results in two ways: (a) handling more than two priority classes, and (b) devising computationally efficient algorithms for scheduling and dropping. The results of this phase of research are summarized in [?]. From the summer of 1998 until the present, we have continued to work on this problem. We have discovered a more general and elegant method for scheduling multiple priority classes in an efficient way. While the algorithm is simple, the proof of its correctness is rather complex. We aim to have this work complete by June 1999. One or two journal papers, in addition to at least one conference publication, will be prepared on the basis of this material.

### 3.1.3 Capacity of Fading Channels

This paper [35] summaries some of our recent work on the application of the concepts of capacity per unit cost and reliability function per unit cost to models of fading channels. The cost is taken to be the energy, or a certain fourth moment functional that is sensitive to the burstiness of the signals, and is related to the ambiguity function of the input signal. The channel is assumed to be a Wide-Sense Stationary and Uncorrelated Scattering (WSSUS) channel. More of this work will be available in [36], and in a planned journal paper. The majority of Vijay Subramanian's Ph. D. thesis support derived from the the FRI contract. Vijay plans to complete his Ph. D. in the summer of 1999.

### 3.1.4 A problem arising in code synchronization in FH-CDMA

We studied a random multiple-access system, where T active stations among M stations contend over a common medium in L minislots. Each active station transmits in a subset of these minislots, the subsets chosen by the stations being mutually independent. A success is said to occur if during at least one minislot there is a single transmission; otherwise, a failure occurs. We devised policies that attempted to minimize the probability of failure. We assumed that the number of active users T is not known a priori, so that the worst case failure probability, obtained by maximizing over T up to some assumed upper bound on T. Comparisons of the probability of failure that we achieved against lower bounds that we derived, show that our strategies nearly minimizes the maximum-over-T failure probability. The application we have in mind is that there are L minislots at the front of each packet transmission slot. A station identifies itself and the hopping pattern that is will use in the rest of the slot that follows.

### 3.1.5 Wireless support of TCP/IP

We have shown how to support TCP/IP, the Internet transport protocol, over wireless links, and what performance to expect. Our work provides the first analytical approach to design and performance analysis. In particular, we demonstrate analytically [19] that TCP-aware link layer error recovery is an excellent approach to wireless-wireline interface design for the support of TCP. This work builds on a basic understanding of TCP developed in [22].

Connections over heterogeneous networks encounter large bandwidth-delay products and *random* loss (i.e., loss that cannot be attributed to congestion). Since TCP/IP cuts back its sending rate for any loss (since it interprets all losses as congestion), its performance can deteriorate seriously if random losses occur frequently. In particular, if the end-to-end packet loss probability seen by TCP is $q$, and the bandwidth-delay product is $W$, then we have shown that TCP gives poor throughput if $qW^2$ is large [22]. Thus, systems should be engineered so as to keep the end-to-end loss probability seen by TCP below $1/W^2$. In [19], we put this rule of thumb to work by considering TCP performance over a Rayleigh faded link. We use a link layer retransmission scheme which delivers packets in order to TCP and thus hides wireless losses from TCP, so that the only remaining losses seen by TCP are at the buffer at the wireless-wireline interface. We show that the buffer size required to attain the required end-to-end loss probability of $1/W^2$ is moderate. A close match between analysis and simulations lend further weight to our design approach. Finally, we give an asymptotic argument that shows that the interface buffer size required to make this approach work scales only *logarithmically* with the bandwidth-delay product for very general classes of wireless channels.

We have made substantial progress on the issue of providing service guarantees over wireless links. We have considered a wireless downlink in which a single transmitter is sending real-time data to different receivers over different Rayleigh fading channels. Error control coding with interleaving is used to deal with the fading. The approach consists of providing a deterministic delay guarantee and a statistical loss guarantee. Since loss can occur due to either buffer overflow or due to loss on the wireless link, it is essential to partition the allowable delay in an optimum way between buffering and interleaving. We provide a framework for doing this systematically, while providing mechanisms for statistical traffic multiplexing. Results have appeared at the International Symposium on Information Theory in 1998 (ISIT'98).

Despite the termination of the FRI program, we are continuing this line of research with DoD support from an ARO contract for research in "Communications in the Digital Battlefield: Fundamental Problems in the Design of Heterogeneous Networks."

### 3.1.6 Dynamic congestion control using SACKs

Since adequate link layer error recovery may not always be available, it is of interest to design transport protocols that can operate in unfriendly environments. We proposed in 1996 a transport protocol [26] that modifies the congestion control mechanism in TCP to take advantage of selective acknowledgments (SACKs). The performance of this protocol in a heterogeneous environment is far superior to that of TCP. It is worth noting that, while SACKs have been proposed in the Internet Engineering Task Force (IETF) and have been previously shown to produce some improvement in the performance of TCP with its *current* congestion control mechanism, the fundamental performance problems of TCP in a wireless

environment cannot be solved without modification of the congestion control mechanism.

The poor performance of TCP in the presence of random loss is because the congestion control algorithm in TCP does not distinguish random loss from sustained congestion. This in turn is partly because TCP uses *cumulative acknowledgments,* and therefore cannot accurately identify how many, and which, packets are lost and should be retransmitted. In our work, we have examined the performance gains that could result from the additional information that could be obtained using *selective acknowledgments.* We have considered one specific form of selective acknowledgment, and have considered one specific dynamic window-based scheme (with dynamics similar to that of the TCP congestion window) designed to exploit it. The performance gains over current forms of TCP are substantial, and motivate further investigation into how best to include selective acknowledgments in TCP. We have also considered a fixed window scheme with selective acknowledgments in order to develop analytical guidelines for estimating the sequence number space and the destination buffer (as a function of the bandwidth-delay product) required to support end-to-end selective acknowledgments. We have found that these grow as $WlogW$, where $W$ is the bandwidth-delay product, and as $\frac{1}{\log(1/q)}$, where $q$ is the probability of random loss.

One of our key achievements is the development of a novel framework for reliable data transport over heterogeneous networks. End-to-end data transport protocols have two main functions: error recovery and congestion control. The information required by the sender to perform these functions is provided by acknowledgements (ACKs) from the receiver. The Internet transport protocol, TCP/IP, uses cumulative acknowledgements (CACKs), which provide a robust but minimal mechanism for error recovery which is inadequate for heterogeneous networks with random loss. Furthermore, TCP's congestion control mechanism is based on counting ACKs, and is therefore vulnerable to loss of ACKs on the reverse path, particularly when the latter may be slower than the forward path, as in asymmetric networks. Our contributions are as follows:
(a) We show that a simple enhancement of CACK provides sufficient information for end-to-end *congestion control.* We term this ACK format total ACKs (TACKs). Modification of TCP-Reno to exploit TACKs leads to significant performance improvements for asymmetric networks, eliminating timeouts during Reno's fast recovery phase. TACKs do not improve the *error recovery* capability of TCP, however, so that the modified TCP-Reno is still vulnerable to random loss.
(b) We devise a novel ACK format that uses TACKs for congestion control, and negative ACKs (NACKs) for efficient error recovery. Typically, the main concern with NACKs is that of robustness to ACK loss, and we address this using an implementation that provides enough redundancy to provide such robustness.
(c) We use the TACK+NACK acknowledgement format as the basis for a new transport protocol that provides efficient error recovery and dynamic congestion control. The protocol provides large performance gains over TCP in an environment with random loss, and is robust against loss of ACKs in the reverse path. In particular, the protocol gives high

throughput upto a designed level of random loss, independent of the bandwidth-delay product. This is in contrast to TCP, whose throughput deteriorates drastically if the random loss probability is higher than the inverse square of the bandwidth-delay product. Efforts have been focused on producing a Request For Comment (RFC) in order to disseminate our ideas to the Internet Engineering Task Force (IETF). The work described above was the subject of an invited presentation at INFORMS'98 and has been presented at ACM SIGMETRICS'98.

### 3.1.7 Providing Quality of Service Guarantees

Quality of Service (QoS) guarantees to real time traffic has been considered through the example of a Rayleigh faded wireless downlink. Methods for statistical multiplexing have been considered, and it was shown that QoS provisioning in this context requires consideration of traffic statistics, choice of link layer error recovery scheme, as well as wireless channel statistics. To the best of our knowledge, this is the first work that provides detailed consideration of all these factors, and shows how important joint optimization across all the system parameters is for efficient design. The work has appeared at the International Symposium on Information Theory (ISIT'98) and the International Conference on Universal Portable Communications (ICUPC'98), and has been submitted for journal publication.

### 3.1.8 Location Tracking and Position Reporting

Diminishing cell sizes and/or the use of increasingly directed antennas, coupled with bursty or intermittent transmission, complicate wireless acquisition and synchronization. It may be desirable that explicit position update messages be issued. There is a basic tradeoff, since increasing the rate of updates can increase the speed of paging or acquisition, but it also increases channel congestion and network load. There is also an interaction between the policy used for issuing updates, and the policy used for paging. The basic tradeoff, and the interaction between location updates and paging, are investigated in [23].

Motion is modeled as a discrete-time Markov chain, and an iterative optimization approach is presented that seeks to minimize the total cost of registration and paging. Given a particular paging policy, the optimal registration policy is found through an infinite-horizon, discounted cost dynamic programming framework. Given a particular registration policy, the optimal paging policy is a maximum likelihood ordering of the cell locations. Iterations on these conditionally optimal policies are performed until convergence is achieved.

Various motion models are considered, including motion in one-dimensional ring and two-dimensional rectangular and hexagonal layouts. In general, regions in which the mobile station continues without attempting registration tend to follow the expected path of the mobile station. The continuation regions tend to get larger as the successful registration penalty increases and as the registration failure probability decreases. Additionally, it is shown that the iterative optimization algorithm does not necessarily produce globally optimal pairs of policies. The algorithm can produce non-optimal fixed-point solutions depending on initial

conditions and motion parameters.

### 3.1.9 Channel Carrying: A Novel Handoff Scheme for Mobile Cellular Networks

We have examined a new scheme that addresses the call handoff problem in mobile cellular networks. Efficiently solving the handoff problem is important for guaranteeing Quality of Service (QoS) to already admitted calls in the network. Our scheme is based on a new approach called *channel carrying*: when a mobile user moves from one cell to another, under certain mobility conditions, the user is allowed to *carry* its current channel into the new cell. We have proposed a new channel assignment scheme to ensure that this movement of channels will not lead to any extra co-channel interference or channel locking. In our scheme, the mobility of channels relies entirely on *localized information*, and no global coordination is required. Therefore, the scheme is simple and easy to implement. We have developed a hybrid channel carrying scheme that allows the maximization of performance under various constraints. We have found numerical results comparing our scheme with the traditional channel reservation and borrowing techniques. We have found that our scheme outperforms the reservation scheme over a broad range of traffic parameters and also outperforms the channel borrowing scheme under high loads. The results of this research have been reported in [6] and [7].

### 3.1.10 New Localized Channel Sharing Scheme for Cellular Networks

Enhancing system capacity while maintaining quality of service is an important issue in wireless cellular networks. A new localized channel sharing scheme has been found to address this problem. Our basic idea is to allow channels to be shared between adjacent cells. We have proposed a fixed channel assignment scheme to maximize channel reuse efficiency while allowing channel sharing. We have shown that our sharing scheme can also facilitate handoff processing. An important feature of our sharing scheme is that channel management is localized between adjacent cells, and no global coordination or optimization is required, thus making it suitable for implementation.

We have obtained simulation results comparing our scheme with the conventional channel assignment and handoff techniques. We found that our scheme improves system capacity over a broad range of traffic parameters and a variety of quality of service requirements. The results of this research have been reported in [8], [9], and [10].

### 3.1.11 An Efficient Scheme to Reduce Handoff Dropping in LEO Satellite Systems

The problem of handoffs in cellular networks is compounded in a low-earth orbit (LEO) satellite-based cellular network due to the relative motion of the satellites themselves with respect to a stationary observer on earth. Typically, the velocity of motion of mobiles can be ignored when compared to the very high velocity of the footprints of satellites. We have

exploited this property of the LEO satellite systems and proposed a handoff scheme based on [10] that results in a significant decrease in handoff dropping. For the same handoff dropping probability, our scheme has significantly lower new call blocking probability than the conventional reservation scheme. We have presented an analytical approximation that is in very good accord with simulation results. The results of this effort have been reported in [11].

### 3.1.12 Channel Sharing Scheme for Packet-Switched Cellular Networks

We have examined an approach for sharing channels to improve network utilization in packet-switched cellular networks. The scheme exploits unused resources in neighboring cells without the need for global coordination. A minimax approach to optimizing the allocation of channels in this sharing scheme has been formulated, a distributed algorithm to achieve this objective has been developed, and the convergence has been studied. Simulation results have shown that the distributed channel sharing scheme performs better than the fixed channel scheme over a wide variety of traffic conditions. The results of this effort have been reported in [12].

### 3.1.13 CDMA Systems in Fading Channels: Admissibility, Network Capacity, and Power Control

Due to the fast-growing demand for network capacity in wireless networks, the characterization of network capacity has become a fundamental and pressing issue. While there have been considerable efforts on CDMA systems at both the physical layer and network layer, the network capacity of imperfect power-controlled CDMA systems with linear receivers in fading environments are less well-understood. Hence, we have studied a single-cell synchronous CDMA system with matched filter receivers, assuming known distributions of received powers. We have found necessary and sufficient conditions on the admissibility for both single class and multiple class systems with random signatures. For systems with deterministic signatures, we have found a necessary and sufficient condition on the admissibility for single class systems, but only a sufficient condition for multiple class systems. We have also identified the network capacity of single class systems for both the random signature case and the deterministic signature case. The network capacity can be uniquely expressed in terms of the users' QoS requirements and the distributions of the received powers. We have found the tightest upper bound on the network capacity over all possible distributions of received powers, and have explored the concepts of effective target SIR and effective bandwidth, which play an important role in determining the admissibility and, hence, the network capacity. The results of this effort have been reported in [14], [15], and [16].

### 3.1.14 A Static Power Control Scheme for Wireless Cellular Networks

We have found a novel static power control scheme to improve system capacity in wireless cellular networks. Our basic idea is to reduce intercellular interference and improve the

capture probability by an *a priori* assignment of power-levels in different cells. We have formulated and solved an optimal scheduling problem for our scheme. We have determined that the optimal scheduling policy is a simple form of bang-bang control. Our scheduling solution has been illustrated by considering two specific cases with uniform and nonuniform fairness constraints. We have evaluated, via numerical analysis and simulation, both throughput and delay of the new scheme, and have compared these performance metrics with other schemes. Our scheme can achieve significant performance improvements, in terms of both maximum throughput and throughput-delay tradeoff, over a wide range of capture ratio values. The results of this effort have been reported in [13] and [17].

### 3.1.15 Analysis of a Distributed Power Control Algorithm

A wireless communication system consisting of mobile users communicating to base stations over a common radio channel has been analyzed for a low complexity uplink power control algorithm. At each iteration, each user needs only a single bit of information from its assigned base station indicating whether its SIR is above or below its desired level. If it is above, the user decreases its power level by a fixed amount (in dB); otherwise, the power level is increased by a fixed amount. This type of algorithm has been shown to be effective in simulation studies of various types of systems. Because of the fixed step sizes, the algorithm does not actually converge to the optimal power assignment, but we have proven its stability and some performance guarantees in terms of analytically derived bounds on the convergence error. We have shown that the convergence error can be made as small as desirable, at the cost of reducing the convergence rate. We have not considered mobility, but rather assumed that the network parameters are held constant while the algorithm runs. The results of this effort have been reported in [18].

## 3.2 Adaptive Coded Modulation for Spread-Spectrum Communication Systems (Wayne Stark, Univ. of MI; D. Sarwate, Univ. of IL, U. Madhow, Univ. of IL; Jim Lehnert, Purdue Univ.)

### 3.2.1 Cancelling Interference and Combining Multipath with a Linear Receiver and Long Sequences

We have examined blind adaptive signal processing algorithms that work by taking several samples of the correlator output resulting from the spread-spectrum signal during the time interval when multipath is arriving at the radio's antenna, and comparing them with samples taken later. Through a process of projecting in the direction of the signal plus noise and then projecting onto the space orthogonal to the noise, it is possible to determine the coefficients for a tapped delay line that follows the matched filter performing the correlation. Multipath can be combined and interference can be rejected simultaneously, and if an antenna array is available, the same algorithm can accommodate the antenna array and steer a beam toward the correct transmitter while producing nulls in the direction of interferers. An important aspect of our work is that it applies to the case of long sequences, which are used in the current spread-spectrum cellular standard and must be used in military systems for security. Many had thought that projection techniques required short sequences and hence had limited application. The net result of this research is to increase the resistance to interference and to again achieve a better SNR in the link budget of the system. This work is described in [42]. The role of the chip waveform selection for improving the performance of such systems is described in [43].

### 3.2.2 Cancelling Interference and Fading Channel Estimation for Multicarrier Spread Spectrum

The near-far problem has been a classic difficulty for DS/SSMA systems. The problem is that an interfering transmitter that is close to a receiver can overpower faint signals. Even though the spread-spectrum modulation provides significant processing gain that helps to extract faint signals, practically the gain is often not enough. We have devised for use in multi-carrier spread-spectrum systems a demodulation scheme that excises interference and adjusts for fading. This scheme is shown to provide great gains in dealing with the near-far problem. This result in described in [41].

### 3.2.3 Meeting the Welch Bound with Equality

A signal set whose root-mean-square inner product magnitude equals the Welch lower bound id called a WBE signal set. WBE signal sets are of interest in synchronous CDMA communication systems. We have studied the signal-to-noise ratio for CDMA communication systems using WBE signal sets. The results are reported in [44].

### 3.2.4 Design of Frequency Hopping Patterns

Careful design of the frequency-hopping patterns used in a frequency-hopped communication system can lead to gains in performance. Well-known methods of frequency-hopping pattern construction lead to patterns whose average Hamming correlation properties are optimal, but which have some local Hamming correlation properties that are less than desirable. For example, the Lempel-Greenberger hopping patterns have the undesirable property that collisions between two different patterns can occur in bursts. Such bursts of collisions lead to bursts of errors and to difficulties in the design of the error-control coding systems for frequency-hopped communication systems. Shorter classes of hopping patterns based on Reed-Solomon codes also have optimal average Hamming correlation but have the undesirable property that most of the patterns hop to only one-half of the available frequency slots. We have discovered a new class of frequency-hop patterns whose periods are intermediate between the short Reed-Solomon code patterns and the much longer Lempel-Greenberger patterns. The average Hamming correlation properties of these patterns are very slightly inferior to the Reed-Solomon patterns and the Lempel-Greenberger patterns, but the new patterns exhibit neither the bursts of collisions that are characteristic of the Lempel-Greenberger patterns nor the poor spectral spreading properties characteristic of Reed-Solomon patterns. Thus, these patterns can be used to improve the performance of frequency-hop communication systems.

The new frequency-hop patterns also have the very interesting property that the collisions occur in a very "systematic" fashion. That is, if two patterns collide during the i-th and jth dwells (say) of the first n dwells, then they will also collide during the (n+i)-th and the (n+j)-th dwells. Here, n is much smaller than the period of the hopping patterns, so that the patterns have a good deal of substructure. Since collisions are often detectable (in fact, the good performance of many of the error-control schemes is predicated on the perfect detection of collisions and the erasure of the corresponding transmitted symbols), the receiver knows where collisions are going to occur in the future. By examining multiple dwells spaced n dwells apart, the receiver can make a more reliable decision as to whether these dwells have collisions in them. The periodicity of the collisions also improves the speed of the decoder in the error-control system. For example, if an interleaved Reed-Solomon code of length n is being used for erasures-and-errors decoding, then the erasure locator polynomial need not be calculated each time because it is the same for each successive received codeword.

An alternative strategy for exploiting the properties of these frequency-hopped patterns uses a feedback channel by means of which the receiver can inform the transmitter of the locations of the collisions. Armed with this knowledge, the transmitter might use adaptive transmission strategies. For example, the transmitter might maintain radio silence during the affected dwells, thus reducing power consumption (as well as reducing interference for the other transmitter.) Of course, such interruptions reduce the data throughput, but this can be ameliorated by increasing the code rate – in the absence of collisions, less powerful error correcting codes can be used. Further details can be found in [24].

We have also considered simple strategies for reducing the number of errors due to collisions in a frequency-hop communication system. One method leads to a very slight reduction

in data rate, but a significant improvement in performance at the limit when the error-control coding system is faced the maximum number of errors that it is designed to correct. The effect of this on the overall performance of the system has been studied.

### 3.2.5 Adaptive Coding

Coding and modulation schemes for direct-sequence spread-spectrum (DS-SS) systems with multiple-access (MA) interference in a fading environment have been considered. Our goal has been to adapt the code to different environments. Communication in an environment with a large amount of interference requires low transmission (code) rate while small levels of interference allows high rate transmission. We have considered the following coded modulation systems: a conventional 64-ary orthogonal code, a trellis coded Nordstrom-Robinson (TCNR) code, and a trellis coded Reed-Muller (TCRM) code. Each of these is concatenated with a (63,k) Reed-Solomon (RS) outer code. The performance measure of interest is error probability and throughput. These are evaluated by making a Gaussian approximation on the multiple-access interference. Our results show, given an error probability requirement, and a certain data rate, a maximum number of users for each of the three DS-SS schemes can be determined. This indicates the receiver can adjust the coding and modulation scheme to achieve the given requirement. In addition to the above, two additional research areas have been explored. several new avenues of research have begun. These include the examination of turbo codes for frequency-hopped spread-spectrum systems subject to jamming, and the optimization of a product code using Reed-Solomon codes to frequency-hopped spread-spectrum with partial-band jamming. This research work is detailed in Milcom '97.

### 3.2.6 Multi-User Demodulation Schemes

Several multiuser demodulation schemes for a direct-sequence code-division multiple access (DS-CDMA) system that provide soft-outputs to enhance single-user soft-decision decoders have been considered [32]. First, we derived an optimum soft-output multiuser estimation (OSOME) algorithm for asynchronous CDMA channels with white Gaussian noise (WGN). The algorithm generates a posteriori probabilities (APP) for coded bits given the received signal. This forward-recursive algorithm requires complexity and storage exponential in the number of users K and linear in the decision lag L. Second, we developed a reduced-computation suboptimal version of this algorithm (SSOME) which compares favorably in complexity and storage with the multiuser soft-output Viterbi algorithm (SOVA). Furthermore, we have shown that the Bayesian conditional decision feedback estimation (BCDFE) algorithm provides symbol APP estimates that can be considerably improved upon by a slight modification. We derived the modified BCDFE algorithm for whitened multiuser channels. Simulation results of a 4-user, convolutionally coded, asynchronous CDMA system indicate that the SSOME algorithm with L=K-1 achieves a 0.4-0.5 dB gain over SOVA with much greater lag (and complexity) and keeps within 0.25 dB of the OSOME algorithm. Moreover, the modified BCDFE algorithm provides a good performance/complexity tradeoff.

### 3.2.7 Decision Feedback Sequence Estimation for Unwhitened ISI Channels with Applications to Multiuser Detection

Decision feedback sequence estimation (DFSE), which is a reduced-complexity alternative to maximum likelihood sequence estimation, can be used effectively for equalization of inter-symbol interference as well as for multiuser detection. The algorithm performs very well for whitened (minimum-phase) channels. For non-minimum-phase channels, however, the algorithm is not very effective. Moreover, DFSE requires a noise-whitening filter, which may not be feasible to compute for time-varying channels like a multiuser DS-CDMA channel. Noise-whitening is also cumbersome for applications that involve bi-directional equalization such as the GSM system. In such conditions, it is desirable to use the Ungerboeck formulation for sequence estimation which operates directly on the discrete-time unwhitened statistic obtained from conventional matched filtering. Unfortunately, decision feedback sequence estimation based on matched filter statistics is severely limited by untreated interference components. We have identified the anti-causal interference components using an error probability analysis. This has lead us to a modified unwhitened decision feedback sequence estimator (MUDFSE) where the components are canceled using tentative decisions. We have obtained approximate error probability bounds for the proposed algorithm. Performance results indicate that the modified algorithm used on unwhitened channels with relatively small channel correlations provides similar performance/complexity tradeoffs as the DFSE used on the corresponding whitened *minimum-phase* channels. The algorithm is especially attractive for multiuser detection for asynchronous direct sequence CDMA channels with long spreading codes, where it can achieve near-MLSE performance with exponentially lower complexity.

### 3.2.8 Reduced Trellis and Tree Search Algorithms: The Effect of The Receive Filter and The Branch Metric

We have examined the role of the receive filter and the branch metric in decision feedback sequence estimation (DFSE) and M-algorithm receivers. We have considered a generalized receiver which consists of a front-end filter (matched to the overall channel response or the transmit filter response) followed by a general transversal processing filter and a reduced trellis or tree search algorithm. A first event error analysis of the generalized receiver has indicated that a proper combination of the processing filter and the branch metric is necessary to avoid bias (untreated interference components) in the receiver. Bias occurs in a DFSE or M-algorithm receiver due to a mismatch between the processing filter and the branch metric. We have shown that the processing filter must either be the appropriate noise-whitening filter or the zero-forcing filter in order to achieve unbiasedness. The branch metric for the reduced trellis and tree search algorithms for each case of matched filtering has been obtained. The well-known DFSE and M-algorithm receivers, where the search algorithm operates on whitened statistics, belong to the class of unbiased receivers, while the receivers where the search algorithm operates on standard matched filter statistics belong to the class of biased receivers. We have characterized the error performance of various DFSE and truncated

memory MLSE receivers in terms of a parameter called the *error distance*, which includes the effect of noise enhancement. We have shown that the whitening filter DFSE receiver is optimum among unbiased DFSE and truncated memory MLSE receivers (with pre-filtering) in the sense that it maximizes the error distance. We have obtained upper bounds on the symbol error probability of the various DFSE receivers and outlined a generating function approach to evaluate the bounds. Simulation and analytical results have been obtained for the case of a symbol-sampled channel model and a fractionally-sampled channel model.

### 3.2.9 A New Fractional MLSE Receiver for Time-varying Channels

We have derived a new maximum-likelihood sequence estimation (MLSE) receiver that operates on fractionally-spaced samples obtained at the output of an analog filter matched to the transmit pulse-shaping filter. A fractional MLSE receiver was proposed by Hamied *et al.* that requires a fixed noise-whitening filter to whiten noise samples at the output of the transmit matched filter. Due to the presence of nulls in the Nyquist bandwidth of practical pulse-shaping filters like the square-root raised cosine filter, the noise-whitening filter has a long slowly-damped delay response and any practical length truncation results in significant distortion. The new receiver does not need noise-whitening. The branch metric of the Viterbi algorithm in the receiver accounts for the correlation in the noise samples. The receiver is insensitive to sampler timing phase. An adaptive form of the receiver requires only one step prediction of medium response coefficients. These features make the receiver attractive for fast time-varying channels.

### 3.2.10 Combined Decision-Feedback Multiuser Detection/Soft-Decision Decoding for CDMA Channels

We have evaluated the performance of decision-feedback multiuser detectors with coding for CDMA channels. A combined multiuser detection/soft-decision decoding scheme is proposed which allows total control over the reliability of decision-feedback mechanism. Its performance is compared to that of conventional detection and linear-decorrelation detection with soft-decision decoding. Simulation and analysis is undertaken for synchronous CDMA channels. It is found that the scheme works very well especially for weak users and when multiuser interference is large. However, strong users do not gain much with this scheme over a linear-decorrelation detector.

### 3.2.11 Soft-Output Multiuser Estimation for Asynchronous CDMA Channels

We have considered several multiuser demodulation schemes for a direct-sequence code-division multiple access (DS-CDMA) system that provide soft-outputs to enhance single-user soft-decision decoders. First, we have derived an optimum soft-output multiuser estimation (OSOME) algorithm for asynchronous CDMA channels with white Gaussian noise (WGN). The algorithm generates *a posteriori probabilities* (APP) for coded bits given the received signal. This forward-recursive algorithm requires complexity and storage exponential in the

number of users $K$ and linear in the decision lag $L$. Second, we have outlined a reduced-computation suboptimal version of this algorithm (SSOME) which compares favorably in complexity and storage with multiuser soft-output Viterbi algorithm (SOVA). Furthermore, we have noted that the Bayesian conditional decision feedback estimation (BCDFE) algorithm [?] provides symbol APP estimates that can be considerably improved upon by a slight modification. The modified BCDFE algorithm for whitened multiuser channels has been derived. Finally, simulation results of a 4-user, convolutionally coded, asynchronous CDMA system have been obtained. The results indicate that the SSOME algorithm with $L = K - 1$ achieves a $0.4 - 0.5$ dB gain over SOVA with much greater lag (and complexity) and keeps within 0.25 dB of the OSOME algorithm. Moreover, the modified BCDFE algorithm provides a good performance/complexity tradeoff.

### 3.2.12 Decision Feedback Sequence Estimation for Unwhitened ISI and Multiuser CDMA Channels

Decision feedback sequence estimation (DFSE), which is a reduced-complexity alternative to maximum likelihood sequence estimation, performs very well for whitened (minimum-phase) inter-symbol interference (ISI) channels. However, it may not be feasible to compute the whitening filter for many time-varying channels like the multiuser asynchronous direct-sequence CDMA channel. Moreover, the performance of DFSE is not very good for many non-minimum-phase whitened ISI channels and for channels for which it is desirable to perform bidirectional equalization as in the GSM system. In these scenarios, it is beneficial to use the Ungerboeck formulation for sequence estimation which operates directly on the discrete-time unwhitened statistic obtained from conventional matched filtering. We have shown that conventional decision-feedback sequence estimation in the Ungerboeck form is interference limited. An error probability analysis has led us to a modified unwhitened decision feedback sequence estimator (MUDFSE). Simulation results have indicated that the modified algorithm used on unwhitened ISI channels with low to moderate dispersion, provides similar performance/complexity tradeoffs as the DFSE used on the corresponding whitened *minimum-phase* channels. The algorithm is especially attractive for multiuser detection for asynchronous DS-CDMA channels with long spreading codes, where sizable gains over the (unwhitened) M-algorithm are obtained.

### 3.2.13 Decision Feedback Sequence Estimation for Unwhitened ISI Channels

A form of decision-feedback sequence estimation (DFSE) has been examined for unwhitened inter-symbol interference (ISI) channels. DFSE, which is a reduced-complexity alternative to maximum likelihood sequence estimation, performs very well on whitened (minimum-phase) ISI channels. However, it may not be feasible to compute the whitening filter for many time-varying channels like the multiuser asynchronous direct-sequence CDMA channel. On such channels, it is desirable to use the Ungerboeck formulation, which operates directly on discrete-time unwhitened statistic obtained from conventional matched filtering. Unfortunately, decision-feedback sequence estimation for unwhitened channels is interference limited

because the decision statistic depends on both past and future inputs. Specifically, the decision rule that chooses the path with the best accumulated metric leading to a reduced state, fails to account for interference from the future inputs not included in the reduced state. We have proposed a modified decision rule to be integrated into the Ungerboeck form of sequence estimation which is not sensitive to channel phase. It can be implemented as a single stage or a multistage scheme depending on the amount of dispersion present in the channel. Simulation results have indicated that the algorithm used on unwhitened channels with low to moderate dispersion, provides similar performance/complexity tradeoffs as the DFSE used on the corresponding whitened minimum-phase channels. The algorithm is especially attractive for multiuser asynchronous DS-CDMA channels with long spreading codes.

### 3.2.14 A Family of Soft-Output Multiuser Demodulators for Coded Asynchronous CDMA Channels

We have considered a soft-output multiuser demodulation for asynchronous CDMA channels with coding and interleaving. First, we derive an optimum soft-output multiuser estimation (OSOME) algorithm for linearly-modulated Gaussian CDMA channels. The forward-recursive algorithm generates *a posteriori* probabilities (APP) for modulator-input symbols given the received signal, which can be fed directly to single-user soft-decision decoders. Second, we have outlined a reduced-state soft-output multiuser estimation (RSOME) scheme, with complexity exponential in a parameter called memory order chosen arbitrarily (smaller than channel memory). These algorithms can be employed with conventional matched filtering and do not require noise whitening. Finally, we have obtained simulation results of a four-user coded asynchronous CDMA system. The results indicate that the OSOME algorithm achieves a $0.4 - 0.6$ dB gain over soft-output Viterbi algorithm (SOVA) in a power controlled environment and the reduced-state schemes provide a desirable performance-complexity tradeoff.

### 3.2.15 Type-II Hybrid ARQ Protocol with Adaptive Coding and Spread-Spectrum

It is desirable to utilize information in packets with errors whenever possible. For example, if a packet is received with one more bit than the utilized error control code can correct, a packet with extra parity information can be sent to correct that error so that the original packet is useful. When the channel is good, extra parity information does not need to be sent. However, when the channel degrades, the extra parity is needed. Adaptive coding is achieved by sending fewer packets, and hence parity bits, when the channel is good and sending more parity packets when the channel degrades.

We have applied the type-II hybrid ARQ protocol in a slotted DS-SSMA packet radio system [30]. Using the improved Gaussian approximation technique, we have performed static analysis on such a system to obtain packet success probabilities. Moreover, we have employed two-dimensional Markov chains to analyze the dynamic behavior of the system. Based on this model, we have upper and lower bounded the performance of the type-II

hybrid ARQ protocol by considering a superior scheme and an inferior scheme, respectively. We have obtained the steady state throughput and delay performances and the optimal retransmission probabilities of the two bounding schemes. Finally, using a sample system as an example, we have shown how to derive the design criteria for the transmitter buffers in order to achieve the system capacity with minimum delay.

### 3.2.16 PAM/QAM Signal Sets for Trellis-Coded Spread-Spectrum Systems

The same effect as is achieved by adaptive coding can be achieved by utilizing the structure of modulation schemes such as quadrature amplitude modulation (QAM). When the channel is good, a decision is made among all the points in the signal constellation corresponding to the modulation, and when the channel is bad, a decision is made among a subset of the points in that constellation. In order to ascertain the benefits of high dimensional modulations such as QAM, the performance of coded QAM schemes in multiple-access interference must be determined.

An expression in matrix form for the multiple-access interference (MAI) in an asynchronous direct-sequence spread-spectrum multiple-access communication system with cascaded sequences, arbitrary chip waveforms, and trellis-coded modulation (TCM) with a PAM or QAM signal set, has been obtained. TCM provides significant coding gain, while cascaded sequences decrease the correlation between the MAI of adjacent data intervals. The expression has been used to calculate arbitrarily accurate probability density functions (pdf's) of the MAI in the TCM system and to derive an accurate approximation of the MAI variance. This has also helped to illustrate some properties of the MAI by separating contributing parameters into different matrices. We have derived an approximation of the upper union bound on the bit error probability and investigated its applicability. The results [33] show that cascaded sequence schemes can greatly reduce the pairwise error probabilities until the length of the cascaded sequence becomes greater than that of the error weight sequence under consideration.

### 3.2.17 Pairwise Error Probabilities in Coded Spread-Spectrum Systems in Rayleigh Fading Channels

Radio links encountered on the digital battlefield are typically coded and suffer from fading. In order to assess spread-spectrum links in such an environment, it is necessary to focus on the channel state information (CSI) that is available and also on the pairwise error probabilities between codewords or paths through a trellis.

Arbitrarily tight upper and lower bounds on the pairwise error probability (PEP) of a trellis-coded or convolutional-coded direct-sequence spread-spectrum multiple-access (DS/SSMA) communication system over a Rayleigh fading channel have been derived [34]. A new set of probability density functions (pdf's) and cumulative distribution functions (cdf's) of the multiple-access interference (MAI) statistic has been derived, and a modified bounding technique has been proposed to obtain the bounds. The upper bounds and lower bounds together specify the accuracy of the resulting estimation of the PEP, and give an indication of the

system error performance with imperfect channel state information (CSI). Several suboptimum decoding schemes have been proposed and their performances have been compared to that of the optimum decoding scheme by the average pairwise error probability (APEP) values. The approach can be used to accurately study the multiple-access capability of the coded DS/SSMA system without numerical integrations.

### 3.2.18 Blind adaptation for interference suppression in DS-CDMA

We have provided a method [25] for blind spatiotemporal adaptation for interference suppression in direct-sequence CDMA with short spreading sequences.

### 3.2.19 Pipelined architectures for adaptive interference suppression algorithms

We have provided pipelined architectures for high-speed low-power implementations of adaptive interference suppression algorithms for direct-sequence CDMA [21].

## 3.3 Antenna Array Processing (Michael Zoltowski, Purdue Univ.)

The goal of this research has been to develop space-time RAKE receivers for direct-sequence spread-spectrum communication systems that achieve two primary goals: (1) optimal combination of the desired user's multipath in a RAKE-like receiver fashion and (2) simultaneous cancellation of strong multiple-access interference and jammers. The effort has concentrated on the development and analysis of reduced dimension space-time RAKE receivers that yield the following two advantages: (1) reduced computational complexity and (2) faster convergence to near optimum SINR in the symbol decision statistic. The effort has proceeded along the following lines:

- Convergence Analysis and Tracking Ability of Reduced Dimension Blind Space-Time Rake Receivers for DS-CDMA
- Joint Angle and Delay Estimation for Reduced Dimension Space-time Rake Receiver With Application to IS-95 CDMA Uplink
- Blind 2-D RAKE Receivers Based on RLS-type Space-Time Adaptive Filtering for DS-CDMA System

Each of these three efforts is briefly summarized below.

### 3.3.1 Convergence Analysis and Tracking Ability of Reduced Dimension Blind Space-Time Rake Receivers for DS-CDMA

We have examined reduced dimension blind space-time RAKE receivers for classical DS-CDMA that cancel strong multiple-access interference while optimally combining the desired user's multipath. After passing the output of each antenna through a matched filter, whose impulse response is an oversampled version of the time-reverse of the spreading waveform of the desired user, one estimates the reduced dimension signal plus interference space-time correlation matrix during that portion of the bit interval where the RAKE fingers occur, and the reduced dimension interference-alone space-time correlation matrix during that portion of the bit interval away from the fingers. It was shown that the weight vector yielding the optimum signal-to-interference-plus-noise ratio for bit decisions is the largest generalized eigenvector of the resulting matrix pencil.

In this work, we have compared the asymptotic SINR and convergence rate of full dimension space-time processing with that of reduced dimension processing based on simultaneous time and space compressing transformations. We have shown through theoretical analysis and supporting simulations that if the space and time compressing transformations are designed judiciously, reduced dimension 2D RAKE receivers offer faster convergence with respect to output SINR as a function of the number of symbols received than that achieved with a full dimension space-time RAKE receiver, at the expense of only a slight loss in asymptotic SINR. Applications to the IS-95 uplink were developed along with supporting simulations. In addition, simulations involving a mobile moving 75 mph were conducted demonstrating the tracking capabilities of the reduced dimension 2D RAKE receiver.

### 3.3.2 Joint Angle and Delay Estimation for Reduced Dimension Space-time Rake Receiver With Application to IS-95 CDMA Uplink

We have developed an algorithm for joint estimation of the angle of arrival (AOA) and delay of each dominant multipath for the desired user for use in a reduced dimension space-time RAKE receiver for DS-CDMA communications that is near-far resistant. After estimating the desired spatio-frequency signal vector, we have proposed the 2D unitary ESPRIT algorithm as our estimator, which provides closed-form as well as automatically paired AOA-delay estimates. We effectively have a single snapshot of 2D data and thus require 2D smoothing for extracting multiple snapshots. The comparative performance of two 2D smoothing schemes, called pre-eigenanalysis and post-eigenanalysis 2D smoothing, respectively, has been examined. The space-time data model for the IS-95 uplink was investigated. The performance of a reduced dimension space-time RAKE receiver for the IS-95 uplink using the AOA-delay estimates has been assessed through Monte-Carlo simulations.

Simulation results show that our algorithms can accurately estimate the AOA and delay for each multipath under near-far conditions. The AOA information is useful for FDD downlink beamforming and source localization for an emergency geolocation (911) service. The pre-eigenanalysis 2D smoothing algorithm offers better performance than the post-eigenanalysis 2D smoothing algorithm. The paired AOA and delay information may be used to the reduce dimensionality of the space-time 2D RAKE receiver. Our simulation results show that better separation between the value of the true Walsh symbol decision variable and the other 63 decision variables may be achieved by using the knowledge of the paired angle-delay estimates, as opposed to that obtained with full dimension space-time processing. This better performance results from the faster convergence toward the optimal weight vector due to the reduced dimensionality under conditions of limited available symbols where channel characteristics remain approximately stationary. The simulation results have revealed that the performance of the joint AOA-delay estimator and the resulting reduced space-time RAKE receiver is quite promising. Work has included examination of the choice of subarray size employed in 2D smoothing and a comparison of the performance of the joint AOA-delay estimator to the CRB(Cramer-Rao Bound).

### 3.3.3 Blind 2-D RAKE Receivers Based on RLS-type Space-Time Adaptive Filtering for DS-CDMA System

We have developed a blind 2D RAKE receiver for CDMA that cancels strong multi-user access interference and optimally combines multipath. The weight vector yielding the optimum signal-to-interference-plus-noise ratio for bit decisions is the largest generalized eigenvector of the spatio-frequency (spatio-temporal) correlation matrix pencil. However, the eigen-analysis based algorithm is on the order of $O(N^3)$ computational complexity and the resulting spatio-frequency (spatio-temporal) correlation matrix pencil is of large dimension. This detracts from the real-time applicability of that scheme. A blind 2-D RAKE receiver was thus developed based on an RLS-type space-time adaptive filtering scheme which offers $O(N^2)$ computational complexity and competitive performance. The applicability of the

scheme to the IS-95 uplink has also been addressed in a decision-directed fashion.

# 4 Integration of Research and Technology Transfer

Attempts have been made to obtain other awards and to continue and expand industrial and university cooperation in order to accomplish technology transfer. This activity has occurred because of our notification that support has ended for the Focused Research Programs across the country.

# References


[1] B. Hajek and P. Seri, "On causal scheduling of multiclass traffic with deadlines," CSL Technical report UILU-ENG-98-2220, August 1997.

[2] B. Hajek and P. Seri, "On causal scheduling of multiclass traffic with deadlines," *Proceedings 1998 IEEE International Symposium on Information Theory*, Cambridge, MA, p. 166, August 1998.

[3] P. Seri, "Causal Scheduling of Multiclass Traffic with Deadlines and Priorities," MS Thesis, CSL Technical report UILU-ENG-98-2211, June 1998.

[4] Vijay G. Subramanian and B. Hajek, Capacity and Reliability Function per Fourth Moment Cost for WSSUS Fading Channels, " To appear, *Proc. IEEE Information Theory and Communications Workshop*, Kruger National Park, South Africa, June 1999.

[5] P. Bruneteau, *One-success random access without feedback for a bounded number of active stations*, MS Thesis, CSL Technical report UILU-ENG-98-2214, June 1998.

[6] J. Li, N. B. Shroff, and E. K. P. Chong, "Channel Carrying: A Novel Handoff Scheme for Mobile Cellular Networks," in *Proceedings of the 1997 IEEE INFOCOM* (16th Annual Joint Conference of the IEEE Computer and Communication Societies), Kobe, Japan, April 9–11, pp. 909–917, 1997.

[7] J. Li, N. B. Shroff, and E. K. P. Chong, "Channel Carrying: A Novel Handoff Scheme for Mobile Cellular Networks," *IEEE/ACM Transactions on Networking*, to appear.

[8] J. Li, N. B. Shroff, and E. K. P. Chong, "A Channel Sharing Scheme to Improve System Capacity and Quality of Service in Wireless Cellular Networks," in *Proceedings of the Third IEEE Symposium on Computers and Communications (ISCC'98)*, pp. 700–704, Athens, Greece, June 30–July 2, 1998.

[9] J. Li, N. B. Shroff, and E. K. P. Chong, "The Study of a Channel Sharing Scheme in Wireless Cellular Networks including Handoffs," in *Proceedings of the 1999 IEEE INFOCOM*, New York, New York, March 21–25, 1999, to appear.

[10] J. Li, N. B. Shroff, and E. K. P. Chong, "A New Localized Channel Sharing Scheme for Cellular Networks," *Wireless Networks*, to appear.

[11] S. Kalyanasundaram, E. K. P. Chong, and N. B. Shroff, "An Efficient Scheme to Reduce Handoff Dropping in LEO Satellite Systems," in *Proceedings of the 17th IEEE Symposium on Reliable Distributed Systems*, Purdue University, West Lafayette, Indiana, October 20–23, 1998, to appear.

[12] S. Kalyanasundaram, J. Li, E. K. P. Chong, and N. B. Shroff, "Channel Sharing Scheme For Packet-Switched Cellular Networks," in *Proceedings of the 1999 IEEE INFOCOM*, New York, New York, March 21–25, 1999, to appear.

[13] J. Li, N. B. Shroff, and E. K. P. Chong, "A Static Power Control Scheme for Wireless Cellular Networks," in *Proceedings of the 1999 IEEE INFOCOM*, New York, New York, March 21–25, 1999, to appear.

[14] J. Zhang and E. K. P. Chong, "Admissibility and Network Capacity of Power-Controlled CDMA Systems in Fading Channels," in *Proceedings of the 36th Annual Allerton Conference on Communication, Control and Computing*, Monticello, Illinois, September 23–25, 1998, to appear.

[15] J. Zhang and E. K. P. Chong, "CDMA Systems with Random Spreading in Fading Channels: Network Capacity and Power Control," in *Proceedings of the 1999 IEEE INFOCOM*, New York, New York, March 21–25, 1999, to appear.

[16] J. Zhang and E. K. P. Chong, "CDMA Systems in Fading Channels: Admissibility, Network Capacity, and Power-Control," submitted to *IEEE Transactions on Information Theory.*

[17] J. Li, N. B. Shroff, and E. K. P. Chong, "A Static Power Control Scheme for Wireless Cellular Networks," submitted to *IEEE/ACM Transactions on Networking.*

[18] J. Herdtner and E. K. P. Chong, "Analysis of a Simple Distributed Power Control Algorithm," in *Proceedings of the 36th Annual Allerton Conference on Communication, Control and Computing*, Monticello, Illinois, September 23–25, 1998, to appear.

[19] H. Chaskar, T. V. Lakshman, U. Madhow, "On the design of interfaces for TCP/IP over wireless," *Proc. IEEE Milcom '96,* October 1996.

[20] B. Hajek, A. Krishna, R.O. LaMaire, "On the capture probability for a large number of stations," IEEE Transactions on Communications, vol. 42, pp. 254-260, February 1997.

[21] L. He and U. Madhow, "Pipelined MMSE equalizers for direct-sequence spread-spectrum CDMA channels," *Proc. International Conf. Univ. Personal Commun. (ICUPC'96),* Boston, MA, September 29-October 2, 1996.

[22] T. V. Lakshman and U. Madhow, "The performance of TCP/IP for networks with high bandwidth-delay products and random loss," to appear, *IEEE/ACM Transactions on Networking,* June 1997.

[23] K. Mitzel, *Iterative Optimization of Registration and Paging Policies in Cellular Networks*, M.S. Thesis and CSL Technical Report, B. Hajek, advisor. January 1997.

[24] D. V. Sarwate and D. A. Losada, "A new class of frequency-hop patterns," *Proceedings of the 1997 IEEE International Symposium on Information Theory*, Ulm, Germany ,p. 125 June 29 - July 5, 1997.

[25] V. Subramaniam and U. Madhow, "Blind Demodulation of Direct-Sequence CDMA Signals Using an Antenna Array," *Proc. Conf. Inform. Sci. Sys. (CISS'96),* Princeton, NJ, March 1996.

[26] J. Waldby and U. Madhow, "Dynamic window-based flow control with end-to-end selective acknowledgments," *Proc. 3rd International Workshop on Mobile Multimedia Communications (MoMuC-3),* Princeton, NJ, September 25-27, 1996.

[27] A. Naguib, A. Paulraj, and T. Kailath, "Capacity Improvement with Base-Station Antenna Array in Cellular CDMA," *IEEE Trans. Veh. Technology,* vol. 43, pp. 691-698, Aug. 1994.

[28] Hui Liu and M. D. Zoltowski, "Blind Equalization in Antenna Array CDMA Systems," *IEEE Trans. on Signal Processing, Spec. Issue on Signal Processing for Adv. Digital Communications,* Jan. 1997, pp.161-172.

[29] A. Naguib, A. Paulraj, and T. Kailath, "Capacity Improvement with Base-Station Antenna Array in Cellular CDMA," *IEEE Trans. Veh. Technology,* vol. 43, pp. 691-698, Aug. 1994.

[30] Q. Zhang, T. F. Wong, and J. S. Lehnert, "Performance of an Adaptive Coding Scheme for a DS/SSMA System," *IEEE Transactions on Communications* , vo. 47, no. 2, pp. 281-290, February 1999.

[31] Tan F. Wong, Tat M. Lok, James S. Lehnert, and Michael D. Zoltowski, "A Linear Receiver for Direct-Sequence Spread-Spectrum Multiple Access Systems With Antenna Arrays and Blind Adaptation," *IEEE Trans. on Information Theory,* vol. 44, pp. 659-676, March 1998.

[32] Abdulrauf Hafeez and Wayne E. Stark, "Soft-output multiuser estimation for asynchronous CDMA channels," *Proceedings of the 1997 IEEE Vehicular Technology Conference,* pp. 465–469, May 1997.

[33] T. T. Chen and J. S. Lehnert, "TCM/SSMA communication systems with cascaded-sequences and PAM/QAM signal sets," *IEEE Transactions on Communications,* vol. 46, no. 7, pp. 950-956, July 1998.

[34] T. T. Chen and J. S. Lehnert, "Bounds on the Pairwise Error Probability of Coded DS/SSMA Communications Systems in Rayleigh Fading Channels," *IEEE Transactions on Communications,* vol. 46, no. 12, pp. 1685-1692, December 1998.

[35] Vijay G. Subramanian and B. Hajek, "Capacity and reliability functions per unit cost for WSSUS fading channels," To appear, *Proc. 33rd Annual Conference on Information Sciences and Systems,* Johns Hopkins University, March 1999.

[36] Vijay G. Subramanian and B. Hajek, Capacity and Reliability Function per Fourth Moment Cost for WSSUS Fading Channels, " To appear, *Proc. IEEE Information Theory and Communications Workshop*, Kruger National Park, South Africa, June 1999.

[37] P. Bruneteau, *One-success random access without feedback for a bounded number of active stations*, MS Thesis, CSL Technical report UILU-ENG-98-2214, June 1998.

[38] B. Hajek and P. Seri, "On causal scheduling of multiclass traffic with deadlines", CSL Technical report UILU-ENG-98-2220, August 1997.

[39] B. Hajek and P. Seri, "On causal scheduling of multiclass traffic with deadlines," *Proceedings 1998 IEEE International Symposium on Information Theory*, Cambridge, MA, p. 166, August 1998.

[40] P. Seri, "Causal Scheduling of Multiclass Traffic with Deadlines and Priorities," MS Thesis, CSL Technical Report UILU-ENG-98-2211, June 1998.

[41] T. M. Lok, T. F. Wong, and J. S. Lehnert, "Blind adaptive signal reception for MC-CDMA systems in Rayleigh fading channels," *IEEE Transactions on Communications*, vol. 47, no. 3, pp. 464-471, March 1999.

[42] T. F. Wong, T. M. Lok, J. S. Lehnert, and M. D. Zoltowski, "A Linear Receiver for direct-sequence spread-spectrum multiple-access systems with antenna arrays and blind adaptation," *IEEE Transactions on Information Theory* , vol. 44, pp. 659-676, March 1998.

[43] T. F. Wong, T. M. Lok, and J. S. Lehnert, "Asynchronous Multiple-Access Interference Suppression and Chip Waveform Selection with Aperiodic Random Sequences," *IEEE Transactions on Communications*, vol. 47, no. 1, pp. 103-144, January 1999.

[44] D. V. Sarwate, "Meeting the Welch bound with equality," *International Conference on Sequences and Their Applications*, December 14 – 17, 1998, Singapore (to appear in Discrete Math/Theoretical Computer Science series volume to be published later by Springer-Verlag).

# Included Papers

Research papers appear in the order of the list of papers submitted or published under ARO sponsorship shown early in this report. Papers may be missing if they have been submitted with earlier interim progress reports, or if the author of a particular manuscript has taken the responsibility of directly providing the manuscript to the Army Research Office.

### 3.2 The Welch Bounds

It was shown in [18] that

$$\sum_{m \in \mathcal{M}} |g_{k,l}(m)|^2 = \sum_{m \in \mathcal{M}} g_k(m)(g_l(m))^*. \tag{11}$$

holds for the aperiodic, periodic, and odd correlation functions. More recently, it has been noted [28] that the same proof shows that polyphase correlation functions also satisfy this identity. Thus, as described in [21], it follows from (11) that

$$\sum_{k=1}^{K} \sum_{l=1}^{K} \sum_{m \in \mathcal{M}} |g_{k,l}(m)|^2 = K^2 N^2 + \sum_{m \in \mathcal{M}^*} \left| \sum_{k=1}^{K} g_k(m) \right|^2. \tag{12}$$

Thus the following generalization of Proposition 1 holds [16], [21], [28].

**Proposition 16.** *The aperiodic and polyphase correlation functions (which include the periodic and odd correlation functions as special cases) for a signal set satisfy the following lower bound:*

$$\sum_{k=1}^{K} \sum_{l=1}^{K} \sum_{m \in \mathcal{M}} |g_{k,l}(m)|^2 \geq K^2 N^2 \tag{13}$$

*where equality holds in (13) if and only if*

$$\sum_{k=1}^{K} g_k(m) = 0 \text{ for all } m \in \mathcal{M}^*. \tag{14}$$

Since the left side of (13) includes $K$ in-phase autocorrelations with total value $KN^2$, the Welch bounds on the RMS correlation are as follows:

$$g_{\text{rms}} \geq \sqrt{N \frac{NK - N}{MK - 1}} \tag{15}$$

while the more familiar form is

$$g_{\max} \geq \sqrt{N \frac{NK - N}{MK - 1}}. \tag{16}$$

The bounds for the polyphase correlations (including periodic and odd correlations) are slightly larger than the right side of (4) but are nonetheless still slightly smaller than $\sqrt{N}$. The bounds for aperiodic correlation are slightly smaller than $\sqrt{N/2}$ since $M = 2N - 1$ in this case.

Welch obtained the bounds (15) and (16) for the periodic and aperiodic correlation functions as a direct consequence of the inner product bound (3). Thus, in [33], it was shown that for periodic and aperiodic correlations functions,

$$\sum_{k=1}^{K}\sum_{l=1}^{K}\sum_{m\in\mathcal{M}}|g_{k,l}(m)|^{2s} \geq \frac{K^2N^{2s}M}{\binom{M+s-1}{s}}. \tag{17}$$

Mow [15] has shown that a straightforward modification of Welch's argument proves (17) for odd correlation functions as well, and a further simple modification shows that (17) holds for polyphase correlations as well.

### 3.3 Complementary Signal Sets

Sets of signals satisfying the relation

$$\sum_{k=1}^{K} C_k(m) = 0 \text{ for all } m \neq 0 \tag{18}$$

are called complementary signal sets [5], [22], [30].

**Proposition 17.** *The aperiodic and polyphase correlation functions (which include the periodic and odd correlation functions as special cases) for a complementary signal set satisfy*

$$\sum_{k=1}^{K}\sum_{l=1}^{K}\sum_{m}|g_{k,l}(m)|^2 = K^2N^2$$

*and thus meet the Welch bound (15) on RMS correlation with equality.*

Various designs for complementary signal sets are given in [5], [22], and [30]. However, in hindsight, it seems that it is really very easy to construct a complementary signal set. The author did not find an explicit reference to cite for the following construction, but its elementary nature suggests that it has undoubtedly been noted by several researchers already.

**Proposition 18.** *Every WBE signal set is a complementary signal set.*

Proposition 18 and the results of Section II imply that a surprisingly large number of signal sets are actually complementary signal sets. For example, almost all "interesting" codes and their cosets are complementary signal sets. As a special case, it was noted in [22] that irreducible cyclic codes and their cosets are complementary signal sets, and in particular, the expurgated set of Gold sequences of Proposition 12 is a complementary signal set.

## 4 WBE Signal Sets in Asynchronous CDMA Systems

### 4.1 The Signal-to-Noise Ratio Parameters

The signal-to-noise ratio (SNR) for asynchronous binary CDMA communication systems was defined by Pursley [17] and has been the subject of considerable study since. Let

$$\mu_{k,i}(n) = \sum_{l=1-N}^{N-1} C_{k,i}(l)[C_{k,i}(l+n)]^* = \sum_{l=1-N}^{N-1} C_k(l)[C_i(l+n)]^* \qquad (19)$$

where the second equality follows from a generalization of (11) (see, e.g. Eq. (5.24) in [24].) In [17] it is shown that the variance of the multiple-access interference in a receiver that is synchronized to the $i$-th signal is proportional to the *SNR parameter*

$$r_i = \sum_{k \neq i} 2\mu_{k,i}(0) + \mathrm{Re}[\mu_{k,i}(1)] \approx R_i = \sum_{k \neq i} 2\mu_{k,i}(0).$$

Now suppose that the set of signature sequences is a WBE signal set or, more generally, a complementary signal set. Then, from (18), (19), and the property $C_i(-l) = [C_i(l)]^*$ of the aperiodic autocorrelation function, it follows that

$$r_i = 2(K-1)N^2 - 4\sum_{l=1}^{N-1} |C_i(l)|^2 + 2(K-2)N\mathrm{Re}[C_i(1)] - 2\mathrm{Re}\left(\sum_{l=1}^{N-2} C_i(l)[C_i(l+1)]^*\right) \qquad (20)$$

and thus

$$R_i = 2(K-1)N^2 - 4\sum_{l=1}^{N-1} |C_i(l)|^2. \qquad (21)$$

The sum $\sum_l |C_i(l)|^2$ in (21) is called the sidelobe energy of the signal $x^{(i)}$ and is nonzero (except for TDMA signal sets). Hence, $R_i < 2(K-1)N^2$ (and generally, $r_i < 2(K-1)N^2$ also) for all interesting WBE signal sets. Consider instead a CDMA communication system in which the $K$ signature sequences are chosen via random sampling (with replacement) from the $(N, N)$ code as in Section II.J. Then, both $R_i$ and $r_i$ have expected value $2(K-1)N^2$. Thus, since each $R_i$ is smaller than $2(K-1)N^2$ for WBE signal sets, these signal sets appear to be somewhat better than random sequences with respect to this measure of performance. Another curious aspect of (21) is that the *larger* the sidelobe energy, the smaller the variance of the multiple-access interference. Signals with *small* sidelobe energy are usually preferred as signature sequences in CDMA communication systems on the grounds that such signals perform better over multipath

channels and are easy to acquire. Hence, considerable effort has been expended in the past on searches for signals with small sidelobe energy. Paradoxically, Eq. (21) implies that from the point of view of multiple-access interference, it would have been better if the searches had tried to find signals with the largest sidelobe energy instead of the smallest!

In most instances, $R_i$ or $r_i$ must be determined via numerical evaluation of the autocorrelation function values needed in (20) or (21). It has already been shown that $R_i < 2(K-1)N^2$ for complementary signal sets, but it is not obvious without computation whether $r_i < 2(K-1)N^2$ also. In some cases, however, it is possible to state more specific results.

- The complementary pairs of binary sequences described by Taki *et al.* [29] have the property that $C_{k,i}(l) = 0$ for all even values of $l$. It follows from (19) that $r_i = R_i < 2(K-1)N^2$ for any collection of such complementary pairs of sequences.
- If the sequence $\boldsymbol{x}^{(i)}$ alternately takes on real and imaginary values, then $C_i(l)$ is real for even values of $l$ and imaginary for odd values of $l$. It follows that $\mathrm{Re}[C_i(l)C_i^*(l+1)] = 0$ and hence $r_i = R_i < 2(K-1)N^2$. Of course, the signal set must be a WBE signal set (or complementary signal set) for this to hold, but this requirement is easily satisfied. If alternate columns of the signal matrix of a real-valued WBE signal set $\mathcal{X}$ are multiplied by $\pm j$, then, according to Proposition 3, the resulting signal set $\hat{\mathcal{X}}$ is also a WBE signal set. In particular, if $\mathcal{X}$ is a *binary* WBE signal set, then $\hat{\mathcal{X}}$ is a WBE signal set over the quaternary alphabet $\{+1, -1, +j, -j\}$. Such quaternary signals are a special case of the EOE sequences described by Fukumasa, Kohno, and Imai [4] and can also be thought of as being derived from binary sequences via the elementary Method B of [9].

### 4.2 SNR Parameters for Some Cyclic WBE Signal Sets

Many of the constructions of WBE signal sets of length $N$ in Section II are based on cyclic codes of length $N$. The signature sequences used in CDMA applications are often required to have full period $N$, and WBE signal sets of this type are considered in the next result.

**Proposition 19.** *If a WBE signal set $\mathcal{X}$ is either a coset or a union of cosets of a linear cyclic code $\mathcal{C}$ all of whose nonzero codewords have period $N$, then,*

$$\sum_{i=1}^{K} |C_i(l)|^2 = K(N-l), \quad 1 \le l \le N-1, \tag{22}$$

$$\bar{R}(\mathcal{X}) = \frac{1}{K}\sum_{i=1}^{K} R_i = 2(K-1)N^2 - 2N^2 + 2N, \tag{23}$$

$$\textit{and} \quad \bar{r}(\mathcal{X}) = \frac{1}{K}\sum_{i=1}^{K} r_i \le 2(K-1)N^2 - N^2 - N + 2. \tag{24}$$

### 4.3 Optimal Shifts of WBE Signal Sets

Since $\bar{R}(\mathcal{X}) = 2(K-1)N^2 - 2N^2 + 2N$ for a cyclic WBE signal satisfying the hypotheses of Proposition 19, at least one signal has $R_i$ no larger than this. However, other $R_k$ may be somewhat larger though (21) guarantees that each is smaller than $2(K-1)N^2$. Now, $T^m\mathcal{X}$, the $m$-th left cyclic shift of $\mathcal{X}$, is also a WBE signal set satisfying the hypotheses of Proposition 19. But $R_i^{(m)}$, the SNR parameter for $T^m x^{(i)}$, need not be the same as $R_i^{(0)} = R_i$ [18], [19], [24]. Thus, for any given $i$, one can search for the shift $m$ that minimizes $R_i^{(m)}$. Unfortunately, since $\bar{R}(T^m\mathcal{X}) = \bar{R}(\mathcal{X})$ is fixed, a decrease in the SNR parameter for one signal is always accompanied by an increase in the SNR parameter for other signals. Thus, a better solution might be to search for that $m$ which minimizes $\max_{1\le i\le K} R_i^{(m)}$.

Since $\bar{r}(\mathcal{X}) \le 2(K-1)N^2 - N^2 - N + 2$ for the class of WBE signal sets satisfying the hypotheses of Proposition 19, at least one $r_i$ is as small as this. In fact, since this bound is quite loose, one can hope to find that at least one $r_i$ is as small as $\bar{R}(\mathcal{X}) = 2(K-1)N^2 - 2N^2 + 2N$. It sometimes happens that all the $r_i$ are smaller than $2(K-1)N^2$, but, in contrast to the situation for $R_i$, there is no guarantee that this will always happen. As in the previous paragraph, for any given $i$, one can choose an $m$ that minimizes $r_i^{(m)}$. Unlike the situation with $\bar{R}$, however, $\bar{r}(T^m\mathcal{X}) \ne \bar{r}(\mathcal{X})$ in general, so that it is possible to choose $m$ to minimize $\bar{r}(T^m\mathcal{X})$ and obtain the best average performance, or to minimize $\max_{1\le i\le K} r_i^{(m)}$ so as to obtain the best worst-case performance.

Thus, given a WBE signal set $\mathcal{X}$ satisfying the hypotheses of Proposition 19, one can choose a cyclically shifted set $T^m\mathcal{X}$ to minimize various SNR parameters. The performance improvement is not very large, but is often large enough to make the computational effort worthwhile. It is also worth keeping in mind that the kinds of searches discussed here shift all the signals in $\mathcal{X}$ by the same $m$. If the shifts applied to the signals are not the same, the resulting signal set is no longer a WBE signal set, and the above results may no longer apply. Nonetheless, it is possible that SNR parameters might be reducible to the same level as those of a WBE signal set or even further. Indeed, even for nonWBE signal sets, it is usually possible to reduce the SNR parameters below $2(K-1)N^2$ but the computational effort in searching over $K^N$ shifts is formidable, and only restricted searches are generally feasible. The advantage of beginning with a WBE signal set is that some measure of goodness of performance is guaranteed by the results described above *without* any search, and the results can be improved somewhat by a much narrower search.

### 4.4 Subsets of WBE Signal Sets

WBE signal sets have too many signals to be of use in practical CDMA systems since the number of simultaneous transmissions that can be supported is generally much smaller than the signature sequence length $N$. On the other hand, the results proved above require the cancellations described in (18) and these hold only when the entire set is used. Since subsets of WBE signal sets are generally

This result was proved earlier for cosets of irreducible binary cyclic codes. Recently, it has been proved for a class of quaternary sequences.

**Corollary 19.1.** *(Sarwate [23]): Proposition 19 holds for any coset of an irreducible binary cyclic code. In particular, it holds for the coset which forms the expurgated set of Gold sequences described in Proposition 12.*

**Corollary 19.2.** *(Sun and Leib [28]): Proposition 19 holds for $\mathcal{A}^-$, an expurgated quadriphase signal set obtained from the Family $\mathcal{A}$ described by Boztaş, Hammons and Kumar [3].*

Family $\mathcal{A}$ is a *quaternary* supercode of a *binary* $m$-sequence code, and the signal set $\mathcal{A}^-$, which consists of one nonbinary signal from each nonbinary cyclic equivalence class of $\mathcal{A}$, is a quaternary coset of the binary $m$-sequence code. As an example of this, note that Table II of [3] lists the 9 nonzero cycle representatives in a Family $\mathcal{A}$ of period 7, of which the first is the binary $m$-sequence $v = 2002022$ and the second a quaternary sequence $u = 3221211$. Adding the cyclic shifts of the first sequence to the second produces (cyclic shifts of) the rest of the sequences in the Table. In other words, if different cycle representatives are chosen, the signals in Table II of [3] can be expressed as the set $\{v, u, u+v, u+Tv, \ldots, u+T^6v\}$ while the signal set $\mathcal{A}^-$ is $\{u, u+v, u+Tv, \ldots, u+T^6v\}$. Thus, $\mathcal{A}^-$ is a quaternary coset of the binary $m$-sequence code $\{0, v, Tv, \ldots, T^6v\}$, and the expurgation is remarkably similar to that used to obtain the expurgated set of Gold sequences.

Sun and Leib [28] have also asserted with respect to $\mathcal{A}^-$ that

> "... it is remarkable that the average user interference of this family at optimal phases outperforms the ideal random sequences."

Actually, according to Proposition 19, a very large class of signal sets enjoys this property, and the fact that (24) holds for $\mathcal{A}^-$ is not remarkable at all. Indeed, the property is a result of the underlying cyclic structure and does not depend at all on the coset representative – an *arbitrary* choice of quaternary sequence $u$ in the above would have worked just as well! Nor is it necessary to find optimal phases for the family – any choice of phase of the quaternary sequence $u$ gives the same result. What is actually remarkable is that Proposition 19 can be used to construct a signal set for which *all* the SNR parameters $r_i$ are smaller than $2(K-1)N^2$. The construction is as follows. Choose alternate symbols of the coset representative from the subsets $\{0,2\}$ and $\{1,3\}$ of $Z_4$ respectively. Then the signals are alternately real-valued and imaginary-valued as described in the previous subsection. Hence, $\bar{r}(\mathcal{X}) = \bar{R}(\mathcal{X})$ equals the right side of (23). Furthermore, each $r_i = R_i < 2(K-1)N^2$, which is a better result than can be guaranteed via Proposition 19 for $\mathcal{A}^-$. However, such a signal set is not necessarily a good choice for CDMA applications. The two corollaries above are of importance because the signal sets are interesting because of their *maximum* correlation properties – the good SNR parameter properties are just an added attraction. The SNR parameter properties by themselves do not provide guidance in signal selection. Note, for example, that Proposition 19 also holds for a multiset formed by the union of a coset with itself, but the resulting signal set is of no interest for CDMA applications.

# Combined Decision-Feedback Multiuser Detection/Soft-Decision Decoding for CDMA Channels

Abdulrauf Hafeez and Wayne E. Stark*
Dept. of Elect. Engineering and Computer Science
University of Michigan, Ann Arbor, MI-48109

*Abstract*–This paper evaluates the performance of decision-feedback multiuser detectors with coding for CDMA channels. A combined multiuser detection/soft-decision decoding scheme is proposed which allows total control over the reliability of decision-feedback mechanism. Its performance is compared to that of conventional detection and linear-decorrelation detection with soft-decision decoding. Simulation and analysis is undertaken for synchronous CDMA channels. It is found that the scheme works very well especially for weak users and when multiuser interference is large. However, strong users do not gain much with this scheme over a linear-decorrelation detector.

## 1 Introduction

Conventional detection for a direct sequence code-division multiple-access (DS-CDMA) system employs a bank of matched filters, matched to the signature waveforms of individual users, followed by decision devices. This scheme suffers from severe degradation if the signal strength of some interfering users is dominant. The linear-decorrelation detector (LDD) does a multidimensional linear filtering operation on the matched filter outputs, which completely decorrelates the signal component of each user with those of the interferering users. This detector performs significantly better than the conventional detector. However, since it employs channel inversion to get rid of MAI, it enhances noise. The maximum likelihood sequence detector minimizes the sequence error probability and has complexity that grows exponentially with the number of users, making it infeasible for implementation.

Several low-complexity, sub-optimum multiuser detectors have been proposed in recent years but most of the research done so far on multiuser detection has considered uncoded transmissions, with a few exceptions [1]. Error control coding, however is important in a noisy and interference limited environment to obtain satisfactory performance.

A family of single-stage decision-feedback multiuser detectors (DFMD) has been proposed for asynchronous CDMA channels in [2]. In these detectors, users make decisions in the order of decreasing signal strength. The MAI affecting a given symbol of a given user is classified as causal and anticausal depending on whether decisions for the symbols causing the interference are available or not. A DFMD eliminates anti-causal MAI using zero-forcing filtering and attempts to cancel causal MAI using decision feedback. It is shown in [2] that the improvement in performance with a DFMD is appreciable over the LDD, especially when MAI is large. The detectors have a nearly ideal near-far resistance. Another desirable feature of these detectors is that their serial structure allows combining multiuser detection with soft-decision decoding for maximum benefit. Note that many of the low-complexity detectors proposed in recent years can not easily be combined with true soft-decision decoding. Examples include the multistage detector proposed by Varanasi and Aazhang[3] which employs successive interference cancellation and the post-processing likelihood detector of Seshadri and Hoeher (see [1] for references).

In this paper we investigate the performance of single-stage DFMD with convolutional coding and soft-decision Viterbi decoding (SDD) over synchronous CDMA channels in additive white Gaussian noise (AWGN). Varying the depth of trellis truncation of the Viterbi decoder allows control over the reliability of decisions fed back. We compare the performance of combined DFMD/SDD with conventional and LDD with coding using simulation and analysis. Performance bounds are derived for a two-user coded synchronous case.

## 2 Combined DFMD/SDD: Model

Consider a coded asynchronous CDMA system with $K$ users. The baseband signal of the $k$th user is:

$$x^k(t) = \sum_{i=-\infty}^{\infty} c_i^k \sqrt{r w_k} s_k(t - iT)$$

where $c_i^k$ are antipodal channel symbols of duration $T$ obtained by encoding binary information symbols of energy $w_k$ with a rate $r$ code and then mapping into $\{+1, -1\}$. $s_k(t)$ is the normalized signature waveform of the $k$th user, $s_k(t) = 0$ for $t \notin [0, T]$. Using the $D$ transform, the input symbol stream of the $k$th user is written as

$$c^k(D) = \sum_{i=-\infty}^{\infty} c_i^k D^i.$$

The input symbol vector of $K$ users is given by

$$c(D) = (c^1(D), c^2(D), \ldots, c^K(D))^T.$$

*This research was supported by NSF under Grant NCR-9115969 and by the Army Research Office under contract number DAAH04-95-I-0246.

The receiver observes the sum of the transmitted signals in additive white Gaussian noise (AWGN).

$$r(t) = \sum_{k=1}^{K} x^k(t - \tau_k) + n(t)$$

where $\tau_k \in [0, T]$ is the relative delay between users and $n(t)$ is WGN with power spectral density $N_0/2$. The received signal is filtered by a bank of matched filters, each matched to the corresponding signature waveform. The sampled output of the matched filter $v(D)$, where $v(D) = (v^1(D), v^2(D), \ldots, v^K(D))^T$ is given by

$$v(D) = S(D)Wc(D) + z(D)$$

where $W = \text{diag}(\sqrt{rw_1}, \sqrt{rw_2}, \ldots, \sqrt{rw_K})$ and $S(D)$ is the channel spectrum

$$S(D) = R_{-1}D^{-1} + R_0 + R_1 D$$

where $R_i^{kl} = \int_{-\infty}^{\infty} s_k(t-\tau_k)s_l(t-\tau_l+iT)dt$. $z(D)$ is colored Gaussian noise with spectrum $S_z(D) = (N_0/2)S(D)$. $S(D)$ is real-symmetric and non-singular on the unit circle. It can be factored as

$$S(D) = F^T(D^{-1})F(D)$$

$F(D)$ and $F(D)^{-1}$ are both causal and stable matrix filters. $F(D)$ has the following form

$$F(D) = F_0 + F_1 D + F_2 D^2 + \cdots \qquad (1)$$

where $F_0$ is lower triangular (See [4] for references). Note that the definition of causality implied here defines the "*past*" for each component $k$ of a vector process at time $i$ as given by all components at times $i$-1,$i$-2,... and the components 1, 2,..., $k$-1 at time $i$, and the "*present*" as the component itself.

The single-stage decision-feedback multiuser detector proposed in [2] consists of an anticausal forward filter $G(D)$ as a zero-forcing filter that eliminates multiuser interference from "*future*" symbols and a strictly causal feedback filter $B(D)$ that attempts to cancel multiuser interference from "*past*" symbols. The optimum forward and feedback filters that would maximize the ideal signal-to-noise ratio (SNR) at the input to the decision devices are shown to be[2]

$$G(D) = (F^T(D^{-1}))^{-1} \ , \ B(D) = (F(D) - \text{diag}(F_o))W \qquad (2)$$

Note that $G(D)$ is the whitening filter for the process $v(D)$ and $y(D)$ is the resulting whitened process

$$y(D) = G(D)v(D) = F(D)Wc(D) + n(D)$$

where $n(D)$ is WGN.

The detector proposed in [2] orders the users in decreasing symbol energy. In the $i$-th sampling time, user 1 makes its decision first based on the corresponding output of the forward filter ($y_i^1$) and the decisions

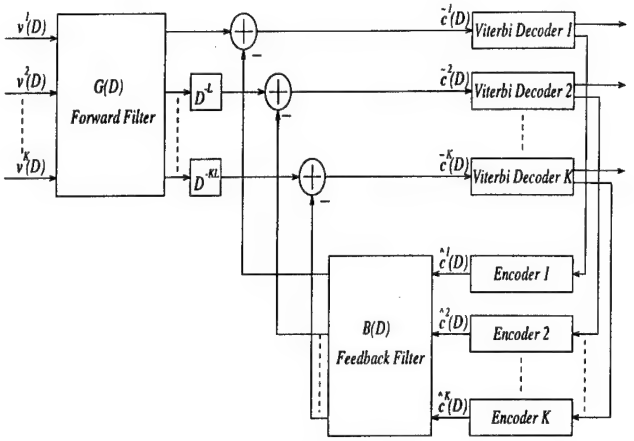


Figure 1: Combined Decision-Feedback Multiuser Detector/Soft-Decision Decoder ($L$=Truncation depth of the feedback device).

of all users made at sampling times $i$-1,$i$-2,.... User 2 makes its decision next based on $y_i^2$, the decision made by user 1 for the $i$-th sampling time and the past decisions of all users, and so on.

The multiuser receiver structure we propose is shown in Figure 1. The decision-feedback mechanism feeds back tentative decisions for convolutionally encoded symbols ($\hat{c}^k(D)$, $k = 1, 2, \ldots$) obtained from the trellis of corresponding decoders at depth $L$, where $L$ is less than or equal to the truncation depth of the Viterbi decoder. Since the decision of user 2 at the $i$-th sampling time depends on the decision of user 1 at the same sampling time, user 2's decoder runs at a lag of $L$ units behind the decoder of user 1, and so on for other decoders. Thus the total detection delay of a $K$ user system is $KL$.

## 3 Performance analysis

### 3.1 Bounds: two-user synchronous system

The input to the Viterbi decoders in Figure 1 is

$$\tilde{c}(D) = G(D)v(D) - B(D)\hat{c}(D).$$

Substituting $G(D)$ and $B(D)$ from (2), we get

$$\begin{aligned} \tilde{c}(D) &= \text{diag}(F_0)Wc(D) + n(D) \\ &\quad + (F(D) - \text{diag}(F_0))W(c(D) - \hat{c}(D)) \end{aligned} \qquad (3)$$

Note that $F(D) = F_0$ for a synchronous CDMA system. Thus $B(D)$ is lower-triangular with zero diagonal elements. For a two-user system, (3) simplifies to

$$\tilde{c}^1(D) = F_0^{11}\sqrt{rw_1}c^1(D) + n^1(D) \qquad (4)$$

$$\tilde{c}^2(D) = F_0^{22}\sqrt{rw_2}c^2(D) + n^2(D) + 2F_0^{12}\sqrt{rw_1}\Delta c^1(D) \qquad (5)$$

where $\Delta c^1(D) = \left(\frac{c^1(D) - \hat{c}^1(D)}{2}\right)$. Since user 1 sees WGN only, an upper bound on its bit error probability

can be found [5] by substituting $E_s = (F_0^{11})^2 r w_1$ in

$$P_{b_1} \leq Q\left(\sqrt{\frac{2d_f E_s}{N_0}}\right) \exp\left(\frac{d_f E_s}{N_0}\right) A(x)\Big|_{x=e^{-E_s/N_0}} \quad (6)$$

where $d_f$ is the free distance of the code and $A(x)$ is obtained as

$$A(x) = \frac{\partial}{\partial y} G(x,y,z)\Big|_{y=z=1}. \quad (7)$$

$G(x,y,z)$ is the transfer function of the code, given by

$$G(x,y,z) = \sum_i \sum_j \sum_k g_{ijk} x^i y^j z^k$$

where $g_{ijk}$ is the number of paths on the trellis of length $k$ with Hamming weight $i$, corresponding to information vectors of Hamming weight $j$, that diverge from the all-zero path at a node and remerge with it.

For user 2, we assume that the all-zero codeword is sent. We find the probability that a path having Hamming weight $d$ that diverges from the all-zero path at a node and then remerges with it, accumulates higher metric over the unmerged segment or equivalently the decision variable

$$\sum_{l=1}^{d} Z_l^2 = F_0^{22}\sqrt{rw_2}\,d + \sum_{l=1}^{d} n_l^2 + 2F_0^{12}\sqrt{rw_1}\sum_{l=1}^{d}\Delta c_l^1$$

is less than zero[1]. (Code symbol 0 is mapped to +1). $n_l^2, l = 1,2,\ldots$ are independent Gaussian random variables with mean 0 and variance $N_0/2$. We model $\Delta c_l^1, l = 1,2,\ldots$, decision errors of user 1 fed back to user 2, as i.i.d. random variables with distribution

$$\Delta c_l^1 = \begin{cases} +1 & \frac{1}{2}P_{c_1} \\ -1 & \frac{1}{2}P_{c_1} \\ 0 & 1 - P_{c_1} \end{cases}$$

where $P_{c_1}$ is the probability of code symbol error of user 1[2] derived in [6]. Since at the output of a Viterbi decoder, we usually get errors in bursts, $\Delta c_l^1$ are not independent. But we can assume independence if we assume an interleaver which randomizes all error bursts at the output of decoder 1 before feedback. However, for all practical purposes an interleaver is not required.

Using the above model, we get the pairwise error probability as

$$P_2(d) = \sum_{k_1=k_2=0, k_1+k_2\leq d}^{d} \binom{d}{k_1, k_2} \left(\frac{1}{2}P_{c_1}\right)^{k_1+k_2} (1-P_{c_1})^{d-k_1-k_2} Q\left(\frac{F_0^{22}\sqrt{2r\frac{w_2}{N_0}}\,d + 2F_0^{12}\sqrt{2r\frac{w_1}{N_0}}(k_1-k_2)}{\sqrt{d}}\right)$$

[1]Note that the superscripts in $Z_l^2$ and $n_l^2$ identify user 2.

[2]Note from Figure 1 that it's the code symbols that are fed back not the information symbols.

Thus,

$$P_{b_2} \leq \sum_{d=d_f}^{\infty} A_d P_2(d) \quad (8)$$

where $A_d$ is the coefficient of the term $x^d$ in the expansion of $A(x)$. We also obtain a relatively loose closed-form union bound for $P_{b_2}$ (see [6] for derivation)

$$P_{b_2} \leq \frac{1}{2}T(x)\Big|_{x=Z} \quad \text{for} \quad \frac{w_1}{N_0} \leq \frac{w_2}{N_0}\left(\frac{F_0^{22}}{2F_0^{12}}\right)^2 \quad (9)$$

where

$$Z = \exp\left(-\frac{(F_0^{22})^2 r w_2}{N_0}\right)\left[1 + 2P_{c_1}\sinh^2\left(\frac{F_0^{22}|F_0^{12}|\sqrt{w_1 w_2}}{N_0}\right)\right]. \quad (10)$$

Combining (8) and (9), we get a tight closed form upper bound, which we call a compound union bound

$$P_{b_2} \leq \frac{1}{2}T(x)\Big|_{x=Z} + \sum_{d=d_f}^{N+d_f-1} A_d\left[P_2(d) - \frac{1}{2}Z^d\right] \quad (11)$$

where $N$ is arbitrary.

### 3.2 DFMD, LDD and the conventional detector: multiuser synchronous system

We consider a system with $K$ equal energy users. For each detector, we find the first-order statistic for the $l$-th code symbol of the $k$-th user:

**DFMD** Assuming that $c_l^k = +1$ is sent, the statistic is given by

$$Z_l^k = F_0^{kk}\sqrt{rw} + n_l^k + 2\sqrt{rw}I_l^k$$

where $F_0^{kk} \leq 1\ \forall\ k$ *and* $I_l^k = \sum_{m=1}^{k-1} F_0^{mk}\Delta c_l^m$. $I_l^k$ is the residual multiuser interference that affects the $l$-th symbol of the $k$-th user and comes from the decision errors of the lower-indexed interfering users.

We model $\Delta c_l^m, m = 1,2,\ldots,k-1$ as i.i.d. random variables with distribution

$$\Delta c_l^m = \begin{cases} +1 & \frac{1}{2}P_{c_1} \\ -1 & \frac{1}{2}P_{c_1} \\ 0 & 1 - P_{c_1} \end{cases}$$

where $P_{c_1}$ is the probability of code symbol error of user 1. We note that if a decision-error in the $l$-th symbol of user $i$ forces user $j$ $(j \geq i)$ to make an error when it is fed back in the absence of noise, $\Delta c_l^i$ and $\Delta c_l^j$ would have opposite signs. This means that the correlation among $\Delta c_l^m, m = 1,\ldots,k-1$ is such that they tend to cancel each other out when added. Thus our assumption about residual multiuser interference (that it is the sum of independent r.v.'s $\Delta c_l^m$) should be pessimistic.

Using this model for $\Delta c_l^m$, we approximate $I_k^l$ as a Gaussian random variable with mean zero and variance $P_{c_1} \sum_{m=1}^{k-1} (F_0^{mk})^2$. $I_l^k$ is independent of the noise component $n_l^k$ that affects user $k$. Letting $D_l^k = \sqrt{\frac{2}{N_0}} \frac{Z_l^k}{F_0^{kk}}$, we get

$$D_l^k = \sqrt{2r(w/N_0)} + N_k \qquad (12)$$

where $N_k$ is a Gaussian r.v. with mean 0 and variance

$$\mathrm{Var}(N_k) = \frac{1}{(F_0^{kk})^2} \left[ 1 + 8r \frac{w}{N_0} P_{c_1} \sum_{m=1}^{k-1} (F_0^{mk})^2 \right]. \qquad (13)$$

**LDD** The first-order statistic for LDD, normallized by $\sqrt{\frac{2}{N_0}}$ is given by (12) where $N_k$ has variance

$$\mathrm{Var}(N_k) = \frac{1}{(H^{kk})^2} = \int_0^1 [S(e^{j2\pi f})^{-1}]^{kk} df \geq 1 . \qquad (14)$$

In the synchronous case, if all users have equal cross-correlations, then $H^{kk} = ((F_0)_{k \times k})^{11} \ \forall \ k$.

**The Conventional Detector** The matched filter output for the $l$-th symbol of the $k$-th user given that a +1 is sent can be normallized by $\sqrt{\frac{2}{N_0}}$ to get (12) where $N_k$ has variance

$$\mathrm{Var}(N_k) = \left[ 1 + 2r \frac{w}{N_0} \sum_{m=1, m \neq k}^{K} (R_0^{mk})^2 \right]. \qquad (15)$$

## 4 Simulation Results & Analysis

We simulated a two-user synchronous CDMA system with rate $\frac{1}{2}$, memory 4, convolutional encoding and Viterbi decoding with 8-level quantization. We employed length 31 spreading sequences for the coded system and length 63 spreading sequences for the uncoded system. Note that for a synchronous two-user system, decision-feedback multiuser detection involves zero-forcing detection for user 1 and complete decision-feedback interference cancellation for user 2. Thus for user 1, DFMD is the same as LDD. Bit-error probability of user 2 with DFMD is compared to that with conventional and LDD in Fig. 2. Truncation depths $L$—4,8,16 and 32 are used for the feedback mechanism in the coded system. With all truncation depths decision-feedback detection outperforms linear-decorrelation for the normal operating range of the system (SNR1$\geq$SNR2). When multiuser interference is large (SNR1$\gg$SNR2), $L = 4$ is as good as $L = 32$, and both achieve the single-user bound. This happens because the tentative decisions of user 1 are reliable even when obtained from the trellis at small depth, owing to the high SNR of the interfering user. Figure 2 shows how the near-far resistance of DFMD with coding depends on $L$. For the code used, the minimum truncation depth ($L_{min}$) which does not result in appreciable performance loss due to truncation is known to be 15. It can be seen

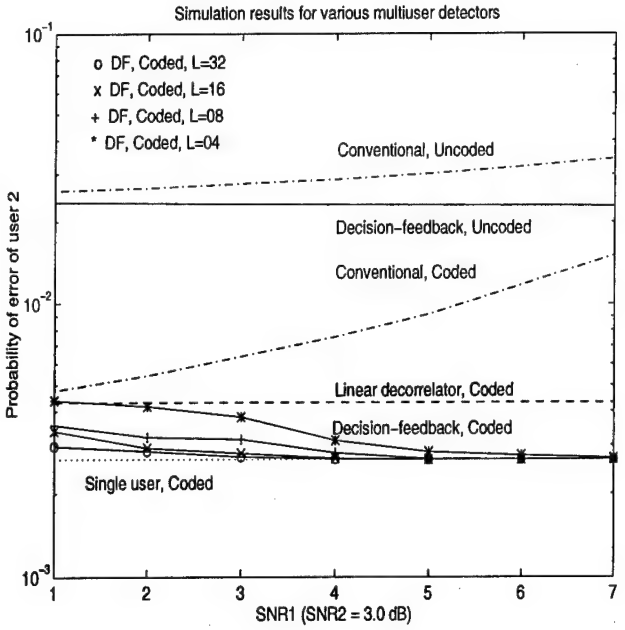


Figure 2: Simulation Results.

that for $L \geq L_{min}$, the effect on the near-far resistance of the detector is negligible. Thus if variable detection delay is allowable, weak users can virtually achieve single-user performance at all interference conditions by adjusting $L$ according to the levels of multiuser interference.

Performance bounds are shown in Fig. 3. By combining the loose union bound of (9) with an arbitrary number of exact union bound terms, we get a tighter upper bound. For finite truncation $L$, the bounds diverge for SNR1<4.0 dB.

In Table 1, we compare the variance of the first-order statistic for the various detectors as given by (13), (14) and (15). The system considered is a coded, synchronous CDMA system with $K$ equal energy users. The computations are done assuming that all users employ length 63 Gold sequences that have equal cross-correlations. $P_{c_1}$ is determined assuming rate $\frac{1}{2}$, memory 4, convolutional coding. For the conventional detector, this corresponds to a strictly power-controlled system. However, the variance of the first-order statistic for this detector blows up with the number of users. The gain obtained by LDD over the conventional detector goes from 1.2 dB when $K = 4$, to 5.3 dB when $K = 20$. The performance of users with decision-feedback detection improves with their order. For user 1, the variance of the statistic is the same as that with LDD because its detection strategy is the same with both detectors. For the $K$-th user, the variance of the statistic is the lowest because the detector attempts to cancel multiuser interference from all interfering users and does not employ any zero-forcing. The highest order user gains 0.65 dB over linear-decorrelator in a 4-user system. We observe that when the number of

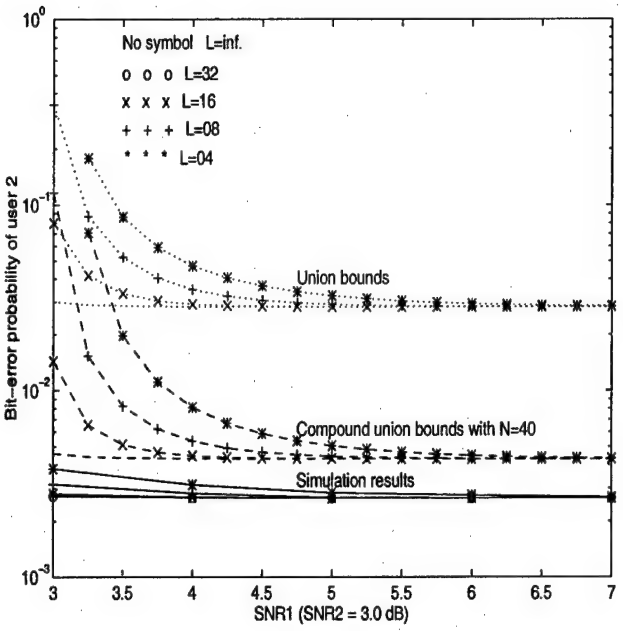


Figure 3: Performance bounds for combined DFMD/SDD (SNR2 = 3.0 dB).

| User order | Conventional | LDD | DFMD |
|---|---|---|---|
| Four equal energy users: | | | |
| 1 | 1.555 | 1.166 | 1.166 |
| 2 | 1.555 | 1.166 | 1.131 |
| 3 | 1.555 | 1.166 | 1.079 |
| 4 | 1.555 | 1.166 | 1.002 |
| Twenty equal energy users: | | | |
| 1 | 4.476 | 1.308 | 1.308 |
| 2 | 4.476 | 1.308 | 1.305 |
| 3 | 4.476 | 1.308 | 1.301 |
| 4 | 4.476 | 1.308 | 1.297 |
| 5 | 4.476 | 1.308 | 1.293 |
| 6 | 4.476 | 1.308 | 1.288 |
| 7 | 4.476 | 1.308 | 1.283 |
| 8 | 4.476 | 1.308 | 1.277 |
| 9 | 4.476 | 1.308 | 1.271 |
| 10 | 4.476 | 1.308 | 1.264 |
| 11 | 4.476 | 1.308 | 1.257 |
| 12 | 4.476 | 1.308 | 1.249 |
| 13 | 4.476 | 1.308 | 1.240 |
| 14 | 4.476 | 1.308 | 1.229 |
| 15 | 4.476 | 1.308 | 1.214 |
| 16 | 4.476 | 1.308 | 1.194 |
| 17 | 4.476 | 1.308 | 1.170 |
| 18 | 4.476 | 1.308 | 1.142 |
| 19 | 4.476 | 1.308 | 1.108 |
| 20 | 4.476 | 1.308 | 1.044 |

Table 1: Variance of first-order statistic for various multiuser detectors ($N_o = 1$).

users is large, a fraction of low-order users do not gain much with decision-feedback detection over complete linear-decorrelation (See Table 1). Thus it may be practical to employ complete linear-decorrelation for the first few lowest-order users and decision-feedback detection for the rest of them, thereby reducing overall detection delay.

## 5 Conclusions

Combined decision-feedback multiuser detection and soft-decision Viterbi decoding is proposed for asynchronous CDMA channels with convolutional coding. Simulation and analytical results are obtained for the synchronous case. However, they also provide valuable insight into the more general asynchronous case. The scheme combines all the benefits of decision-feedback interference cancellation with the gains of soft-decision decoding. It allows us flexibility to control the reliability of decisions fed back and we get a tradeoff between overall delay of the receiver and performance at medium or low levels of interference. At high levels of multiuser interference, weak users can achieve the single user bound even with low truncation lengths of the feedback mechanism because the decisions made by the stronger interferers are reliable. If variable detection delay is allowable, then weak users can be made to approach single-user bound for all levels of interference. The zero-forcing forward filter limits the performance gain achievable by the strong users in a synchronous CDMA system.

## References

[1] P. Hoeher, "On Channel Coding and Multiuser Detection for DS-CDMA", ITG-Fachberichte. Berlin: VDE-Verlag, No. 124, pp. 55–66, 1994.

[2] A. Duel-Hallen, "A Family of Multiuser Decision-Feedback Detectors for Asynchronous Code-Division Multiple-Access Channels", IEEE Trans. Comm. , Vol. 43, No. 2/3/4, pp. 421-434, Feb. /March/April 1995.

[3] M. K. Varanasi and B. Aazhang, "Multistage Detection in Asynchronous Code-Division Multiple-Access Communications", IEEE Trans. Comm. , Vol. 38, No. 4, April 1990.

[4] A. Duel-Hallen, "Equalizers for Multiple Input/ Multiple Output Channels and PAM Systems with Cyclostationary Input Sequences", IEEE Journal Selected Areas in Comm. , Vol. 10, No. 3, pp. 630-639, April 1992.

[5] A. J. Viterbi, "Principles of Digital Communication and Coding", "McGraw-Hill", 1979.

[6] To be submitted to IEEE Transactions on Communications.

# Soft-Output Multiuser Estimation for Asynchronous CDMA Channels

Abdulrauf Hafeez[1] and Wayne E. Stark
Dept. of Elect. Engineering and Computer Science
University of Michigan, Ann Arbor, MI 48109-2122.

**Abstract**: In this paper, we consider several multiuser demodulation schemes for a direct-sequence code-division multiple access (DS-CDMA) system that provide soft-outputs to enhance single-user soft-decision decoders. First, we derive an optimum soft-output multiuser estimation (OSOME) algorithm for asynchronous CDMA channels with white Gaussian noise (WGN). The algorithm generates *a posteriori probabilities* (APP) for coded bits given the received signal. This forward-recursive algorithm requires complexity and storage exponential in the number of users $K$ and linear in the decision lag $L$. Second, we outline a reduced-computation suboptimal version of this algorithm (SSOME) which compares favorably in complexity and storage with multiuser soft-output Viterbi algorithm (SOVA). Furthermore, we note that the Bayesian conditional decision feedback estimation (BCDFE) algorithm [3] provides symbol APP estimates that can be considerably improved upon by a slight modification. We derive the modified BCDFE algorithm for whitened multiuser channels. Finally, we present simulation results of a 4-user, convolutionally coded, asynchronous CDMA system. The results indicate that the SSOME algorithm with $L = K-1$ achieves a $0.4-0.5$ dB gain over SOVA with much greater lag (and complexity) and keeps within 0.25 dB of the OSOME algorithm. Moreover, the modified BCDFE algorithm provides a good performance/complexity tradeoff.

## 1 Introduction

Multiuser CDMA systems suffer from multiple-access interference (MAI), noise and other channel impairments. Two techniques are generally used to combat MAI. The first is multiuser demodulation for which there has been considerable research. The second technique is the combination of coding and interleaving. In order to make the most of error control coding, the demodulator must provide soft-inputs to the decoders in the form of likelihoods, symbol APP's, erasures, etc.. Unfortunately most multiuser detection algorithms ignore the possibility of generating this reliability information and concentrate instead on minimizing the demodulated error rate. In this paper, we attempt to derive multiuser algorithms that estimate code symbol APP's and can be effectively combined with error control coding and interleaving.

Recently considerable amount of work has been done in symbol-by-symbol detection techniques for channels with ISI ([1] and [3]). The optimum soft-output algorithm (OSA) of [1] can be applied to the multiuser case, but this requires noise whitening. Despite the strides made in the whitening technique [7], it requires sizable complexity and is not very suitable for long spreading sequences and time varying channels. Hayes et. al. derived an optimal symbol-by-symbol detection (OSSD) algorithm for ISI channels with correlated noise (after matched filtering) [2]. They and other authors, however, over-estimated the complexity of this algorithm. We derive an optimum soft-output multiuser estimation (OSOME) algorithm based on their scheme. The complexity of this algorithm is at par with the OSA but does not require noise whitening. The OSOME algorithm is an optimum demodulator for a coded multiuser CDMA system with ideal interleaving, in the sense that without exploiting any information about coding in the demodulation process, it supplies each individual decoder with as much information as possible about the sequence of modulator-input symbols for the corresponding user while suppressing the irrelevant information about other user's sequences. This is called user-separating demodulation in [8].

The recursion in the OSOME algorithm can be reduced to add-compare-select operations only. The resulting suboptimal version called SSOME has a recursion similar to the sub-optimum soft-output algorithm (SSA) of [1] but differs in the way symbol APP's are generated.

Bayesian Conditional Decision Feedback Estimation (BCDFE) proposed in [3] for ISI channels is a reduced-complexity symbol-by-symbol estimation scheme that employs an efficient method of trellis truncation. While the scheme is capable of providing good hard decisions on symbols, it fails to deliver good estimates of symbol APP's. Fortunately, this can be fixed by a simple modification. The modified BCDFE algorithm is considered for multiuser estimation. This algorithm requires noise whitening.

Simulation is undertaken to compare the performance of these algorithms with SOVA [4]. In addition, the complexity of these algorithms are compared.

[1]This work was supported in part by the Army Research Office under grant DAAH04-95-I-0246 and by Ericsson Inc.

**Corollary 12.2.** Any *coset of an* m*-sequence code or extended* m*-sequence code is an MWBE signal set.*

Also, as noted above, the *entire* Gold code is a WBE signal set. Constructions similar to the one in Proposition 12 can also be applied to various other classes of codes described in [24] to obtain WBE signal sets.

## 2.6 Binary Very Nearly MWBE Signal Sets

Cosets of the $m$-sequence codes and extended $m$-sequence codes are MWBE signal sets, but *supercodes* of these codes generally are not MWBE signal sets. In two interesting cases, however, certain supercodes of binary MWBE signal sets are *very nearly* MWBE signal sets in the sense that $I_{\max} = \sqrt{N}$ and equality very nearly holds in (5).

The extended small Kasami codes are $(2^{2n}, 3n)$ extended binary cyclic codes whose parity-check polynomials are of the form $M_\alpha(x)M_\gamma(x)$ where $\alpha \in GF(2^{2n})$ and $\gamma \in GF(2^n)$ are primitive elements and $\gamma = \alpha^{2^n+1}$ (cf. Chapter 8.7 of [13]). The inner products take on values $\pm 2^n = \pm\sqrt{N}$ and 0 only. Thus, equality *very nearly* holds in (5) for these WBE signal sets. One could even say that these *small Kasami signal sets* are asymptotically MWBE signal sets in the sense that the ratio of the maximum inner product magnitude to the right side of (5) approaches 1 as $N \to \infty$.

The $(2^{2n}, 4n)$ binary *nonlinear* Kerdock code (cf. Chapter 15 of [13]) is a union of cosets of the extended $m$-sequence code and is thus a WBE signal set. Unfortunately, the complement of each codeword is also a codeword, and the inner product of the signals corresponding to these two codewords is $-N$. The inner product of the signals corresponding to any two noncomplementary codewords takes on values $\pm 2^n = \pm\sqrt{N}$ and 0. It follows that the $(2^{2n}, 4n-1)$ subcode obtained by choosing either a codeword or its complement from the Kerdock code gives a signal set of size $N^2/2$ and length $N$ with $I_{\max} = 2^n = \sqrt{N}$ and these *Kerdock signal sets* are asymptotically MWBE signal sets. The Kerdock signal sets are also optimum in the sense of being the largest possible binary signal sets for which $I_{\max} = \sqrt{N}$. This was noted by Levenshtein [11] who showed that if $I_{\max} \leq \sqrt{N}$, then $K \leq N^2/2$ for binary signal sets. In contrast to the Kerdock signal sets, the extended Gold codes of the same length have $N^2$ signals and thus are twice the size. However, these codes have $I_{\max} = 2\sqrt{N}$ which is also twice as large. In fact, the $(2^{2n}, 5n)$ extended large Kasami codes give an even larger signal set with $N^{5/2}$ signals for which $I_{\max} = 2\sqrt{N}$ also [24].

The signal sets described above have lengths $2^{2n}$. The Kasami construction cannot be used for lengths $2^{2n+1}$, while the Kerdock codes of length $N = 2^{2n+1}$ are linear and have the same parameters as the extended Gold codes, viz. $K = N^2$ and $I_{\max} = \sqrt{2N}$. Of course, since $\sqrt{N} = 2^{(2n+1)/2}$ is not an integer, there are no nearly MWBE signal sets for these lengths. However, since Sidelnikov [26] has shown that for *binary* signal sets of size $N^2$, $I_{\max} > \sqrt{2N-2}$, the Kerdock and Gold code sets are optimal with respect to this bound [24].

## 2.7 WBE Signal Sets over Prime Power Alphabets

Many of the results stated above are also applicable to codes over prime-power fields $GF(p^s)$, but often do not produce any new classes of signal sets. This is because the results hold only when the elements of $GF(p^s)$ are mapped to the complex $p$-th roots of unity (and not to the $p^s$-th roots of unity) via $x \rightarrow \exp(j2\pi \mathrm{Tr}(x)/p)$ where $\mathrm{Tr}(\cdot)$ denotes the trace function from $GF(p^s)$ to $GF(p)$.

In practical applications, however, there is often the need to design signals over prime-power alphabets such as the quaternary alphabet $\{+1, j, -1, -j\}$. Unfortunately, codes over $GF(2^2)$, when used as described above, yield binary signals and not quaternary signals. One solution to this difficulty is to use codes over $\mathcal{Z}_4$ as described in Proposition 7. Codes over $\mathcal{Z}_4$ have attracted a great deal of research interest in recent years [6],[8], and many new results are available. A somewhat different solution is described below wherein signals over a $q$-ary alphabet are constructed from short codes over $GF(q)$. Interestingly, this construction allows the use of an *arbitrary* one-one mapping from $GF(q)$ to the complex $q$-th roots of unity.

**Proposition 13.** *Let $\mathcal{C}$ denote a linear $(N, k)$ code over the field $GF(q)$ with the property that no code symbol $C_m$ is a nonzero multiple of another code symbol $C_n$. Let $S(\mathcal{C})$ be a signal matrix obtained by mapping the codeword matrix $\hat{S}(\mathcal{C})$ to the complex $q$-th roots of unity via an* arbitrary *one-one mapping. Then $S(\mathcal{C})$ is a WBE signal set of size $K = q^k$ and length $N$.*

Thus, one can use codes over $GF(2^2)$ to construct WBE signal sets over the quaternary alphabet just as one can use codes over $\mathcal{Z}_4$. However, although both types of signal sets have the WBE property, codes over $\mathcal{Z}_4$ often can be designed to have smaller $I_{\max}$ than the codes over $GF(2^2)$. Finally, note that $N$ cannot exceed $(q^k - 1)/(q - 1)$ if this construction is used.

## 2.8 WBE Signal Sets of Arbitrary Size

WBE signal sets of obtained from codes are of size size $q^k$ (or $L \cdot q^k$) where $q^k \geq N$. It is thus of interest to consider whether a WBE signal set of size $K$ and length $N$ exists for *any* given $K \geq N > 1$. The answer is trivially Yes if one uses a $(N, 1)$ code over $\mathcal{Z}_K$. A more interesting construction is as follows.

**Proposition 14.** *Given any $N > 1$ and any $K = p_1^{k_1} p_2^{k_2} \ldots p_n^{k_n} \geq N$, there exists a WBE signal set of size $K$ and length $N$ over the complex $r$-th roots of unity where $r$ is a divisor of $p_1 p_2 \ldots p_n$.*

The idea here is to apply Proposition 5 to the $(p_i^{k_i}, k_i)$ extended cyclic codes to construct a WBE signal set of size $K$ and length $K$ and then shorten it in accordance with Proposition 4. Thus, given any $N > 1$, one can construct a WBE signal set of size $K$ and length $N$ for each $K \geq N$. Note, however, that since $K$ and $K + 1$ are relatively prime, the WBE signal sets of these sizes provided by Proposition 14 are over completely different alphabets. Of course, a

little thought about the condition for equality in Proposition 1 shows that it is not possible to augment *any* WBE signal set by just one signal and still retain the WBE property.

Just as it is not possible to add one signal to a WBE signal set and still retain the WBE property, it is not possible to delete one signal from a WBE signal set and still retain the WBE property. More generally, while there might exist subsets of WBE signal sets that are themselves WBE signal sets (for example, when a WBE signal set is the union of two WBE signal sets), *not all* subsets of a WBE signal set are WBE signal sets.

**Proposition 15.** *Let $\mathcal{X}$ denote a WBE signal set of size $K$ and length $N$. Then, for each $L < K$, at least one subset $\mathcal{Y} \subset \mathcal{X}$ of size $L$ is not a WBE signal set. However, if $\mathcal{Y}$ is a WBE signal set, then so is its complement $\mathcal{X} - \mathcal{Y}$.*

In fact, for at least one subset $\mathcal{Y}$,

$$I_{\rm rms}(\mathcal{Y}) \geq I_{\rm rms}(\mathcal{X}) = \sqrt{N\frac{K-N}{K-1}} > \sqrt{N\frac{L-N}{L-1}}$$

and thus this $\mathcal{Y}$ is not a WBE signal set. Indeed, for most values of $L$, *no* subset of size $L$ is a WBE signal set.

### 2.9 Random Signal Sets

The standard model for a randomly chosen signal set $\mathcal{X}$ over a $p$-ary alphabet is that the entries in the $K \times N$ signal matrix $M(\mathcal{X})$ are $KN$ independent identically distributed complex-valued discrete random variables uniformly distributed on the complex $p$-th roots of unity. It is easily verified that the signals have energy $N$ and that for $k \neq l$, $E[|\langle x^{(k)}, x^{(l)}\rangle|^2] = N$. Thus, for a randomly chosen signal set $\mathcal{X}$,

$$E\left[\sum_{k=1}^{K}\sum_{l=1}^{K}|\langle x^{(k)}, x^{(l)}\rangle|^2\right] = K(K-1)N + KN^2 > K^2N$$

so that the average randomly chosen set of signals is not a WBE signal set. Note that $E[(I_{\rm rms}(\mathcal{X}))^2] = N$ which is slightly larger than the minimum value $N(K-N)/(K-1)$ given by the Welch bound (4).

The standard model for randomly chosen signal sets is convenient because the independence of the symbols greatly simplifies system analyses. An equivalent model is that the $K$ signals are a *random sample with replacement* from the $(N, N)$ code over $GF(p)$ described in Corollary 7.4. Sampling with replacement allows for the possibility that the same signal might be chosen more than once and thus $I_{\rm rms}(\mathcal{X}) = \sqrt{N}$. On the other hand, a more appropriate model might be to construct $\mathcal{X}$ by random sampling *without replacement* so that all the signals in $\mathcal{X}$ are guaranteed to be distinct. Since the $(N, N)$ code is a WBE signal set, Proposition 15 shows that

$$E[(I_{\rm rms}(\mathcal{X}))^2] = N\frac{p^N - N}{p^N - 1} = (I_{\rm rms}(\mathcal{C}))^2 > N\frac{K-N}{K-1}$$

where $\mathcal{C}$ denotes the $(N, N)$ code. Although the average random subset $\mathcal{X}$ is not a WBE signal set under this interpretation either, it is worth noting that the RMS inner product magnitude for randomly chosen signals *is* smaller than $\sqrt{N}$ under this interpretation.

### 2.10 Information Theory and WBE Signal Sets

The most important point to keep in mind in the analysis of communication systems that use WBE signal sets is that the various properties of WBE signal sets do not always apply to subsets. In particular, subsets of WBE signal sets are not necessarily WBE signal sets. Consider then, the result in [14] that if a WBE signal set is used, then the mean-square interference in a correlation receiver for the $l$-th transmitted signal is the same for all values of $l$, that is,

$$\sum_{k \neq l} |\langle x^{(k)}, x^{(l)} \rangle|^2 = KN - N^2, \quad 1 \leq l \leq K. \tag{7}$$

Now suppose that only $L < K$ transmitters are active. Since some signals are no longer present at the receiver input, the mean-square interference in all the $L$ active receivers is reduced, and is smaller than $KN - N^2$. Thus, absence of some signals improves the performance of the rest. However, unless the active subset happens to be a WBE signal set also, the mean-square interference in all the receivers will not be *uniformly* reduced to $LN - N^2$. Indeed, it is easy to show that for all choices of $l$ and $L$, the *average* mean-square interference in the $l$-th receiver when $L-1$ *other* transmitters are active is $LN - N^2 + N(N-1)(K-L)/(K-1) > LN - N^2$, and thus for at least one choice of $L-1$ other transmitters, the mean-square interference in the $l$-th receiver is worse than that promised by the WBE signal theory. In short, one cannot simply replace $K$ with $L$ in (7) when only $L$ transmitters are active. The WBE property is quite fragile and does not hold for subsets or for variations from the stated conditions.

A fixed assignment of a WBE signal set to transmitters does not retain the WBE property when some transmitters are silent. Thus, suppose that $K$ transmitters use a WBE signal set and can simultaneously transmit at rate $R$ so that the *symmetric* rate vector $(R, R, \ldots, R)$ is achieved. If the first transmitter is silent, the rest can still transmit via their assigned signals from the WBE signal set at rate $R$ so that rate vector $(0, R, R, \ldots, R)$ can be achieved. In fact, since the interference is less, higher rates should be achievable, but without a detailed study of the WBE signal set, it is not clear what "symmetric" rate vector $(0, R', R', \ldots, , R')$ (where $R' > R$) can be achieved. Indeed, the entire rate region achievable by a fixed assignment of a WBE signal set (that is, the set of rate vectors $(R_1, R_2, \ldots, R_K)$ at which it is possible to transmit via use of the WBE signal set) seems difficult to compute without detailed knowledge of the structure of the WBE signal set. A variable assignment of signals to transmitters (depending on which transmitters have data to send at any given time) does not work either because there may not be a WBE signal set of the right size. For example, the size of a binary WBE signal set is either 2 or a multiple of 4 which is not helpful if exactly 13 transmitters wish to be active.

In studying the capacity region of multiple-access channels, one might wish to use different WBE signal sets to achieve different rate vectors. For any given $K \geq N$, Proposition 14 can be used to construct WBE signal sets of sizes $K, K-1, K-2, \ldots$. Thus, no matter which $L < K$ transmitters are active, one could assign a WBE signal set of size $L$ to the active transmitters, and each active receiver would uniformly suffer a mean-square multiple-access interference of $LN - N^2$. Unfortunately, these various signal sets are over different alphabets, so that the achievable rates are not directly comparable since they apply to different multiple-access channels. On the other hand, if the different alphabets are combined into a single alphabet, then this large alphabet has size $p_1 p_2 \ldots p_s$ where $p_1, p_2, \ldots, p_s$ are all the primes that do not exceed $K$. In the absence of multi-user interference and channel noise, any transmitter can send $\log_2 p_1 p_2 \ldots p_s$ bits per symbol over the channel, so the capacity is quite large. On the other hand, only a small subset of the alphabet is used by the WBE signal sets described above, so that the rate vectors that can be achieved by the use of WBE signal sets may well turn out to be a very small subset of the actual capacity region.

In summary, an insistence on always using a WBE signal set may be a hindrance rather than an advantage, and the simplifications in the analysis due to the uniform interference level might be insufficient to overcome the disadvantages. Subsets of WBE signal sets do not enjoy the WBE properties and results on WBE signal sets are not always applicable to the subsets.

## 3 Bounds on Correlation Functions

The bounds on inner products discussed in the previous section are of interest in studies of synchronous CDMA communication systems. Analyses of asynchronous CDMA communication systems lead to the consideration of various correlation functions of the signals (see, for example, [24]), and bounds on the magnitudes of these are studied in this section.

### 3.1 The Correlation Functions

As before, let $\mathcal{X}$ denote a set of $K$ signals of length $N$ and energy $N$, and let $S(\mathcal{X})$ denote the signal matrix. Now, however, it is not necessary to insist that $K \geq N$. For signals $x^{(k)}, x^{(l)} \in \mathcal{X}$, the *aperiodic* crosscorrelation function $C_{x^{(k)},x^{(l)}}(m)$ for $x^{(k)}$ and $x^{(l)}$ (more simply, $C_{k,l}(m)$) is defined as

$$C_{k,l}(m) = C_{x^{(k)},x^{(l)}}(m) = \begin{cases} \sum_{n=0}^{N-1-m} x_n^{(k)} (x_{n+m}^{(l)})^*, & 0 \leq m \leq N-1, \\ \sum_{n=0}^{N-1+m} x_{n-m}^{(k)} (x_n^{(l)})^*, & 1-N \leq m < 0, \\ 0, & |m| \geq N. \end{cases} \tag{8}$$

For $0 \leq m < N$, the *periodic* crosscorrelation function $\theta_{x^{(k)},x^{(l)}}(m) = \theta_{k,l}(m)$ and the *odd* crosscorrelation function $\hat{\theta}_{x^{(k)},x^{(l)}}(m) = \hat{\theta}_{k,l}(m)$ are given by

$$\theta_{k,l}(m) = C_{k,l}(m) + C_{k,l}(m-N) \text{ and } \hat{\theta}_{k,l}(m) = C_{k,l}(m) - C_{k,l}(m-N), \quad (9)$$

and have been studied extensively in the context of asynchronous CDMA systems using biphase modulation. Consideration of $Q$-ary modulation in CDMA systems leads to the study of the *polyphase* crosscorrelation function [4], [28] which is defined as

$$\theta_{k,l}^{(\gamma)}(m) = C_{k,l}(m) + \gamma C_{k,l}(m-N). \quad (10)$$

where $\gamma$ is a unit-magnitude complex number. Note also that $\theta_{k,l}^{(\gamma)}(0) = \langle x^{(k)}, x^{(l)} \rangle$ for all $\gamma$. If $k = l$, we get the autocorrelation functions which are usually denoted by $C_k(m)$, $\theta_k(m)$, $\hat{\theta}_k(m)$, and $\theta_k^{(\gamma)}(m)$ respectively. All the autocorrelation functions have the same value for zero offset: $\theta_k(0) = \hat{\theta}_k(0) = C_k(0) = \theta_k^{(\gamma)}(0) = \langle x^{(k)}, x^{(k)} \rangle = N$.

Many results in this section apply to all of the correlation functions described above. Let $g(\cdot)$ denote any of the correlation functions and let the index set $\mathcal{M}$ be defined as

$$\mathcal{M} = \begin{cases} \{m : 1-N \leq m \leq N-1\}, \text{ if } g(\cdot) = C(\cdot), \\ \{m : 0 \leq m \leq N-1\}, \qquad \text{if } g(\cdot) = \theta^{(\gamma)}(\cdot),\ \theta(\cdot),\ \hat{\theta}(\cdot). \end{cases}$$

Let $\mathcal{M}^* = \mathcal{M} - \{0\}$, and $M = |\mathcal{M}|$ denote the cardinality of $\mathcal{M}$. The maximum crosscorrelation value $g_{c,\max}(\mathcal{X})$ and maximum out-of-phase autocorrelation value $g_{a,\max}(\mathcal{X})$ are defined to be

$$g_{c,\max}(\mathcal{X}) = \max_{k \neq l} \max_{m \in \mathcal{M}} |g_{k,l}(m)| \quad \text{and} \quad g_{a,\max}(\mathcal{X}) = \max_{k} \max_{m \in \mathcal{M}^*} |g_k(m)|$$

The maximum correlation value is $g_{\max}(\mathcal{X}) = \max\{g_{c,\max}(\mathcal{X}), g_{a,\max}(\mathcal{X})\}$. The RMS correlation value is obtained by averaging all $K(K-1)M + K(M-1) = K(KM-1)$ correlation magnitudes and is thus

$$\begin{aligned} (g_{\text{rms}}(\mathcal{X}))^2 &= \frac{1}{K(KM-1)} \left[ \sum_{k=1}^{K} \sum_{l=1}^{K} \sum_{m \in \mathcal{M}} |g_{k,l}(m)|^2 - KN^2 \right] \\ &= \frac{1}{K(KM-1)} \left[ K(K-1)M(g_{c,\text{rms}}(\mathcal{X}))^2 + K(M-1)(g_{a,\text{rms}}(\mathcal{X}))^2 \right] \end{aligned}$$

where $g_{c,\text{rms}}(\mathcal{X})$ is the the RMS crosscorrelation value obtained by averaging over the $K(K-1)M$ crosscorrelation magnitudes, and $g_{a,\text{rms}}(\mathcal{X})$ is the RMS autocorrelation value obtained by averaging over the $K(M-1)$ out-of-phase autocorrelation magnitudes. Note also that $g_{c,\max} \geq g_{c,\text{rms}}$, $g_{a,\max} \geq g_{a,\text{rms}}$, and $g_{\max} \geq g_{\text{rms}}$.

Here, puncturing means deletion of symbols, that is, columns of the signal matrix, of the extended $m$-sequence code with $k$ information symbols. Next, consider cyclic codes of length $N$ and extended cyclic codes of length $N+1$. If the parity-check polynomial $h(z)$ is of period $N$, then the residues of $x^i$ mod $h(z)$, $0 \leq i \leq N-1$ are distinct, and hence each code symbol is a different linear function of the information symbols. Thus we have the following result.

**Proposition 11.** *Suppose that $N$ is not a multiple of $p$. Then,*

- *A cyclic code of length $N$ over $GF(p)$ is a WBE signal set if and only if its parity-check polynomial $h(z)$ has period $N$.*
- *An extended cyclic code of length $N+1$ over $GF(p)$ is a WBE signal set if and only if its parity-check polynomial $h(z)$ has period $N$.*

One way of ensuring that $h(z)$ has period $N$ is to require that $h(z)$ be divisible by an irreducible polynomial of period $N$.

**Corollary 11.1.** *If $N$ is not a multiple of $p$, then cyclic codes of length $N$ and extended cyclic codes of length $N+1$ over $GF(p)$ are WBE signal sets if the parity-check polynomial $h(z)$ is divisible by an irreducible polynomial of period $N$ over $GF(p)$.*

As an example, the binary Gold *codes* are $(2^n-1, 2n)$ cyclic codes with parity-check polynomials $M_\alpha(x)M_\beta(x)$ where $M_\alpha(x)$ and $M_\beta(x)$ denote the minimal polynomials of primitive elements $\alpha$, $\beta \in GF(2^n)$ and the $m$-sequences $u$ and $v$ generated by $M_\alpha(x)$ and $M_\beta(x)$ are a *preferred pair* of $m$-sequences [24]. The representatives of the cyclic equivalence classes of the codewords in this code can be expressed as $\{v, u, u+v, u+Tv, u+T^2v, \ldots, u+T^{N-1}v\}$ where $T$ is the left cyclic shift operator and $N = 2^n-1$, and constitute the well-known class of Gold *sequences* [24]. According to Corollary 11.1, Gold codes are WBE signal sets, as indeed are all supercodes of the $m$-sequence codes and the extended $m$-sequence codes. In fact, the extended $(2^n, 2n)$ Gold codes and Gold-like codes [24] are WBE signal sets of length $N = 2^n$ and size $N^2 = 2^{2n}$ for which $I_{\max} = 2^{\lfloor (n+2)/2 \rfloor}$ which equals $2\sqrt{N}$ or $\sqrt{2N}$ according as $n$ is even or odd.

### 2.5 Some Interesting Cosets of Cyclic Codes

Massey and Mittelholzer [14] noted that the Gold *sequence* set described above is very nearly a coset of an $m$-sequence code.

**Proposition 12.** *(Massey and Mittelholzer [14]): The expurgated set of Gold sequences $\{u, u+v, u+Tv, u+T^2v, \ldots, u+T^{N-1}v\}$ is a WBE signal set.*

In fact, from Proposition 9 and Corollary 7.2, it follows that

**Corollary 12.1.** *The expurgated set of Gold sequences is an MWBE signal set.*

Of course, as noted in [14], *any* coset of an $m$-sequence code is an WBE signal set. More strongly, it follows from Corollary 7.2 that

### 2.4 Cyclic and Extended Cyclic Codes

Let $h(z)$ denote an irreducible polynomial of degree $k$ and period $N$ over $GF(p)$. Then, the codewords of the $(N, k)$ cyclic code with parity-check polynomial $h(z)$ can be represented as

$$C^{(\zeta)} = (\mathrm{Tr}(\alpha^0 \cdot \zeta), \mathrm{Tr}(\alpha^1 \cdot \zeta), \mathrm{Tr}(\alpha^2 \cdot \zeta), \ldots, \mathrm{Tr}(\alpha^{N-1} \cdot \zeta)) \tag{6}$$

where $\alpha^{-1}$ is a root of $h(z)$. Since the code symbols are different linear functions, it follows from Corollary 7.1 that the code is a WBE signal set. Now suppose that this code is extended to include the zero function $\mathrm{Tr}(0 \cdot \zeta)$ as a code symbol. This extra symbol is, in fact, an "overall parity check" since

$$\sum_{i=0}^{N-1} \mathrm{Tr}(\alpha^i \cdot \zeta) = \mathrm{Tr}\left(\sum_{i=0}^{N-1} \alpha^i \cdot \zeta\right) = \mathrm{Tr}\left(\left(\sum_{i=0}^{N-1} \alpha^i\right) \cdot \zeta\right) = \mathrm{Tr}(0 \cdot \zeta).$$

Hence, this extended cyclic code is also a WBE signal set which proves

**Proposition 8.** *If $h(z)$ is an irreducible polynomial of degree $k$ and period $N$ over $GF(p)$, then the $(N, k)$ cyclic code, and the $(N+1, k)$ extended cyclic code, with parity-check polynomial $h(z)$ are WBE signal sets.*

When the parity-check polynomial $h(z)$ is a *primitive* polynomial of degree $k$, the cyclic $(p^k-1, k)$ code is called a maximal-length sequence code (henceforth $m$-sequence code), and the $(p^k, k)$ extended code is called an extended $m$-sequence code. Binary $m$-sequence codes and extended binary $m$-sequence codes are WBE signal sets [14]. In fact, these sets (and more generally, $p$-ary $m$-sequence codes and extended $m$-sequence codes) are MWBE signal sets. Note also that the signal matrices of extended binary $m$-sequence codes are $2^k \times 2^k$ Hadamard matrices.

**Proposition 9.** *If $h(z)$ is a primitive polynomial of degree $k$ over $GF(p)$, then*

- *m-sequence code: the $(p^k-1, k)$ cyclic code with parity-check polynomial $h(z)$ is a nonorthogonal MWBE signal set.*
- *Extended m-sequence code: The $(p^k, k)$ extended cyclic code with parity-check polynomial $h(z)$ is an orthogonal MWBE signal set.*

The signal matrix for the extended $m$-sequence code is a $p^k \times p^k$ orthogonal matrix whose entries are complex $p$-th roots of unity. In contrast, the discrete Fourier transform (FDMA) signal matrix for this length is a $p^k \times p^k$ matrix whose entries are complex $p^k$-th roots of unity.

The $m$-sequence codes and the extended $m$-sequence codes are well-known in the literature as simplex signal sets and orthogonal signal sets. They also form the basis for the following observations about WBE signal sets derived from linear codes.

**Proposition 10.** *An $(N, k)$ code is a WBE signal set if and only if it is equivalent under column permutation to a punctured extended m-sequence code with $k$ information symbols.*

Both these results are straightforward generalizations of the Massey and Mittelholzer [14] result that a linear binary code $\mathcal{C}$ is a WBE signal set if and only if its dual code has no codewords of Hamming weight 2. An equivalent result due to Assmus and Mattson is that linear binary codes satisfying the stated condition have mean-square Hamming weight $N(N+1)/4$ (cf. [34]).

The remainder of this section only considers codes over finite fields, but many of the results also apply to codes over $\mathcal{Z}_q$. For codes over $GF(p)$, it is convenient to think of the $k$ information symbols as an element $\zeta$ of the extension field $GF(p^k)$. Since any linear function from $GF(p^k)$ to $GF(p)$ is of the form $z \to \mathrm{Tr}(\alpha \cdot z)$ where $\mathrm{Tr}(z) = z + z^p + z^{p^2} + \ldots + z^{p^{k-1}}$ is the trace function from $GF(p^k)$ to $GF(p)$ and $\alpha \in GF(p^k)$ [13], a codeword in this linear code can be expressed as

$$C^{(\zeta)} = (\mathrm{Tr}(\alpha_1 \cdot \zeta), \mathrm{Tr}(\alpha_2 \cdot \zeta), \mathrm{Tr}(\alpha_3 \cdot \zeta), \ldots, \mathrm{Tr}(\alpha_N \cdot \zeta))$$

where $\alpha_1, \alpha_2, \ldots, \alpha_N$ are $N$ different elements of $GF(p^k)$. Note that at most one of the $\alpha_i$ can be 0.

It is convenient to simply call $\mathcal{C}$ a WBE signal set whenever $S(\mathcal{C})$ is a WBE signal set. A *coset* of $\mathcal{C}$ is $a + \mathcal{C} = \{a + c : c \in \mathcal{C}\}$ where $a$ is a vector of length $N$ over $GF(p)$. Then, $S(a+\mathcal{C}) = S(\mathcal{C})U$ where is a unitary matrix. From Proposition 3, it follows that if $\mathcal{C}$ is a WBE (MWBE) signal set, then so is $a+\mathcal{C}$. This is a minor generalization of a result noted in [14] for binary codes.

**Corollary 7.2.** *Cosets of codes*

- *If $\mathcal{C}$ is a WBE signal set, then any coset of $\mathcal{C}$ is a WBE signal set.*
- *If $\mathcal{C}$ is a MWBE signal set, then any coset of $\mathcal{C}$ is a MWBE signal set.*

From Proposition 2 it follows that

**Corollary 7.3.** *If $\mathcal{C}$ is a WBE signal set, then the union of any number of cosets of $\mathcal{C}$ is a WBE signal set.*

In fact, since the entire space $[GF(p)]^N$ is a union of cosets of $\mathcal{C}$, we have

**Corollary 7.4.** *The $(N, N)$ code over $GF(p)$ is a WBE signal set.*

Of course, this result is also immediate from Corollary 7.1 since each codeword symbol in this code is a different information symbol. Notice that $I_{\max} = N$ for this WBE signal set even though $I_{\mathrm{rms}} < \sqrt{N}$, thus showing once again that the WBE property does not guarantee small values of $I_{\max}$.

The only codes excluded by the hypotheses of Corollary 7.1 are those with repeated symbols (whether zero or nonzero). Codes with repeated symbols are usually of interest only for very noisy channels; generally, better performance is obtained if different parity check equations specify the various code symbols. Thus, colloquially, Corollary 7.1 says that almost all interesting codes are WBE signal sets. Some especially interesting codes are considered next.

**Proposition 6.** *There exists a binary WBE signal set of size $K$ if and only if $K$ equals 2 or is a multiple of 4.*

$K \times K$ Hadamard matrices provide binary MWBE signal sets of size $K$ and length $K$. However, even for those multiples of 4 for which the existence of a $K \times K$ Hadamard matrix has not been demonstrated, it is possible to construct a binary WBE signal set of size $K$ and length $N < K$.

More generally, linear codes are the source of large classes of WBE signal sets over small alphabets, and these are considered next.

### 2.3 WBE Signal Sets from Linear Codes

Let $\mathcal{C}$ denote a linear $(N, k)$ code over $GF(p)$, $p$ a prime, with the property that each code symbol $C_m$ is a different linear function of the $k$ information symbols. Since there are only $p^k$ different linear functions of $k$ variables, it must be that $p^k \geq N$. Let $\hat{S}(\mathcal{C})$ denote the $p^k \times N$ matrix whose rows are the $p^k$ codewords of $\mathcal{C}$. Since the code symbols are linear functions, then for any given column of $\hat{S}(\mathcal{C})$, either each element of $GF(p)$ occurs $p^{k-1}$ times in the column, or every entry in the column is zero. The latter occurs if and only if the corresponding code symbol is the zero function. Since different code symbols must be different functions, $\hat{S}(\mathcal{C})$ can have *at most one* all-zero column. For $m \neq n$, the code symbols $C_m$ and $C_n$ are different linear functions, and hence $C_m - C_n$ is a *nonzero* linear function of the information symbols. It follows that the difference of two columns of $\hat{S}(\mathcal{C})$ has the property that each field element occurs $p^{k-1}$ times in the difference.

In communications applications, codewords are mapped into complex-valued vectors by mapping $x \in GF(p)$ onto $\exp(j2\pi x/p)$. This mapping is used to convert $\hat{S}(\mathcal{C})$ into a signal matrix $S(\mathcal{C})$ whose elements are the complex $p$-th roots of unity. The inner product of two columns is

$$\langle y^{(m)}, y^{(n)} \rangle = \sum_{i=1}^{p^k} \exp(j2\pi(C_m^{(i)} - C_n^{(i)})/p) = p^{k-1} \sum_{l=0}^{p-1} \exp(j2\pi l/p) = 0$$

because $C_m^{(i)} - C_n^{(i)}$ takes on each value $0, 1, \ldots, p-1$ an equal number of times as $i$ varies from 1 to $p^k$, and the sum of the complex $p$-th roots of unity is 0.

All of the above also applies to linear codes over the integer ring $\mathcal{Z}_q$ with the minor modification that in some cases, $C_m^{(i)} - C_n^{(i)}$ may take on all values $0, 1, \ldots, r-1$ in a subring $\mathcal{Z}_r$ equally often. Hence, the following result holds:

**Proposition 7.** *(Helleseth and Kumar [8]): If $\mathcal{C}$ is a linear $(N, k)$ code over $\mathcal{Z}_q$ such that the code symbols $C_m$ are different linear functions of the information symbols, then $S(\mathcal{C})$ is a WBE signal set of size $K = q^k$ and length $N$.*

**Corollary 7.1.** *Proposition 7 holds for linear codes over $GF(p)$.*

**Proposition 4.** *Let $\mathcal{X}$ denote a WBE signal set of size $K$ and length $N$. If all the entries in a column of $S(\mathcal{X})$ are complex numbers of unit magnitude, then the set $\hat{\mathcal{X}}$ obtained by deleting this column of $S(\mathcal{X})$ is a WBE signal set of size $K$ and length $N-1$.*

Proposition 4 can be applied to the FDMA signal set but not to the TDMA signal set described above. Also, deletions of columns generally do not preserve the MWBE property.

Propositions 2 and 3 together allow the design of very large WBE signal sets with distinct signals (or WBE signal multisets if one so wishes.) For all of these, $I_{\text{rms}}$ *equals* the right side of (4) which is slightly smaller than $\sqrt{N}$. However, this does not mean that *all* the inner product magnitudes are smaller than $\sqrt{N}$. In fact, $I_{\max}$ can be considerably larger than $\sqrt{N}$. For example, $I_{\max} = N$ for the union of two TDMA (or FDMA) WBE signal sets. More generally, a result in [33] shows that $I_{\max}$ exceeds $\sqrt{N}$ for large signal sets, even though $I_{\text{rms}} < \sqrt{N}$ for a WBE signal set.

The union construction of Proposition 2 requires the WBE sets to be of the same length. It is also possible to combine WBE sets of different lengths via the Kronecker product construction to produce a larger WBE signal set with longer signals. Recall that if $A$ and $B$ are $K \times N$ and $\hat{K} \times \hat{N}$ matrices respectively, then their Kronecker (or tensor) product is the $K\hat{K} \times N\hat{N}$ matrix $A \otimes B$ given by

$$A \otimes B = \begin{bmatrix} a_{1,1}B & a_{1,2}B & \cdots & a_{1,N}B \\ a_{2,1}B & a_{2,2}B & \cdots & a_{2,N}B \\ \vdots & \vdots & \ddots & \vdots \\ a_{K,1}B & a_{K,2}B & \cdots & a_{K,N}B \end{bmatrix}.$$

WBE signal sets retain the WBE property when combined via the Kronecker product construction.

**Proposition 5.** *If $S(\mathcal{X})$ and $S(\hat{\mathcal{X}})$ are WBE signal sets of sizes $K$ and $\hat{K}$ respectively and lengths $N$ and $\hat{N}$ respectively, then $S(\mathcal{X}) \otimes S(\hat{\mathcal{X}})$ is a WBE signal set of size $K\hat{K}$ and length $N\hat{N}$.*

**Corollary 5.1.** *The Kronecker product of two MWBE signal sets is an MWBE signal set if and only if the constituent MWBE signal sets are orthogonal MWBE signal sets.*

## 2.2 WBE Signal Sets over Small Alphabets

The construction of WBE signal sets over small alphabets is of importance for practical applications. The essential results for binary signals are given in [14]. In this chapter, these results are re-stated and generalized to larger alphabets.

Consider first that the inner product of two signals of length $N$ over the binary alphabet $\{+1, -1\}$ equals $N - 2d$ where $d$ is the *Hamming distance* between the signals.

It follows from (1) and (3) that for a signal set of size $K$ and length $N$,

$$I_{\text{rms}} \geq \sqrt{N\frac{K-N}{K-1}} \tag{4}$$

which is a form of Welch's bound. Since $I_{\max} \geq I_{\text{rms}}$, the Welch bound [33] is usually stated as

$$I_{\max} = \max_{k \neq l} |\langle x^{(k)}, x^{(l)} \rangle| \geq \sqrt{N\frac{K-N}{K-1}}. \tag{5}$$

If equality holds in (1), then the signal set is said to meet the Welch bound (4) on $I_{\text{rms}}$ with equality, and is called a WBE signal set [14]. Similarly, signal sets which meet the Welch bound (5) on $I_{\max}$ with equality can be called MWBE signal sets. The inner product magnitudes of MWBE signal sets satisfy

$$|\langle x^{(k)}, x^{(l)} \rangle| = \sqrt{N\frac{K-N}{K-1}} \quad \text{for all } k \neq l.$$

Examples of MWBE signal sets are the $N \times N$ discrete Fourier transform matrix with $(k,l)$-th element $\exp(j2\pi kl/N)$ where $j = \sqrt{-1}$, and $\sqrt{N} \cdot I$ where $I$ is the $N \times N$ identity matrix. These sets contain $N$ orthogonal signals of length $N$ and will be called orthogonal MWBE signal sets. These orthogonal MWBE signal sets correspond to frequency-division multiple-access (FDMA) and time-division multiple-access (TDMA) signaling respectively.

**Proposition 2.** *(Massey and Mittelholzer [14]): If $\mathcal{X}$ and $\hat{\mathcal{X}}$ are WBE signal sets of length $N$ and sizes $K$ and $\hat{K}$, then $\mathcal{X} \cup \hat{\mathcal{X}}$ is a WBE signal set of size $K + \hat{K}$ and length $N$.*

Note that it is not necessary that $\mathcal{X}$ and $\hat{\mathcal{X}}$ be different signal sets. For example, if the TDMA (or FDMA) signal set is used for both $\mathcal{X}$ and $\hat{\mathcal{X}}$, then the larger (multi)set has $2N$ signals of length $N$. All inner products are 0 except for $\langle x^{(k)}, \hat{x}^{(k)} \rangle = N$, $1 \leq k \leq K$, and both sides of (1) have value $4N^3$. However, $I_{\max}(\mathcal{X} \cup \hat{\mathcal{X}}) = N$. These signaling schemes in effect divide the $2N$ transmitters into $N$ pairs with each pair using its allotted time slot (or frequency slot) as a two-user adder channel. As a final comment, note that the union of two MWBE signal sets is generally not a MWBE signal set.

Given a WBE signal set $\mathcal{X}$ of size $K$ and length $N$, Proposition 2 allows the construction of a WBE signal multiset of size $LK$ as the union of $L$ copies of $\mathcal{X}$. It is also possible to transform $\mathcal{X}$ into a different set $\hat{\mathcal{X}}$ so as to ensure that the signals in $\mathcal{X} \cup \hat{\mathcal{X}}$ are distinct. Several "WBE-preserving" transformations such as cyclic shifts, multiplication of rows or columns of $S(\mathcal{X})$ by constants of unit magnitude, etc., are described in [14]. The next two propositions describe general transformations that include all these WBE-preserving transformations as special cases.

**Proposition 3.** *If $S(\mathcal{X})$ is a WBE (MWBE) signal set of size $K$ and length $N$, then $DS(\mathcal{X})U$, where $D$ is a $K \times K$ diagonal unitary matrix and $U$ is a unitary matrix, is a WBE (MWBE) signal set $\hat{\mathcal{X}}$ of size $K$ and length $N$.*

## 2 Bounds on Inner Products

### 2.1 WBE Signal Sets

Let $\mathcal{X} = \{x^{(1)}, x^{(2)}, \ldots, x^{(K)}\}$ denote a set of $K$ complex-valued vectors of length $N$ where, to avoid special cases, it is assumed that $K \geq N > 1$. The vectors in $\mathcal{X}$ need not be distinct, that is, $\mathcal{X}$ can be a multiset. The signal matrix $S(\mathcal{X})$ of $\mathcal{X}$ is defined to be the $K \times N$ matrix whose $k$-th row is $x^{(k)} = (x_0^{(k)}, x_1^{(k)}, \ldots, x_{N-1}^{(k)})$, $1 \leq k \leq K$. The set $\mathcal{X}$ will be called a *signal set* of size $K$ and length $N$ if all the rows of $S(\mathcal{X})$ in $\mathcal{X}$ have energy $N$, that is, $\|x^{(k)}\|^2 = \langle x^{(k)}, x^{(k)} \rangle = \sum_{i=0}^{N-1} |x_i^{(k)}|^2 = N$ for all $k$, $1 \leq k \leq K$. Conversely, any $K \times N$ matrix whose rows all have energy $N$ specifies a signal set $\mathcal{X}$ of size $K$ and length $N$. The *maximum* inner product magnitude $I_{\max}(\mathcal{X})$ of a signal set $\mathcal{X}$ is defined by

$$I_{\max}(\mathcal{X}) = \max_{k \neq l} |\langle x^{(k)}, x^{(l)} \rangle|.$$

The *root-mean-square* (RMS) inner product magnitude $I_{\text{rms}}(\mathcal{X})$ is the square root of the average value of $|\langle x^{(k)}, x^{(l)} \rangle|^2$ over all $k \neq l$. Thus,

$$I_{\text{rms}}(\mathcal{X}) = \left[ \frac{1}{K(K-1)} \sum_{k=1}^{K} \sum_{l \neq k,\ l=1}^{K} |\langle x^{(k)}, x^{(l)} \rangle|^2 \right]^{1/2}.$$

When the signal set is obvious from the context, it is convenient to just write $I_{\max}$ and $I_{\text{rms}}$. Note also that $I_{\max} \geq I_{\text{rms}}$.

**Proposition 1.** *(Massey and Mittelholzer [14]): For any signal set $\mathcal{X}$,*

$$\sum_{k=1}^{K} \sum_{l=1}^{K} |\langle x^{(k)}, x^{(l)} \rangle|^2 \geq K^2 N \tag{1}$$

*with equality if and only if the* columns $y^{(0)}, y^{(1)}, \ldots, y^{(N-1)}$ *of $S(\mathcal{X})$ are orthogonal vectors of energy $K$, that is,*

$$\langle y^{(m)}, y^{(n)} \rangle = \begin{cases} K, & m = n, \\ 0, & m \neq n. \end{cases} \tag{2}$$

Welch [33] used a different argument to prove the more general result

$$\sum_{k=1}^{K} \sum_{l=1}^{K} |\langle x^{(k)}, x^{(l)} \rangle|^{2s} \geq \frac{K^2 N^{2s}}{\binom{N+s-1}{s}}. \tag{3}$$

Note that (1) is the special case $s = 1$ of (3). However, the condition for equality stated in Proposition 1 was not known before.

title and the statement of the main results in [33]. Recently, however, Massey and his colleagues [14], [20], have considered sets of vectors for which the RMS magnitude of the inner product equals the Welch lower bound. The capacity of code-division multiple-access (CDMA) systems in which these so-called WBE signal sets are used as the signature sequences has been studied in [20]. Following this, other authors [31], [32] have considered the signal-to-interference ratio in CDMA systems when WBE signal sets are used as signature sequences.

In this chapter, both the RMS magnitude and the maximum magnitude of the inner product are considered. Signal sets whose maximum inner product magnitude equals the Welch bound (hereafter called MWBE signal sets) form a subclass of WBE signal sets, and are also described. The results in [14] are generalized in several obvious ways from linear binary codes and their cosets to linear nonbinary codes and their cosets, and from WBE signal sets to MWBE signal sets. It is shown that almost all interesting codes are WBE signal sets – indeed, in stark contrast to the folk theorem that "all codes are good except the ones we can think of" one can assert that

"All codes are WBE signal sets except the ones we *don't want* to think of!"

Some of the WBE signal sets described in [14] are actually MWBE signal sets. Large sets of signals whose maximum inner product magnitudes are only very slightly larger than the Welch bound are also described. All these constructions provide signal sets whose sizes and alphabets are restricted in various ways. A new result in this chapter is a Kronecker product construction that provides WBE signal sets of arbitrary size. A construction of WBE signal sets over alphabets whose size is a prime power is also described. The most important practical application of the latter result is to the design of signal sets over quaternary alphabets for use in quadriphase communication systems. Next, it is noted that subsets of WBE signal sets generally are not WBE signal sets. The effect of this on system analyses and information-theoretic analyses of channel capacity is briefly described.

For asynchronous CDMA communication systems, various correlation parameters of the signal sets are more important than the inner products. The Welch lower bounds [33] on the RMS and maximum magnitudes of the periodic, odd, and aperiodic correlation functions have been studied previously [18], [21], [23], [24]. The same bounds also apply to the RMS and maximum magnitudes of the more-recently introduced polyphase correlation functions [4], [28] which include the periodic and odd correlation functions as special cases. Welch also proved more general bounds on the periodic and aperiodic correlation function magnitudes. It is noted that these also apply to the polyphase correlation functions. It is also noted that signal sets (such as WBE signal sets) that meet the Welch bounds on RMS correlation are also complementary signal sets. Finally, the chapter considers the signal-to-noise ratio parameter [17] for asynchronous CDMA communication systems that use WBE signal sets as signature sequences. It is noted that in many cases, better than average performance can be guaranteed if WBE signal sets are used. The chapter concludes with a brief discussion of these results.

# Meeting the Welch Bound with Equality

Dilip V. Sarwate

Department of Electrical and Computer Engineering
and the Coordinated Science Laboratory
1308 West Main Street
Urbana IL 61801 USA
Email: sarwate@comm.csl.uiuc.edu

**Abstract.** A signal set whose root-mean-square inner product magnitude equals the Welch lower bound is called a WBE signal set. WBE signal sets are of interest in synchronous CDMA communication systems. This chapter surveys the known results on WBE signal sets and extends them in several ways. In particular, WBE signal sets over signal alphabets whose size is a prime power (the most important case is the quaternary alphabet), and arbitrary-size WBE signal sets over small alphabets are constructed. Constructions are also described for signal sets whose maximum inner product magnitudes equal (or are only very slightly larger than) the Welch bound. Similarly, signal sets whose root-mean-square correlation magnitudes equal the Welch lower bound on correlations are of interest in asynchronous CDMA communication systems. It is shown that the root-mean-square correlation magnitude of all WBE signal sets (and many more) equals the Welch bound. Finally, the signal-to-noise ratio for CDMA communication systems using WBE signal sets is studied.

## 1 Introduction

A quarter-century ago, Welch [33] published a collection of lower bounds on the maximum magnitude of the inner products of a set of unit-norm complex-valued vectors, and used these results to deduce lower bounds on the maximum magnitudes of the periodic and aperiodic correlation functions for sets of periodic sequences. The method used was a familiar one – Welch found lower bounds on the root-mean-square (RMS) magnitude, and then asserted that the maximum magnitude could not be smaller than these lower bounds. In the years that followed the publication of the Welch bounds, the statement

"The set satisfies the Welch bound with equality"

was generally understood [1], [8], [10], [15], [21] to mean that the *maximum* magnitude of the parameter under consideration was equal to the corresponding lower bound given in [33]. Indeed, this interpretation is supported by both the

[0] Chapter 11 of *Sequences and Their Applications: Proceedings of SETA'98*, C. Ding, T. Helleseth, and H. Niederreiter (eds.), DMTCS Series, Springer-Verlag, 1999.

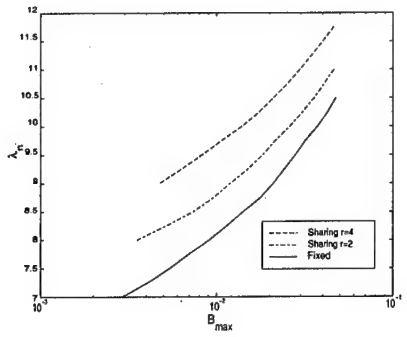


**Figure 4. Plot of optimal $\lambda_n$ versus $B_{max}$ in the linear case**

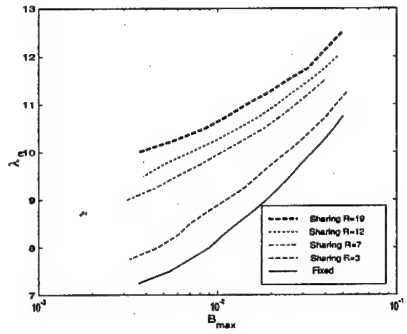


**Figure 5. Plot of optimal $\lambda_n$ versus $B_{max}$ in the 2-D case**

$$\text{subject to} \qquad P_b \leq B_{max} \tag{2}$$

A similar optimization problem is defined for the FCA scheme, except that $\lambda_n$ is the only tuning parameter in that case. In Figure 4, we plot the optimal values of $\lambda_n$ versus $B_{max}$ for both schemes for the linear case with $r = 2$ and $r = 4$. In Figure 5, we plot the optimal values of $\lambda_n$ versus $B_{max}$ for both schemes for the 2-D case with $R = 3, 7, 12$, and 19. For both figures, we use $\mu = 1$. To make our results comparable for different minimum reuse factors, we keep $N/r = 15$ for all the curves in Figure 4. Thus, $N = 30$ when $r = 2$, and $N = 60$ when $r = 4$. Similarly, in Figure 5, we set $N/R = 15$ for all $R$.

From Figures 4 and 5, we observe that for any $P_b \leq B_{max}$ constraint, our channel sharing scheme allows a higher call rate than the FCA scheme. For a typical constraint of $P_b \leq 10^{-2}$, our scheme can admit approximately 20% more calls into the network than the FCA scheme with $r = 4$ in the linear case or with $R = 7$ in the 2-D case. Note that in the 2-D case, even with the minimum possible reuse factor $R = 3$, our scheme outperforms the FCA scheme by more than 10%. Of course, when the reuse factor becomes larger, the improvement also increases (e.g., 30% for $R = 19$). Also, as shown in the figures, for lower blocking probability constraints, the improvement is even greater.

We next investigate the protocol complexity for those optimal combined sharing schemes obtained for Figures 4 and 5. We first estimate the expected number of inter-cell communications used to serve a call arrival, by dividing the total number of sharing requests that have been submitted in simulation to the total number of call arrivals. Here we count all sharing request signals, including those that are not granted. We find that the expected number of sharing requests per call arrival does not exceed 0.2 in all the cases shown in Figure 4, and 0.6 for those in Figure 5. There is a difference between the linear and 2-D cases, because in the latter, each cell has more adjacent cells, and thus more sharing requests have to be sent. We next estimate the expected number of intra-cell channel swappings needed to serve a call arrival, by dividing the total number of channel swappings observed in simulation to the total number of call arrivals. We find that the maximum number of channel swappings per call arrival needed is less than 0.04 for the combined sharing schemes in Figure 4, and less than 0.25 for those in Figure 5. These results suggest that the computational overhead to implement our protocol is not significant.

## 5. Conclusion

We have presented a novel channel sharing scheme to improve system capacity in wireless cellular systems. Our basic idea is to allow channels to be shared between adjacent cells without co-channel coordination with other cells. For this purpose, we introduce the concept of meta-cells to facilitate localized channel management. Further, to maximize channel reuse efficiency, we develop a channel assignment method based on the distance measure between meta-cells. An attractive feature of the channel sharing scheme is that it does not require complex power control techniques, global channel coordination, or on-line optimization, which simplifies its implementation. In this paper, we only consider the channel assignment problem without taking into account call handoff. In [3], we describe how the channel sharing scheme can be applied to address the call handoff problem. We find that our scheme significantly reduces handoff blocking probability and improves system capacity over a large range of traffic conditions.

## References

[1] H. Jiang and S. Rappaport. CBWL: A new channel assignment and sharing method for cellular communication systems. *IEEE Transactions on Vehicle Technology*, 43:313–322, May 1994.

[2] I. Katzela and M. Naghshineh. Channel assignment schemes for cellular mobile telecommunication systems: a comprehensive survey. *IEEE Personal Communications Magazine*, pages 10–31, June 1996.

[3] J. Li. *Intercellular coordination schemes for improving spectrum utilization in wireless cellular networks.* Ph.D. dissertation, Purdue University, West Lafayette, Indiana, 1998.

assigned an idle channel, and the state of that channel is then changed to "BUSY." Otherwise, we attempt to obtain an idle accessible channel from some sharing cell, as follows. We first look up all accessible channels currently labeled "DISABLED" in the local cell, and get a list of the sharing cells associated with those "DISABLED" accessible channels. We then choose one of the sharing cells on this list, and send it a *sharing request*. The sharing cell, upon receiving the sharing request, then executes the procedure described below. If the sharing request is granted, we accept the arriving call by assigning the accessible channel specified in the return message from the sharing cell, and setting the state of that channel "BUSY". If the request is denied, we proceed to send another sharing request to one of the remaining sharing cells on the list. The process is continued until the sharing request is accepted, or denied by all sharing cells on the list, in which case the call is rejected (blocked).

When a sharing request is received from a sharing cell, we first check whether there is any accessible channel $U$, associated with that sharing cell, currently labeled "IDLE" in the local cell. If so, we grant the sharing request by sending back the identification number of channel $U$ in the return message, and setting channel $U$ "DISABLED" in the local look-up table. Otherwise, we attempt to obtain such an idle channel $U$ by *swapping channels* as follows. We check whether there is any accessible channel $V$ currently labeled "IDLE" in the local cell. If so, we find a user currently using an accessible channel $U$ associated with the sharing cell. That user then releases channel $U$ and grabs channel $V$, so that we can grant the sharing request by returning the identification number of channel $U$, and setting channel $U$ as "DISABLED" in the local look-up table. If no accessible channels are in the "IDLE" state, we reject the sharing request.

When a call leaves the local cell, we simply label the associated channel "IDLE."

The following are some of the important features of our channel sharing protocol.

1. *Channel sharing within a meta-cell is localized* between two adjacent cells and can therefore be done in a decentralized fashion. No global coordination is necessary in our protocol. The major computational effort in the local cell includes communication with the sharing cells and channel swappings.

2. *Channel utilization is improved*, because channels are assigned to meta-cells, instead of being assigned to cells. Specifically, an idle channel can be accessed by calls in either of its component cells, thus effectively reducing the fraction of idle periods of channels.

3. *Call blocking may be decreased*, since users have access to statistically more portion of channel capacity. For example, in the linear cellular system, each cell is covered by two overlapping meta-cells. Users in each cell may thus have access to $\frac{2N}{r'}$ channels (at most), compared with $\frac{N}{r}$ channels using the FCA scheme. Note that $\frac{2N}{r'} = \frac{2N}{r+1} > \frac{N}{r}$, since $r \geq 2$. Therefore, our scheme can provide more channel capacity than the FCA scheme. It can be shown that a similar result holds for the 2-D case as well.

## 4. Combined Scheme and Simulation Results

It is instructive to compare the effective channel capacity using our sharing scheme and the FCA scheme. As we pointed out above, in an individual cell, the number of accessible channels in our scheme is generally larger than that of the FCA scheme. Note that, however, this number is an upper bound for the effective channel capacity since it assumes that the statistical sharing advantage can be fully exploited. On the other hand, if we totally ignore the statistical sharing advantage, we may then obtain a lower bound for the channel capacity. The effective channel capacity using our sharing scheme is bounded by these two extreme scenarios, and depends on the extent to which the statistical sharing advantage is actually obtained.

Next, we describe a combined scheme that attempts to maximize the effective channel capacity for each cell. Specifically, we divide the $N$ given channels into two distinct groups of size $N_1$ and $N_2$ such that $N = N_1 + N_2$. The first group of $N_1$ channels is assigned to cells using the FCA scheme, and thus cannot be shared between adjacent cells. The remaining group of $N_2$ channels, however, is assigned to meta-cells according to our channel sharing assignment scheme, and can be shared within meta-cells, the same as in the previous sections.

Varying $N_2$ allows us to maximize the effective channel capacity. Specifically, the parameter $N_2$ enables us to trade off the potential advantage from statistical sharing with a reduction in the average number of channels for each cell. The larger the value of $N_2$ in the combined scheme, the more the gain we expect from statistical sharing, but at the same time the higher the price we pay by reducing the average number of channels for each cell.

We next numerically compare the performance of the combined channel sharing scheme with the FCA scheme. We investigate both the linear and 2-D hexagonal cases by simulation. Our simulation model for the linear cellular system consists of 30 cells, where each cell has two adjacent cells. The boundary cells on the two sides are then connected to each other to avoid "edge" effects at the boundaries. To model the 2-D cellular system, we use a 36-cell configuration, with each cell having six adjacent cells. Again, the cells on the boundary of one side of the configuration are connected to the cells on the boundary of the other side. For both the linear and 2-D cases, calls are assumed to arrive at each cell according to a Poisson process with rate $\lambda_n$. The time until a call terminates is assumed to be exponentially distributed with mean $1/\mu$.

We compare the maximum call arrival rate $\lambda_n$ that can be admitted by our channel sharing scheme and the FCA scheme, respectively, for various values of the blocking probability $P_b$. More precisely, we define the following optimization problem for our sharing scheme:

$$\underset{\lambda_n, N_2}{\text{maximize}} \quad \lambda_n$$

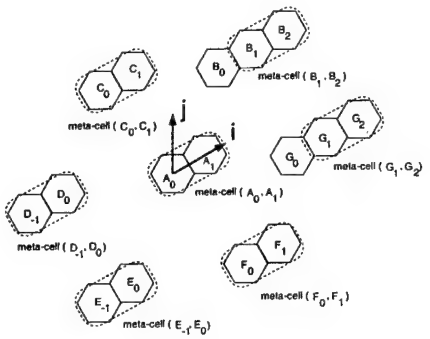


**Figure 3. Configuration of co-channel meta-cells in the case of $p + 1 \geq q$.**

radius of a single cell. In general, the minimum reuse factor $R$ can be represented by $R = p^2 + pq + q^2$, where $p$ and $q$ are nonnegative integers satisfying $p + q \geq 2$. Without loss of generality, we assume that $q \geq p$ in the following.

As in the linear case, a meta-cell here consists of two adjacent neighboring cells. To allow for channel sharing, we assign channels to meta-cells, under the minimum reuse distance constraint in terms of meta-cells. For our purpose, the distance measure between two meta-cells is defined in the same way as in Equation (1), and we attempt to deploy co-channel meta-cells as close as possible. In the remainder of this section, we describe this channel assignment scheme.

Consider an arbitrary cell $A_0$ in the hexagonal cellular system as shown in Figure 3, and establish a set of coordinates $i$-$j$ originating at the center of cell $A_0$, where the two axes form a $60^o$ angle, and the unit distance along the axes is $\sqrt{3}\rho$. Then, the minimum reuse distance $\Delta$ is equal to $R$ coordinate units in this set of coordinates. The center of any hexagon $Z$ can be designated by a pair of coordinates $(i_Z, j_Z)$, with $i_Z$ and $j_Z$ integers. Let $B_0$, $C_0$, $D_0$, $E_0$, $F_0$, and $G_0$ denote six hexagons with centers at the coordinates $(p, q)$, $(-q, p + q)$, $(-p - q, p)$, $(-p, -q)$, $(q, -p - q)$, and $(p + q, -p)$, respectively (see Figure 3). Note that their distances to cell $A_0$ (centered at $(0, 0)$) are equal and given by $p^2 + pq + q^2 = R$ units. In the conventional FCA scheme, cells $B_0$, $C_0$, $D_0$, $E_0$, $F_0$, and $G_0$ are assigned the same set of channels as cell $A_0$.

Let $A_1$ be the adjacent right neighboring cell of $A_0$ along the $i$-axis as shown in Figure 3, i.e., $(i_{A_1}, j_{A_1}) = (i_{A_0} + 1, j_{A_0}) = (1, 0)$. We next focus on meta-cell $(A_0, A_1)$. Note that in the 2-D case, meta-cells may have three distinct orientations, and each meta-cell may have six neighboring co-channel meta-cells. Consequently, there are an infinite number of different ways to deploy co-channel meta-cells, including irregular (non-repetitive) deployment patterns. For the sake of simplicity and regularity, here we restrict ourselves to deployment methods in which all co-channel meta-cells are of the same orientation. In other words, for any co-channel meta-cell of $(A_0, A_1)$, two components are adjacent along the $i$-axis. Therefore, we can identify any co-channel meta-cell of reference meta-cell $(A_0, A_1)$ by its left component.

It turns out that for different values of $p$ and $q$, we need different methods to deploy co-channel meta-cells of reference meta-cell $(A_0, A_1)$, depending on whether $p + 1 \geq q$. For simplicity, here we discuss only the case of $p + 1 \geq q$. The values of $R$ within this category are $3, 7, 12, 19$, etc. It can be shown that in this case, as illustrated in Figure 3, the meta-cells whose left components are respectively $B_1$, $C_0$, $D_{-1}$, $E_{-1}$, $F_0$, and $G_1$, can be deployed as co-channel meta-cells of reference meta-cell $(A_0, A_1)$, where the centers of cells $B_1$, $D_{-1}$, $E_{-1}$, and $G_1$ are given respectively as follows: $(i_{B_1}, j_{B_1}) = (p + 1, q)$, $(i_{D_{-1}}, j_{D_{-1}}) = (-p - q - 1, p)$, $(i_{E_{-1}}, j_{E_{-1}}) = (-p - 1, -q)$, and $(i_{G_1}, j_{G_1}) = (p + q + 1, -p)$. Furthermore, we have shown that when assigning channels according to this co-channel meta-cell deployment, the channel reuse factor is

$$R' = R + p + q.$$

A detailed proof and further discussion of the above co-channel meta-cell deployment are given in [3].

## 3. Channel Sharing Protocol

We next develop a channel sharing protocol to exploit this sharing feature of our scheme. For the sake of description, we focus our attention on a particular (arbitrary) cell, which we call the *local cell*. Recall from the previous section that using our channel assignment scheme, each cell in the cellular network is always covered by several overlapping meta-cells, called the *covering meta-cells* of that cell. We call channels that are assigned to the covering meta-cells of the local cell the *accessible channels*, since users in the local cell may have access to those channels.

At any given instance, each accessible channel can be used in only either the local cell or one of the adjacent cells. In other words, not all the accessible channels can be used by the local cell at a given instance. Those channels that can be used by the local cell are called enabled channels. To coordinate the use of accessible channels between the local cell and the corresponding sharing cells, the local cell maintains a look-up table, in which each accessible channel occupies one entry, recording the current state of that channel. The state of this entry may be "DISABLED", "IDLE", or "BUSY". A channel labeled "DISABLED" is not enabled in the local cell. This indicates that the channel is currently enabled in the sharing cell associated with that channel. The local cell can use only those accessible channels labeled "BUSY" or "IDLE". In this case the labels further indicate whether channels are currently occupied by mobile users in the local cell.

Our protocol can be described in three main parts, corresponding to three different possible scenarios: *arrival of a call, sharing request from a sharing cell,* and *departure of a call.*

When a call arrives, we check if there are any accessible channels labeled "IDLE" in the look-up table of the local cell. If there are, the arriving call is accepted and

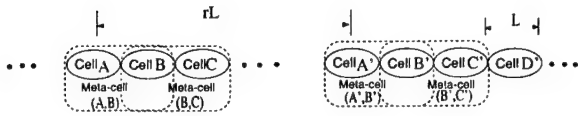


**Figure 1. Meta-cells in the 1-D cellular system.**

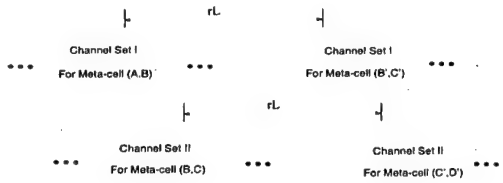


**Figure 2. Meta-cell based channel assignment scheme in the 1-D cellular system.**

used in cell $A'$. Such a channel borrowing scheme requires excessive exchange of channel usage information between remote cells, and channel utilization may also be decreased at high traffic loads [1].

In our scheme, we attempt to alleviate call blocking by sharing channels between neighboring cells. To facilitate the description of our scheme, we first introduce the concept of *meta-cell*. A meta-cell is a fixed collection of neighboring cells (typically a pair of two adjacent cells). For example, Figure 1 shows a family of meta-cells in a linear (1-D) cellular system, each comprising a pair of two adjacent cells. Each meta-cell is designated by a pair $(X, Y)$, where $X$ and $Y$ are individual cells called the *component cells* of that meta-cell. For example, in Figure 1, cells $A$ and $B$ are components of meta-cell $(A, B)$. As before, we assume that we have a distance measure for meta-cells (e.g., based on the distance measure $d$ between cells).

The main idea of our channel assignment scheme is to allocate channels to meta-cells in such a way that a maximum number of channels can be assigned to each meta-cell while any two meta-cells assigned the same channels satisfy the minimum reuse distance requirement, i.e., the distance measure, now with respect to two meta-cells, is no shorter than $\Delta$. Our channel assignment scheme, done at the meta-cell level, is different from the usual channel assignment scheme which is done at the cell level. In particular, channels are assigned not to individual cells but to meta-cells. A user in a given cell can use any channel that is assigned to a meta-cell to which the given cell belongs, with the usual proviso that only one user can use a given channel within a given meta-cell at a given instance. Our channel allocation scheme allows channels to be shared between neighboring cells (namely, cells belonging to the same meta-cell). Note that relative to the usual FCA scheme, in our sharing scheme we need to coordinate between cells in a meta-cell. However, since meta-cells consist only of neighboring cells, the scheme should be easy to implement.

In the following, we illustrate our channel assignment scheme for two typical cellular systems: linear and 2-D hexagonal. We develop methods to deploy meta-cells assigned the same channels as close as possible, while not violating the minimum reuse distance requirement.

Consider again Figure 1. For this simple linear cellular system, the distance measure $d_{X,Y}$ between two cells $X$ and $Y$ is usually given as $d_{X,Y} = |c_X - c_Y|$, where $c_X$ and $c_Y$ denote the positions of the centers of cells $X$ and $Y$, respectively. Suppose that the minimum reuse distance is $\Delta = rL$, where $L$ is the width of a single cell and $r$ is an integer. Cells that are assigned the same set of channels are called *co-channel cells*. Therefore, in the FCA scheme, co-channel cells are exactly $r$ cells apart. Let $N$ denote the total number of distinct channels that are available in this linear cellular system. Thus, the total number of distinct channels allocated to each cell is $N/r$. The integer $r$ is called the *reuse factor*.

To assign channels to meta-cells, we next derive the *distance measure* $d_{(X,Y),(X',Y')}$ between two meta-cells $(X, Y)$ and $(X', Y')$. Recall that in our scheme, when a channel is assigned to a meta-cell, it can be used by a mobile user in any cell belonging to that meta-cell. Thus, we have to ensure that the distance measure between any component cells of two meta-cells assigned the same set of channels complies with the minimum reuse distance requirement. Consequently, we define $d_{(X,Y),(X',Y')}$ as the minimum of the distance measures between the component cells of meta-cells $(X, Y), (X'Y')$, i.e.,

$$d_{(X,Y),(X',Y')} \triangleq \min\{d_{X,X'}, d_{X,Y'}, d_{Y,X'}, d_{Y,Y'}\}. \quad (1)$$

For example, in Figure 1, the distance measure between meta-cells $(A, B)$ and $(A', B')$ is given by $(r-1)L$, which is the distance between cells $B$ and $A'$.

We call meta-cells that are assigned the same set of channels *co-channel meta-cells*. To allocate a maximum number of channels to each meta-cell, co-channel meta-cells have to be deployed as close as possible. Therefore, we assign the same set of channels to meta-cells that are exactly the minimum reuse distance apart, i.e., $rL$ in this case. For example, in Figure 2, meta-cells $(A, B)$ and $(B', C')$ are assigned the same set of channels. It is easy to show that, using our scheme, each meta-cell is assigned $N/(r+1)$ distinct channels. In other words, the reuse factor of our channel assignment scheme is

$$r' = r + 1.$$

In the planar or 2-D case, the cellular configuration is usually assumed to be hexagonal. As in the linear case, the distance $d_{X,Y}$ between two cells $X$ and $Y$ is usually defined as the distance between their centers. Let $N$ denote the total number of distinct channels available in this hexagonal cellular system. In the FCA scheme, co-channel cells are exactly a distance of $\Delta$, the minimum reuse distance, apart. Consequently, each cell is assigned $N/R$ channels, where $R$ is the minimum reuse factor. It has been shown that $R$ can be determined from $\Delta$ by $R = (1/3)(\Delta/\rho)^2$, where $\rho$ is the

Proc. 3rd IEEE Symp. on Comp. & Comm. (ISCC'98)

# A Channel Sharing Scheme To Improve System Capacity in Wireless Cellular Networks *

Junyi Li Ness B. Shroff† Edwin K.P. Chong
School of Electrical and Computer Engineering
Purdue University
West Lafayette, IN 47907, U.S.A.
E-mail: {junyi, shroff, echong}@ecn.purdue.edu

## Abstract

*Enhancing system capacity is an important issue in wireless cellular networks. In this paper, we present a new channel sharing scheme to address this problem. Our basic idea is to allow channels to be shared between adjacent cells. We propose a fixed channel assignment scheme to maximize channel reuse efficiency while allowing channel sharing. An important feature of our sharing scheme is that channel management is localized between adjacent cells, and no global coordination or optimization is required, thus simplifying implementation. We provide simulation results comparing our scheme with the fixed channel assignment scheme.*

## 1. Introduction

Worldwide focus on wireless networking research has intensified in recent years. Compared to its wired counterpart, wireless spectrum is a much more scarce resource. Thus, enhancing system capacity is of great importance in wireless networks. The use of cellular technology is a common means to this end. In a cellular system, the service area is divided into cells, and the wireless spectrum is reused among those cells. We refer to the unit of wireless spectrum needed to serve a single user as a *channel*. For example, in a TDMA system, a time-slot is viewed as a channel. We adopt the usual assumption that channels used in one cell cannot be used in other cells that are closer than the *minimum reuse distance*. A significant body of research has been conducted on efficiently allocating channels to individual cells under this minimum reuse distance constraint [2]. There are, in general, two types of channel allocation schemes: Fixed Channel Allocation (FCA) and Dynamic Channel Allocation (DCA).

In this paper, we propose a novel channel sharing scheme to improve system capacity in wireless cellular networks. The basic idea in our channel sharing scheme is to allow channels to be shared between adjacent cells; i.e., channels can be used by any user in either cell, without coordinating with other cells for the use of the same channels. In this way, channel management can be localized within adjacent cells. Further, to avoid the need for centralized optimization, we propose a new fixed channel assignment scheme that attempts to keep the co-channel reuse distance as close as possible while allowing channel sharing.

## 2. Localized Channel Sharing Assignment Scheme

Consider a set of cells in a cellular system. Each cell contains a base station, which communicates with mobile users in that cell. Associated with the cellular system is a set of channels, which are to be allocated to the cells. In each cell, an individual channel can be used by only one mobile user in the cell for communication with the base station. The same channel can be reused in two different cells as long as they (the cells) satisfy a *minimum reuse distance requirement*. To elaborate, we assume that we are given a distance measure $d$, where $d_{X,Y}$ is the distance between cells $X$ and $Y$. We are also given a parameter $\Delta$ that represents the *minimum reuse distance*. Two cells $X$ and $Y$ are said to satisfy the minimum reuse distance requirement if $d_{X,Y} \geq \Delta$.

In the conventional FCA scheme, each channel is assigned to cells that are exactly a distance $\Delta$ apart. For example, cells $A$ and $A'$ are assigned the same set of channels. In cellular systems using the FCA scheme, calls in a cell can only use those channels assigned to that cell. Call blocking results if such a channel is not available. Channel borrowing is one way to reduce call blocking. Specifically, if at the time the call arrives at cell $B$, cell $B$ does not have any idle channel, but cell $A$ has some idle channels, then cell $B$ may borrow one of the idle channels to serve the new call. To achieve this, however, we need to coordinate the use of channels in the co-channel cells of cell $A$. For example, channels that are borrowed by cell $B$, cannot be

*This research was supported in part by AT&T special purpose grant 670-1285-2569, by the National Science Foundation through grants NCR-9624525, CDA-9422250, CDA 96-17388, ECS-9410313, and ECS-9501652, and by the U.S. Army Research Office through grant DAAH04-95-1-0246.

†Please address all correspondence to this author, Tel. +1 765 494 3471, Fax. +1 765 494 3358.

| Algorithm | Compare | Add | Multiply | Divide | Exp | Storage |
|---|---|---|---|---|---|---|
| OSOME | 1 | $2^{K-1}(2A_v + L - K + 4)$ | $2^K(L-K+2)$ | 1 | $2^K$ | $2^{K-1}[f + f(L-K+1)]$ |
| SSOME | $2^{K-1}(L-K+2)$ | $2^{K-1}(2A_v + 2L - 2K + 6)$ | 0 | 1 | $2^K$ | $2^{K-1}[f + (f+1)(L-K+1)]$ |
| SSOME1 | $2^{K-1}(L-K+3)$ | $2^{K-1}(2A_v + 2L - 2K + 4)$ | 0 | 1 | 1 | $2^{K-1}[f + (f+1)(L-K+1)]$ |
| SOVA | $2^{K-1}(L-K+3)$ | $2^{K-1}(2A_v + 3e + 4)$ | $2^K(e)$ | $2^{K-1}$ | $2^{K-1}$ | $2^{K-1}[f + (f+1)(L-K+1)]$ |
| BCDFE | $2^{J+1}(L-J)+1$ | $2^J(2A_v + 4)$ | $2^J(3)$ | $2^{J+1}$ | $2^{J+1}$ | $2^J(f + L - J)$ |
| MBCDFE | $2^J(K-J-1)+1$ | $2^J(2A_v + L - J + 4)$ | $2^J(2L - 2J + 3)$ | $2^{J+1}$ | $2^{J+1}$ | $2^J[f(L-J+1) + K - J - 1]$ |

Table 1: Complexity in number of operations per iteration ($f$ = #bits required to store a floating point number, $e$ = #places where the code bits corresponding to two converging paths differ.)

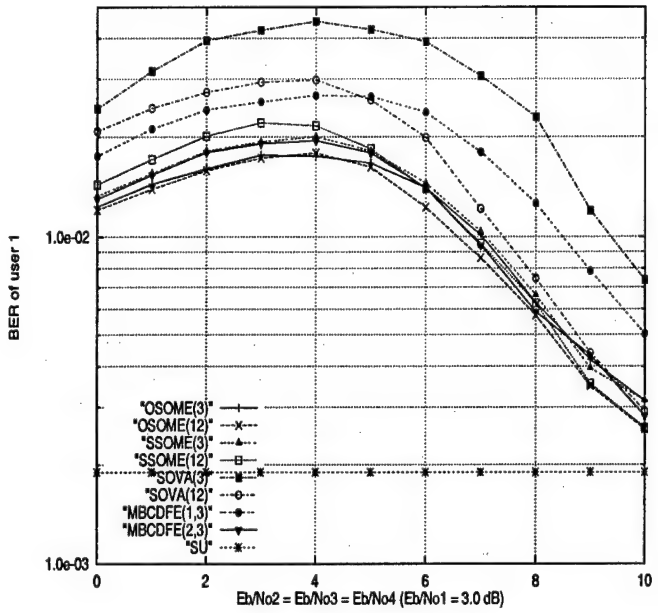


Figure 3: BER performance of various algorithms in near-far situation.

BER curves of all schemes tend to single user under extreme conditions of MAI. Thus Fig.2 depicts almost worst case performance for user 1 given its $E_b/N_0$. Note that MBCDFE(1,3) outperforms SOVA(12) under power control if the background noise is not too high. Although the application of MBCDFE requires whitening, its performance/complexity tradeoff is highly desirable.

Table 1 compares the complexity of various algorithms with binary symbols where it is assumed that $A_v$ add operations are required to compute $V(.)$ in (8) (or the equivalent quantity for other algorithms). Note that the complexity of OSOME(L) is on the order of $2^{K-1}(L-K+1)$. SSOME mainly consists of add-compare-select operations and exponentiation is only used for soft-output generation. The complexity of MBCDFE(J,L) is on the order of $2^J(L-J)$. The modified version requires some extra storage and computation.

In conclusion, the suboptimal soft-output multiuser estimation algorithm with decision lag equal to $K-1$ manages to extract most of the benefits of soft-output demodulation with a simple forward recursion that can be implemented without whitening. So the algorithm is suitable to use with long spreading codes and time-varying channel conditions like fast fading. Adaptive complexity reduction techniques like the T-algorithm and T-algorithm with soft-limiting, can be applied to all schemes discussed in this paper.

# References


[1] Y. Li, B. Vucetic, Y. Sato, "Optimum Soft-Output Detection for Channels with Intersymbol Interference", *IEEE Trans. Information Theory*, Vol. 41, No. 3, May 1995.

[2] J. F. Hayes, T. M. Cover and J. B. Riera, "Optimal Sequence Detection and Optimal Symbol-by-Symbol Detection: Similar Algorithms", *IEEE Trans. Comm.*, Vol. COM-30, No. 1, Jan. 1982.

[3] G. Lee, S. B. Gelfand and M. P. Fitz, "Bayesian Decision Feedback Techniques for Deconvolution", *IEEE Journal on Selected Areas in Comm.* , Vol. 13, No. 1, pp. 155-165, Jan. 1995.

[4] J. Hagenauer and P. Hoeher, "A Viterbi Algorithm with Soft-Decision Outputs and its Applications", *Proc. Globecom*, Vol. 3, pp. 47.1.1-47.1.7, Nov. 1989.

[5] S. Verdu, "Minimum Probability of Error for Asynchronous Gaussian Multiple-Access Channels", *IEEE Trans. Information Theory*, Vol. IT-32, No. 1, pp. 85-96, Jan. 1986.

[6] Z. Xie, C. K. Rushforth, R. T. Short, "Multiuser Signal Detection Using Sequential Decoding", *IEEE Trans. Comm.* , Vol. 38, No. 5, May 1990.

[7] L. Wei, L. K. Rasmussen, "A Near Ideal Noise Whitening Filter for an Asynchronous Time-Varying CDMA System", *IEEE Trans. Comm.* , Vol. 44, No. 10, Oct. 1996.

[8] M. Rupf, F. Tarkoy, J. L. Massey, "User-Separating Demodulation for Code-Division Multiple-Access Systems", *IEEE J. Selected Areas Comm.* , Vol. 12, No. 5, June 1994.

stores the quantities $\mathrm{p}(\beta_n|z^n)$ and $\mathrm{p}(b_{n-i}=b|z^n,\beta_n)$ for $J \le i \le L$ and $b \in \{u_1, u_2, \ldots, u_{M-1}\}$. Note that $\beta_n$ is a truncated state comprising of $J$ most recent bits.

$$\mathrm{p}(\beta_n|z^n) = \frac{\sum_{b_{n-J}} \mathrm{p}(\beta_n, b_{n-J}, z_n|z^{n-1})}{\sum_{b_{n-J},\beta_n} \mathrm{p}(\beta_n, b_{n-J}, z_n|z^{n-1})} \quad (22)$$

where

$$\begin{aligned}&\mathrm{p}(\beta_n, b_{n-J}, z_n|z^{n-1})\\ &\quad = \mathrm{p}(z_n|z^{n-1}, b_n, \beta_{n-1})\mathrm{p}(\beta_{n-1}|z^{n-1})\mathrm{p}(b_n) \quad (23)\end{aligned}$$

$$\mathrm{p}(b_{n-J}|z^n,\beta_n) = \frac{\mathrm{p}(\beta_n, b_{n-J}, z_n|z^{n-1})}{\sum_{b_{n-J}} \mathrm{p}(\beta_n, b_{n-J}, z_n|z^{n-1})} \quad (24)$$

$$\begin{aligned}&\mathrm{p}(b_{n-i}=b|z^n,\beta_n)\\ &\quad = \sum_{b_{n-J}} \mathrm{p}(b_{n-i}=b|z^n,\beta_n,b_{n-J})\mathrm{p}(b_{n-J}|z^n,\beta_n)\\ &\quad = \sum_{b_{n-J}} \mathrm{p}(b_{n-i}=b|z^{n-1},\beta_{n-1})\mathrm{p}(b_{n-J}|z^n,\beta_n), \quad (25)\\ &\qquad \text{for } J+1 \le i \le L\end{aligned}$$

The second equality follows from the assumption that given $z^{n-1}$ and $\beta_{n-1}$, $b_{n-i}$ $(J+1 \le i \le L)$ is conditionally independent of $z_n$ and $b_n$ (Not true unless $J = K-1$).

To compute $\mathrm{p}(z_n|z^{n-1}, b_n, \beta_{n-1})$ in (23), suppose we had made hard decisions on bits $b_{n-i}$, $J+1 \le i \le K-1$ conditioned on the previous state $\beta_{n-1}$ as follows:

$$\hat{b}(n-i|z^{n-1},\beta_{n-1}) = \mathrm{argmax}_{b_{n-i}} \mathrm{p}(b_{n-i}|z^{n-1},\beta_{n-1})$$

Assuming that these decisions are correct, we get

$$\begin{aligned}&\mathrm{p}(z_n|z^{n-1}, b_n, \beta_{n-1}) =\\ &\quad \mathrm{p}\left(z_n \left| b_n, \beta_{n-1}, \hat{b}(n-i|\beta_{n-1}, z^{n-1}),\ J+1 \le i \le K-1\right.\right)\end{aligned}$$

which is a known Gaussian pdf. Thus the modified BCDFE(J,L) algorithm consists of these steps: For all states $\beta_n$, compute $\mathrm{p}(\beta_n|z^n)$, $\mathrm{p}(b_{n-J}|z^n,\beta_n)$ for all values of $b_{n-J}$, and $\mathrm{p}(b_{n-i}=b|z^n,\beta_n)$ for $b \in \{u_1, u_2, \ldots, u_{M-1}\}$ and $J+1 \le i \le L$, using (22), (24) and (25) respectively. Given each state $\beta_n$, make hard decisions on bits $b_{n-i}$, $J \le i \le K-2$ (these decisions will be used to calculate $\mathrm{p}(z_{n+1}|z^n, b_{n+1}, \beta_n)$ in the next iteration). Store $\mathrm{p}(\beta_n|z^n)$, $\mathrm{p}(b_{n-i}=b|z^n,\beta_n)$ $(J \le i \le L-1$ and $b \in \{u_1, u_2, \ldots, u_{M-1}\})$ and $\hat{b}(n-i|z^n,\beta_n)$ $(J \le i \le K-2)$. At lag $L$, obtain:

$$\mathrm{p}(b_{n-L}|z^n) = \sum_{\beta_n} \mathrm{p}(b_{n-L}|z^n,\beta_n)\mathrm{p}(\beta_n|z^n)$$

The BCDFE algorithm [3] makes hard decisions on symbols $b_{n-i}$, $J \le i \le L-1$ conditioned on the state by quantizing $\mathrm{p}(b_{n-i}=b|z^n,\beta_n)$. It stores these hard decisions and updates them recursively. Due to this, the symbol APP's obtained at lag $L$ are not as accurate as in the algorithm we described here which updates and stores $\mathrm{p}(b_{n-i}=b|z^n,\beta_n)$ directly (25) and uses hard decisions only to truncate the state. Note that MBCDFE(K-1,L) is the same as OSA(L).

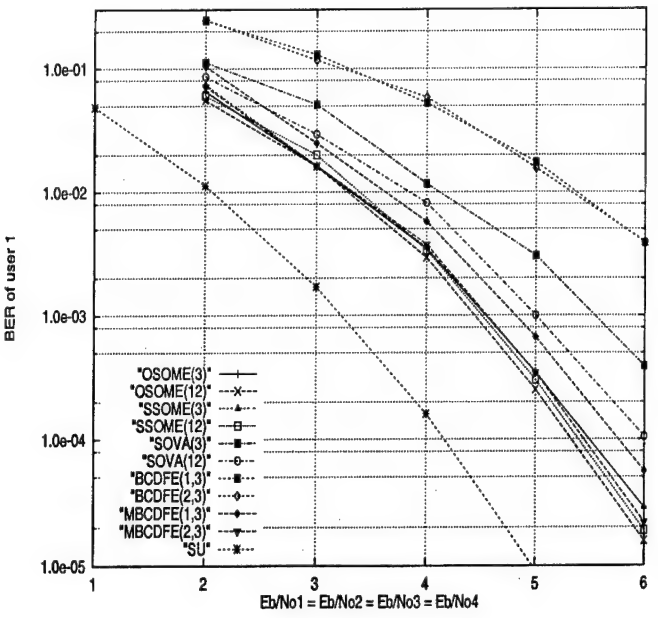


Figure 2: BER performance of various algorithms.

# 3 Simulation results

We simulate an asynchronous CDMA system with four users that employ BPSK modulation and rate $\frac{1}{2}$, memory 4 convolutional encoding over an AWGN channel. User correlations used are given by:

$$\begin{aligned}H(D) &= \sum_{m=-1}^{1} H(m)D^m\\ &= \frac{1}{7}\begin{bmatrix} 7 & -4-D & 1+2D & -D \\ -4-D^{-1} & 7 & -4-D & 3 \\ 1+2D^{-1} & -4-D^{-1} & 7 & -2+D \\ -D^{-1} & 3 & -2+D^{-1} & 7 \end{bmatrix}\end{aligned}$$

Code symbol sequences of all users are interleaved by a $30 \times 30$ interleaver. Fig.2 shows the BER of user 1 versus the signal-to-noise ratio ($E_b/N_0$) in perfect power control. Each simulation was run for a count of 500 errors. It can be seen that the BER curves of OSOME(3), OSOME(12), SSOME(3), SSOME(12) and MBCDFE(2,3) lie in a band of width 0.2 dB. OSOME(12) loses about 1.2 dB over single user. SSOME(3) achieves a $0.4-0.5$ dB gain over SOVA(12) in the range $3-6$ dB. Note that SSOME(3) requires only state metrics (and no path metrics) to be computed. We have not plotted curves for SSOME1 because SSOME1(3) is the same as SOVA(3) and SSOME1(12) approaches the performance of SSOME(12). The modified BCDFE algorithms gain $1.0-2.0$ dB over the original BCDFE because the soft outputs of the later are no better than hard decisions.

Fig.3 shows the BER of user 1 versus $E_b/N_0$ of interfering users (with $E_b/N_0$ of user 1 fixed at 3.0 dB). $10^5$ data symbols were counted for each simulation. The

Note that $\mathrm{p}(\sigma_N, r^N(t)) = \mathrm{C}f(\sigma_N, y^N)$ and $\mathrm{p}(\sigma_N, b_{N-i} = b, r^N(t)) = \mathrm{C}f_i(\sigma_N, b, y^N)$. Thus for $K-1 \le i \le N-1$,

$$\mathrm{p}(b_{N-i} = b | r^N(t)) = \frac{\sum_{\sigma_N} f_i(\sigma_N, b, y^N)}{\sum_{\sigma_N} f(\sigma_n, y^N)} \qquad (13)$$

Equations (11), (12) and (13) complete the recursion of the OSOME algorithm. Note that it's not necessary to observe the entire signal $r^N(t)$. Close to optimum estimates can be obtained for bits $b^{n-L}$ with $L$ sufficiently large, by observing $r^n(t)$ only. With this in mind, we outline the OSOME(L) algorithm as follows:

For each iteration $n$ $(n = 1, 2, \ldots, N)$, recursively compute and store the state metrics given by (12). For each $n \ge K$, $i = K-1, K, \ldots, L$ and $b \in \{u_1, u_2, \ldots, u_{M-1}\}$, also compute and store the path metrics given by (11). For each $n > L$ and $b \in \{u_1, u_2, \ldots, u_{M-1}\}$, obtain symbol APP's as:

$$\mathrm{p}(b_{n-L} = b | r^n(t)) = \frac{\sum_{\sigma_n} f_L(\sigma_n, b, y^n)}{\sum_{\sigma_n} f(\sigma_n, y^n)} \qquad (14)$$

$$\mathrm{p}(b_{n-L} = u_M | r^n(t)) = 1 - \sum_{i=1}^{M-1} \mathrm{p}(b_{n-L} = u_i | r^n(t))$$

Note that if data symbols of all users are equiprobable a priori, then $\mathrm{p}(b_n)$ can be dropped from all computations.

## 2.2 SSOME

Here we reduce the recursion described in the previous section to add-compare-select operations mostly and get the SSOME(L) algorithm. For this we define:

$$m(\sigma_n, y^n) \triangleq \max_{b^{n-K+1}} [\mathrm{U}(y^n, b^n)/N_0 + \log \mathrm{p}(b^n)], \qquad (15)$$

$$m_i(\sigma_n, b, y^n) \triangleq \max_{b^{n-K+1} | b_{n-i} = b} [\mathrm{U}(y^n, b^n)/N_0 + \log \mathrm{p}(b^n)], \quad \text{for } K-1 \le i \le n-1. \qquad (16)$$

Then a derivation similar to (11) can be used to show that

$$m_i(\sigma_n, b, y^n) = \max_{b_{n-K+1} | b_{n-i} = b} [m_i(\sigma_{n-1}, b, y^{n-1}) + \mathrm{V}(y_n, \sigma_{n-1}, b_n)] + \log \mathrm{p}(b_n) \qquad (17)$$

and

$$m(\sigma_n, y^n) = \max_{b_{n-K+1}} [m(\sigma_{n-1}, y^{n-1}) + \mathrm{V}(y_n, \sigma_{n-1}, b_n)] + \log \mathrm{p}(b_n) \qquad (18)$$

Note that recursive application of (18) for each state $\sigma_n$ while keeping path history of the best sequence $\hat{b}^{n-K+1}(\sigma_n)$ leading to state $\sigma_n$ would yield maximum likelihood hard decisions for the composite data sequence $b^N$. Let $b^N_{N-i} = b_1, \ldots, b_{N-i-1}, b_{N-i+1}, \ldots, b_N$, then note that:

$$\mathrm{p}\left(\sigma_N, b^{N-K+1} = \hat{b}^{N-K+1}(\sigma_N), r^N(t)\right) = \mathrm{C}\exp[m(\sigma_N, y^N)], \text{ and}$$

$$\mathrm{p}\left(\sigma_N, b^{N-K+1}_{N-i} = \hat{b}^{N-K+1}_{N-i}(\sigma_N), b_{N-i} = b, r^N(t)\right) = \mathrm{C}\exp[m_i(\sigma_N, b, y^N)].$$

The SSOME(L) algorithm consists of these steps: For each iteration $n$ $(n = 1, 2, \ldots, N)$, recursively compute and store the state metrics given by (18). For each state $\sigma_n$ keep the best path comprising of the latest $L-K+1$ hard decisions $\underline{\hat{b}}(\sigma_n)$ leading to state $\sigma_n$ as in the Viterbi algorithm. For each $n \ge K$, recursively update and store the path metrics given by (17) for $i = K-1, K, \ldots, L$ and $b \ne \hat{b}_{n-i}(\sigma_n)$ (Note that $m_i(\sigma_n, \hat{b}_{n-i}(\sigma_n), y^n) = m(\sigma_n, y^n)$, so there is no need to store it separately). For each $n > L$ and $b \in \{u_1, u_2, \ldots, u_M\}$, approximate symbol APP's as:

$$\mathrm{p}(b_{n-L} = b | r^n(t)) = \frac{\sum_{\sigma_n} \exp[m_L(\sigma_n, b, y^n)]}{\sum_{\sigma_n, b} \exp[m_L(\sigma_n, b, y^n)]} \qquad (19)$$

The above recursion is similar to that of SSA [1], except the latter estimates symbol APP's by:

$$\mathrm{p}(b_{n-L} = b | r^n(t)) = \frac{\exp[m_L(\sigma_n^*, b, y^n)]}{\sum_b \exp[m_L(\sigma_n^*, b, y^n)]}$$

where $\hat{\sigma_n^*} = \mathrm{argmax}_{m(\sigma_n, y^n)}$. We will call this scheme SSOME1(L).

## 2.3 Modified BCDFE

In this section, we modify the BCDFE algorithm of [3] and apply it to the multiuser channel. The sampled matched filter output given by (3) can also be expressed as [6]

$$y_i = \sum_{j=i-K+1}^{i+K-1} b_j \sqrt{w_{\kappa(j)}} H_{\kappa(i),\kappa(j)}(\eta(i) - \eta(j)) + n_i \qquad (20)$$

where the Gaussian noise samples $n_i$ are correlated with $E[n_i n_j] = \frac{N_0}{2} H_{\kappa(i),\kappa(j)}(\eta(i) - \eta(j))$. A noise whitening filter can be used [7] to make the statistic uncorrelated (while maintaining its sufficiency for estimating the transmitted data sequence), to get

$$z_i = \sum_{j=i}^{i-K+1} b_j \sqrt{w_{\kappa(j)}} F_{i,j} + n_i' \qquad (21)$$

where $\{z_i\}_{i=1}^N$ is the whitened statistic, $F_{i,j}$ are stable coefficients obtained from the factorization of matrix $G$ [7] and $E[n_i' n_j'] = \frac{N_0}{2}$. Hereafter we assume that $F_{i,j}$ can be perfectly estimated prior to demodulation. Note that given $b_n, b_{n-1}, \ldots, b_{n-K+1}$, $\{z_i\}_{i=1}^N$ is a sequence of i.i.d. Gaussian random variables with mean $\sum_{j=i}^{i-K+1} b_j \sqrt{w_{\kappa(j)}} F_{i,j}$ and variance $\frac{N_0}{2}$.

Consider the receiver of Fig.1 with the "matched filter bank" (giving out $y_i$) replaced by a "whitened matched filter" (giving out $z_i$). Let $z^n = z_1, z_2, \ldots, z_n$, $\beta_n = b_n, b_{n-1}, \ldots, b_{n-J+1}$ where $1 \le J \le K-1$ and $L \ge K-1$. The modified BCDFE algorithm recursively computes and

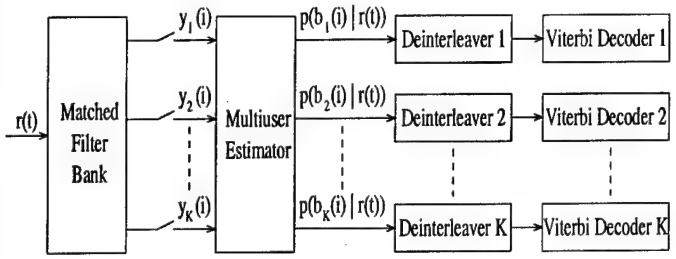


Figure 1: Receiver for an asynchronous CDMA system.

## 2 System Model

Consider a Gaussian CDMA channel shared by $K$ users who transmit (after coding and interleaving) independent data streams by modulating assigned signal waveforms. The received signal $r(t)$ is the sum of $K$ delayed signals and an additive WGN process $n(t)$ with power spectral density $N_0/2$

$$r(t) = \sum_{j=0}^{N'} \sum_{k=1}^{K} b_k(j)\sqrt{w_k} s_k(t - jT - \tau_k) + n(t),\ t \in \mathbf{R} \quad (1)$$

where

$$s_k(t) = \sqrt{2} a_k(t) \cos(\omega_c t + \theta_k)$$

$b_k(j)$ is the $(j+1)$th data bit of user $k$ ($b_k(j) \in \{u_1, u_2, \ldots, u_M\}$, a finite alphabet). $s_k(t)$ is the waveform transmitted by user $k$ during a $T$-second bit interval. $a_k(t)$, $\tau_k$, $\theta_k$ and $w_k$ are respectively the normalized spreading sequence, the time delay, the carrier phase and the symbol power of user $k$. $\omega_c$ is the carrier frequency. Equation(1) can also be expressed as

$$r(t) = \sum_{i=1}^{N} b_{\kappa(i)}(\eta(i))\sqrt{w_{\kappa(i)}} s_{\kappa(i)}\left(t - \eta(i)T - \tau_{\kappa(i)}\right) + n(t) \quad (2)$$

In the above equation, $i = K\eta(i) + \kappa(i) - 1$, $\kappa(i) - 1$ is the remainder of $i$ mod $K$, $\eta(i)$ is the integer part of $i/K$, and $N = (N'+1)K$ is the composite message length of $K$ users. The composite data sequence $\{b_{\kappa(i)}(\eta(i))\}_{i=1}^{N}$ is to be estimated upon observing the received signal $r(t)$.

The receiver structure is shown in Fig.1. We assume that the receiver is able to estimate perfectly the signal powers, the time delays and the phase lags of all users prior to demodulation. Also assume without loss of generality, that the time delays of users are in increasing order. The matched filter output of user $\kappa(i)$ at time $\eta(i)$ is

$$y_{\kappa(i)}(\eta(i)) = \int_{-\infty}^{\infty} s_{\kappa(i)}\left(t - \eta(i)T - \tau_{\kappa(i)}\right) r(t) dt,\quad i = 1, 2, \ldots, N \quad (3)$$

For notational brevity let $b^N = \{b_i\}_1^N = \{b_{\kappa(i)}(\eta(i))\}_{i=1}^N$, $y^N = \{y_i\}_1^N = \{y_{\kappa(i)}(\eta(i))\}_{i=1}^N$ and $r^N(t) = \{r(t), t \in [\tau_{\kappa(1)}, \eta(N)T + \tau_{\kappa(N)}]\}$. It has been shown [5] that

$$\mathrm{p}(r^N(t)|b^N) = \mathrm{C} \exp[\mathrm{U}(y^N, b^N)/N_0]$$

where C is a positive scalar independent of $b^N$ and

$$\mathrm{U}(y^N, b^N) = \sum_{i=1}^{N} b_i \sqrt{w_{\kappa(i)}} \left[2y_i - b_i\sqrt{w_{\kappa(i)}} - 2\sum_{j=1}^{K-1} b_{i-j}\sqrt{w_{\kappa(i-j)}} G_{K-j,\kappa(i)}\right] \quad (4)$$

where $b_i = 0$ for $i \le 0$ and $i > N$, and

$$G'_{i,j} = \begin{cases} H_{i+j,j}(-1) & \text{if } i+j \le K \\ H_{i+j-K,j}(0) & \text{if } i+j > K \end{cases} \quad (5)$$

$$H_{\kappa(i),\kappa(j)}(m) = \int_{-\infty}^{\infty} s_{\kappa(i)}\left(t - \tau_{\kappa(i)}\right) s_{\kappa(j)}\left(t + mT - \tau_{\kappa(j)}\right) dt, \quad (6)$$

for $i, j = 1, 2, \ldots, K$.

### 2.1 OSOME

In this section, we determine a recursion for $\mathrm{p}(b_i|r^N(t))$. Let $\sigma_N = b_N, b_{N-1}, \ldots, b_{N-K+2}$, then (4) can be written as

$$\mathrm{U}(y^N, b^N) = \mathrm{U}(y^{N-1}, b^{N-1}) + \mathrm{V}(y_N, \sigma_{N-1}, b_N) \quad (7)$$

where

$$\mathrm{V}(y_N, \sigma_{N-1}, b_N) = b_N\sqrt{w_{\kappa(N)}} \left[2y_N - b_N\sqrt{w_{\kappa(N)}} - 2\sum_{j=1}^{K-1} b_{N-j}\sqrt{w_{\kappa(N-j)}} G_{K-j,\kappa(N)}\right] \quad (8)$$

For $n = 1, 2, \ldots, N$, define:

$$f(\sigma_n, y^n) \triangleq \sum_{b^{n-K+1}} \exp[\mathrm{U}(y^n, b^n)/N_0]\mathrm{p}(b^n), \quad (9)$$

$$f_i(\sigma_n, b, y^n) \triangleq \sum_{b^{n-K+1}, b_{n-i}=b} \exp[\mathrm{U}(y^n, b^n)/N_0]\mathrm{p}(b^n), \quad \text{for } K-1 \le i \le n-1. \quad (10)$$

Now

$$\begin{aligned} & f_i(\sigma_n, b, y^n) \\ &= \sum_{b^{n-K+1}, b_{n-i}=b} \exp[\mathrm{V}(y_n, \sigma_{n-1}, b_n)] \\ &\quad \cdot \exp[\mathrm{U}(y^{n-1}, b^{n-1})/N_0]\mathrm{p}(b^n) \\ &= \sum_{b_{n-K+1}, b_{n-i}=b} \exp[\mathrm{V}(y_n, \sigma_{n-1}, b_n)]\mathrm{p}(b_n) \\ &\quad \cdot \sum_{b^{n-K}, b_{n-i}=b} \exp[\mathrm{U}(y^{n-1}, b^{n-1})/N_0]\mathrm{p}(b^{n-1}) \\ &= \sum_{b_{n-K+1}, b_{n-i}=b} \exp[\mathrm{V}(y_n, \sigma_{n-1}, b_n)]\mathrm{p}(b_n) \\ &\quad \cdot f_i(\sigma_{n-1}, b, y^{n-1}) \end{aligned} \quad (11)$$

Where the first equality follows from (7) and the second one follows from the assumption that $\{b_i\}_{i=1}^N$ are independent and the fact that $\mathrm{V}(y_n, \sigma_{n-1}, b_n)$ does not depend on $b^{n-K}$. From (11), it follows that

$$f(\sigma_n, y^n) = \sum_{b_{n-K+1}} \exp[\mathrm{V}(y_n, \sigma_{n-1}, b_n)]\mathrm{p}(b_n) f(\sigma_{n-1}, y^{n-1}) \quad (12)$$

not WBE signal sets, they do not enjoy the properties described in Proposition 19 except in an average sense – a situation that is similar to that discussed in Proposition 15. For any given $i$, there are $\binom{K-1}{L-1}$ subsets of size $L$ that include $x^{(i)}$. Any other $x^{(k)}$ belongs to $\binom{K-2}{L-2}$ of these subsets. Hence, (23) and (24) imply that the following result holds:

**Proposition 20.** *For any signal $x^{(i)}$ in a WBE signal set $\mathcal{X}$ satisfying the hypotheses of Proposition 19, and any $L$, $2 \leq L \leq K$, there exists a $\mathcal{Y} \subset \mathcal{X}$ of size $L$ such that $x^{(i)} \in \mathcal{Y}$ and*

$$R_i \leq 2(L-1)N^2 - \frac{L-1}{K-1}\left(2N^2 - 2N\right)$$

$$r_i \leq 2(L-1)N^2 - \frac{L-1}{K-1}\left(N^2 + N - 2\right)$$

The right sides of the above inequalities are just $(L-1)/(K-1)$ times the right sides of (23) and (24). In fact, these quantities are respectively the average values of $R_i$ and the bound on $r_i$ over all subsets of $\mathcal{X}$ that contain $x^{(i)}$ and $L-1$ other signals. Note that the values obtained are smaller than $2(L-1)N^2$ but the improvement over random sequences is not as much as with the full WBE signal set. Unfortunately, although the $i$-th signal is guaranteed to achieve a good SNR, the other signals in the set do not necessarily also achieve a good SNR. In contrast, for a WBE signal set, *all* the $K$ signals achieve values of $R_i$ smaller than $2(K-1)N^2$. Note that Sun and Leib [28] have proved a slightly different version of Proposition 20. Their result is that, averaged over all subsets $\mathcal{Y} \subset \mathcal{A}^-$ of size $L$, the value of $\bar{r}(\mathcal{Y})$ is bounded by $(L-1)/(K-1)$ times the right side of (24), just as in Proposition 20 above. It is easily shown that the Sun-Leib result also holds for the class of WBE signals described in Proposition 19.

## 5 Concluding Remarks

Signal sets that meet the Welch bounds on the maximum magnitude of the inner product or the correlation functions are not easy to find. In contrast, finding signal sets that meet the Welch bounds on the RMS magnitudes is almost trivially easy – *almost all* linear codes (and their cosets) meet the latter bounds, with rates and minimum distances hardly being of any concern. Thus, meeting the Welch bound on the RMS magnitudes is far too broad a criterion for signal design, and the traditional measures for signal performance should not be discarded. The recent interest in proving various information-theoretic results via the use of WBE signal sets is also somewhat puzzling. It would seem that almost any result which holds only when the signals form a WBE signal set could have been proved long ago since (at least in terms of mean-square Hamming weights) it has been known for nearly forty years that most binary linear codes are WBE signal sets! Finally, it is worth re-emphasizing that subsets of WBE signal sets usually are not WBE signal sets, and thus, careful analysis is needed to determine the performance of systems that use WBE signal sets.

## 6 Acknowledgments

This research was supported in part by the Joint Services Electronics Program under Grant N00014-90-J-1270, and in part by the U. S. Army Research Office under Focused Research Initiative Grant DAAH01-95-1-0216.

## References

1. W. O. Alltop, "Complex sequences with low periodic correlations," *IEEE Trans. Inform. Theory*, vol. IT-26, pp. 350–354, May 1980.
2. I. F. Blake and R. C. Mullin, *The Mathematical Theory of Coding*, New York: Academic Press, 1975.
3. S. Boztaş, R. Hammons, and P. V. Kumar, "4-phase sequences with near-optimum correlation properties," *IEEE Trans. Inform. Theory*, vol. 38, pp. 1101-1113, May 1992.
4. H. Fukumasa, R. Kohno, and H. Imai, "Design of pseudonoise sequences with good odd and even correlation properties for DS/CDMA," *IEEE J. Selected Areas Commun.*, vol. 12, pp. 828-836, June 1994.
5. M. J. E. Golay, "Complementary series," *IRE Trans. Inform. Theory*, vol. IT-7, pp. 82-87, April 1961.
6. A. R. Hammons, Jr., P. V. Kumar, A. R. Calderbamk. N. J. A. Sloane, and P. Solé, "The $Z_4$ linearity of Kerdock, Preparata, Goethals, and related codes," *IEEE Trans. Inform. Theory*, vol. 40, pp. 301-319, March 1994.
7. T. Helleseth and P. V. Kumar, "Pseudonoise sequences," in *The Communications Handbook*, J. D. Gibson (ed.), Piscataway, NJ: IEEE Press, 1997.
8. T. Helleseth and P. V. Kumar, "Sequences with low correlation," in *Handbook of Coding Theory*, V. Pless (ed.), Elsevier Press (1998).
9. S. M. Krone and D. V. Sarwate, "Quadriphase sequences for spread-spectrum multiple-access communication," *IEEE Trans. Inform. Theory*, vol. IT-30, pp. 520-529, May 1984.
10. P. V. Kumar and C.-M. Liu, "On lower bounds to the maximum correlation of complex, roots-of-unity sequences," *IEEE Trans. Inform. Theory*, vol. 36, pp. 633-640, May 1990.
11. V. I. Levenshtein, "Bounds on the maximum cardinality of a code with bounded modulus of the inner product," *Soviet Math. Dokl.*, vol. 25, pp. 526-531, 1982.
12. F. J. MacWilliams and N. J. A. Sloane, "Pseudorandom sequences and arrays," *Proc. IEEE*, vol. 64, pp. 1715-1729, December 1976.
13. F. J. MacWilliams and N. J. A. Sloane, *Theory of Error Correcting Codes*. Amsterdam: North Holland, 1977.
14. J. L. Massey and T. Mittelholzer, "Welch's bound and sequence sets for code-division multiple-access systems," in *Sequences II: Methods in Communication, Security, and Computer Science*, R. Capocelli, A. De Santis, and U. Vaccaro, (eds.), pp. 63-78, New York: Springer-Verlag, 1993.
15. W. H. Mow, "On the bounds on odd correlation of periodic sequences," *IEEE Trans. Inform. Theory*, vol. 40, pp. 954-955, May 1994.
16. W. H. Mow, "Optimal sequence sets meeting Welch's lower bound," *Proc. 1995 IEEE Int'l. Symp. Inform. Theory*, (Whistler, Canada: September 17–22, 1995) p. 89.

17. M. B. Pursley, "Performance evaluation for phase-coded spread-spectrum multiple-access communication – Part I: System analysis," *IEEE Trans. Commun.*, vol. COM-25, pp. 795-799, August 1977.
18. M. B. Pursley and D. V. Sarwate, "Evaluation of correlation parameters for periodic sequences," *IEEE Trans. Inform. Theory*, vol. IT-23, pp. 508-513, July 1977.
19. M. B. Pursley and D. V. Sarwate, "Performance evaluation for phase-coded spread-spectrum multiple-access communication – Part II: Code sequence analysis," *IEEE Trans. Commun.*, vol. COM-25, pp. 800-803, August 1977.
20. M. Rupf and J. L. Massey, "Optimum sequence multisets for synchronous code-division multiple-access channels," *IEEE Trans. Inform. Theory*, vol. 40, pp. 1261–1266, July 1994.
21. D. V. Sarwate, "Bounds on crosscorrelation and autocorrelation of sequences," *IEEE Trans. Inform. Theory*, vol. IT-25, pp. 720–724, November 1979.
22. D. V. Sarwate, "Sets of complementary sequences," *Electronics Letters*, vol. 19, pp. 711-712, September 1983.
23. D. V. Sarwate, "Mean-square correlation of shift register sequences," *IEE Proceedings*, vol. 131, Part F, pp. 101–106, April 1984.
24. D. V. Sarwate and M. B. Pursley, "Crosscorrelation properties of pseudorandom and related sequences," *Proc. IEEE*, vol. 68, pp. 593–619, May 1980.
25. H. D. Schotten, "Mean-square correlation parameters of code sequences in DS-CDMA systems," *Proc. 1997 IEEE Int'l. Symp. Inform. Theory*, (Ulm, Germany: June 29–July 4, 1997), p. 486.
26. V. M. Sidelnikov, "On mutual correlation of sequences," *Soviet Math. Dokl.*, vol. 12, pp. 197-201, 1971.
27. S. G. S. Shiva, "Some results on binary codes with equidistant words," *IEEE Trans. Inform. Theory*, vol. IT-15, pp. 328-329, March 1969.
28. F.-W. Sun and H. Leib, "Optimal phases for a family of quadriphase CDMA sequences," *IEEE Trans. Inform. Theory*, vol. 43, pp. 1205-1217, July 1997.
29. Y. Taki, H. Miyakawa, M. Hatori, and S. Namba, "Even-shift orthogonal sequences," *IEEE Trans. Inform. Theory*, vol. IT-15, pp. 295-300, March 1969.
30. C.-C. Tseng and C. L. Liu, "Complementary sets of sequences," *IEEE Trans. Inform. Theory*, vol. IT-18, pp. 644-652, September 1972.
31. P. Viswanath, V. Anantharam, and D. Tse, "Optimal sequences, power control and capacity of synchronous CDMA systems with linear multiuser receivers," *Proc. 1998 IEEE Inform. Theory Workshop*, (Killarney, Ireland: June 22-26, 1998), pp. 134-135.
32. P. Viswanath and V. Anantharam, "Optimal sequences and sum capacity of synchronous CDMA systems," *Proceedings of the 36th Allerton Conference on Communication, Control, and Computing*, (Monticello, Illinois: September 23-25, 1998), pp. 272-281.
33. L. R. Welch, "Lower bounds on the maximum cross correlation of signals," *IEEE Trans. Inform. Theory*, vol. IT-20, pp. 397-399, May 1974.
34. N. Zierler, "A note on the mean square weight for group codes," *Information and Control*, vol. 5, pp. 87-89, January 1962.

# A Linear Receiver for Direct-Sequence Spread-Spectrum Multiple-Access Systems with Antenna Arrays and Blind Adaptation

Tan F. Wong, Tat M. Lok, *Member, IEEE*, James S. Lehnert, *Senior Member, IEEE*, and Michael D. Zoltowski, *Senior Member, IEEE*

***Abstract*— A linear receiver for direct-sequence spread-spectrum multiple-access communication systems under the aperiodic random sequence model is considered. The receiver consists of the conventional matched filter followed by a tapped delay line with the provision of incorporating the use of antenna arrays. It has the ability of suppressing multiple-access interference (MAI) and narrowband interference in some weighted proportions, as well as combining multipath components without explicit estimation of any channel conditions. Under some specific simplified channel models, the receiver reduces to the minimum variance distortionless response beamformer, the RAKE receiver, a notch filter, or an MAI suppressor. The interference rejection capability is made possible through a suitable choice of weights in the tapped delay line. The optimal weights can be obtained by straightforward but computationally complex eigenanalysis. In order to reduce the computational complexity, a simple blind adaptive algorithm is also developed.**

***Index Terms*—Adaptive signal detection, antenna arrays, code-division multiaccess, interference suppression, pseudonoise-coded communication.**

## I. Introduction

MANY researchers have investigated receiving structures to suppress interference, especially multiple-access interference (MAI), in direct-sequence spread-spectrum multiple-access (DS/SSMA) systems. Verdú [1] worked out the optimum multiuser detector, which is near–far resistant, for DS/SSMA systems over additive white Gaussian noise (AWGN) channels. Lupas and Verdú [2] considered simpler linear receivers to reject MAI. Roughly speaking, the main working principle of these receivers is to project the signature sequence of the desired user onto the space orthogonal to the signature sequences of the interferers. Other MAI rejection receivers based on the minimum mean-squared error (MMSE) criterion are also developed in [3]–[7] (see [13] for a survey of the literature). They are adaptive in nature by making use of the cyclostationarity of the received signal. Recently, Honig *et al.* [8] proposed a blind adaptive linear receiver which eliminated the need for training sequences as in [3]–[7]. Another way to suppress MAI is to explore the spatial relationship between a user and the interferers and to utilize the steering capability of an antenna array. Kohno, *et al.* [9], [10], and Naguib, *et al.* [11], [12] worked in this direction. Kohno [9] also suggested a combination of spatial processing techniques and some of the MAI rejection structures described above.

In most of these papers, the MAI suppression schemes are developed under the periodic sequence assumption, in which the signature sequences employed to spectrally spread the data sequences are periodic with period equal to a data symbol duration. This assumption differs significantly from the IS-95 standard [16] in which signature sequences with much longer periods are employed. With sequences having long periods, the receiver considered in [1] is too complex for practical implementations. The decorrelator receiver in [2] would also have to be modified in every symbol period. Hence, its applicability is also limited. Moreover, as the cyclostationarity assumption in [3]–[8] may not hold any more, the adaptive receivers in [3]–[8] may not be capable of rejecting MAI with the use of long signature sequences. On the other hand, the efficacy of the spatial processing techniques should remain provided the interferers and the desired user are not clustered spatially. The challenge, however, is to develop a receiving structure which can effectively employ spatial processing techniques to reject MAI with the use of long signature sequences.

To facilitate such a development, we consider in this paper DS/SSMA systems with aperiodic signature sequences. As the sequences are aperiodic, it is reasonable to model each element of them to be an independent random variable. Hence, we adopt the aperiodic random sequence model which provides a good approximation to the long signature sequences employed in practical systems. We consider a decentralized linear receiver composed of the conventional matched filter (despreader) followed by a tapped delay line (TDL) with the provision of incorporating the use of antenna arrays. We point out that the observables in the proposed receiving structure are the output samples (possibly faster than the chip rate) from the despreader. This distinguishes this work from many others ([4]–[8]) in which the observables are outputs from the chip-matched filter. Details of the receiving structure and the channel model are given in Section II. We note that an approximate decorrelating multiuser detector, which is

Manuscript received February 1, 1996; revised September 9, 1997. This material is based upon work supported by the U. S. Army Research Office under Grant DAAH04-95-1-0246. The material in this paper was presented in part at the IEEE Military Communications Conference (MILCOM '96), McLean, VA, October 21–24, 1996.

The authors are with the School of Electrical and Computer Engineering, Purdue University, West Lafayette, IN 47907-1285 USA.

Publisher Item Identifier S 0018-9448(98)00657-9.

applicable to systems with long signature sequences, is also developed in [15]. The major difference between this work and [15] is that the receiver in [15] is centralized, and is developed under the deterministic sequence model.

The weights in the TDL are chosen to maximize the signal-to-noise ratio (SNR), which is defined in Section IV. Optimal choices under the minimum mean square error (MMSE) and the constrained minimum output energy (CMOE) criteria are also considered. In fact, we show in Section IV that the three criteria are asymptotically equivalent when the number of chips per symbol $N$ approaches infinity. The performance of the receiver is examined for a multipath fading channel with MAI, narrowband interference, and AWGN. It turns out that the proposed receiver has the ability of suppressing MAI and narrowband interference in some weighted proportions, as well as combining multipath components simultaneously. It actually unifies the minimum variance distortionless response (MVDR) beamformer, the RAKE receiver, a notch filter, and an MAI suppressor. As shown in Section V, it reduces to these structures under simplified channel models.

In the development of Sections IV and V, there is a certain parallelism between the MMSE-based receivers in [3]–[8] and the receiver proposed in this paper. Although this parallelism might lead to similar properties and practical implications, it cannot be obtained as a direct consequence from the results derived in [3]–[8] since the structures of the receivers and the underlying system models are different in our case. In order to establish the results in Sections IV and V, we need two important asymptotic properties of the despread received signal at output of the matched filter which are derived in Section III. The first property is that the despread received signal is cyclostationary, and the second one is that the correlation matrix of the desired signal component is of rank one. These two properties form the basis of most of the work developed in this paper.

Sections VI and VII address the implementation issues. In Section VI, we see that optimal weights under the maximum SNR criterion can be obtained by straightforward eigenanalysis. In practice, we do not have prior knowledge of the channel parameters. Based on the asymptotic properties of the despread received signal, we develop a simple method to estimate and optimize the SNR simultaneously from two different observations of the despread received signal, namely, a signal-plus-interference observation and an interference-only observation. In [11] and [12], Naguib *et al.* employed a similar approach by using the spread and despread received signals to estimate the SNR. However, that approach does not work under the asynchronous model considered in this paper. The eigenanalysis algorithms are computationally complex for time-varying channels. Because of the cyclostationarity of the despread received signal, it is possible to construct adaptive algorithms to obtain the weights in the TDL. Based on the CMOE, we develop a computationally simple blind adaptive algorithm for the optimization to eliminate the need for training sequences.

Using the blind adaptive algorithm developed in Section VII, the proposed receiver requires the same amount of information as the conventional matched filter receiver, namely, the signature sequence and the synchronization information (the timing and the carrier phase) of the desired user. The receiver is decentralized in nature, i.e., each receiver works independently for a single user. The proposed receiving structure is useful in both the base station and the mobile units in wireless DS/SSMA systems because it is decentralized and can reject interference with a single algorithm. Note that even if only a single element antenna is used in a mobile unit due to physical constraints, the proposed receiver still combats narrowband interference and combines multipath components.

## II. System Model

In this section, we describe the model of the DS/SSMA system. We assume that there are $K$ simultaneous users in the system.

The $k$th user, for $1 \le k \le K$, generates a data sequence

$$b^{(k)} = (\cdots, b_0^{(k)}, b_1^{(k)}, \cdots, b_{N-1}^{(k)}, \cdots)$$

with a symbol duration of $T$ seconds. We assume that the data symbols $b_j^{(k)}$ are random variables with $E[|b_j^{(k)}|^2] = 1$. Note that this assumption is satisfied, apart from a trivial scaling factor, by almost all coded and uncoded data symbols.

The $k$th user is provided a randomly generated signature sequence

$$a^{(k)} = (\cdots, a_0^{(k)}, a_1^{(k)}, \cdots, a_{N-1}^{(k)}, \cdots).$$

The elements $a_i^{(k)}$ are independent random variables such that $E[a_i^{(k)}] = 0$ and

$$E[|a_i^{(k)}|^2] = |E[a_i^{(k)2}]|^2 = E[|a_i^{(k)}|^4] = 1.$$

The sequence $a^{(k)}$ is used to spectrally spread the data symbols to form the signal

$$a_k(t) = \sum_{i=-\infty}^{\infty} b_{\lfloor i/N \rfloor}^{(k)} a_i^{(k)} \psi(t - iT_c) \tag{1}$$

where the chip duration $T_c$ is given by $T_c = T/N$, $N$ is the number of chips per symbol interval, and $\psi(t)$ is the common chip waveform for all signals. The chip waveform $\psi(t)$ is time-limited to the interval $[0, T_c]$, and normalized so that

$$\int_0^{T_c} |\psi(t)|^2 dt = T_c.$$

The transmitted signal for the $k$th user, for $1 \le k \le K$, can be expressed as

$$\mathrm{Re}\left[\sqrt{2P_k} a_k(t - T_k) \exp\left(j\omega_c(t - T_k)\right)\right] \tag{2}$$

where $P_k$ is the power for the $k$th signal, $\omega_c$ is the carrier frequency, and $T_k$ is the delay that models the asynchronous system.

Without loss of generality, throughout the paper we will consider the signal from the first user as the communicating signal and the signals from all other users as interfering signals.

We now describe the channel model. We assume that the channel is a multipath fading channel corrupted by narrowband interferers as well as AWGN with two-sided power spectral

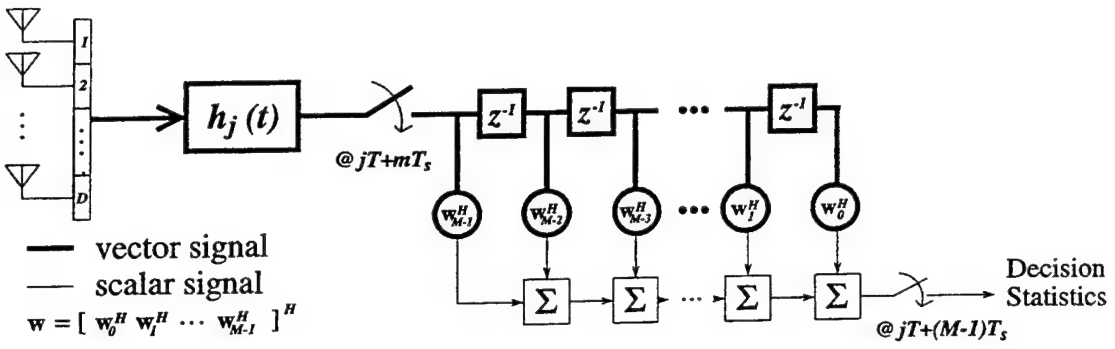


Fig. 1. Linear receiver for the $j$th data symbol.

density $N_0/2$. We assume that there are $K_B$ narrowband interferers. Each narrowband interfering signal is assumed to be a pure tone.

We assume that the signals are received by an antenna array of $D$ elements. The signal vector received by the antenna array in complex baseband notation is given by

$$\boldsymbol{r}(t) = \boldsymbol{y}(t) + \boldsymbol{n}_I(t) + \boldsymbol{n}_B(t) + \boldsymbol{n}_W(t) \tag{3}$$

where $\boldsymbol{n}_W(t)$ represents AWGN. We assume that the AWGN is also spatially white. The signal contribution $\boldsymbol{y}(t)$ is given by

$$\boldsymbol{y}(t) = \sqrt{2P_1}\sum_{\lambda=1}^{L_1} g_{1,\lambda}a_1(t - T_1 - \tau_{1,\lambda})e^{-j\omega_c(T_1+\tau_{1,\lambda})}\boldsymbol{d}_{1,\lambda}. \tag{4}$$

The MAI contribution $\boldsymbol{n}_I(t)$ is given by

$$\boldsymbol{n}_I(t) = \sum_{k=2}^{K}\sqrt{2P_k}\sum_{\lambda=1}^{L_k} g_{k,\lambda}a_k(t - T_k - \tau_{k,\lambda}) \cdot e^{-j\omega_c(T_k+\tau_{k,\lambda})}\boldsymbol{d}_{k,\lambda}. \tag{5}$$

The narrowband interference contribution $\boldsymbol{n}_B(t)$ is given by

$$\boldsymbol{n}_B(t) = \sum_{k=K+1}^{K+K_B}\sqrt{2P_k}g_k e^{j\delta_k t}\boldsymbol{d}_k. \tag{6}$$

In (4) and (5), $L_k$ is the number of propagation paths from the $k$th transmitter to the antenna array. The parameters $\tau_{k,\lambda}$, $g_{k,\lambda}$, and $\boldsymbol{d}_{k,\lambda}$ represent the delay, the complex gain, and the array response vector associated with the $\lambda$th path of the signal from the $k$th transmitter. In (6), the parameters $P_k$, $g_k$, $\delta_k$, and $\boldsymbol{d}_k$ represent the power, the complex gain, the frequency deviation from $\omega_c$, and the array response vector associated with the tone indexed by $k$ for $K+1 \le k \le K+K_B$. Without loss of generality, we assume that $\delta_k \neq \delta_l$ for $k \neq l$.

To facilitate the derivation of the receiver, we assume that the communication channel is time-invariant. In particular, the number, the powers, the frequencies (for narrowband interferers), the locations, and the delay profiles of the users and the interferers are fixed (but unknown). Only the data, the signature sequences, and the AWGN are random. It turns out that the resulting receiver is able to adapt quickly. Therefore, such an assumption does not affect the usefulness of the receiver.

We assume that we have achieved synchronization with the path of the signal from the desired user that arrives earliest at the antenna array. Hence, we may assume $T_1 = 0, \tau_{1,1} = 0$, and $\tau_{1,\lambda} > 0$ for $2 \le \lambda \le L_1$. We also assume that $\tau_{1,\lambda} \le \tau_{\max}$ for all $\lambda$ where $\tau_{\max}$ is the maximum delay spread of the channel. For coherent detection, we may assume the phase angle of $g_{1,1}$ and that of the first element of the array response vector $\boldsymbol{d}_{1,1}$ to be zero.

The receiver is shown in Fig. 1. To detect the $j$th symbol $b_j^{(1)}$, the received signal $\boldsymbol{r}(t)$ is passed through a matched filter with impulse response $h_j(t)$ where

$$h_j(t) = \sum_{i=0}^{N-1} a_{i+jN}^{(1)*}\psi^*(-t - iT_c). \tag{7}$$

The despread received signal at the output of the matched filter $\tilde{\boldsymbol{r}}_j(t)$ is sampled once every $T_s$ seconds to give a sample vector of length $D$, where $T_c/T_s = S$ is the number of sample vectors per chip interval. Note that for simplicity in notation, the matched filter in (7) is set to be noncausal. To get a causal matched filter, we can simply delay the impulse response of the filter described by (7). Consequently, we have to delay the sampling by the same amount of time. If $S$ is an integer, we have the equivalent multirate implementation of the matched filter as shown in Fig. 2. Since $\tau_{1,\lambda} \le \tau_{\max}$ for all $\lambda$, only the first $M = \lceil(\tau_{\max} + T_c)/T_s\rceil$ sample vectors in the $j$th symbol interval contain significant contributions from the signal of the desired user. The $M$ sample vectors $\tilde{\boldsymbol{r}}_j(jT), \tilde{\boldsymbol{r}}_j(jT+T_s), \cdots, \tilde{\boldsymbol{r}}_j(jT+(M-1)T_s)$ are concatenated to give the vector $\boldsymbol{v}_j$ of length $MD$.

Finally, the decision statistic for the $j$th symbol interval is formed by $\boldsymbol{w}^H\boldsymbol{v}_j$, where $\boldsymbol{w}$ is a weight vector whose components remain to be determined. Notice that there is a complex scaling introduced by the weight vector in the decision statistics. However, such a scaling is immaterial if differential encoding is applied.

In order to facilitate the process of optimizing the weight vector, a counterpart of $\boldsymbol{v}_j$ that contains *mainly* noise and interference contributions is needed. More precisely, we pick an integer $M'$ such that $M'T_c > MT_s$. The $M$ sample vectors

$$\tilde{\boldsymbol{r}}_j(jT + M'T_c), \tilde{\boldsymbol{r}}_j(jT + M'T_c + T_s), \cdots, \tilde{\boldsymbol{r}}_j(jT + M'T_c + (M-1)T_s)$$

are taken and concatenated to give the vector $\hat{\boldsymbol{v}}_j$ of length $MD$. Note that the timing difference between each element of $\hat{\boldsymbol{v}}_j$ and the corresponding element of $\boldsymbol{v}_j$ is $M'T_c$, an integral multiple of the chip duration.

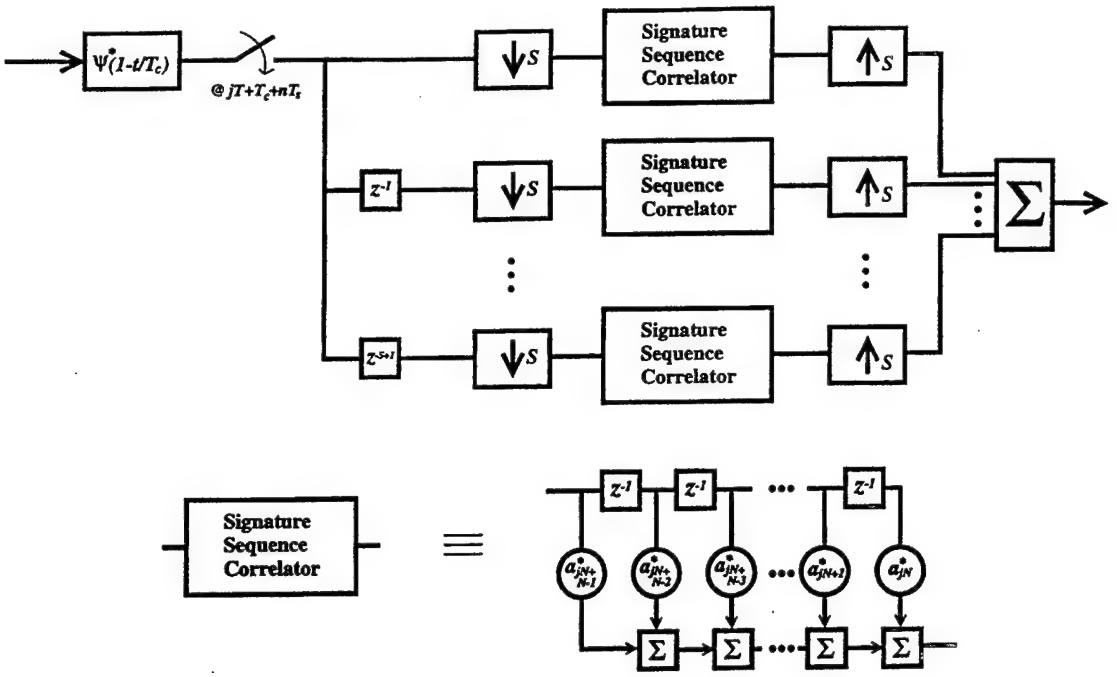


Fig. 2. Equivalent multirate implementation of the matched filter.

In developing the above sampling scheme, we have assumed that the maximum delay spread of the channel $\tau_{\max}$ cannot be larger than several $T_c$, which is typical in most wireless cellular systems employing DS/SSMA. Otherwise, the size of the sample vectors could be large. If $\tau_{\max}$ is, indeed, large, other sampling schemes might be used to reduce the size of the sample vectors. For example, we can estimate the arrival times of the paths and sample only at those instances.

## III. Correlation Properties

In this section, we consider the correlation properties of the samples of despread received signal at the output of the matched filter. Without loss of generality, we consider the samples associated with the detection of the symbol $b_0^{(1)}$.

The despread signal at the output of the matched filter $\tilde{\boldsymbol{r}}_0(t)$, for $t \geq 0$, is given by

$$\tilde{\boldsymbol{r}}_0(t) = \tilde{\boldsymbol{y}}(t) + \tilde{\boldsymbol{n}}_I(t) + \tilde{\boldsymbol{n}}_B(t) + \tilde{\boldsymbol{n}}_W(t) \tag{8}$$

where $\tilde{\boldsymbol{y}}(t)$, $\tilde{\boldsymbol{n}}_I(t)$, $\tilde{\boldsymbol{n}}_B(t)$, and $\tilde{\boldsymbol{n}}_W(t)$ are the matched filter output due to the desired signal, the MAI, the narrowband interference, and the thermal noise components, respectively. It is easy to see that the random processes $\tilde{\boldsymbol{y}}(t)$, $\tilde{\boldsymbol{n}}_I(t)$, $\tilde{\boldsymbol{n}}_B(t)$, and $\tilde{\boldsymbol{n}}_W(t)$ are uncorrelated. Hence, the correlation matrix $\boldsymbol{R}_{\tilde{\boldsymbol{r}}}(t,s)$ defined as $E[\tilde{\boldsymbol{r}}_0(t)\tilde{\boldsymbol{r}}_0^H(s)]$ is given by

$$\boldsymbol{R}_{\tilde{\boldsymbol{r}}}(t,s) = \boldsymbol{R}_{\tilde{\boldsymbol{y}}}(t,s) + \boldsymbol{R}_{\tilde{\boldsymbol{n}}_I}(t,s) + \boldsymbol{R}_{\tilde{\boldsymbol{n}}_B}(t,s) + \boldsymbol{R}_{\tilde{\boldsymbol{n}}_W}(t,s) \tag{9}$$

where

$$\begin{aligned}\boldsymbol{R}_{\tilde{\boldsymbol{y}}}(t,s) &= E[\tilde{\boldsymbol{y}}(t)\tilde{\boldsymbol{y}}^H(s)] \\ &= 2P_1T^2 \sum_{\lambda=1}^{L_1}\sum_{\nu=1}^{L_1} g_{1,\lambda}g_{1,\nu}^* e^{-j\omega_c(\tau_{1,\lambda}-\tau_{1,\nu})}\, \boldsymbol{d}_{1,\lambda}\, \boldsymbol{d}_{1,\nu}^H \\ &\quad \cdot \left[\hat{\psi}(t-\tau_{1,\lambda})\hat{\psi}^*(s-\tau_{1,\nu}) + \frac{1}{N}\sum_{\substack{i=-\infty \\ i\neq 0}}^{\infty} \right. \\ &\quad \cdot \hat{\psi}(t-iT_c-\tau_{1,\lambda})\hat{\psi}^*(s-iT_c-\tau_{1,\nu}) \\ &\quad + \frac{1}{N}\sum_{\substack{i=-N+1 \\ i\neq 0}}^{N-1} \frac{N-|i|}{N}\hat{\psi}(t+iT_c-\tau_{1,\lambda}) \\ &\quad \left. \cdot \hat{\psi}^*(s-iT_c-\tau_{1,\nu})\right]\end{aligned} \tag{10}$$

$$\begin{aligned}\boldsymbol{R}_{\tilde{\boldsymbol{n}}_I}(t,s) &= E[\tilde{\boldsymbol{n}}_I(t)\tilde{\boldsymbol{n}}_I^H(s)] \\ &= \sum_{k=2}^{K}\frac{2P_kT^2}{N}\sum_{\lambda=1}^{L_k}\sum_{\nu=1}^{L_k} g_{k,\lambda}g_{k,\nu}^* e^{-j\omega_c(\tau_{k,\lambda}-\tau_{k,\nu})} \\ &\quad \cdot \boldsymbol{d}_{k,\lambda}\boldsymbol{d}_{k,\nu}^H \cdot \sum_{i=-\infty}^{\infty}\hat{\psi}(t-iT_c-T_k-\tau_{k,\lambda}) \\ &\quad \cdot \hat{\psi}^*(s-iT_c-T_k-\tau_{k,\nu})\end{aligned} \tag{11}$$

$$\begin{aligned}\boldsymbol{R}_{\tilde{\boldsymbol{n}}_B}(t,s) &= E[\tilde{\boldsymbol{n}}_B(t)\tilde{\boldsymbol{n}}_B^H(s)] \\ &= \sum_{k=K+1}^{K+K_B}\sum_{l=K+1}^{K+K_B}\frac{2\sqrt{P_kP_l}T^2}{N} g_k g_l^* e^{-j(\delta_k t-\delta_l s)} \\ &\quad \cdot \Psi(\delta_k)\Psi^*(\delta_l)\frac{\sin(NT_c(\delta_k-\delta_l)/2)}{N\sin(T_c(\delta_k-\delta_l)/2)} \\ &\quad \cdot e^{-j(N-1)(\delta_k-\delta_l)T_c/2}\, \boldsymbol{d}_k\, \boldsymbol{d}_l^H\end{aligned} \tag{12}$$

and

$$\begin{aligned}\boldsymbol{R}_{\tilde{\boldsymbol{n}}_W}(t,s) &= E[\tilde{\boldsymbol{n}}_W(t)\tilde{\boldsymbol{n}}_W^H(s)] \\ &= N_0T\hat{\psi}(t-s)\boldsymbol{I}_{D\times D}.\end{aligned} \tag{13}$$

$$\begin{bmatrix} R_{\tilde{r}}(0,0) & R_{\tilde{r}}(0,T_s) & \cdots & R_{\tilde{r}}(0,(M-1)T_s) \\ R_{\tilde{r}}(T_s,0) & R_{\tilde{r}}(T_s,T_s) & & \vdots \\ \vdots & & \ddots & \vdots \\ R_{\tilde{r}}((M-1)T_s,0) & \cdots & \cdots & R_{\tilde{r}}((M-1)T_s,(M-1)T_s) \end{bmatrix}. \tag{20}$$

In (10)–(13), the function $\hat{\psi}(\cdot)$ is the autocorrelation of the chip waveform defined by

$$\hat{\psi}(t) = \frac{1}{T_c}\int_{-\infty}^{\infty} \psi(s)\psi^*(s-t)\,ds \tag{14}$$

and the function $\Psi(\cdot)$ is the Fourier transform of $\psi^*(\cdot)$ defined by

$$\Psi(\delta) = \frac{1}{T_c}\int_0^{T_c} e^{-j\delta T_c s}\psi^*(s)\,ds. \tag{15}$$

Notice that for fixed $t$ and $s$, the sums involving $\hat{\psi}(\cdot)$ in (10) and (11) contain only finite numbers of nonzero terms because $\hat{\psi}(\cdot)$ is time-limited to $[-T_c, T_c]$.

We observe two important asymptotic properties of the correlation matrix $\boldsymbol{R}_{\tilde{r}}(t,s)$ which will be needed in later sections. First, from (10)[1]

$$\lim_{N\to\infty} \boldsymbol{R}_{\tilde{y}}(t,s) = \tilde{\boldsymbol{z}}(t)\tilde{\boldsymbol{z}}(s)^H \tag{16}$$

where

$$\tilde{\boldsymbol{z}}(t) = \sqrt{2P_1}T\sum_{\lambda=1}^{L_1} g_{1,\lambda}e^{-j\omega_c\tau_{1,\lambda}}\hat{\psi}(t-\tau_{1,\lambda})\,\boldsymbol{d}_{1,\lambda} \tag{17}$$

i.e., when the number of chips per symbol is large, we can neglect the effect of interchip interference and approximate the correlation matrix of the desired signal component as an outer product of two vectors.

Secondly, we see from (11) that $\tilde{\boldsymbol{n}}_I(t)$ is cyclostationary with period $T_c$, that is, for any integer $i$

$$\boldsymbol{R}_{\tilde{\boldsymbol{n}}_I}(t,s) = \boldsymbol{R}_{\tilde{\boldsymbol{n}}_I}(t+iT_c, s+iT_c). \tag{18}$$

Moreover, it is obvious from (13) that $\tilde{\boldsymbol{n}}_W(t)$ is wide-sense-stationary. We also notice from (12) that $\tilde{\boldsymbol{n}}_B(t)$ is asymptotically cyclostationary with period $T_c$ when $N$ approaches infinity because of the fact that

$$\lim_{N\to\infty} \frac{\sin(NT_c(\delta_k-\delta_l)/2)}{N\sin(T_c(\delta_k-\delta_l)/2)} = \begin{cases} 1, & \text{if } \delta_k \equiv \delta_l \pmod{2\pi/T_c} \\ 0, & \text{otherwise.} \end{cases} \tag{19}$$

Combining all these, we see that the overall noise and interference component in $\tilde{\boldsymbol{r}}_0(t)$ is asymptotically cyclostationary with period $T_c$ when $N$ approaches infinity.

[1] The limiting argument here can be interpreted as the convergence in matrix 2-norm. Recall that the 2-norm of a matrix $\boldsymbol{A}$ is defined [18, Ch. 2] as $\|\boldsymbol{A}\| = \sup_{\boldsymbol{x}\neq\boldsymbol{0}}(\|\boldsymbol{A}\boldsymbol{x}\|/\|\boldsymbol{x}\|)$, where the operator $\|\cdot\|$ denotes both the 2-norm of a matrix and the Euclidean norm of a vector. Throughout this paper, all limiting arguments concerning matrices and vectors are interpreted as convergences in 2-norm for matrices and in Euclidean norm for vectors, respectively.

With $\boldsymbol{R}_{\tilde{r}}(t,s)$, we find that the correlation matrix

$$\boldsymbol{R}_{\boldsymbol{v}} \triangleq E[\boldsymbol{v}_0\boldsymbol{v}_0^H]$$

of the sample vector $\boldsymbol{v}_0$ described in Section II is given by (20) at the top of this page.

Inheriting its properties from $\boldsymbol{R}_{\tilde{r}}(t,s)$, $\boldsymbol{R}_{\boldsymbol{v}}$ can also be decomposed into two parts, namely,

$$\boldsymbol{R}_{\boldsymbol{v}} = \boldsymbol{R}_{\boldsymbol{z}} + \boldsymbol{R}_{\boldsymbol{n}}. \tag{21}$$

The first part, $\boldsymbol{R}_{\boldsymbol{z}}$, is due to the desired signal contribution in $\boldsymbol{v}_0$. Just as $\boldsymbol{R}_{\tilde{y}}(t,s)$, $\boldsymbol{R}_{\boldsymbol{z}}$ is also asymptotically equal to an outer product of two vectors when $N$ tends to infinity. More precisely,

$$\lim_{N\to\infty} \boldsymbol{R}_{\boldsymbol{z}} = \boldsymbol{z}\boldsymbol{z}^H \tag{22}$$

where

$$\boldsymbol{z} = \begin{bmatrix} \tilde{\boldsymbol{z}}(0) \\ \tilde{\boldsymbol{z}}(T_s) \\ \vdots \\ \tilde{\boldsymbol{z}}((M-1)T_s) \end{bmatrix}. \tag{23}$$

The second part, $\boldsymbol{R}_{\boldsymbol{n}}$, is due to the overall noise and interference contribution in $\boldsymbol{v}_0$, which is asymptotically cyclostationary with period $T_c$.

Similarly, the correlation matrix $\boldsymbol{R}_{\hat{\boldsymbol{v}}} \triangleq E[\hat{\boldsymbol{v}}_0\hat{\boldsymbol{v}}_0^H]$ of the sample vector $\hat{\boldsymbol{v}}_0$, has the same form as $\boldsymbol{R}_{\boldsymbol{v}}$ except that $\boldsymbol{R}_{\tilde{r}}(iT_s, jT_s)$ is replaced by

$$\boldsymbol{R}_{\tilde{r}}(M'T_c + iT_s, M'T_c + jT_s), \qquad \text{for } 0 \le i, j \le M-1.$$

It can also be decomposed into two parts. The first part, which we denote by $\boldsymbol{R}_{\hat{\boldsymbol{z}}}$, is due to the desired signal contribution in $\hat{\boldsymbol{v}}_0$. Since $M'T_c > MT_s \ge \tau_{\max} + T_c$, (10) shows that $\lim_{N\to\infty}\boldsymbol{R}_{\hat{\boldsymbol{z}}} = \boldsymbol{0}$. This is the reason why we say that $\hat{\boldsymbol{v}}_0$ contains mainly noise and interference contributions. The second part, which we denote by $\boldsymbol{R}_{\hat{\boldsymbol{n}}}$, is due to the overall noise and interference contributions in $\hat{\boldsymbol{v}}_0$. From the asymptotic cyclostationarity of the overall interference, $\boldsymbol{R}_{\hat{\boldsymbol{n}}} = \boldsymbol{R}_{\boldsymbol{n}}$ when $N$ tends to infinity. Consequently, we have

$$\lim_{N\to\infty} (\boldsymbol{R}_{\boldsymbol{v}} - \boldsymbol{R}_{\hat{\boldsymbol{v}}}) = \boldsymbol{z}\boldsymbol{z}^H. \tag{24}$$

Equations (22) and (24) will be employed repeatedly in all the following sections.

## IV. Optimal Weight Vector

In this section, we consider optimal choices of the weight vector $\boldsymbol{w}$ according to three criteria, namely, the maximum signal-to-noise ratio (MSNR), the minimum mean-squared error (MMSE), and the constrained minimum output energy (CMOE) criteria. MSNR, which is closely related to the minimization of error probability, is the main criterion while MMSE and CMOE are useful in adaptive algorithm development. As shown in Proposition 1, the three criteria are actually asymptotically equivalent. Notice that the equivalence of three similar criteria has been established in [7] and [8]. However, the results are based on the deterministic periodic sequence model, which is quite different from the aperiodic random sequence model used in this paper.

### A. Maximum Signal-to-Noise Ratio (MSNR)

We first consider the weight vector that maximizes SNR defined by, for $\boldsymbol{w} \neq \mathbf{0}$

$$\mathrm{SNR}(\boldsymbol{w}) = \frac{\boldsymbol{w}^H \boldsymbol{R}_z \boldsymbol{w}}{\boldsymbol{w}^H \boldsymbol{R}_n \boldsymbol{w}}. \tag{25}$$

Note that the existence of the AWGN component guarantees that the matrix $\boldsymbol{R}_n$ is positive definite. Hence, the SNR defined in (25) is always finite and the matrix pencil $(\boldsymbol{R}_z, \boldsymbol{R}_n)$ is regular [17, Ch. X]. Moreover, since both $\boldsymbol{R}_z$ and $\boldsymbol{R}_n$ are Hermitian, all of the generalized eigenvalues associated with the matrix pencil are real [17, Ch. X]. It can be shown [17, Ch. X] that the weight vector that maximizes the SNR is the generalized eigenvector associated with the largest generalized eigenvalue of the matrix pencil $(\boldsymbol{R}_z, \boldsymbol{R}_n)$. Since, for $\boldsymbol{w} \neq \mathbf{0}$

$$\frac{\boldsymbol{w}^H \boldsymbol{R}_v \boldsymbol{w}}{\boldsymbol{w}^H \boldsymbol{R}_n \boldsymbol{w}} = \mathrm{SNR}(\boldsymbol{w}) + 1 \tag{26}$$

the optimal weight vector is also the generalized eigenvector associated with the largest generalized eigenvalue of the matrix pencil $(\boldsymbol{R}_v, \boldsymbol{R}_n)$. Since $\boldsymbol{R}_{\hat{v}}$ closely approximates $\boldsymbol{R}_n$, it is conceivable that the optimal weight vector may be approximated by the generalized eigenvector associated with the largest generalized eigenvalue of the matrix pencil $(\boldsymbol{R}_v, \boldsymbol{R}_{\hat{v}})$ when $N$ is large. This approximation will be justified in Proposition 1.

### B. Minimum Mean-Squared Error (MMSE)

We may also find the weight vector that minimizes the mean-squared error, defined by

$$\mathrm{MSE}(\boldsymbol{w}) = E[|b_0^{(1)} - \boldsymbol{w}^H \boldsymbol{v}_0|^2]. \tag{27}$$

It is well known [20] that the MSE is minimized by

$$\tilde{\boldsymbol{w}}_N = \arg\min_{\boldsymbol{w}} [\mathrm{MSE}(\boldsymbol{w})] = \boldsymbol{R}_v^{-1} \boldsymbol{z} \tag{28}$$

for a particular $N$.

### C. Constrained Minimum Output Energy (CMOE)

As our objective is to suppress the interference component in the received sample vector, we can choose $\boldsymbol{w}$ so that the output energy is minimized with the constraint that the desired signal component is fixed, which is exactly the idea of the MVDR beamformer. More precisely, we define the output energy as

$$\sigma(\boldsymbol{w}) = \boldsymbol{w}^H \boldsymbol{R}_v \boldsymbol{w} \tag{29}$$

and choose $\boldsymbol{w}$ to be $\hat{\boldsymbol{w}}_N$ where

$$\hat{\boldsymbol{w}}_N = \arg\min_{\boldsymbol{w}^H \boldsymbol{z} = c} \sigma(\boldsymbol{w}) \tag{30}$$

for some constant $c \neq 0$ and a particular $N$. By the method of Lagrange multipliers, it can be shown [20] that the MMSE solution in (28) is also the solution of (30) when $c = \boldsymbol{z}^H \boldsymbol{R}_v^{-1} \boldsymbol{z}$. Moreover, the solution of (30) for any $c \neq 0$ is a scalar multiple of the MMSE solution.

We note that the MMSE and CMOE criteria are basically equivalent since they share a common solution. They are asymptotically equivalent to the MSNR criterion according to the following proposition whose proof can be found in Appendix I.

*Proposition 1:* Let $\boldsymbol{w}_N$ be an eigenvector associated with the largest generalized eigenvalue of the matrix pencil $(\boldsymbol{R}_v, \boldsymbol{R}_{\hat{v}})$ and $\overline{\boldsymbol{w}}_N = \boldsymbol{R}_n^{-1} \boldsymbol{z}$ for a particular $N$. Let $\tilde{\boldsymbol{w}}_N$ and $\hat{\boldsymbol{w}}_N$ be defined as in (28) and (30), respectively. Then, for any $\varepsilon > 0$, when $N$ is sufficiently large

$$\max_{\boldsymbol{w} \neq 0} [\mathrm{SNR}(\boldsymbol{w})] - \mathrm{SNR}(\boldsymbol{w}_N) < \varepsilon$$

$$\max_{\boldsymbol{w} \neq 0} [\mathrm{SNR}(\boldsymbol{w})] - \mathrm{SNR}(\overline{\boldsymbol{w}}_N) < \varepsilon$$

$$\max_{\boldsymbol{w} \neq 0} [\mathrm{SNR}(\boldsymbol{w})] - \mathrm{SNR}(\tilde{\boldsymbol{w}}_N) < \varepsilon$$

$$\max_{\boldsymbol{w} \neq 0} [\mathrm{SNR}(\boldsymbol{w})] - \mathrm{SNR}(\hat{\boldsymbol{w}}_N) < \varepsilon.$$

## V. Optimalities of the Receiver

In this section, we consider the behavior of the proposed receiver under different situations. Under appropriate conditions, the receiver reduces to the MVDR beamformer, a notch filter for suppressing narrowband interference, the RAKE receiver, or an MAI suppressor. Notice that some of these properties have been developed independently for other receivers proposed in [3]–[8] under the periodic sequence model. Under the aperiodic random sequence model, we are able to unify these properties into a single linear receiving structure.

### A. MVDR Beamformer

To illustrate the beamforming capability of the proposed receiver, we consider an AWGN channel with MAI only. Hence, $\boldsymbol{n}_B(t) = 0, L_k = 1$, and $g_{k,1} = \exp(j\theta_k)$ for $1 \leq k \leq K$, where $\theta_k$ is the phase shift for the $k$th user signal. Since we assume synchronization with the signal from the first user, we have $\theta_1 = 0$. The absence of multipath fading also implies that $\tau_{\max} = 0$.

Suppose that the output of the matched filter $\tilde{\boldsymbol{r}}_0(t)$ is sampled once every bit interval at $t = jT$. Then $M = 1$ and $\boldsymbol{v}_0 = \tilde{\boldsymbol{r}}(0)$. Hence, from (10)–(13), for any $N$, $\boldsymbol{R}_z = \boldsymbol{R}_{\tilde{\boldsymbol{y}}}(0,0) = \boldsymbol{z}\boldsymbol{z}^H$, and $\boldsymbol{R}_n = \boldsymbol{R}_{\tilde{n}_I}(0,0) + \boldsymbol{R}_{\tilde{n}_W}(0,0)$, where $\boldsymbol{z} \doteq \sqrt{2P_1}Tg_1 \boldsymbol{d}_{1,1}$. Notice that the vector $\boldsymbol{z}$ is just the array response vector $\boldsymbol{d}_{1,1}$ of the desired user. Maximizing the SNR defined in (25) is equivalent to minimizing the

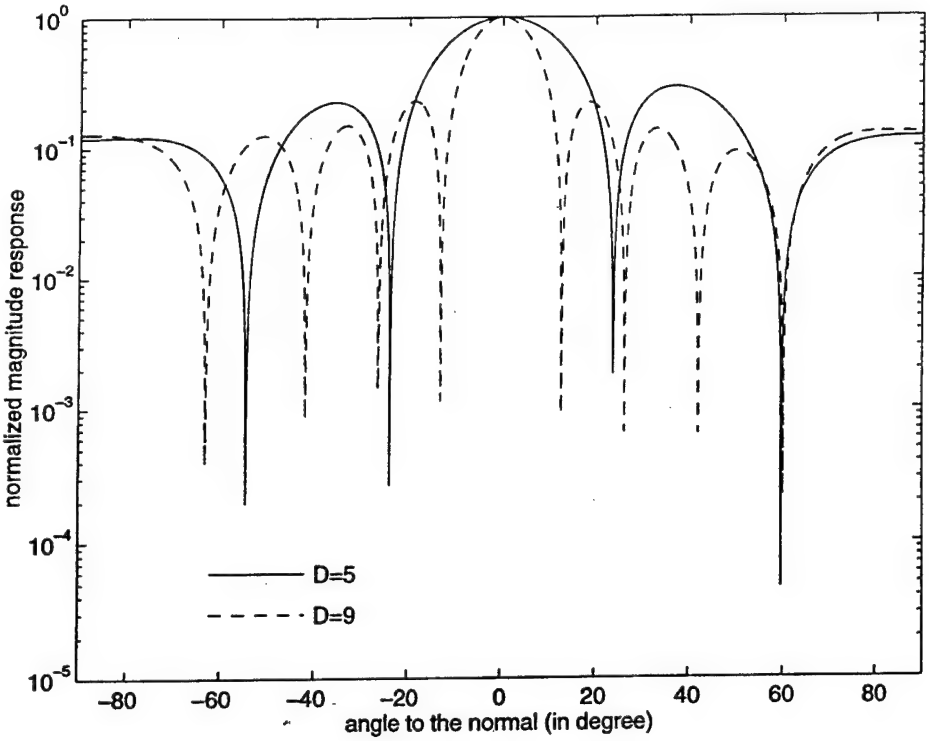


Fig. 3. Directional magnitude response of the beamformer example.

noise variance $\boldsymbol{w}^H \boldsymbol{R}_n \boldsymbol{w}$ subject to the constraint that the signal strength $\boldsymbol{w}^H \boldsymbol{d}_{1,1}$ is kept constant. This is exactly the operation performed by the MVDR beamformer [20].

As an example,[2] we consider a two-user system. The received power of the interferer is 20 dB stronger than that of the desired user, i.e., $P_2|g_2|^2 = 100P_1|g_1|^2$. The signal of the desired user comes at 0° whereas the interferer signal comes at 60°. Fig. 3 shows realizations of the normalized directional magnitude responses of the optimal receiver output for a five-element array and a nine-element array. The spatial selectivity of the receiver is shown by the deep nulls at 60°.

Next, we show the performance of the receiver when the number of interferers increases. The received power of each interferer is 20 dB stronger than that of the desired user. The signal of the desired user comes at 0° whereas each interferer signal comes at an independent and uniformly distributed random angle. The average[3] maximum SNR achievable by the receiver using antenna with different numbers of elements is plotted in Fig. 4. Obviously, we see the advantage of using an antenna array with more elements than a single antenna.

### *B. Notch Filter for Suppressing Narrowband Interference*

To illustrate the notch filtering capability of the proposed receiver, we consider an AWGN channel with the presence of a single user and a single-tone narrowband interferer only, i.e., $K = 1$, $K_B = 1$, $L_1 = 1$, and $\boldsymbol{n}_I(t) = 0$. Moreover, we also assume that a single-element antenna is being used, i.e., $D = 1$. In this way, the effect of notch filtering can be singled out from the spatial selectivity of a multielement antenna array.

Suppose that the output of the matched filter $\tilde{\boldsymbol{r}}_0(t)$ is sampled once every $T_c$ seconds and $M$ samples are taken to form the vector $\boldsymbol{v}_0$. Using the results in Section III, a straightforward calculation shows that $\boldsymbol{R}_z = \boldsymbol{z}\boldsymbol{z}^H$, and

$$\boldsymbol{R}_n = \boldsymbol{e}_2 \boldsymbol{e}_2^H + N_0 T \boldsymbol{I}_{M\times M} \tag{31}$$

where

$$\boldsymbol{e}_2 = \sqrt{\frac{2P_2}{N}} T|g_2||\Psi(\delta_2)|[1 e^{j\delta_2 T_c} \cdots e^{j(M-1)\delta_2 T_c}]^H$$

and $\boldsymbol{z} = \sqrt{2P_1}T[1 \quad 0 \quad \cdots \quad 0]^T$. The optimal weight vector is given by

$$\overline{\boldsymbol{w}} = \boldsymbol{R}_n^{-1}\boldsymbol{z} = \frac{1}{N_0 T}\left[\boldsymbol{z} - \sqrt{\frac{NP_1|g_1|^2}{P_2|g_2|^2}}\frac{1}{C}\boldsymbol{e}_2\right] \tag{32}$$

where

$$C = M + \frac{N_0}{2P_2 T|g_2|^2|\Psi(\delta_2)|^2/N}. \tag{33}$$

From (33), we see that when the narrowband noise dominates, $C \approx M$.

Taking a closer look at the definition of $\boldsymbol{e}_2$, we observe that components of the vector $\boldsymbol{e}_2$ are just the samples of the single-tone interference contribution $\tilde{\boldsymbol{n}}_B(t)$. From (32)

$$\frac{\overline{\boldsymbol{w}}^H \boldsymbol{e}_2}{\overline{\boldsymbol{w}}^H \boldsymbol{z}} = \sqrt{\frac{P_2|g_2|^2}{NP_1|g_1|^2}} \cdot \frac{C-M}{C-1}. \tag{34}$$

[2]For this and all other examples in this paper, we assume binary data sequences and binary signature sequences with the use of a rectangular chip waveform. The bits in the data sequences are equally probable and independent. Moreover, we always assume $N = 127$ and the existence of AWGN with one-sided power spectral density $N_0$ such that the signal-to-thermal-noise ratio (STNR) is 15 dB.

[3]The word "average" here, and in the following examples, means that the value referred to is obtained by averaging over 500 realizations.

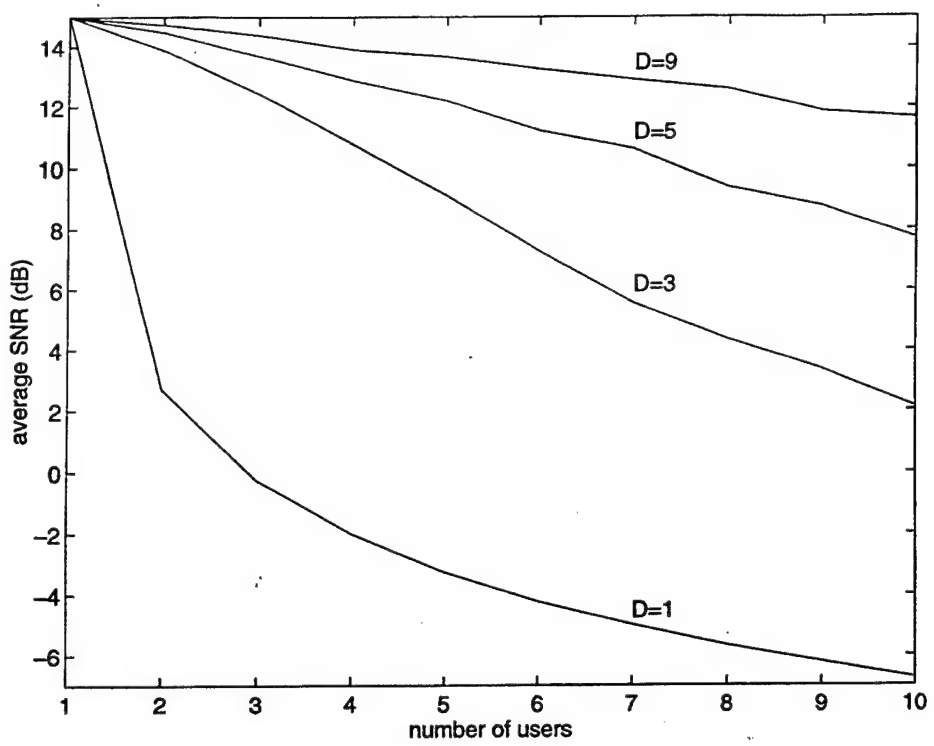


Fig. 4. Average maximum SNR achievable in the beamformer example.

When $M > 1$, we can see from (34) that the relative strength of the narrowband noise component is mitigated by the weighting operation. In particular, when the narrowband noise dominates over the wideband AWGN, $C \approx M$. The ratio of the narrowband noise magnitude to the signal magnitude in (34) is almost zero. This means that the weighting operation acts as a digital filter to notch out the single-tone interference component, $\boldsymbol{e}_2$, from the matched filter sample vector $\boldsymbol{v}_0$.

As an example, consider a single-user, single-element antenna system with a single-tone interferer. The received power of the single-tone interferer is 20 dB above that of the user. The frequency of the interferer is exactly the carrier frequency, i.e., $\delta_2 = 0$. Fig. 5 shows the frequency responses of the optimal receiver for $M = 5$ and $M = 9$. The notch-filtering nature of the receiver is shown readily in the frequency response.

For the case of multitone interference ($K_B > 1$), the argument is basically the same. As an example, we consider the situation where the received power of each narrowband interferer is 20 dB above that of the user. The frequency offset (from the carrier frequency) of each tone is uniformly distributed on $[-1/2T_c, 1/2T_c)$. The average maximum SNR achievable by the receiver is plotted against the number of multitone interferes $K_B$ in Fig. 6 for different values of $M$.

### C. RAKE Receiver

We consider a single-user communication system in a multipath fading channel with AWGN, i.e., $K = 1$, $\boldsymbol{n}_I(t) = 0$, and $\boldsymbol{n}_B(t) = 0$. Again, we assume a single-element antenna is employed to eliminate the spatial selective capability of the proposed receiver structure, i.e., $D = 1$.

We begin with a simple case in which the path delays $\tau_{1,\lambda}$, for $2 \le \lambda \le L_1$, are integral multiples of $T_c$ and we sample the matched filter output $\tilde{\boldsymbol{r}}_0(t)$ every $T_c$ seconds, i.e., $T_s = T_c$. We assume there are altogether $M$ paths which have path delays ranging from 0 to $(M-1)T_c$. For compatibility with the model we introduced in Section II, we can simply set the gains of the nonexisting paths to zero. Using the correlation properties of the various components in Section III, one can obtain easily that $\boldsymbol{R}_n = N_0 T \boldsymbol{I}_{M\times M}$ and

$$\boldsymbol{R}_z = \boldsymbol{z}\boldsymbol{z}^H + O(1/N) \tag{35}$$

where

$$\boldsymbol{z} = \sqrt{2P_1}T[g_{1,1}e^{j\omega_c} \;\; g_{1,2}e^{j2\omega_c} \;\; \cdots \;\; g_{1,M-1}e^{j(M-1)\omega_c}]^H.$$

From Proposition 1, for sufficiently large $N$, the optimal weight vector is approximately given by

$$\overline{\boldsymbol{w}} = \boldsymbol{R}_n^{-1}\boldsymbol{z} = \frac{1}{N_0 T}\boldsymbol{z}. \tag{36}$$

Hence, the optimal weight vector is just the vector $\boldsymbol{z}$ since a scalar constant is immaterial in the maximization of the SNR. Since the components of $\boldsymbol{z}$ are the path gains of the lowpass equivalent representation of the paths, the optimal weighting operation is to combine the energy in each path coherently. This is exactly the characteristics of a RAKE receiver [21].

In general, it is unlikely that all the path delays are integral multiples of the chip duration. Therefore, in order to achieve a finer resolution, we sample the matched filter output $\tilde{\boldsymbol{r}}_0(t)$ at a rate higher than the chip rate, i.e., $T_s < T_c$. Following the development in the simple case above, $\boldsymbol{R}_z$ still takes the form in (35) with the $m$th, $m = 0, 1, \cdots, M-1$, element of $\boldsymbol{z}$ given by $\tilde{\boldsymbol{z}}(mT_s)$ defined in (17). In fact, the vector $\boldsymbol{z}$ is

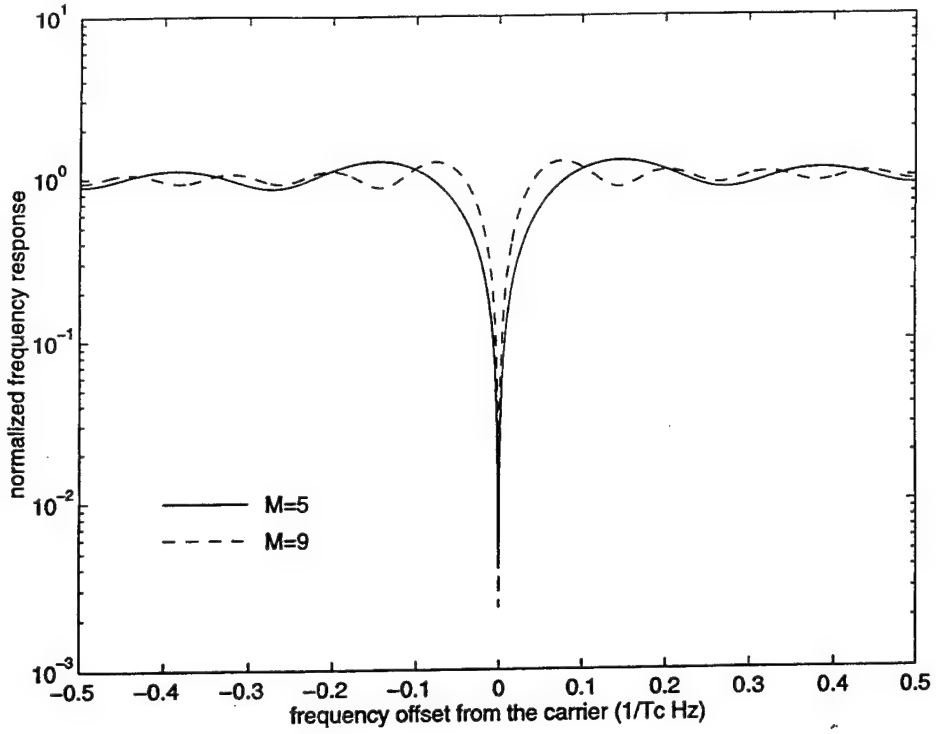


Fig. 5. Frequency response of the notch filter example.

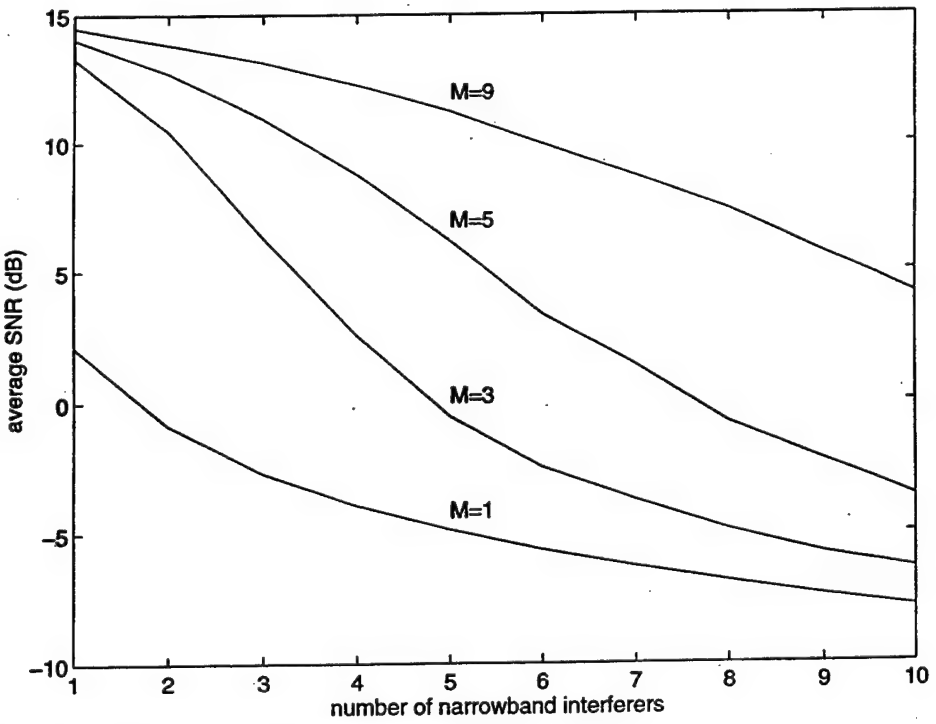


Fig. 6. Average maximum SNR achievable in the notch filter example.

just the oversampling counterpart of the path gain vector in the simple case. Unlike the simple case, the noise covariance matrix $\boldsymbol{R}_n$ is no longer the identity matrix. Nevertheless, it is easy to see that $\boldsymbol{R}_n$ is a positive definite Hermitian matrix. Hence, we have the decomposition $\boldsymbol{R}_n = \boldsymbol{G}\boldsymbol{G}$, where $\boldsymbol{G}$ is the square root of $\boldsymbol{R}_n$. Note that $\boldsymbol{G}$ is Hermitian and invertible. For sufficiently large $N$, the optimal weight vector is well approximated by

$$\overline{\boldsymbol{w}}^H = (\boldsymbol{G}^{-1}\boldsymbol{z})^H \cdot \boldsymbol{G}^{-1}. \tag{37}$$

The optimal weighting operation described by (37) can be decomposed into two operations in cascade. We can treat

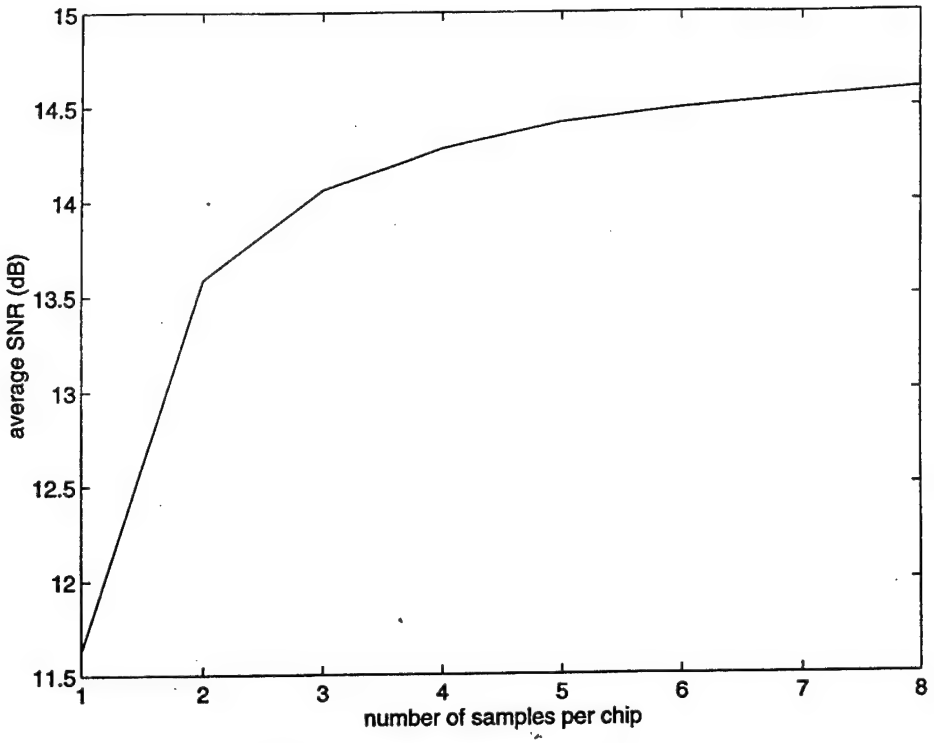


Fig. 7. Average maximum SNR achievable in the RAKE receiver example.

the linear operation defined by $G^{-1}$ as a noise whitening filter. Then the linear operation defined by $(G^{-1}z)^H$ is just a digital filter matched to response of $z$ after the noise whitening operation. Notice that since the noise samples are not independent in this case, a direct coherent combination of the paths as in the RAKE receiver is not optimal. This is why the noise whitening filter is needed.

We use an example to show the advantage of sampling more than once in each chip. The single-user, single-element antenna system is used for a multipath fading channel. There are five paths, i.e., $L_1 = 5$, and the complex path gains are independent zero-mean complex Gaussian random variables with equal variance such that the total average power of the five paths is equal to the original transmitted power $P_1$. Except the first path, we assume each path arrives with a uniformly distributed delay ranging from $[0, \tau_{\max})$ independently, where $\tau_{\max} = 5T_c$. The average maximum SNR achievable by the receiver is plotted against the number of samples in a chip, $S$, in Fig. 7. As we expect, the average performance is better when $S$ increases. Note that the vector size $M$ increases with $S$, and hence performance improves at the expense of complexity.

### D. MAI Suppressor

For simplicity, we consider a communication system with two users on an AWGN channel, i.e., $K = 2$. There is no narrowband interference or multipath effect, i.e., $n_B(t) = 0$, $L_k = 1$, and $g_{k,1} = \exp(j\theta_k)$ for $k = 1, 2$. Again, we assume a single-element antenna is being used, i.e., $D = 1$. Moreover, the matched filter output $\tilde{r}(t)$ is sampled every $T_c$ seconds, i.e., $T_s = T_c$ and we use the first $M$ samples of $\tilde{r}(t)$ to form the vector $v_0$.

Using the results in Section III, we obtain that $R_z$ is, again, given by (35) and $z = \sqrt{2P_1}T[1\ 0\ \cdots\ 0]^T$ as in the notch filter case. On the other hand, when the chips of the interferer do not align with those of the desired user, $R_n$ is tri-diagonal and some form of optimal combining is performed. In fact, the prewhitening explanation in the previous section can be employed to justify the optimal weighting operation in this case with the modification that only one path is present this time. To illustrate the above argument by example, we consider a single-element antenna system with two users. The power of the interferer is 20 dB above the desired user. Fig. 8 shows the maximum SNR achievable by the receiver when $T_{2,1}$ varies for different values of $M$. The maximum suppression is about 1.5 dB when $T_{2,1} = 0.5$. Notice that MAI suppression is achieved by exploring the asynchrony between the interferers and the desired user. This result is related to that in [14]. The major differences are that in [14], a prewhitening filter is applied *before* the conventional matched filter, and the delays of the interferers are assumed to be random instead of deterministic.

### E. Spatially and Temporally Noise-Whitening Matched Filter

The prewhitening argument in Section V-C can be generalized to the case of general multiuser, multielement antenna systems over multipath fading channels with AWGN. Since the generalization is straightforward, we state the result without going through the derivation. When $N$ is large, the optimal weight vector is approximately given by (37) where, now, the vector $z$ is the response vector, including the spatial information, of the matched filtered channel with the desired user signal as input. The noise component $n$ in the sample

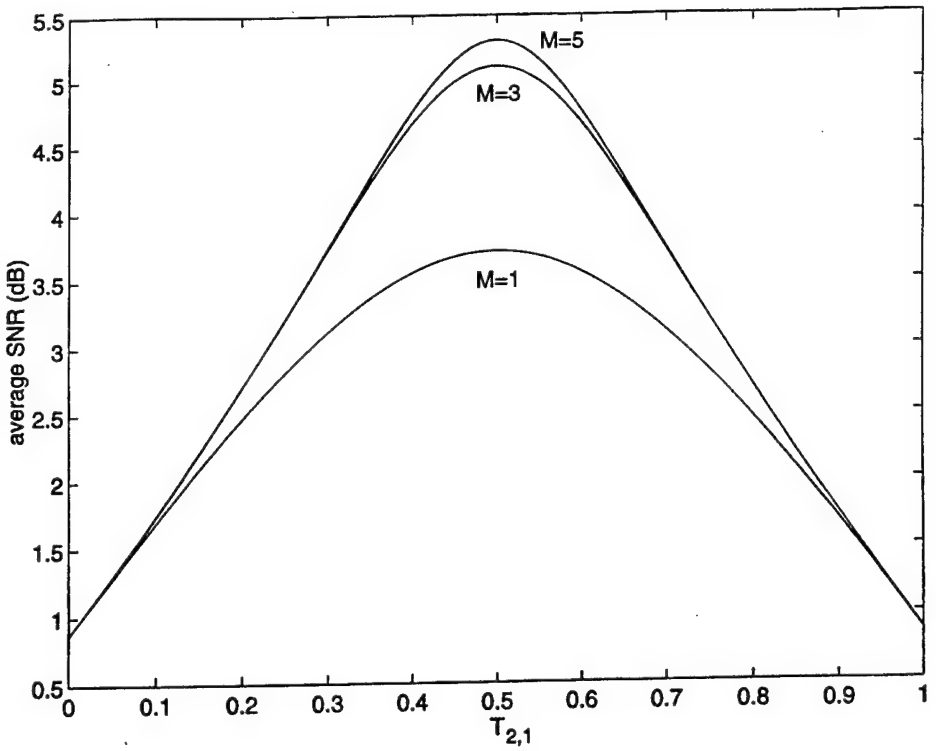


Fig. 8. Average maximum SNR achievable in the MAI suppressor example.

vector $\boldsymbol{v}_0$ includes the MAI, narrowband interference, and the AWGN components. The crucial point is that a whitening operation still exists. Therefore, the weighting operation can still be viewed as noise-whitening discrete-time matched filter as in Section V-C. However, since the noise component vector $\boldsymbol{n}$ contains spatial and temporal information, the receiver, in this case, can be interpreted as a spatially and temporally noise-whitening matched filter. This point of view is related to that in [10].

## VI. Eigenanalysis Algorithms

In this section, we consider a class of nonadaptive algorithms to obtain the optimal weight vector. As discussed in Section IV, the optimal weight vector is the generalized eigenvector of the matrix pencil $(\boldsymbol{R}_z, \boldsymbol{R}_n)$. However, the correlation matrices $\boldsymbol{R}_z$ and $\boldsymbol{R}_n$ are usually not known. In Section IV-A, we suggest a method to circumvent this difficulty by employing the similarity in the statistical structures of the sample vectors $\boldsymbol{v}_0$ and $\hat{\boldsymbol{v}}_0$. The generalized eigenvector of the matrix pencil $(\boldsymbol{R}_v, \boldsymbol{R}_{\hat{v}})$ is approximately the optimal weight vector when the number of chips per symbol, $N$, is large. Note that this condition is usually satisfied in all DS/SSMA systems. The advantage of this formulation is that both $\boldsymbol{R}_v$ and $\boldsymbol{R}_{\hat{v}}$ can be estimated directly using the samples taken from the output of the matched filter in Fig. 1. Any consistent estimators of the correlation matrices $\boldsymbol{R}_v$ and $\boldsymbol{R}_{\hat{v}}$ can be used. The consistency and Lemma 2 in Appendix I guarantee the average SNR obtained by using the estimates of the correlation matrices in the eigenanalysis is close to the maximum SNR when the estimates are good enough.

To conclude the discussion above, we consider two examples and use them to demonstrate the dependence of the average SNR obtained by the algorithm stated above on the accuracy of the estimates of the correlation matrices $\boldsymbol{R}_v$ and $\boldsymbol{R}_{\hat{v}}$. The two examples are the first example given in Section V-A and the example given in Section V-C with the restriction that the paths arrive exactly at the chip boundaries and we sample once per chip, respectively. In both of the examples, we take $M' = 31$ and use the time average correlation matrices as the estimators for the correlation matrices, i.e.,

$$\hat{\boldsymbol{R}}_v = \frac{1}{J}\sum_{j=0}^{J-1} \boldsymbol{v}_j \boldsymbol{v}_j^H \tag{38}$$

$$\hat{\boldsymbol{R}}_{\hat{v}} = \frac{1}{J}\sum_{j=0}^{J-1} \hat{\boldsymbol{v}}_j \hat{\boldsymbol{v}}_j^H. \tag{39}$$

Figs. 9 and 10 show the average SNR obtained in the first example and the second example for different values of $J$, respectively. Also shown in the figures are the average maximum SNR achievable by the receiver and the average SNR when no weighting is performed, i.e., only the first element of the sample vector is used as the decision statistic. It is clear in both cases that the average SNR increases as $J$ increases. When $J$ is large, the estimates of the correlation matrices are accurate, and hence, the average SNR is close to the maximum SNR. For these two examples, we need about 20 symbols to get an average SNR of 1 dB below the maximum value. For slowly time-varying channels, we can modify the estimators in (38) and (39) by applying a window with a carefully chosen width.

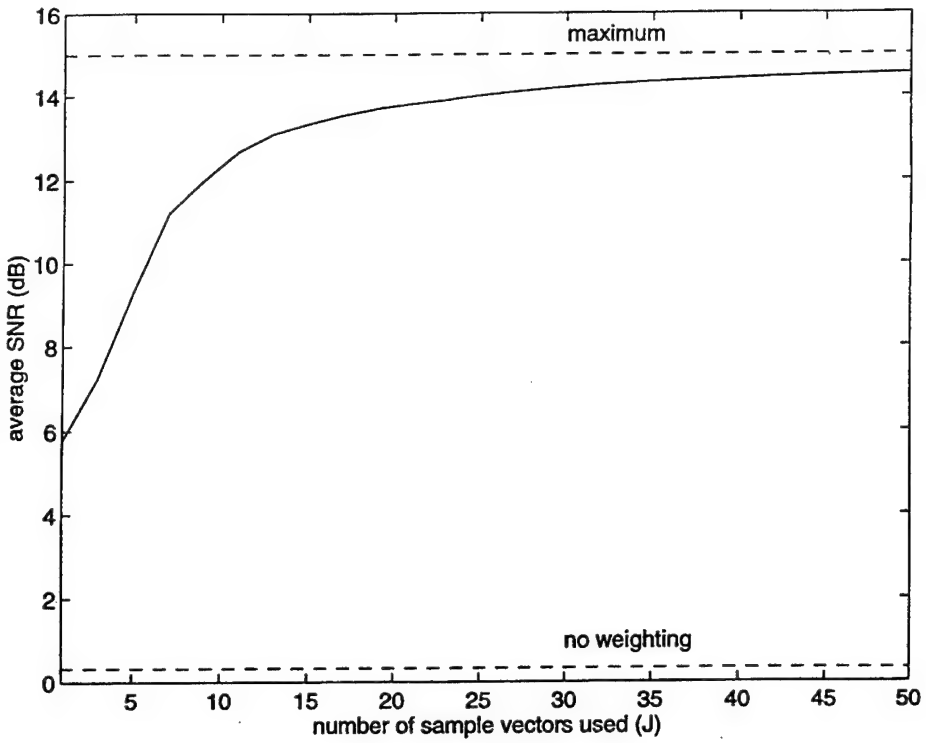


Fig. 9. Average SNR obtained by the eigenanalysis algorithm in the beamformer example.

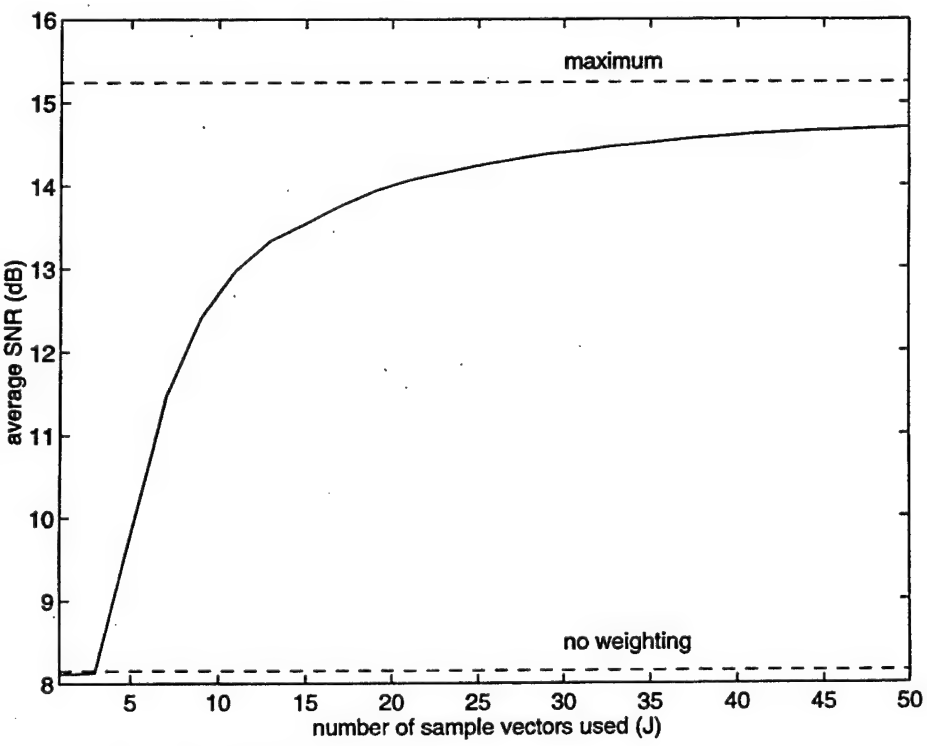


Fig. 10. Average SNR obtained by the eigenanalysis algorithm in the RAKE receiver example.

## VII. Adaptive Algorithms

The major disadvantage of the eigenanalysis algorithms stated in Section VI is the computational complexity involved in obtaining the generalized eigenvector. It limits the size of the weight vector. As shown in Section IV, the MMSE and the CMOE criteria are asymptotically equivalent to MSNR. Similar to [7] and [8], the consideration of MMSE and CMOE provides simple methods to develop adaptive algorithms. Consideration of MMSE naturally leads to the well-known LMS algorithm when training sequences are

available. However, the requirement of training sequences is undesirable in some DS/SSMA systems, especially, when the communication channels are time-varying. With the CMOE criterion, we now develop a blind adaptive algorithms to obtain the optimal weight vector.

From the previous discussion, we know that direct estimates of $z$ from the samples at the output of the matched filter are not readily available. However, from (24), the correlation matrices $R_v$ and $R_{\hat{v}}$, and hence the matrix $zz^H$ can be easily estimated from the sample vectors $v_j$ and $\hat{v}_j$. Therefore, if we have an adaptive algorithm which only requires the knowledge of the matrices $R_v$ and $zz^H$, we can approximate this algorithm by using estimates of $R_v$ and $zz^H$ instead. This is similar to the development of the LMS algorithm from the steepest descent algorithm. Unlike the LMS algorithm, the resulting algorithm would be a blind adaptive algorithm since no training sequence is needed.

The asymptotic equivalence of CMOE and MSNR suggests that we can determine the optimal weight vector by constrained minimization of the output energy $\sigma(w)$ when $N$ is sufficiently large. Assume that the matrices $R_v$ and $zz^H$ are given. Consider the matrix $P_z$ defined by

$$P_z = \frac{zz^H}{z^H z}. \tag{40}$$

Notice that it defines a projection operation onto the space spanned by the vector $z$. Since $z^H z$ is just the trace of the matrix $zz^H$, we can obtain $P_z$ from $zz^H$. The gradient vector of the function $\sigma(w)$ is $g_\sigma(w) = R_v w$. Restricted by the constraint $w^H z = c$, we cannot descend in the direction opposite to $g_\sigma(w)$ as in the steepest descent algorithm. Let $\tilde{g}_\sigma(w)$ be the component of $g_\sigma(w)$ which is orthogonal to the vector $z$

$$\tilde{g}_\sigma = (I - P_z)R_v w. \tag{41}$$

Note that the vector $\tilde{g}_\sigma$ is determined directly by $P_z$ and $R_v$. It is easy to see that descending in the direction opposite to $\tilde{g}_\sigma(w)$ does not violate the constraint $w^H z = c$. Therefore, we set up an adaptive algorithm which descends in that direction to solve the constrained minimization problem.

*Algorithm 1:* For $j \geq 1$

$$w(j) = [I - \mu(I - P_z)R_v]w(j-1) \tag{42}$$

where $\mu > 0$ and $w(0)^H z = c$.

The following proposition, whose proof is given in Appendix II, summaries the convergence of Algorithm 1. It solves, iteratively, the constrained minimization problem whenever $\mu$ is chosen to be adequately small.

*Proposition 2:* Given any $w(0)$ such that $w(0)^H z = c$. for $j \geq 1$, update $w(j)$ as in Algorithm 1. Suppose $\mu$ is chosen such that

$$0 < \mu < \frac{2}{\lambda_{\max}} \tag{43}$$

where $\lambda_{\max}$ is the largest eigenvalue of the matrix $(I - P_z)R_v$, then

$$\lim_{j\to\infty} w(j) = \left[\frac{z^H w(0)}{z^H R_v^{-1} z}\right]\tilde{w}_N. \tag{44}$$

Moreover, as $j$ increases, $\sigma(w(j)) \downarrow |z^H w(0)|^2 / z^H R_v^{-1} z$.

Unfortunately, it is shown in Appendix II that Algorithm 1 is numerically unstable even when $\mu$ satisfies the condition in Proposition 2. To stabilize the algorithm, we may put some restrictions on the vector $w(j)$ at each iteration. By restricting $w(j)$ at each iteration, the constraint $w(j)^H z = c$ may not be satisfied at each iteration. Instead of considering the minimization problem of the output energy, we define, for $w$ such that $w^H z \neq 0$,

$$\tilde{\sigma}(w) = \frac{w^H R_v w}{w^H z z^H w} \tag{45}$$

and consider the minimization problem below

$$\min_{w^H z \neq 0} \tilde{\sigma}(w). \tag{46}$$

Note that it reduces to the minimization problem of the output energy if the additional constraint $w^H z = c$ is added.

Proposition 3 below shows that the following numerically stable algorithm solves the constrained minimization problem of $\tilde{\sigma}(w)$ in (46) when $\mu$ is chosen to be adequately small.

*Algorithm 2:*

For $j \geq 1$

$$w(j) = c(j)[I - \mu(I - P_z)R_v]w(j-1) \tag{47}$$

where $\mu > 0$ and $w(0)^H z \neq 0$. At each iteration, the complex constant $c(j)$ is chosen to stabilize the algorithm in the following way.

Fix one $m \in \{1, 2, \cdots, MD\}$. For each $j \geq 1$, let $w_m(j)$ be the $m$th element of $w(j)$. If $w_m(j) \neq 0$, choose $c(j)$ such that $||w(j)|| = 1$ and $\arg(w_m(j)) = 0$. Otherwise, choose $c(j)$ such that $||w(j)|| = 1$ and $\arg(c(j)) = 0$.

*Proposition 3:* Given any $w(0)$ such that $w(0)^H z \neq 0$, for $j \geq 1$, update $w(j)$ as in Algorithm 2. Suppose $\mu$ is chosen such that

$$0 < \mu < \frac{2}{\lambda_{\max}} \tag{48}$$

where $\lambda_{\max}$ is the largest eigenvalue of the matrix $(I - P_z)R_v$, and the $m$th element of $\tilde{w}_N, \tilde{w}_{Nm} \neq 0$, where $m$ is the index fixed in Algorithm 2. Then

$$\lim_{j\to\infty} w(j) = \frac{\exp(-j\arg(\tilde{w}_{Nm}))}{||\tilde{w}_N||}\tilde{w}_N. \tag{49}$$

Moreover, as $j$ increases, $\tilde{\sigma}(w(j)) \downarrow 1/z^H R_v^{-1} z$.

The proof of Proposition 3 and the stability argument of Algorithm 2 can be found in Appendix II.

Note that for Algorithm 2 to give the desired weight vector, we have to choose the initial vector $w(0)$ such that it is not orthogonal to the signal vector $z$. In practical situations with synchronization achieved, the first sample at the output of the matched filter usually carries a significant portion of power. In most cases, it should not be zero. Hence, it is usually a safe choice to start the algorithms with $w(0) = [1 \ 0 \ \cdots \ 0]^T$. Moreover, the algorithm also requires us to fix the phase angle of one of the elements of the weight vector at each iteration. By the same line of reasoning, we can choose this to be the first element.

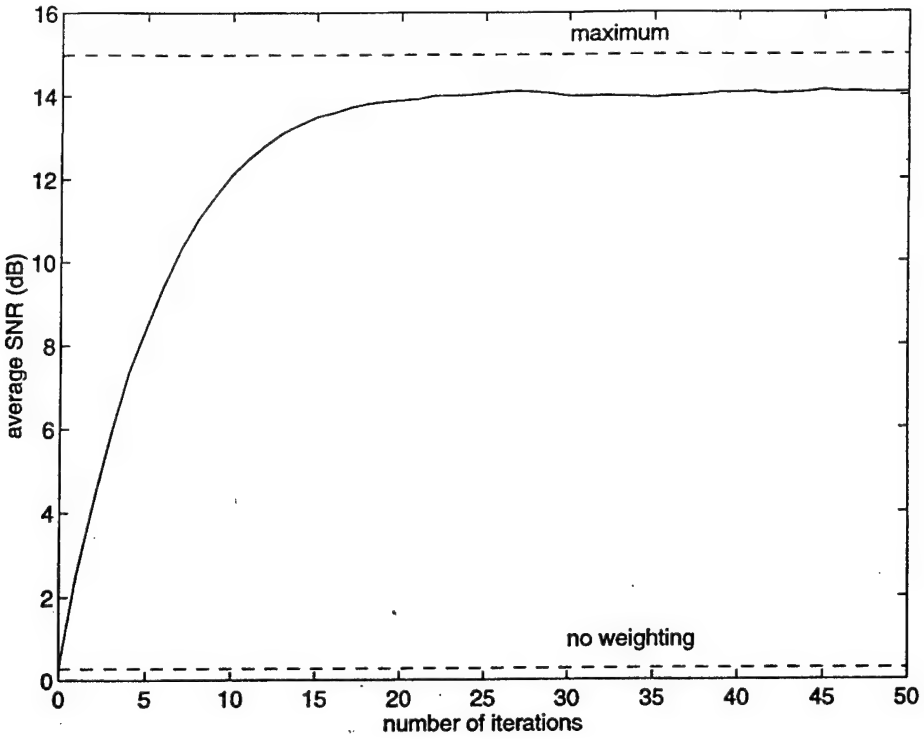


Fig. 11. Average SNR obtained by the blind adaptive algorithm in the beamformer example.

Algorithm 2 requires knowledge of $\boldsymbol{R}_v$ and $\boldsymbol{z}\boldsymbol{z}^H$. To obtain a blind adaptive algorithm, we estimate $\boldsymbol{R}_v$ and $\boldsymbol{R}_{\hat{v}}$ by $\boldsymbol{v}_j\boldsymbol{v}_j^H$ and $\hat{\boldsymbol{v}}_j\hat{\boldsymbol{v}}_j^H$ at the $j$th iteration, respectively. When $N$ is large, it is reasonable to estimate $\boldsymbol{z}\boldsymbol{z}^H$ by $\boldsymbol{v}_j\boldsymbol{v}_j^H - \hat{\boldsymbol{v}}_j\hat{\boldsymbol{v}}_j^H$. Replacing $\boldsymbol{z}\boldsymbol{z}^H$ and $\boldsymbol{R}_v$ in (47) by these estimates, we get the following blind adaptive algorithm.

*Algorithm 3:* For $j \geq 1$

$$\begin{aligned}\boldsymbol{w}(j) &= c(j)\{\boldsymbol{w}(j-1) + \mu[\boldsymbol{v}_j^H\boldsymbol{w}(j-1)] \\ &\quad \cdot [(\hat{\boldsymbol{v}}_j^H\hat{\boldsymbol{v}}_j)\boldsymbol{v}_j - (\hat{\boldsymbol{v}}_j^H\boldsymbol{v}_j)\hat{\boldsymbol{v}}_j]\} \\ &= c(j)\{\boldsymbol{I} + \mu[(\hat{\boldsymbol{v}}_j^H\hat{\boldsymbol{v}}_j)\boldsymbol{I} - \hat{\boldsymbol{v}}_j\hat{\boldsymbol{v}}_j^H]\boldsymbol{v}_j\boldsymbol{v}_j^H\}\boldsymbol{w}(j-1) \quad (50)\end{aligned}$$

where $c(j)$ and $\boldsymbol{w}(0)$ are chosen as in Algorithm 2.

The first form in (50) is for the sake of implementation, while the second form provides a simple intuitive interpretation of the algorithm. Note that the matrix $[(\hat{\boldsymbol{v}}_j^H\hat{\boldsymbol{v}}_j)\boldsymbol{I} - \hat{\boldsymbol{v}}_j\hat{\boldsymbol{v}}_j^H]\boldsymbol{v}_j\boldsymbol{v}_j^H$ represents the operation of first projecting onto the space spanned by $\boldsymbol{v}_j$ and then projecting the result onto the space orthogonal to $\hat{\boldsymbol{v}}_j$. Since $\boldsymbol{v}_j$ contains the signal and noise components and $\hat{\boldsymbol{v}}_j$ contains mainly the noise component, the algorithm can be roughly viewed as projecting the current weight vector to the direction of the noise and signal; then removing the noise part by orthogonal projection; and, finally, changing the current weight vector by a small amount in the resulting direction.

While an exact analysis of Algorithm 3 may be prohibitively difficult, we expect it to retain the numerical stability of Algorithm 2. In fact, we may view the estimation errors of $\boldsymbol{z}\boldsymbol{z}^H$ and $\boldsymbol{R}_v$ as perturbations of the eigenvalues in the proof of Proposition 3. Since Algorithm 2 is stable with respect to perturbations of the eigenvalues, this provides some indications on the convergence of Algorithm 3. Therefore, it is reasonable to choose the initial vector and $\mu$ to satisfy the requirement similar to that in Proposition 3. Note that (48) should be modified to $0 < \mu < 2/(\lambda_{\max}\boldsymbol{z}^H\boldsymbol{z})$, and the randomness in this algorithm actually helps to loosen the orthogonality requirement of the initial vector. We also expect behavior of Algorithm 3 to be similar to that of the LMS algorithm. As a rule of thumb, we should choose $\mu$ such that

$$0 < \mu < \frac{2}{(\text{average energy in } \boldsymbol{v}_j)^2}. \quad (51)$$

We reconsider the two examples in Section VI to demonstrate the behavior of Algorithm 3. In both examples, we start the algorithm by $\boldsymbol{w}(0) = [1\ 0\ \cdots\ 0]^T$, and the first element is chosen to be fixed in phase. $\mu$ is chosen to be half of the upper limit in (51). The results of the beamformer example are given in Figs. 11 and 12. Fig. 11 shows the average SNR achieved by the weight vectors given by the algorithm at each iteration. Fig. 12 gives the Euclidean norm of the vector difference between the weight vectors given by the algorithm and the ideal limit given in (49). Similar results of the RAKE example are plotted in Figs. 13 and 14.

Just like the LMS algorithm, we observe from Figs. 12 and 14 that the weight vectors do not converge to the ideal limits. In fact, they approach the ideal limits closely and exhibit small fluctuations about the ideal limits. Since the weight vectors do not converge to the ideal limits, the maximum SNR is not reached as indicated in Figs. 11 and 13. However, the average SNR achieved after a large number of iterations is less than a quarter of a decibel from the maximum value in the RAKE receiver example, while the corresponding difference in the beamformer example is about 1 dB. In the RAKE receiver

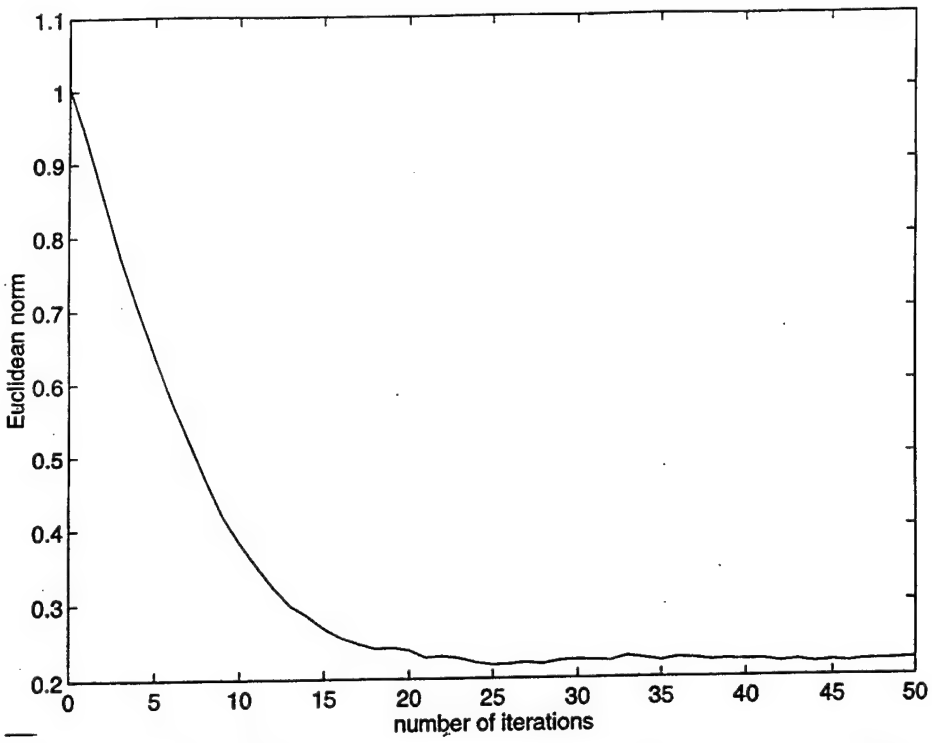


Fig. 12. Euclidean norm of the vector difference between the weight vector and the ideal limit in the beamformer example.

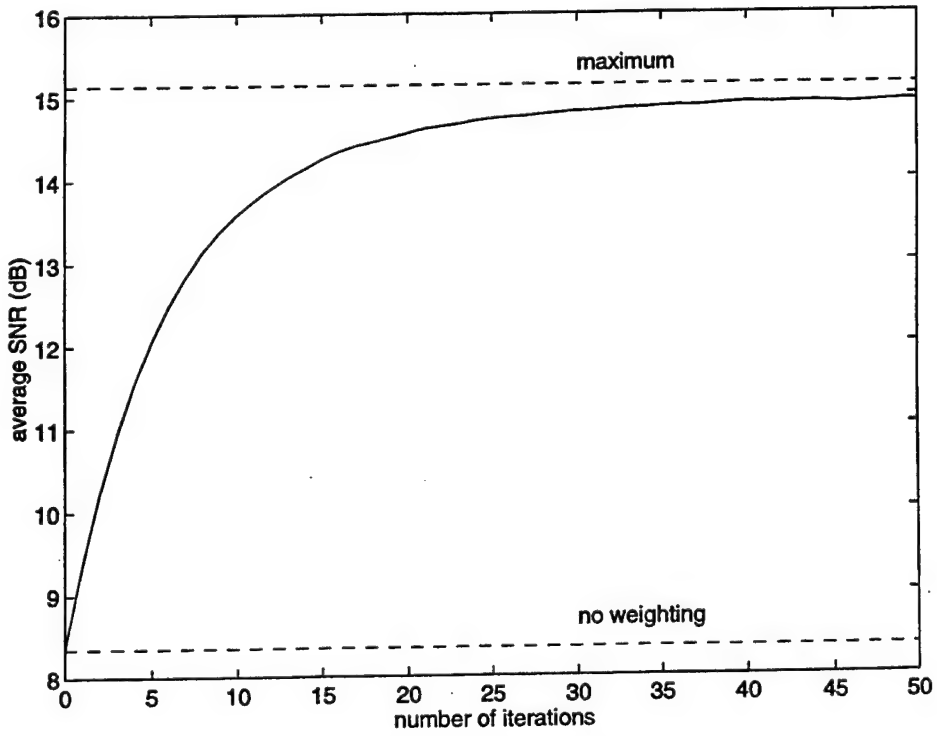


Fig. 13. Average SNR obtained by the blind adaptive algorithm in the RAKE receiver example.

example, it takes about 15 iterations (symbols) to get to an average SNR of 1 dB below the maximum value. That value for the beamformer example is about 20 iterations. Note that the eigenanalysis algorithm in Section VI requires a similar amount of symbols to get to the same average SNR.

We note that better estimators for the matrices $\boldsymbol{z}\boldsymbol{z}^H$ and $\boldsymbol{R}_v$ can also be obtained directly from the matched filter sample vectors $\boldsymbol{v}_j$ and $\hat{\boldsymbol{v}}_j$. However, these better estimators lead to more computationally complex algorithms. Therefore, we restrict our attention to the simple estimators mentioned in this paper. Unlike the adaptive algorithms suggested in [3]–[8], the computational complexity of Algorithm 3 is of the order of $MD$ per iteration which does not depend on the spreading factor $N$.

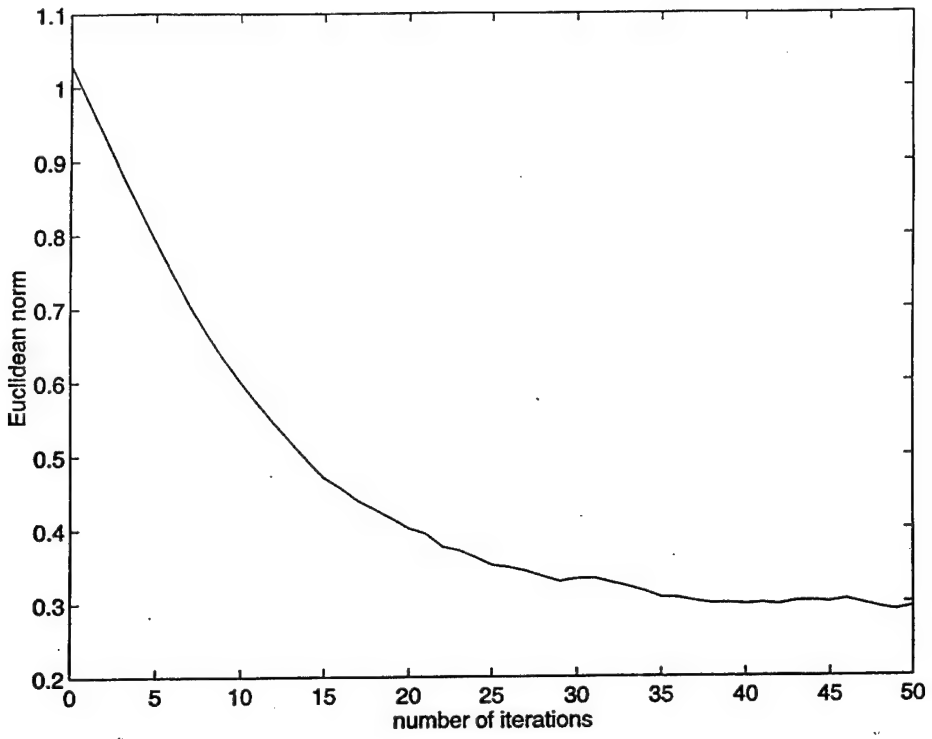


Fig. 14. Euclidean norm of the vector difference between the weight vector and the ideal limit in the RAKE receiver example.

Finally, we point out that Algorithms 1–3 are closely related to the algorithm developed in [8] which is also based on the method of constrained stochastic gradient descent. The major difference is that in [8], the vector equivalent to $\boldsymbol{z}$ is known *a priori*. Therefore, there is no need to obtain estimates of $\boldsymbol{z}\boldsymbol{z}^H$ as in Algorithm 3. On the other hand, since no knowledge of $\boldsymbol{z}$ is required in Algorithm 3, the same algorithm can be employed for the mismatch situations described in [8].

## VIII. Conclusions

In this paper, we have proposed a linear receiving structure which is composed of the conventional matched filter followed by a tapped delay line. The structure of the receiver also incorporates the possible use of an antenna array. When the weights in the tapped delay line are chosen so as to maximize the signal-to-noise ratio, the proposed receiver has a unified capability of rejecting multiple-access and narrowband interferences, and combining multipath components. We have also developed nonadaptive and adaptive algorithms to obtain the optimal weights in the tapped delay line. Among the various algorithms proposed, the blind adaptive algorithm, which is computationally simple and requires the same amount of information as the conventional matched filter receiver, is suitable for practical implementation. Results in this paper are applicable to a wide range of both coded and uncoded direct-sequence spread-spectrum multiple-access systems.

## Appendix I

In this appendix, we prove Proposition 1.

We need the following lemmas on the continuity of eigenvalues and generalized eigenvalues, which are corollaries of results from perturbation theory of matrices ([22, Appendix K], [18, p. 412], or [19]).

*Lemma 1:* Let $\{\boldsymbol{A}_N\}_{N=1}^{\infty}$ be a sequence of Hermitian matrices which converges to the Hermitian matrix $\boldsymbol{A}$. Let $\lambda_{\max}(\boldsymbol{A})$ and $\lambda_{\min}(\boldsymbol{A})$ denote the largest and the smallest eigenvalue of $\boldsymbol{A}$, respectively. Then

$$\lim_{N\to\infty} \lambda_{\max}(\boldsymbol{A}_N) = \lambda_{\max}(\boldsymbol{A}) \tag{52}$$

$$\lim_{N\to\infty} \lambda_{\min}(\boldsymbol{A}_N) = \lambda_{\min}(\boldsymbol{A}). \tag{53}$$

*Lemma 2:* Let $\{\boldsymbol{A}_N\}_{N=1}^{\infty}$ be a sequence of Hermitian matrices which converges to the Hermitian matrix $\boldsymbol{A}$, and $\{\boldsymbol{B}_N\}_{N=1}^{\infty}$ be a sequence of positive definite Hermitian matrices which converges to the positive definite Hermitian matrix $\boldsymbol{B}$. Moreover, let $\lambda_{\max}(\boldsymbol{A}_N, \boldsymbol{B}_N)$ be the largest generalized eigenvalue of the regular matrix pencil $(\boldsymbol{A}_N, \boldsymbol{B}_N)$, and $\lambda_{\max}(\boldsymbol{A}, \boldsymbol{B})$ be the largest generalized eigenvalue of the regular matrix pencil $(\boldsymbol{A}, \boldsymbol{B})$. Then

$$\lim_{N\to\infty} \lambda_{\max}(\boldsymbol{A}_N, \boldsymbol{B}_N) = \lambda_{\max}(\boldsymbol{A}, \boldsymbol{B}). \tag{54}$$

*Proof (of Proposition 1):* From the discussion in Section III, we know that $\lim_{N\to\infty} \boldsymbol{R}_{\boldsymbol{n}}$ exists and it is positive definite. Let $\boldsymbol{R}_{\boldsymbol{n},\infty}$ denote this limit. It can be shown easily that $\boldsymbol{w}_\infty = \boldsymbol{R}_{\boldsymbol{n},\infty}^{-1}\boldsymbol{z}$ is an eigenvector associated with the largest generalized eigenvalue of the matrix pencil $(\boldsymbol{z}\boldsymbol{z}^H, \boldsymbol{R}_{\boldsymbol{n},\infty})$ and the value of that eigenvalue is $\boldsymbol{z}^H\boldsymbol{R}_{\boldsymbol{n},\infty}^{-1}\boldsymbol{z}$. Therefore, from (22) and Lemma 2, we have

$$\lim_{N\to\infty} \max_{\boldsymbol{w}\neq\boldsymbol{0}} [\mathrm{SNR}(\boldsymbol{w})] = \mathrm{SNR}_\infty = \boldsymbol{z}^H\boldsymbol{R}_{\boldsymbol{n},\infty}^{-1}\boldsymbol{z}. \tag{55}$$

Note that $\boldsymbol{w}_N$ is an eigenvector associated with the largest eigenvalue of the matrix pencil $(\boldsymbol{R}_{\boldsymbol{v}} - \boldsymbol{R}_{\hat{\boldsymbol{v}}}, \boldsymbol{R}_{\hat{\boldsymbol{v}}})$. Again the existence of the AWGN component guarantees that $\boldsymbol{R}_{\boldsymbol{v}} - \boldsymbol{R}_{\hat{\boldsymbol{v}}}$ and $\boldsymbol{R}_{\hat{\boldsymbol{v}}}$ satisfy the conditions required for the sequences

$\{A_N\}_{N=1}^{\infty}$ and $\{B_N\}_{N=1}^{\infty}$ in Lemma 2, respectively. Applying Lemma 2 with (24), we have

$$\lim_{N\to\infty} \frac{\boldsymbol{w}_N^H(\boldsymbol{R}_v - \boldsymbol{R}_{\hat{v}})\boldsymbol{w}_N}{\boldsymbol{w}_N^H \boldsymbol{R}_{\hat{v}} \boldsymbol{w}_N} = \mathrm{SNR}_\infty. \tag{56}$$

Since

$$\lim_{N\to\infty} (\boldsymbol{R}_{\hat{v}} - \boldsymbol{R}_n) = 0$$

and

$$\lim_{N\to\infty} (\boldsymbol{R}_v - \boldsymbol{R}_{\hat{v}} - \boldsymbol{R}_z) = 0$$

applying Lemma 1, we can show that

$$\lim_{N\to\infty} \left| \frac{\boldsymbol{w}_N^H(\boldsymbol{R}_v - \boldsymbol{R}_{\hat{v}})\boldsymbol{w}_N}{\boldsymbol{w}_N^H \boldsymbol{R}_{\hat{v}} \boldsymbol{w}_N} - \frac{\boldsymbol{w}_N^H \boldsymbol{R}_z \boldsymbol{w}_N}{\boldsymbol{w}_N^H \boldsymbol{R}_n \boldsymbol{w}_N} \right| = 0. \tag{57}$$

Combining (55)–(57), we have the first inequality in Proposition 1.

Next, since

$$\lim_{N\to\infty} \boldsymbol{R}_n^{-1} = \boldsymbol{R}_{n,\infty}^{-1},$$
$$\lim_{N\to\infty} \overline{\boldsymbol{w}}_N = \boldsymbol{w}_\infty.$$

Since

$$\lim_{N\to\infty} \boldsymbol{R}_v^{-1} = (\boldsymbol{z}\boldsymbol{z}^H + \boldsymbol{R}_{n,\infty})^{-1},$$
$$\lim_{N\to\infty} \tilde{\boldsymbol{w}}_N = (1 + \mathrm{SNR}_\infty)^{-1} \boldsymbol{w}_\infty$$

by the matrix inversion lemma. Moreover, since $\hat{\boldsymbol{w}}_N$ is a complex multiple of $\tilde{\boldsymbol{w}}_N$, $\lim_{N\to\infty} \hat{\boldsymbol{w}}_N$ is just a complex multiple of $\lim_{N\to\infty} \tilde{\boldsymbol{w}}_N$. From (22), we have

$$\lim_{N\to\infty} \frac{\overline{\boldsymbol{w}}_N^H \boldsymbol{R}_z \overline{\boldsymbol{w}}_N}{\overline{\boldsymbol{w}}_N^H \boldsymbol{R}_n \overline{\boldsymbol{w}}_N} = \mathrm{SNR}_\infty. \tag{58}$$

Combining (58) with (55), we have the second inequality in Proposition 1. The other two inequalities can be proved in a similar way.

## Appendix II

In this appendix, we prove Propositions 2 and 3, and give stability arguments of Algorithms 1 and 2.

First, we need the following lemma on the eigenstructure of the matrix $(\boldsymbol{I} - \boldsymbol{P}_z)\boldsymbol{R}_v$.

*Lemma 3:* The matrix $(\boldsymbol{I} - \boldsymbol{P}_z)\boldsymbol{R}_v$ has the diagonalization

$$(\boldsymbol{I} - \boldsymbol{P}_z)\boldsymbol{R}_v = \boldsymbol{Q}\boldsymbol{\Lambda}\boldsymbol{Q}^{-1} \tag{59}$$

where $\boldsymbol{\Lambda}$ is a diagonal matrix whose elements are the eigenvalues $\{\lambda_m\}_{m=1}^{MD}$ of $(\boldsymbol{I}-\boldsymbol{P}_z)\boldsymbol{R}_v$ and $\boldsymbol{Q}$ is an invertible matrix with the corresponding eigenvectors of $(\boldsymbol{I}-\boldsymbol{P}_z)\boldsymbol{R}_v$ as its columns. All the eigenvalues are real and nonnegative, and exactly one of them, say, $\lambda_1$, is zero. Then the first column of $\boldsymbol{Q}$ can be chosen to be $\tilde{\boldsymbol{w}}_N$, the MMSE solution $\tilde{\boldsymbol{w}}_N$ defined in (28).

*Proof:* Note that since $\boldsymbol{R}_v$ is positive definite, $\boldsymbol{R}_v = \boldsymbol{G}\boldsymbol{G}$, where $\boldsymbol{G}$, which is invertible and Hermitian, is the matrix square root of $\boldsymbol{R}_v$. Suppose $\lambda$ is an eigenvalue of $(\boldsymbol{I} - \boldsymbol{P}_z)\boldsymbol{R}_v$ and $\boldsymbol{x}$ is the corresponding eigenvector. Then

$$(\boldsymbol{I} - \boldsymbol{P}_z)\boldsymbol{R}_v\boldsymbol{x} = (\boldsymbol{I} - \boldsymbol{P}_z)\boldsymbol{G}\boldsymbol{G}\boldsymbol{x} = \lambda\boldsymbol{x}. \tag{60}$$

Let $\boldsymbol{y} = \boldsymbol{G}\boldsymbol{x}$, then

$$\boldsymbol{G}(\boldsymbol{I} - \boldsymbol{P}_z)\boldsymbol{G}\boldsymbol{y} = \lambda\boldsymbol{y}. \tag{61}$$

From (60) and (61), since $\boldsymbol{G}$ is invertible, the eigenvalues of $\boldsymbol{G}(\boldsymbol{I} - \boldsymbol{P}_z)\boldsymbol{G}$ and $(\boldsymbol{I} - \boldsymbol{P}_z)\boldsymbol{R}_v$ are the same. Moreover, if $\boldsymbol{x}$ is an eigenvector of $\boldsymbol{G}(\boldsymbol{I} - \boldsymbol{P}_z)\boldsymbol{G}$, then $\boldsymbol{G}^{-1}\boldsymbol{x}$ is an eigenvector of $(\boldsymbol{I} - \boldsymbol{P}_z)\boldsymbol{R}_v$. Since $\boldsymbol{G}(\boldsymbol{I} - \boldsymbol{P}_z)\boldsymbol{G}$ is a positive semidefinite Hermitian matrix, all its eigenvalues, and hence, all the eigenvalues of $(\boldsymbol{I} - \boldsymbol{P}_z)\boldsymbol{R}_v$ are real and nonnegative. Moreover, $\boldsymbol{G}(\boldsymbol{I} - \boldsymbol{P}_z)\boldsymbol{G}$ has the diagonalization

$$\boldsymbol{G}(\boldsymbol{I} - \boldsymbol{P}_z)\boldsymbol{G} = \boldsymbol{U}\boldsymbol{\Lambda}\boldsymbol{U}^H \tag{62}$$

where $\boldsymbol{\Lambda}$ is a diagonal matrix whose elements are the eigenvalues $\{\lambda_m\}_{m=1}^{MD}$ of $\boldsymbol{G}(\boldsymbol{I} - \boldsymbol{P}_z)\boldsymbol{G}$ and $\boldsymbol{U}$ is a unitary matrix with the corresponding eigenvectors of $\boldsymbol{G}(\boldsymbol{I} - \boldsymbol{P}_z)\boldsymbol{G}$ as its columns. Let

$$\boldsymbol{Q} = \sqrt{\boldsymbol{z}^H \boldsymbol{R}_v^{-1} \boldsymbol{z}}\, \boldsymbol{G}^{-1}\boldsymbol{U}.$$

We get (59) from (62).

Set $\lambda = 0$ in (60). Since $\boldsymbol{R}_v$ is invertible, for $\boldsymbol{x} \neq \boldsymbol{0}$, (60) is satisfied when and only when $\boldsymbol{R}_v\boldsymbol{x}$ is parallel to the vector $\boldsymbol{z}$. Moreover, since $\boldsymbol{Q}$ is of full rank, we conclude that exactly one of the eigenvalues of $(\boldsymbol{I} - \boldsymbol{P}_z)\boldsymbol{R}_v$ is zero. By rearranging the columns of $\boldsymbol{U}$ if necessary, we can set $\lambda_1 = 0$ and the first column of $\boldsymbol{Q}$ to be the eigenvector corresponding to $\lambda_1$. Finally, from the fact that

$$\boldsymbol{Q}^H \boldsymbol{R}_v \boldsymbol{Q} = (\boldsymbol{z}^H \boldsymbol{R}_v^{-1} \boldsymbol{z})\boldsymbol{I} \tag{63}$$

the first column of $\boldsymbol{Q}$ is exactly $\tilde{\boldsymbol{w}}_N$. □

Now we can employ Lemma 3 to prove Propositions 2 and 3.

*Proof (of Proposition 2):* Let $\boldsymbol{u}(j) = \boldsymbol{Q}^{-1}\boldsymbol{w}(j)$. We can rewrite (42) as

$$\boldsymbol{u}(j) = (\boldsymbol{I} - \mu\boldsymbol{\Lambda})\boldsymbol{u}(j-1). \tag{64}$$

From (64), the $m$th element of the vector $\boldsymbol{u}(j)$ is given by

$$u_m(j) = (1 - \mu\lambda_m)^j u_m(0) \tag{65}$$

where $u_m(0)$ is the $m$th element of the initial vector $\boldsymbol{u}(0) = \boldsymbol{Q}^{-1}\boldsymbol{w}(0)$. Since $\lambda_1 = 0$ and by (43), $|1 - \mu\lambda_m| < 1$, for $m = 2, 3, \cdots, MD$, we have

$$\lim_{j\to\infty} \boldsymbol{w}(j) = \boldsymbol{Q}[\lim_{j\to\infty} \boldsymbol{u}(j)] = u_1(0)\tilde{\boldsymbol{w}}_N. \tag{66}$$

From (63) and (65)

$$\sigma(\boldsymbol{w}(j)) = (\boldsymbol{z}^H \boldsymbol{R}_v^{-1} \boldsymbol{z}) \sum_{m=1}^{MD} (1 - \mu\lambda_m)^{2j} |u_m(0)|^2. \tag{67}$$

Therefore, (67) shows that $\sigma(\boldsymbol{w}(j)) \downarrow (z^H R_v^{-1} z)|u_1(0)|^2$. Finally, the proof is completed by showing $u_1(0) = z^H \boldsymbol{w}(0)/z^H R_v^{-1} z$. This fact can be shown from the identity

$$(\boldsymbol{Q}^{-1})^H = \frac{1}{z^H R_v^{-1} z} R_v \boldsymbol{Q}. \tag{68}$$

□

*Proof (of Proposition 3):* Similar to (65), we have, for $n = 1, 2, \cdots, MD$

$$u_n(j) = C(j)(1 - \mu\lambda_n)^j u_n(0) \tag{69}$$

where

$$C(j) = \prod_{j'=1}^{j} c(j').$$

For each $j>0$, since $||\boldsymbol{w}(j)|| = 1$, $||\boldsymbol{Q}\boldsymbol{u}(j)|| = 1$. Since $R_v$ is positive definite, so is the matrix $\boldsymbol{Q}^H\boldsymbol{Q}$. Denote the $(m,n)$th element of $\boldsymbol{Q}^H\boldsymbol{Q}$ by $q_{mn}$. Applying these to (69), we get, for $n = 1, 2, \cdots, MD$

$$|u_n(j)| = \left[\sum_{m'=1}^{MD}\sum_{n'=1}^{MD} q_{m'n'} \left(\frac{u_{m'}(0)}{u_n(0)}\right)^* \left(\frac{u_{n'}(0)}{u_n(0)}\right) \cdot \left(\frac{1-\mu\lambda_{m'}}{1-\mu\lambda_n}\right)^j \left(\frac{1-\mu\lambda_{n'}}{1-\mu\lambda_n}\right)^j\right]^{-1/2} \tag{70}$$

if $(1-\mu\lambda_n)u_n(0) \neq 0$. Otherwise, $u_n(j) = 0$. Note that since $z^H\boldsymbol{w}(0) \neq 0$ and $\lambda_1 = 0$, $(1-\mu\lambda_1)u_1(0) \neq 0$. If (48) is satisfied

$$|1-\mu\lambda_1| > |1-\mu\lambda_n|, \qquad \text{for } n = 2, 3, \cdots, MD.$$

Since $q_{11} = ||\tilde{\boldsymbol{w}}_N||^2$, we have from (70)

$$\lim_{j\to\infty} |u_1(j)| = 1/||\tilde{\boldsymbol{w}}_N||$$

and

$$\lim_{j\to\infty} u_n(j) = 0, \qquad \text{for } n = 2, 3, \cdots, MD.$$

Combining these limiting results with the fact that $\boldsymbol{w}(j) = \boldsymbol{Q}\boldsymbol{u}(j)$

$$|w_m(j)| \to |\tilde{w}_{Nm}|/||\tilde{\boldsymbol{w}}_N||.$$

Since $\tilde{w}_{Nm} \neq 0, w_m(j) \neq 0$ for all sufficiently large $j$. Then, $\arg(w_m(j)) = 0$ for all sufficiently large $j$. Hence, we have

$$\lim_{j\to\infty} \arg(u_1(j)) = -\arg(\tilde{w}_{Nm}).$$

This implies that

$$\lim_{j\to\infty} u_1(j) = \exp(-j\arg(\tilde{w}_{Nm}))/||\tilde{\boldsymbol{w}}_N||$$

and, hence, (49).

We notice from (47) that $z^H\boldsymbol{w}(j) = C(j)z^H\boldsymbol{w}(0)$ for all $j>0$. Putting this and (63) in (45), we get

$$\tilde{\sigma}(\boldsymbol{w}(j)) = \frac{z^H R_v^{-1} z}{|z^H\boldsymbol{w}(0)|^2} \sum_{m=1}^{MD} (1-\mu\lambda_m)^{2j}|u_m(0)|^2. \tag{71}$$

Therefore, (71) shows that $\tilde{\sigma}(\boldsymbol{w}(j)) \downarrow 1/z^H R_v^{-1} z$. □

The numerical instability of Algorithm 1 can be seen from (65) by setting $m = 1$. Since $1 - \mu\lambda_1 = 1$, any perturbation on $\lambda_1$ caused by numerical or other reasons may affect the convergence of the element $v_1(j)$, and, hence, the convergence of Algorithm 1. On the other hand, Algorithm 2 is numerically stable when the condition in (48) is satisfied. It can be seen from (70) that the convergence of Algorithm 2 does not depend on the absolute magnitudes of the factors $1 - \mu\lambda_n$, for $n = 1, 2, \cdots, MD$, but on their relative magnitudes. Therefore, as long as the perturbation on $\lambda_1$ is small, the magnitude of $1-\mu\lambda_1$ is still the largest, and hence, Algorithm 2 converges to the desired result.

## REFERENCES


[1] S. Verdú, "Minimum probability of error for asynchronous Gaussian multiple-access channels," *IEEE Trans. Inform. Theory*, vol. IT-32, pp. 85–96, Jan. 1986.

[2] R. Lupas and S. Verdú, "Linear multiuser detectors for synchronous code-division multiple-access channels," *IEEE Trans. Inform. Theory*, vol. 35, pp. 123–136, Jan. 1989.

[3] M. Abdulrahman, A. U. H. Sheikh, and D. D. Falconer, "Decision feedback equalization for CDMA in indoor wireless communications," *IEEE J. Select. Areas Commun.*, vol. 12, no. 4, May 1994.

[4] P. B. Rapajic and B. S. Vucetic, "Adaptive receiver structures for asynchronous CDMA systems," *IEEE J. Select. Areas Commun.*, vol. 12, pp. 685–697, May 1994.

[5] C. N. Pateros and G. J. Saulnier, "An adaptive correlator receiver for direct-sequence spread-spectrum communication," *IEEE Trans. Commun.*, vol. 44, pp. 1543–1552, Nov. 1996.

[6] S. L. Miller, "An adaptive direct-sequence code-division multiple-access receiver for multiuser interference rejection," *IEEE Trans. Commun.*, vol. 43, pp. 1746–1754, Feb./Mar./Apr. 1995.

[7] U. Madhow and M. Honig, "MMSE interference suppression for direct-sequence spread-spectrum CDMA," *IEEE Trans. Commun.*, vol. 42, pp. 3178–3188, Dec. 1994.

[8] M. Honig, U. Madhow, and S. Verdú, "Blind adaptive multiuser detection," *IEEE Trans. Inform. Theory*, vol. 41, pp. 944–960, July 1995.

[9] R. Kohno, H. Imai, M. Hatori, and S. Pasupathy, "Combination of an adaptive array antenna and a canceller of interference for direct-sequence spread-spectrum multiple-access system," *IEEE J. Select. Areas Commun.*, vol. 8, pp. 641–649, May 1990.

[10] M. Nagatsuka and R. Kohno, "A spatially temporally optimal multi-user receiver using an array antenna for DS/CDMA," *IEICE Trans. Commun.*, vol. E78-B, pp. 1489–1497, Nov. 1995.

[11] B. Suard, A. Naguib, G. Xu, and A. Paulraj, "Performance analysis of CDMA mobile communication systems using antenna arrays," in *Proc. ICASSP '93*, vol. VI, Apr. 1993, pp. 153–156.

[12] A. F. Naguib, A. Paulraj, and T. Kailath, "Capacity improvement with base-station antenna array in cellular CDMA," *IEEE Trans. Veh. Technol.*, vol. 43, pp. 691–698, Aug. 1994.

[13] U. Madhow, "Blind adaptive interference suppression for direct-sequence CDMA," invited submission to *Proc. IEEE* (Special Issue on Blind Systems Identification and Estimation), to be published, Sept. 1998.

[14] A. Monk, M. Davis, L. B. Milstein, and C. W. Helstrom, "A noise-whitening approach to multiple-access noise rejection—Part I: Theory and background," *IEEE J. Select. Areas Commun.*, vol. 12, pp. 817–827, June 1994.

[15] N. Mandayam and S. Verdú, "Analysis of an approximate decorrelating detector," *Wireless Personal Commun.*, to be published.

[16] TIA/EIA/IS-95 Interim Standard, *Mobile Station-Base Station Compatibility Standard for Dual Mode Wideband Spread Spectrum Cellular System*, Telecommun. Industry Assoc., Washington, DC, July 1993.

[17] F. R. Gantmacher, *The Theory of Matrices*, vol. I. New York: Chelsea, 1960.

[18] G. H. Golub and C. F. Van Loan, *Matrix Computations*, 2nd ed. Baltimore, MD: Johns Hopkins Univ. Press, 1989.

[19] G. W. Stewart, "Perturbation bounds for the definite generalized eigenvalues problem," *Lin. Alg. and Its Applic.*, vol. 23, pp. 69–86, 1979.

[20] S. Haykin, *Adaptive Filter Theory*, 2nd ed. Englewood Cliffs, NJ: Prentice-Hall, 1991.

[21] J. G. Proakis, *Digital Communications*, 3rd ed. New York: McGraw-Hill, 1995.

[22] A. M. Ostrowski, *Solution of Equations in Euclidean and Banach Spaces*. New York: Academic, 1973.

# Bounds on the Pairwise Error Probability of Coded DS/SSMA Communication Systems in Rayleigh Fading Channels

Tsao-Tsen Chen, *Member, IEEE*, and James S. Lehnert, *Senior Member, IEEE*

*Abstract*— **Arbitrarily tight upper and lower bounds on the pairwise error probability (PEP) of a trellis-coded or convolutional-coded direct-sequence spread-spectrum multiple-access (DS/SSMA) communication system over a Rayleigh fading channel are derived. A new set of probability density functions (pdf's) and cumulative distribution functions (cdf's) of the multiple-access interference (MAI) statistic is derived, and a modified bounding technique is proposed to obtain the bounds. The upper bounds and lower bounds together specify the accuracy of the resulting estimation of the PEP, and give an indication of the system error performance. Several suboptimum decoding schemes are proposed and their performances are compared to that of the optimum decoding scheme by the average pairwise error probability (APEP) values. The approach can be used to accurately study the multiple-access capability of the coded DS/SSMA system without numerical integrations.**

*Index Terms*—**Code division multiaccess, error correction coding, error analysis, fading channels.**

## I. Introduction

PERFORMANCE of trellis-coded modulation (TCM) systems over the Rayleigh fading channel can be evaluated using several different methods [1]–[8], [18]. In [1], a residue method was used to compute the exact pairwise error probability (PEP) of a TCM system with imperfect channel state information (CSI). In [2], tight bounds on the PEP were first obtained, and then the upper bound was expressed in a product form to be used with the transfer function bounding technique [17], [18] to get the upper union bound (UUB) on the bit-error probability (BEP) with ideal CSI. In [4] and [6]–[8], the saddle-point approximation (SAP) method was used to approximate the PEP. In [3] and [5], Chernoff upper bounds on the PEP were derived for both the ideal CSI and no CSI cases. The Chernoff upper bounds then were used with the transfer function bounding technique to get the UUB on the BEP.

In general, Chernoff upper bounds on the PEP's allow the use of the transfer function bounding technique to get the UUB on the BEP over the fading channel, but the result is too loose. On the other hand, it is impractical to compute the exact PEP's (if obtainable) for all the error paths, and only dominant PEP values can be used to approximate the UUB on the BEP. The situation becomes more complex when the multiple-access channel is considered. Arbitrarily tight performance bounds of asynchronous direct-sequence spread-spectrum multiple-access (DS/SSMA) systems have been computed for both the uncoded [10]–[12] and coded [14] systems over the additive white Gaussian noise (AWGN) channel when deterministic spreading sequences with arbitrary chip waveforms are used. In this work, the probability density function (pdf) and cumulative distribution function (cdf) of the multiple-access interference (MAI) statistic from each interfering user were first computed, and then the (one-dimensional) bounding technique [11] was applied to get the results. In this paper, we find that the MAI statistic needed for the computation of the performance bounds of the coded DS/SSMA systems over Rayleigh fading channels is quite different from that over the AWGN channel; in particular, a multidimensional pdf is needed to characterize the MAI statistic, and the support in each dimension of the pdf is nonnegative. Therefore, a new set of pdf's and cdf's of the MAI statistic is derived, and a modified bounding technique is proposed, together with the residue method [1], to obtain the arbitrarily tight upper and lower bounds on the PEP of the coded DS/SSMA systems.

It was shown in [7] and [8] that the SAP method can be used to approximate the PEP for narrowband coded systems over a general class of fading channels, and can avoid some numerical problems. However, in this paper, we focus on the exact PEP only. The exact PEP can serve as a reliable reference to other possible upper bounds on the PEP, and is an indication of the system error performance by itself. Hence, the SAP method is not studied here. Also, the upper union bound on the BEP can be approximated by using the dominant PEP values, but this issue is not discussed here. Several suboptimum decoding schemes are proposed and their performances are compared to that of the maximum-likelihood optimum decoding scheme by the average pairwise error probability (APEP) values. We find that the performance of each suboptimum decoding scheme is very close to that of the optimum decoding scheme under different conditions. The formulas derived in this paper are suitable for TCM systems over a slow Rayleigh fading channel with one- or two-dimensional signal sets, imperfect CSI, coherent detection, and ideal interleaving, and for asynchronous DS/SSMA systems

Paper approved by R. Kohno, the Editor for Spread Spectrum Theory and Applications of the IEEE Communications Society. Manuscript received February 12, 1997; revised March 19, 1998. This paper was presented in part at the IEEE International Conference on Universal Personal Communications (ICUPC), San Diego, CA, October 12–16, 1997.

T.-T. Chen is with the Wireless Systems Core Technology Department, Lucent Technologies, Whippany, NJ 07981 USA.

J. S. Lehnert is with the School of Electrical and Computer Engineering, Purdue University, West Lafayette, IN 47907-1285 USA.

Publisher Item Identifier S 0090-6778(98)09381-7.

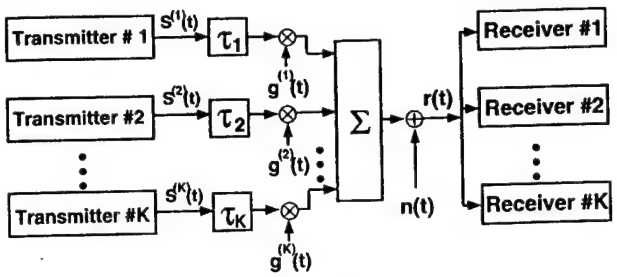


Fig. 1. Baseband equivalent system model.

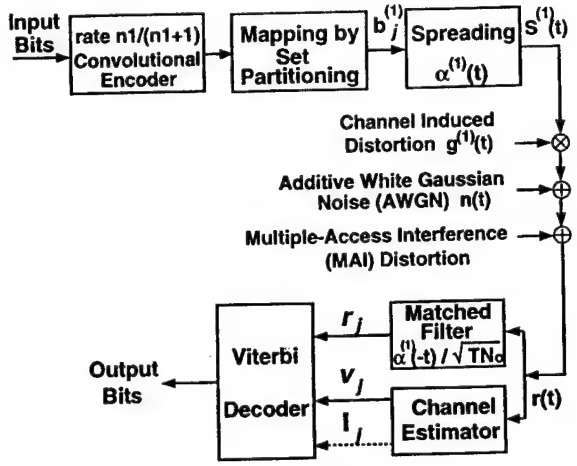


Fig. 2. Transmitter/receiver pair of the first user.

with arbitrary chip waveforms. We call the system under study the TCM/SSMA system. The techniques described in this paper can also be used to analyze convolutional-coded SSMA (CC/SSMA) systems.

The paper is organized as follows. In Section II we present the system model. In Section III we characterize the MAI statistic and propose a modified bounding technique. Section IV uses the residue method and the modified bounding technique to derive the upper and lower bounds on the PEP for both the optimum and suboptimum decoding schemes. Finally, Section V offers some conclusions.

## II. System Model

The system model (see Fig. 1) that we examine is similar to that used frequently in previous studies of asynchronous TCM/SSMA systems [13], [14]. There are $K$ transmitter/receiver pairs (see Fig. 2) sharing a common channel.

### A. Transmitter

The input data sequence is divided into blocks of $n$ bits. Next, $n1$ of these bits select a coset of the signal constellation through a rate $n1/(n1+1)$ convolutional encoder, while the remaining $n2$ select a signal point within the given coset. This is the mapping by set partitioning [16]. We define the $k$th user's baseband coded signal by

$$b^{(k)}(t) = \sum_{j=-\infty}^{\infty} b_j^{(k)} p_T(t - jT) \tag{1}$$

where $\{b_j^{(k)}\}$ is the output symbol sequence from the trellis encoder of the $k$th transmitter, $T$ is the symbol interval, and $p_T(t)$ is the unit pulse on $[0, T)$. We normalize the signal constellation so that the average signal energy equals 1. All signature sequences are deterministic. The signature sequence $\{\alpha_h^{(k)}\}$, where each $\alpha_h^{(k)} \in \{-1, 1\}$, is used to form the $k$th user's spreading waveform that is given by

$$\alpha^{(k)}(t) = \sum_{h=-\infty}^{\infty} \alpha_h^{(k)} \psi(t - hT_c) \tag{2}$$

where $\psi(t)$ is the common chip waveform for all signals. The chip waveform $\psi(t)$ is time-limited to $[0, T_c)$, where the chip duration $T_c$ satisfies $T_c = T/N$, and $N$ is the period of the signature sequence. The chip waveform is also normalized such that $\int_0^{T_c} \psi^2(t)\, dt = T_c$.

The baseband transmitted signal of the $k$th user is given by

$$S^{(k)}(t) = \sqrt{2P}\alpha^{(k)}(t)b^{(k)}(t) \exp(j\phi_k) \tag{3}$$

where $P$ is the power of the transmitted signal, and $\phi_k$ is the phase of the $k$th transmitter.

### B. Receiver

The received baseband signal for all receivers is

$$r(t) = \sum_{k=1}^{K} \sqrt{2P} g^{(k)}(t)\alpha^{(k)}(t - \tau_k)b^{(k)}(t - \tau_k) \exp(j\theta_k) + n(t) \tag{4}$$

where $\{g^{(k)}(t)\}$ is a sequence of independent, zero-mean, complex, Gaussian fading processes with a common variance of $\sigma_g^2 = 1/2\, E\{|g^{(k)}(t)|^2\}$, $\tau_k$ is the time delay parameter that accounts for propagation delay and the lack of synchronism between the transmitters, $\theta_k = \phi_k - \omega_c\tau_k$ is the phase angle of the $k$th carrier, $\omega_c$ is the carrier frequency, and $n(t)$ is the complex envelope of the channel white Gaussian noise with double-sided power spectral density (psd) $N_o$. The notation $E\{\cdot\}$ denotes expectation. We assume that $g^{(k)}(t) = g_j^{(k)}$ over the $j$th interval (i.e., slow fading), and ideal interleaving in this study. Then $g_j^{(k)}$'s are independent and identically distributed (i.i.d.) complex Gaussian random variables, each with zero mean and variance $\sigma_g^2$. Symmetry allows us to consider only the receiver that is listening to the first transmitter (the "desired receiver"). Accordingly, $\tau_1 = \theta_1 = 0$, and for $k \neq 1$, the delays $\tau_k$ and the phase angles $\theta_k$ are random variables that are uniformly distributed on $[0, T)$ and $[0, 2\pi)$, respectively. The average received symbol energy and bit energy are given by $E_s = 2\sigma_g^2 PT$ and $E_b = 1/n\, E_s$, respectively.

Correlation receivers are used to demodulate the received signal (see Fig. 2). The decision statistic of the first user at interval $j$ is given by

$$r_j = u_j^{(1)} b_j^{(1)} + n_j + \sum_{k=2}^{K} u_j^{(k)} I_j^{(k)} \tag{5}$$

where

$$u_j^{(k)} = \sqrt{2PT/N_o}\, g_j^{(k)}, \qquad k = 1, \cdots, K$$

is a zero-mean complex Gaussian random variable with variance $\sigma_u^2 = E_s/N_o$, $n_j$ is a zero-mean complex Gaussian random variable with variance $\sigma_n^2 = 1$, and $I_j^{(k)}$ is the MAI from the $k$th user given by

$$I_j^{(k)} = \frac{1}{T}\left[b_{j-1}^{(k)} R_{k,1}(\tau_k) + b_j^{(k)} \hat{R}_{k,1}(\tau_k)\right] \exp(j\theta_k) \quad (6)$$

where $R_{k,1}(\cdot)$ and $\hat{R}_{k,1}(\cdot)$ are the continuous-time partial crosscorrelation functions of the $k$th and first spreading waveforms defined in [9].

The channel state information (CSI) is available for the desired receiver, and is denoted by the sequence $\boldsymbol{v} = \{v_j\}$, where $v_j$ is the estimate of $u_j^{(1)}$. We assume that $v_j$'s are i.i.d. complex Gaussian random variables with zero mean and variance of $\sigma_v^2$, and the covariance of $u_j^{(1)}$ and $v_j$ is $\sigma_{uv}^2$. The correlation coefficient of $u_j^{(1)}$ and $v_j$ is then given by $u = \sigma_{uv}^2/\sigma_u\sigma_v$. We assume that the desired receiver has perfect knowledge of $u$. If we condition on $v_j$, the random variable $u_j^{(1)}$ is then a complex Gaussian random variable with mean $u(\sigma_u/\sigma_v)v_j \triangleq \beta v_j$ and variance $\sigma_u^2(1-|u|^2) \triangleq \sigma_e^2$. The knowledge of the MAI statistic for the desired receiver (dashed line in Fig. 2) will be discussed in Section IV. We assume either we have perfect knowledge of it (optimum decoding), or no knowledge of it (suboptimum decoding).

## III. Characterization of the MAI Statistic

In this section, we characterize the MAI statistic in a TCM/SSMA system with the Rayleigh fading channel. For simplicity, we study the rectangular chip waveform only. However, we can obtain the results for the arbitrary chip waveform case by applying the techniques used in [10].

Without loss of generality, we assume that an error symbol sequence diverges from the transmitted symbol sequence from the first demodulation interval, and remerges with the transmitted sequence after $L$ intervals. We will see that the error performance of the system under study depends on the MAI $I_j^{(k)}$ through the random vector $\boldsymbol{I}$ given by

$$\boldsymbol{I} = [I_1, I_2, \cdots, I_L] \quad (7)$$

where

$$I_j = \sum_{k=2}^{K} |I_j^{(k)}|^2 \triangleq \sum_{k=2}^{K} \hat{I}_j^{(k)} \quad (8)$$

for $j = 1 \cdots L$, and $I_j^{(k)}$ is as defined in (6). Since the MAI from different interfering users are independent, $\boldsymbol{I}$ can be obtained by the convolution of the random vectors $\boldsymbol{I^{(k)}}$ defined as

$$\boldsymbol{I^{(k)}} = [\hat{I}_1^{(k)}, \hat{I}_2^{(k)}, \cdots, \hat{I}_L^{(k)}] \quad (9)$$

for $k = 2 \cdots K$. It is shown in [9] that for $0 \le \lambda_k T_c \le \tau_k < (\lambda_k + 1)T_c$

$$R_{k,1}(\tau_k) = C_{k,1}(\lambda_k - N)(T_c - s_k) + C_{k,1}(\lambda_k - N + 1)s_k \quad (10)$$

and

$$\hat{R}_{k,1}(\tau_k) = C_{k,1}(\lambda_k)(T_c - s_k) + C_{k,1}(\lambda_k + 1)s_k \quad (11)$$

where $\lambda_k$ is uniformly distributed on the set $\{0, \cdots, N-1\}$, $s_k = \tau_k - \lambda_k T_c$ is uniformly distributed on $[0, T_c)$, and $C_{k,1}(\cdot)$ is the aperiodic crosscorrelation function defined in [9]. Note that the random variables $\lambda_k$ and $s_k$ are independent. By replacing $R_{k,1}(\cdot)$ and $\hat{R}_{k,1}(\cdot)$ by (10) and (11) in (6), we can express $\hat{I}_j^{(k)}$ as

$$\hat{I}_j^{(k)} = [A_{1,j}^{(k)} U_k + A_{2,j}^{(k)}(1-U_k)]^2 + [B_{1,j}^{(k)} U_k + B_{2,j}^{(k)}(1-U_k)]^2 \quad (12)$$

where $U_k = s_k/T_c$ is uniformly distributed on $[0, 1)$, and

$$\begin{aligned}
A_{1,j}^{(k)} &= \frac{1}{N}\left[b_{I,j-1}^{(k)} C_{k,1}(\lambda_k - N + 1) + b_{I,j}^{(k)} C_{k,1}(\lambda_k + 1)\right] \\
A_{2,j}^{(k)} &= \frac{1}{N}\left[(b_{I,j-1}^{(k)} C_{k,1}(\lambda_k - N) + b_{I,j}^{(k)} C_{k,1}(\lambda_k)\right] \\
B_{1,j}^{(k)} &= \frac{1}{N}\left[b_{Q,j-1}^{(k)} C_{k,1}(\lambda_k - N + 1) + b_{Q,j}^{(k)} C_{k,1}(\lambda_k + 1)\right] \\
B_{2,j}^{(k)} &= \frac{1}{N}\left[b_{Q,j-1}^{(k)} C_{k,1}(\lambda_k - N) + b_{Q,j}^{(k)} C_{k,1}(\lambda_k)\right] \quad (13)
\end{aligned}$$

with $b_{I,j}^{(k)} = \mathrm{Re}\left\{b_j^{(k)}\right\}$ and $b_{Q,j}^{(k)} = \mathrm{Im}\left\{b_j^{(k)}\right\}$.

### A. Modified Bounding Technique

In order to evaluate the multiple-access capability, we modify the bounding technique introduced in [11] as follows. We define the discrete random vector $\boldsymbol{D^{(k)}} = [D_1^{(k)}, \cdots, D_L^{(k)}]$, which characterizes $\boldsymbol{I^{(k)}}$, as

$$\boldsymbol{D^{(k)}} = [i_1, \cdots, i_L], \qquad \text{if } \boldsymbol{I^{(k)}} \in \boldsymbol{V}(i_1, \cdots, i_L) \quad (14)$$

where $\boldsymbol{V}(i_1, \cdots, i_L)$ is a cube defined as

$$\begin{aligned}
&\boldsymbol{V}(i_1, \cdots, i_L) \\
&\quad = \left\{(x_1, \cdots, x_L);\ \frac{i_j}{N_u} \le x_j < \frac{i_j + 1}{N_u}, j = 1, \cdots, L\right\} \quad (15)
\end{aligned}$$

$N_u$ is a positive integer, and $\boldsymbol{I^{(k)}}$ is as defined in (9). The probability mass function (pmf) of $\boldsymbol{D^{(k)}}$ is defined as

$$d^{(k)}(i_1, \cdots, i_L) = \Pr\left(\boldsymbol{D^{(k)}} = [i_1, \cdots, i_L]\right). \quad (16)$$

It is examined in the next subsection.

We define the discrete random vector $\boldsymbol{D}$, which characterizes $\boldsymbol{I}$, as $\boldsymbol{D} = \sum_{k=2}^{K} \boldsymbol{D^{(k)}}$. The pmf of $\boldsymbol{D}$ is defined as

$$d(i_1, \cdots, i_L) = \Pr(\boldsymbol{D} = [i_1, \cdots, i_L]). \quad (17)$$

Since the random vectors in the set $\{\boldsymbol{D^{(k)}};\ k = 2, \cdots, K\}$ are independent, $d(\cdot, \cdots, \cdot)$ can be computed by performing a discrete convolution of the discrete densities $d^{(k)}(\cdot, \cdots, \cdot)$. Let the cube $\boldsymbol{VK}(i_1, \cdots, i_L)$ be defined as

$$\begin{aligned}
\boldsymbol{VK}(i_1, \cdots, i_L) = \Bigg\{&(x_1, \cdots, x_L);\ \frac{i_j}{N_u} \le x_j < \frac{i_j + K - 1}{N_u}, \\
&j = 1, \cdots, L\Bigg\}. \quad (18)
\end{aligned}$$

Then the probability mass $d(i_1, \cdots, i_L)$ means part of the probability that $\boldsymbol{I}$ falls in the cube $\boldsymbol{VK}(i_1, \cdots, i_L)$. This will be used to compute the upper and lower bounds on the PEP in Section IV.

### B. PMF of $\boldsymbol{D^{(k)}}$

From (8), (9), (12), and (13), if we condition on the sequence of random variables $\{b_j^{(k)}\}_{j=0}^{L}$ and $\lambda_k$, the random vector $\boldsymbol{I^{(k)}}$ is a quadratic function of the single random variable $U_k$. The conditional pdf and cdf of $\hat{I}_j^{(k)}$ are given in the Appendix. For $L = 1$, the conditional pmf of $\boldsymbol{D^{(k)}}$ is given by

$$d^{(k)}(i_1) = F_{\hat{I}_1^{(k)}}\left(\frac{i_1+1}{N_u}\right) - F_{\hat{I}_1^{(k)}}\left(\frac{i_1}{N_u}\right) \tag{19}$$

where $F_{\hat{I}_1^{(k)}}(\cdot)$ is the cdf of $\hat{I}_1^{(k)}$ that is given in the Appendix. For $L > 1$, the conditional pmf of $\boldsymbol{D^{(k)}}$ is given by

$$d^{(k)}(i_1, \cdots, i_L) = \Pr\left\{\frac{i_j}{N_u} \le \hat{I}_j^{(k)} < \frac{i_j+1}{N_u},\ j = 1, \cdots, L\right\}. \tag{20}$$

We do not have a closed-form formula for (20). However, this expression can be obtained by solving a set of $L$ equations. To obtain the (unconditional) pmf of $\boldsymbol{D^{(k)}}$, we have to average (19) or (20) over $\{b_j^{(k)}\}_{j=0}^{L}$ and $\lambda_k$.

### C. Expected Value of $I_j$

From (12), if we condition on the random variables $A_{1,j}^{(k)}$, $A_{2,j}^{(k)}$, $B_{1,j}^{(k)}$, and $B_{2,j}^{(k)}$, the conditional expected value of $\hat{I}_j^{(k)}$ is given by $1/3\,[(A_{1,j}^{(k)})^2 + A_{1,j}^{(k)} A_{2,j}^{(k)} + (A_{2,j}^{(k)})^2 + (B_{1,j}^{(k)})^2 + B_{1,j}^{(k)} B_{2,j}^{(k)} + (B_{2,j}^{(k)})^2]$. If the average value of the symbols in the signal set is zero, then by averaging over the above random variables, the expected value of $\hat{I}_j^{(k)}$ can be shown to be

$$E\left(\hat{I}_j^{(k)}\right) = \frac{1}{3N^3}\left[2u_{k,1}(0) + u_{k,1}(1)\right] \triangleq M_I^{(k)} \tag{21}$$

where

$$u_{k,1}(i) = \sum_{l=1-N}^{N-1} C_{k,1}(l) C_{k,1}(l+i) \tag{22}$$

and $C_{k,1}(\cdot)$ is the aperiodic crosscorrelation function defined in [9]. The expected value of $I_j$ is then given by

$$E(I_j) = \sum_{k=2}^{K} M_I^{(k)} \triangleq M_I. \tag{23}$$

The value $M_I$ will be used to form a suboptimum decoding metric in Section IV.

## IV. Performance Analysis

In this section, the upper and lower bounds on the PEP are derived for the optimum and several suboptimum decoding schemes. Let the transmitted symbol sequence be $\boldsymbol{b} = \{b_j^{(1)}\}_{j=1}^{L}$ and an error symbol sequence be $\bar{\boldsymbol{b}} = \{\bar{b}_j^{(1)}\}_{j=1}^{L}$, where $L$ is the length of the period in which $\bar{\boldsymbol{b}}$ diverges from $\boldsymbol{b}$. The PEP means the probability that the decoder chooses $\bar{\boldsymbol{b}}$ instead of $\boldsymbol{b}$, and is denoted by $\Pr(\boldsymbol{b} \to \bar{\boldsymbol{b}})$. In order to fairly compare the performances of different decoding schemes, we define the average pairwise error probability (APEP) as

$$\Pr(\boldsymbol{b} \leftrightarrow \bar{\boldsymbol{b}}) = \tfrac{1}{2}\Pr(\boldsymbol{b} \to \bar{\boldsymbol{b}}) + \tfrac{1}{2}\Pr(\bar{\boldsymbol{b}} \to \boldsymbol{b}). \tag{24}$$

Note that the APEP is the Bayes error, and the optimum decoding scheme is the scheme that minimizes the APEP, not the PEP. However, it suffices to give the derivation of the upper and lower bounds on the PEP only.

### A. Optimum Decoding Scheme (SO Scheme)

If we have perfect knowledge of the MAI statistic $\boldsymbol{I}$, then by conditioning on the symbol sequence and the CSI for $u_j^{(1)}$'s, the decision statistics $r_j$'s are independent complex Gaussian random variables and the maximum-likelihood optimum decoding metrics of the correct symbol sequence $\boldsymbol{b}$ and the error symbol sequence $\bar{\boldsymbol{b}}$ are given by

$$\mathrm{M}(\boldsymbol{b}) = \sum_{j=1}^{L}\left[\frac{\left|r_j - \beta v_j b_j^{(1)}\right|^2}{2\sigma_j^2} + \ln(\sigma_j^2)\right] \tag{25}$$

and

$$\mathrm{M}(\bar{\boldsymbol{b}}) = \sum_{j=1}^{L}\left[\frac{\left|r_j - \beta v_j \bar{b}_j^{(1)}\right|^2}{2\bar{\sigma}_j^2} + \ln(\bar{\sigma}_j^2)\right] \tag{26}$$

where

$$\sigma_j^2 = \left|b_j^{(1)}\right|^2 \sigma_e^2 + 1 + \sigma_u^2 I_j \triangleq \sigma_{O,j}^2$$

and

$$\bar{\sigma}_j^2 = \left|\bar{b}_j^{(1)}\right|^2 \sigma_e^2 + 1 + \sigma_u^2 I_j \triangleq \bar{\sigma}_{O,j}^2 \tag{27}$$

for $j = 1 \cdots L$. The parameters $\beta$, $\sigma_e^2$, and $\sigma_u^2$ are defined in Section II-B, and $I_j$ is as defined in (8). In practice, the perfect knowledge of $\boldsymbol{I}$ is not available, and the variances $\sigma_{O,j}^2$ and $\bar{\sigma}_{O,j}^2$ have to be replaced with some approximations. However, the performance of the optimum decoding scheme serves as a benchmark for other suboptimum decoding schemes.

### B. Suboptimum Decoding Schemes

In this subsection, we assume that we have no knowledge of the MAI statistic $\boldsymbol{I}$, and propose three suboptimum decoding schemes. We use the same forms of decoding metrics $\mathrm{M}(\boldsymbol{b})$ and $\mathrm{M}(\bar{\boldsymbol{b}})$ as defined in (25) and (26) and compute the variance terms $\sigma_j^2$ and $\bar{\sigma}_j^2$ by three kinds of approximations, instead of the optimum values $\sigma_{O,j}^2$ and $\bar{\sigma}_{O,j}^2$. Note that the three decoding metrics introduced here are used for either the simplicity or the resulting fairly good performances, and the same approach can be used to get the bounds on the PEP when other possible decoding metrics are used. The approximation values and notations are given as follows.

*First Suboptimum Decoding Scheme (S1 Scheme):* The first suboptimum decoding metric is the optimum decoding metric for the case of no MAI. In this case, we have

$$\sigma_j^2 = \left|b_j^{(1)}\right|^2 \sigma_e^2 + 1$$

and

$$\overline{\sigma}_j^2 = \left|\overline{b}_j^{(1)}\right|^2 \sigma_e^2 + 1 \tag{28}$$

for the $j$th decoding interval. The S1 scheme is useful when the MAI is small or when some MAI cancellation scheme is employed in the receiver.

*Second Suboptimum Decoding Scheme (S2 Scheme):* The second suboptimum decoding metric uses a constant value, say 1, as the variance term. In this case, we have

$$\sigma_j^2 = \overline{\sigma}_j^2 = 1 \tag{29}$$

for each interval $j$. The S2 scheme has the advantage of simplicity, and is useful when the MAI is large.

*Third Suboptimum Decoding Scheme (S3 Scheme):* The third suboptimum decoding metric uses the expected value of the MAI statistic $I_j$ in the approximation of the variance term. In this case, we have

$$\sigma_j^2 = \left|b_j^{(1)}\right|^2 \sigma_e^2 + 1 + \sigma_u^2 M_I$$

and

$$\overline{\sigma}_j^2 = \left|\overline{b}_j^{(1)}\right|^2 \sigma_e^2 + 1 + \sigma_u^2 M_I \tag{30}$$

for the $j$th interval, where $M_I$ is as defined in (23). The performance of the S3 scheme will be shown to be very close to that of the optimum decoding scheme for all MAI conditions. The reason for this is that the pdf of the MAI is highly centered around its expected value. In order to use this scheme, the knowledge of the number of users $K$ is assumed.

### C. PEP of Coded System

In order to investigate the system performance for both the optimum and suboptimum schemes, we use the general metrics (25) and (26) in the following derivation. The decoder will choose $\overline{\boldsymbol{b}}$ instead of $\boldsymbol{b}$ if $\mathrm{M}(\overline{\boldsymbol{b}}) < \mathrm{M}(\boldsymbol{b})$, or

$$\mathcal{D} = \sum_{j=1}^{L} \mathcal{D}_j \le \delta \tag{31}$$

where

$$\mathcal{D}_j = \mathcal{A}_j |r_j|^2 + \mathcal{B}_j |v_j|^2 + C_j r_j v_j^* + C_j^* r_j^* v_j \tag{32}$$

with

$$\mathcal{A}_j = \left(\frac{1}{2\overline{\sigma}_j^2} - \frac{1}{2\sigma_j^2}\right) \tag{33}$$

$$\mathcal{B}_j = \left(\frac{|\beta|^2 \left|\overline{b}_j^{(1)}\right|^2}{2\overline{\sigma}_j^2} - \frac{|\beta|^2 \left|b_j^{(1)}\right|^2}{2\sigma_j^2}\right) \tag{34}$$

$$C_j = \left(\frac{\beta^* \left(b_j^{(1)}\right)^*}{2\sigma_j^2} - \frac{\beta^* \left(\overline{b}_j^{(1)}\right)^*}{2\overline{\sigma}_j^2}\right) \tag{35}$$

and

$$\delta = \ln\left[\prod_{j=1}^{L} \left(\frac{\sigma_j^2}{\overline{\sigma}_j^2}\right)\right]. \tag{36}$$

The notation * above denotes complex conjugate. Given $b_j^{(1)}$ and $I_j$, $r_j$, and $v_j$ are zero-mean complex Gaussian random variables with variances of $(|b_j^{(1)}|^2 + I_j)\sigma_u^2 + 1$ and $\sigma_v^2$, respectively, and a covariance of $b_j^{(1)}\sigma_{uv}^2$. Hence, (32) is a quadratic form of complex Gaussian random variables. Let $\Phi_j(s)$ be the two-sided Laplace transform of the pdf of the random variable $\mathcal{D}_j$. Then with a slight modification to [19] or [20], $\Phi_j(s)$ is given by

$$\Phi_j(s) = \frac{p_{1,j} p_{2,j}}{(s - p_{1,j})(s - p_{2,j})} \tag{37}$$

where

$$\begin{bmatrix} p_{1,j} \\ p_{2,j} \end{bmatrix} = \begin{bmatrix} w_j - \sqrt{w_j^2 - p_{1,j} p_{2,j}} \\ w_j + \sqrt{w_j^2 - p_{1,j} p_{2,j}} \end{bmatrix} \tag{38}$$

are the left plane (LP) and right plane (RP) poles, respectively, with

$$p_{1,j} p_{2,j} = -\frac{\sigma_j^2 \overline{\sigma}_j^2}{|u|^2 d_j^2 \sigma_u^2 \sigma_{O,j}^2} \tag{39}$$

$$w_j = \frac{\sigma_j^2 \overline{\sigma}_{O,j}^2 - \overline{\sigma}_j^2 \sigma_{O,j}^2}{2|u|^2 d_j^2 \sigma_u^2 \sigma_{O,j}^2} + \frac{\sigma_j^2 \left[(1 - |u|^2)\left(|b_j^{(1)}|^2 - |\overline{b}_j^{(1)}|^2\right) + |u|^2 d_j^2\right]}{2|u|^2 d_j^2 \sigma_{O,j}^2} \tag{40}$$

and

$$d_j^2 = \left|b_j^{(1)} - \overline{b}_j^{(1)}\right|^2. \tag{41}$$

Since the random variables $\mathcal{D}_j$'s are independent (we assume ideal interleaving in this study), the two-sided Laplace transform of $\mathcal{D} = \sum_j \mathcal{D}_j$ is given by

$$\Phi_{\mathcal{D}}(s) = \prod_{j \in \eta} \Phi_j(s) \tag{42}$$

where the product is taken over the set $\eta$ of $j$ for which $b_j^{(1)} \ne \overline{b}_j^{(1)}$ and the region of convergence is the vertical strip enclosing the $jw$-axis bounded by the closest poles on either side. If we condition on the MAI statistic $\boldsymbol{I}$, the conditional PEP is a Bromwich contour integral [21], and can be computed by the residue method as

$$\Pr(\boldsymbol{b} \to \overline{\boldsymbol{b}} | \boldsymbol{I}) = \int_{\rho - j\infty}^{\rho + j\infty} [e^{s\delta} \Phi_{\mathcal{D}}(s)/s]\, ds$$

$$= \begin{cases} -\sum \text{Residue } [e^{s\delta} \Phi_{\mathcal{D}}(s)/s]_{\text{RP}_{\text{poles}}}, & \text{if } \delta \le 0 \\ \sum \text{Residue } [e^{s\delta} \Phi_{\mathcal{D}}(s)/s]_{\text{LP}_{\text{poles}}} \cup \{0\}, & \text{if } \delta > 0 \end{cases} \tag{43}$$

where $\rho$ is some constant satisfying $0 < \rho <$ first RP pole of $\Phi_{\mathcal{D}}(s)$ and $\delta$ is as defined in (36).

In order to examine the effect of MAI on the system error performance, we rewrite (39) as

$$p_{1,j}p_{2,j} = -\frac{\left|\bar{b}_j^{(1)}\right|^2 \frac{E_s}{N_o + I_j E_s}(1-|u|^2)+1}{|u|^2 d_j^2 \frac{E_s}{N_o + I_j E_s}} \tag{44}$$

for the optimum decoding scheme. If we fix $E_s$, we see that an increase in $I_j$ can be regarded as an increase in thermal noise psd $N_o$, and, hence, can increase the PEP. By using (18), the upper bound (UB) and lower bound (LB) on the PEP, $\Pr(\boldsymbol{b} \to \bar{\boldsymbol{b}})$, are given by

$$\text{UB} = \sum_{i_1,\cdots,i_L} \Pr\{\boldsymbol{b} \to \bar{\boldsymbol{b}} | \boldsymbol{I} = \boldsymbol{D}_{\text{U}}(i_1,\cdots,i_L)\}\, d(i_1,\cdots,i_L) \tag{45}$$

and

$$\text{LB} = \sum_{i_1,\cdots,i_L} \Pr\{\boldsymbol{b} \to \bar{\boldsymbol{b}} | \boldsymbol{I} = \boldsymbol{D}_{\text{L}}(i_1,\cdots,i_L)\}\, d(i_1,\cdots,i_L) \tag{46}$$

where

$$\boldsymbol{D}_{\text{U}}(i_1,\cdots,i_L) = \left[\frac{i_1+K-1}{N_u},\cdots,\frac{i_L+K-1}{N_u}\right] \tag{47}$$

and

$$\boldsymbol{D}_{\text{L}}(i_1,\cdots,i_L) = \left[\frac{i_1}{N_u},\cdots,\frac{i_L}{N_u}\right]. \tag{48}$$

The bounds become tighter as $N_u$ increases. The UB and LB on the APEP can then be obtained via formulas (24), (45), and (46). From (44), we also see that, since $(E_s/N_o + I_j E_s) \to 1/I_j$ as $E_s/N_o \to \infty$, it is the MAI that limits the system performance.

### D. Numerical Examples

In this subsection, numerical examples are given to illustrate the tightness of the performance bounds derived in this paper. We also compare the performances of the suboptimum decoding schemes (Section IV-B) with that of the optimum decoding scheme (Section IV-A) and suggest the appropriate suboptimum decoding schemes for various CSI, MAI, and signal set conditions. Both the UB and LB are given for the APEP. The SNR, $E_b/N_o = (1/n)E_s/N_o$, equals 20 dB, and the rectangular chip waveform is used throughout the examples. The parameter $N_u$, which controls the tightness of the bounds, equals 4000 in Figs. 3 and 4, and equals 1000 in Fig. 5.

In Fig. 3, we compare one dominant APEP of a TCM/SSMA system with the UUB on the BEP of an uncoded system for the four decoding schemes S0, S1, S2, and S3. Gold sequences with length $N = 127$ [15] are used. For the TCM/SSMA system, an 8-PSK signal set, perfect CSI ($u = 1$), and a rate 2/3, 8-state convolutional encoder [16] are used in the TCM

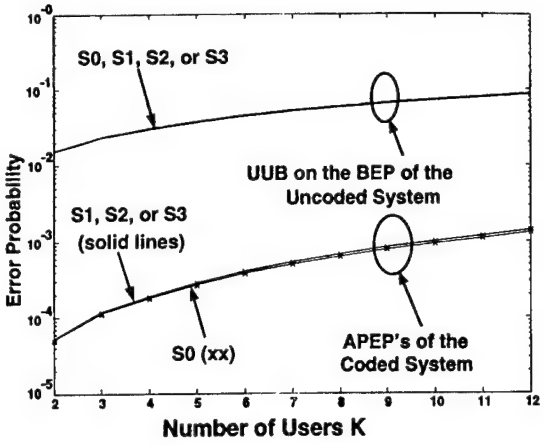


Fig. 3. APEP's of the rate 2/3 TCM/SSMA system with an 8-PSK signal set versus the UUB on the BEP of the uncoded system with a 4-PSK signal set. Various decoding schemes are considered, and both the UB (formula (45)) and LB (formula (46)) are plotted with $N_u = 4000$. The SNR, $E_b/N_o$, is fixed to 20 dB.

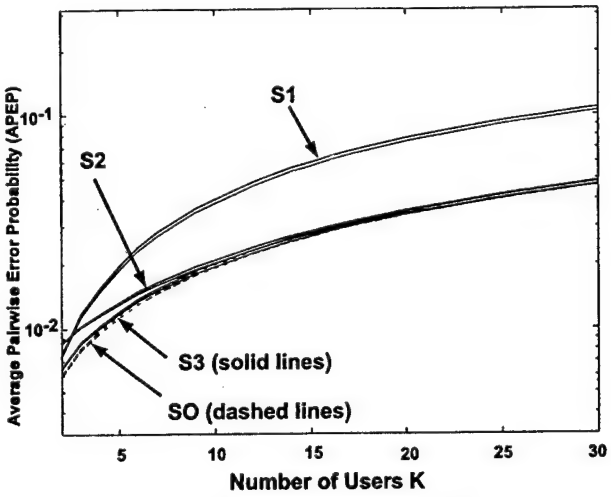


Fig. 4. APEP's of various decoding schemes in an uncoded 16-QAM system. Both the UB (formula (45)) and LB (formula (46)) on the APEP are plotted with $N_u = 4000$. The SNR, $E_b/N_o$, is fixed to 20 dB.

part. The correct and incorrect symbol sequences are chosen to be $\boldsymbol{b} = \{1, 1\}$ and $\bar{\boldsymbol{b}} = \{-1, i\}$, respectively. Hence, we have $L = 2$ and $\eta = \{1, 2\}$. For the uncoded system, a 4-PSK signal set is used and perfect CSI is assumed. Since the equal-energy signal sets (MPSK) are used, the four decoding schemes are equivalent for the uncoded system, and the three suboptimum decoding schemes are equivalent for the coded system. Hence, only one pair of UB and LB is given for the UUB on the BEP of the uncoded system, and two pairs of UB and LB are given for the APEP's of the coded system. It is observed that the performances of the suboptimum decoding schemes and the optimum decoding scheme are very close for all the MAI conditions, which are specified by $K$.

In Fig. 4, we compare the APEP's of various decoding schemes in an uncoded 16-QAM system for the error event with $\boldsymbol{b} = \{1/\sqrt{10}(3+i3)\}$ and $\bar{\boldsymbol{b}} = \{1/\sqrt{10}(-1-i)\}$. Gold sequences with length $N = 127$ [15] are used. Also, the imperfect CSI with $u = 0.99$ is considered. Since the two symbols in the error event do not have the same energy and

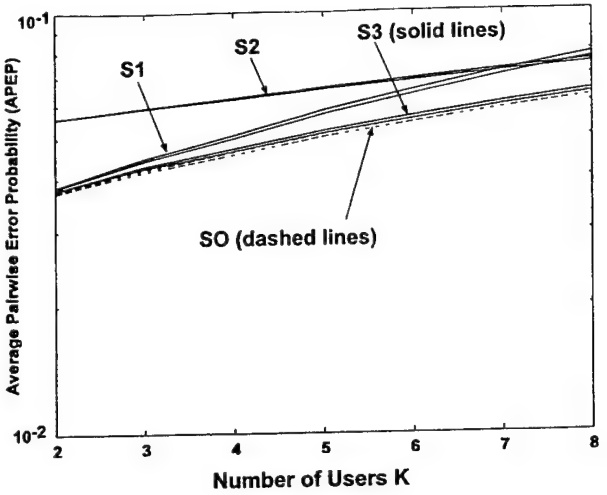


Fig. 5. APEP's of various decoding schemes in the rate 3/4 TCM/SSMA system with a 16-QAM signal set. Both the UB (formula (45)) and LB (formula (46)) on the APEP are plotted with $N_u = 1000$. The SNR, $E_b/N_o$, is fixed to 20 dB.

$|u| \neq 1$, the four decoding schemes are not equivalent. It is observed that the performance of the S3 scheme is very close to the SO scheme for all values of $K$. As expected from the formulations in Section IV-B, the S1 scheme is appropriate for use when the number of users $K$ is small, and the S2 scheme is appropriate for use when the number of users $K$ is large.

In Fig. 5, we compare one APEP of various decoding schemes in a TCM/SSMA system. A 16-QAM signal set and a rate 3/4, 8-state convolutional encoder [16] are used in the TCM part. Gold sequences with length $N = 31$ [15] are used. Also, the imperfect CSI with $u = 0.8$ is considered. Both the UB and LB are given for the APEP, where the correct and incorrect symbol sequences are chosen to be

$$\boldsymbol{b} = \{1/\sqrt{10}(-1-i), 1/\sqrt{10}(3+i3)\}$$

and

$$\overline{\boldsymbol{b}} = \{1/\sqrt{10}(3-i), 1/\sqrt{10}(1-i3)\}.$$

Hence, we have $L = 2$ and $\eta = \{1, 2\}$. We see again that the S3 scheme is appropriate for use for all the MAI conditions. The performance of this system is not very good since both $N$ and $|u|$ are not large in this example.

## V. Conclusion

In this paper, we have derived a new set of pdf's and cdf's of the MAI statistic and have proposed a modified bounding technique to obtain tight upper and lower bounds on the PEP of the coded DS/SSMA system over the slow Rayleigh fading channel with imperfect CSI. The approach yields bounds that can be made arbitrarily tight and avoids numerical integrations. The tight bounds can be used to accurately study the multiple-access capability of the coded DS/SSMA systems and to compare the performances of the suboptimum decoding schemes with that of the optimum decoding scheme.

The comparison among the four decoding schemes are summarized as follows. For the uncoded system, or error event with length $L = 1$ in the coded system, the four decoding schemes are equivalent if an equal-energy signal set is used, or if perfect CSI is assumed. For the error event with length $L > 1$ in the coded system, the three suboptimum decoding schemes are equivalent if an equal-energy signal set is used, or if perfect CSI is assumed. The performances of the suboptimum and optimum schemes are shown to be very close. Finally, if a nonequal-energy signal set is used and imperfect CSI is assumed, the S1 scheme is appropriate for use when the MAI is small, the S2 scheme is appropriate for use when the MAI is large, and the S3 scheme is appropriate for use for all MAI conditions. Hence, the S3 scheme is suggested for use when knowledge of the number of users $K$ is available.

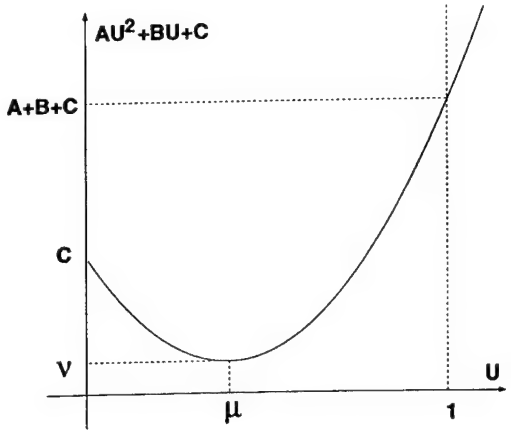


Fig. 6. Plot of $AU^2 + BU + C$ when $0 < \mu < 1/2$.

## VI. Appendix
### pdf and cdf of $A^2 + BU + C$

Suppose that $X = AU^2 + BU + C$, where $A$, $B$, and $C$ are constants such that $\Delta = B^2 - 4AC \leq 0$, $A > 0$, $C \geq 0$, and $U$ is uniformly distributed on $[0, 1)$. Let $\mu$ and $\nu$ be defined as $\mu = -B/2A$ and $\nu = -\Delta/4A$. The case when $0 < \mu < 1/2$ is illustrated in Fig. 6. The random variable $X$ then has the probability density function $f_X(x)$ given by the following:

1) If $\mu < 0$, then

$$f_X(x) = \frac{1}{\sqrt{4Ax + \Delta}}, \qquad \text{for } C \leq x < A + B + C. \tag{49}$$

2) If $\mu = 0$, then

$$f_X(x) = \frac{1}{2\sqrt{A(x - C)}}, \qquad \text{for } C \leq x < A + C. \tag{50}$$

3) If $0 < \mu < 1/2$, then

$$f_X(x) = \begin{cases} \dfrac{2}{\sqrt{4Ax + \Delta}}, & \text{for } \nu < x \leq C \\ \dfrac{1}{\sqrt{4Ax + \Delta}}, & \text{for } C < x < A + B + C. \end{cases} \tag{51}$$

4) If $\mu = 1/2$, then

$$f_X(x) = \begin{cases} \dfrac{2}{\sqrt{4Ax + \Delta}}, & \text{for } \nu < x \leq C \\ \dfrac{1}{-B}, & \text{for } x = C. \end{cases} \tag{52}$$

5) If $1/2 < \mu < 1$, then

$$f_X(x) = \begin{cases} \dfrac{2}{\sqrt{4Ax+\Delta}}, & \text{for } \nu < x < A+B+C \\ \dfrac{1}{\sqrt{4Ax+\Delta}}, & \text{for } A+B+C \le x \le C. \end{cases} \quad (53)$$

6) If $\mu \ge 1$, then

$$f_X(x) = \frac{1}{\sqrt{4Ax+\Delta}}, \text{ for } A+B+C < x \le C. \quad (54)$$

The distribution function of $X$, $F_X(x)$, is given by the following:

1) If $\mu < 0$, then

$$F_X(x) = \frac{1}{2A}\left(\sqrt{4Ax+\Delta} - B\right), \text{ for } C \le x < A+B+C. \quad (55)$$

2) If $\mu = 0$, then

$$F_X(x) = \frac{1}{A}\left(\sqrt{A(x-C)}\right), \qquad \text{for } C \le x < A+C. \quad (56)$$

3) If $0 < \mu < 1/2$, then

$$F_X(x) = \begin{cases} \dfrac{1}{A}\sqrt{4Ax+\Delta}, & \text{for } \nu < x \le C \\ \dfrac{1}{2A}\left(\sqrt{4Ax+\Delta} - B\right), & \text{for } C < x < A+B+C. \end{cases} \quad (57)$$

4) If $\mu = 1/2$, then

$$F_X(x) = \frac{1}{A}\sqrt{4Ax+\Delta}, \qquad \text{for } \nu < x < C. \quad (58)$$

5) If $1/2 < \mu < 1$, then

$$F_X(x) = \begin{cases} \dfrac{1}{A}\sqrt{4Ax+\Delta}, & \text{for } \nu < x < A+B+C \\ \dfrac{1}{2A}\left(\sqrt{4Ax+\Delta} + 2A + B\right), & \text{for } A+B+C \le x \le C. \end{cases} \quad (59)$$

6) If $\mu \ge 1$, then

$$F_X(x) = \frac{1}{2A}\left(\sqrt{4Ax+\Delta} + 2A + B\right), \quad \text{for } A+B+C < x \le C. \quad (60)$$

## REFERENCES


[1] J. Cavers and P. Ho, "Analysis of the error performance of trellis-coded modulations in Rayleigh fading channels," *IEEE Trans. Commun.*, vol. 40, pp. 74–83, Jan. 1992.

[2] S. B. Slimane and T. Le-Ngoc, "Tight bounds on the error probability of coded modulation schemes in Rayleigh fading channels," *IEEE Trans. Veh. Technol.*, vol. 44, pp. 121–130, Feb. 1995.

[3] R. G. McKay, P. J. McLane, and E. Biglieri, "Error bounds for trellis-coded MPSK on a fading mobile satellite channel," *IEEE Trans. Commun.*, vol. 39, pp. 1750–1761, Dec. 1991.

[4] C. Tellambura, Q. Wang, and V. K. Bhargava, "A performance analysis of trellis-coded modulation schemes over Rician fading channels," *IEEE Trans. Veh. Technol.*, vol. 42, pp. 491–501, Nov. 1993.

[5] D. Divsalar and M. K. Simon, "The design of trellis coded MPSK for fading channels: Performance criteria," *IEEE Trans. Commun.*, vol. 36, pp. 1004–1012, Sept. 1988.

[6] C. Tellambura, "Evaluation of the exact union bound for trellis-coded modulations over fading channels," *IEEE Trans. Commun.*, vol. 44, Dec. 1996.

[7] E. Biglieri, G. Caire, and G. Taricco, "Approximating the pairwise error probability for fading channels," *Electron. Lett.*, pp. 1625–1627, Sept. 14, 1995.

[8] E. Biglieri, G. Caire, G. Taricco, and J. Ventura-Traveset, "Simple method for the computation of error probabilities," *Electron. Lett.*, pp. 191–192, Feb. 1, 1996.

[9] M. B. Pursley, "Performance evaluation for phase-coded spread-spectrum multiple-access communication—Part I: System analysis," *IEEE Trans. Commun.*, vol. COM-25, pp. 795–799, Aug. 1977.

[10] R. T. Hsu and J. S. Lehnert, "A characterization of multiple-access interference in generalized quadriphase spread-spectrum communications," *IEEE Trans. Commun.*, vol. 42, pp. 2001–2010, Feb. 1994.

[11] J. S. Lehnert, "An efficient technique for evaluating direct-sequence spread-spectrum multiple-access communications," *IEEE Trans. Commun.*, vol. 37, pp. 851–858, Aug. 1989.

[12] A. T. McDowell, "Dual-phase continuous phase modulation for bandwidth efficient spread-spectrum multiple-access communication," Ph.D. dissertation, Purdue University, West Lafayette, IN, May 1993.

[13] H. Chu, "Trellis-coded modulation for CDMA," Ph.D. dissertation, J. S. Lehnert, Advisor, Purdue University, West Lafayette, IN, May 1994.

[14] T.-T. Chen and J. S. Lehnert, "TCM/SSMA communication systems with cascaded-sequences and PAM/QAM signal sets," *IEEE Trans. Commun.*, to be published.

[15] M. B. Pursley and H. F. A. Roefs, "Numerical evaluation of correlation parameters for optimal phases of binary shift-register sequences," *IEEE Trans. Commun.*, vol. COM-27, pp. 1597–1604, Oct. 1979.

[16] G. Ungerboeck, "Trellis-coded modulation with redundant signal sets—Part II: State of the art," *IEEE Commun. Mag.*, vol. 25, pp. 12–21, Feb. 1987.

[17] E. Zehavi and J. K. Wolf, "On the performance evaluation of trellis codes," *IEEE Trans. Inform. Theory*, vol. IT-33, pp. 196–202, Mar. 1987.

[18] M. K. Simon, E. Biglieri, P. J. McLane, and D. Divsalar, *Introduction to Trellis-Coded Modulation with Application.* New York: McMillan, 1991.

[19] M. Schwartz, W. Bennett, and S. Stein, *Communication Systems and Techniques.* New York: McGraw-Hill, 1966.

[20] J. G. Proakis, *Digital Communications.* New York: McGraw-Hill, 1989.

[21] N. W. McLachlan, *Complex Variable Theory and Transform Calculus.* Cambridge, U.K. Cambridge Univ. Press, 1953.



**Tsao-Tsen Chen** (M'98), for photograph and biography, see p. 890 of the July 1998 issue of this TRANSACTIONS.

**James S. Lehnert** (S'83–M'84–SM'95) received the B.S. (highest honors), M.S., and Ph.D. degrees in electrical engineering from the University of Illinois at Urbana-Champaign in 1978, 1981, and 1984, respectively.

From 1978 to 1984, he was a Research Assistant at the Coordinated Science Laboratory, University of Illinois, Urbana. He was a University of Illinois Fellow from 1978 to 1979 and an IBM Pre-Doctoral Fellow from 1982 to 1984. He has held summer positions at Motorola Communications, Schaumburg, IL, in the Data Systems Research Laboratory, and Harris Corporation, Melbourne, FL, in the Advanced Technology Department. He is currently an Associate Professor of Electrical Engineering at Purdue University, West Lafayette, IN. His current research work is in communication and information theory with emphasis on spread-spectrum communications.

Dr. Lehnert has served as Editor for Spread Spectrum for the IEEE TRANSACTIONS ON COMMUNICATIONS.

# Asynchronous Multiple-Access Interference Suppression and Chip Waveform Selection with Aperiodic Random Sequences

Tan F. Wong, Tat M. Lok, and James S. Lehnert

*Abstract*—**A linear decentralized receiver capable of suppressing multiple-access interference (MAI) for asynchronous direct-sequence code-division multiple-access (DS-CDMA) systems with aperiodic random signature sequences is proposed. Performance bounds on this receiver are also obtained. Using them as performance measures, the problem of chip waveform selection in DS-CDMA systems with the proposed receiver under the near–far scenario is investigated. In particular, the performance of several practical chip waveforms is compared. An LMS-type adaptive algorithm is developed to obtain the parameters needed in the receiver, which only requires the signature sequence and coarse timing information of the desired user.**

*Index Terms*—**Adaptive signal detection, chip waveform, code division multiaccess, interference suppression, spread spectrum.**

## I. Introduction

MANY existing multiuser detection methods (see [1] and [2] for a survey of the literature) for direct-sequence code-division multiple-access (DS-CDMA) systems are developed under the periodic sequence assumption, in which the signature sequences employed to spectrally spread the data sequences are periodic with periods equal to one or, at most, a few data symbol durations. In practice, there are systems, such as IS-95 [3], which employ signature sequences with very long periods. In fact, in IS-95 [3], the period of the signature sequences is so long that the sequences can be regarded as aperiodic. For systems with aperiodic (or very long) signature sequences, the aforementioned multiuser detection methods may not work well.

In this paper, we examine the problem of multiuser communications via the single-user detection point of view, i.e., we treat signals from other users as interference. To this end, we investigate multiple-access interference (MAI) suppression for DS-CDMA systems with random aperiodic signature sequences. Moreover, we assume that users in the system communicate in an asynchronous manner. Details of the system model are given in Section II. In Section III, we develop a linear minimum-mean-squared error (MMSE) receiver, which is closely related to the receivers in [4]–[6] (see Section III for a discussion on the similarities and differences). The linear MMSE receiver changes every symbol period due to the fact that the signature sequences are aperiodic. To reduce complexity, we simplify the linear MMSE receiver to make it take the form of conventional matched filter followed by a continuous-time correlator, which is time-invariant. Aiming further toward a practical implementation, we approximate the continuous-time correlator in the receiver by a discrete-time correlator. The resulting receiver turns out to be a special case of the one considered in [7]. Because of this, the development in Section III can be viewed as a justification for the receiving structures in [7].

The key advantage of this receiver is its implementational simplicity. We will demonstrate in Section V that it is practically sufficient to sample the output of the matched filter a few times and pass the samples to the discrete-time correlator. The major complexity burden of the receiver lies in determining the weights in the correlator. Therefore, the smaller the number of samples taken, the simpler is the receiver. Second, adaptive algorithms can be employed to determine correlator weights. In Section VI, we develop an LMS-type adaptive algorithm to do the job.

Unlike the abundant amount of work on MAI rejection, there is much less work concerning the problem of chip waveform selection in DS-CDMA systems. The chip waveform selection problem for the conventional matched filter receiver is investigated in [8]–[10]. The problem of chip waveform selection with the noise-whitening matched filter receiver is also addressed in [4] and [5]. In this paper, we investigate the chip waveform selection problem for the MMSE receiver proposed under the near–far scenario. As a starting point, we define two performance measures to evaluate the performance of the receiver, namely, the signal-to-noise ratio (SNR) and the near–far efficiency (NFE), in Section IV. The former measures the average SNR in the decision statistic given out by the receiver. The latter indicates the "average robustness" of the receiver in combating MAI. We also develop performance bounds on the receiver proposed by considering the simple case of a system with just a single interferer. Using these bounds, we examine the effect of the chip waveform on

Paper approved by U. Mitra, the Editor for Spread Spectrum/Equalization of the IEEE Communications Society. Manuscript received March 10, 1997; revised May 13 1998 and September 8, 1998. This work was supported in part by the U.S. Army Research Office under Grant DAAH04-95-1-0246 and in part by the Chinese University of Hong Kong Research Committee Funding. This work was presented in part at the IEEE International Conference on Universal Personal Communications (ICUPC'97), San Diego, CA, October 12–16, 1997.

T. F. Wong is with the Department of Electrical and Computer Engineering, University of Florida, Gainesville, FL 32611-6130 USA.

T. M. Lok is with the Department of Information Engineering, Chinese University of Hong Kong, Shatin, Hong Kong.

J. S. Lehnert is with Purdue University, West Lafayette, IN 47907-1285 USA (e-mail: lehnert@purdue.edu).

Publisher Item Identifier S 0090-6778(99)00793-X.

the performance of the receiver considering factors such as bandwidth efficiency, MAI suppression capability, and robustness. In particular, we consider several common sample chip waveforms and evaluate their performance with the receiver proposed. We see that the results, although sharing some similarities with, are significantly different from those in [4], [5], [9], and [10]. These similarities and differences are explained in Section V.

## II. System Model

In this section, we describe the model of the DS-CDMA system. We assume that there are $K+1$ simultaneous users in the system. The $k$th user, for $0 \le k \le K$, generates a sequence of data symbols $b_j^{(k)}$. We assume that the data symbols $b_j^{(k)}$ are random variables with $E[|b_j^{(k)}|^2] = 1$.

The $k$th user is provided a randomly generated signature sequence $a^{(k)}$ given by

$$a^{(k)} = \left(\cdots, a_0^{(k)}, a_1^{(k)}, \cdots, a_{N-1}^{(k)}, \cdots\right). \tag{1}$$

The elements $a_i^{(k)}$ are independent random variables such that $E[a_i^{(k)}] = 0$ and $E[|a_i^{(k)}|^2] = E[|a_i^{(k)}|^4] = 1$.[1] The sequence $a^{(k)}$ is used to generate the spectrally spread signal given by

$$a_k(t) = \sum_{i=-\infty}^{\infty} b_{[i/N]}^{(k)} a_i^{(k)} \psi(t - iT_c) \tag{2}$$

where $T_c$ is the chip separation and $\psi(t)$ is the common chip waveform for all signals. The symbol duration is $T = NT_c$, where $N$ is the number of chips per symbol interval (the processing gain). The chip waveform $\psi(t)$ is assumed to satisfy the Nyquist criterion to minimize the interchip interference and is normalized so that $\int_{-\infty}^{\infty} |\psi(t)|^2\, dt = T_c$. Moreover, we assume that the signature sequence of any user is independent of all other signature sequences and all the data symbol sequences.

The transmitted signal for the $k$th user, for $0 \le k \le K$, can be expressed as

$$\mathrm{Re}\left[\sqrt{2P_k} a_k(t - T_k) \exp(\mathrm{j}\omega_c(t - T_k))\right] \tag{3}$$

where $P_k$ is the power for the $k$th signal, $\omega_c$ is the carrier frequency, and $T_k$ is the delay that models the asynchronous system. We show later that it suffices to assume $T_k \in [0, T_c)$, for $0 \le k \le K$.

Without loss of generality, we consider the signal from the zeroth user as the communicating signal and the signals from all other users as interfering signals throughout the paper. We assume that the communication channel is corrupted by additive white Gaussian noise (AWGN) with two-sided power spectral density $N_0/2$.

Then the signal received at the intended receiver in complex baseband notation is given by

$$r(t) = y(t) + n(t) \tag{4}$$

[1] BPSK and QPSK spreadings are examples under this general model.

where $y(t)$ and $n(t)$ represent the desired signal and the interference components, respectively. The desired signal contribution $y(t)$ is given by

$$y(t) = \sqrt{2P_0} \exp(-\mathrm{j}\phi_0) \sum_{i=-\infty}^{\infty} b_i^{(0)} h_i^{(0)}(t - T_0). \tag{5}$$

The interference $n(t)$ is the sum of the AWGN component $n_W(t)$ and the MAI contribution $n_I(t)$, which is given by

$$n_I(t) = \sum_{k=1}^{K} \sqrt{2P_k} \exp(-\mathrm{j}\phi_k) \sum_{i=-\infty}^{\infty} b_i^{(k)} h_i^{(k)}(t - T_k). \tag{6}$$

In (5) and (6), $h_i^{(k)}(t)$, the $i$th symbol waveform of the $k$th interferer, is given by

$$h_i^{(k)}(t) = \sum_{j=0}^{N-1} a_{iN+j}^{(k)} \psi(t - (iN + j)T_c) \tag{7}$$

and $\phi_k = (\omega_c T_k + \theta_k)$ models the phase angle of the $k$th user's signal.

## III. Receiving Structure

We assume that we have achieved synchronization with the desired user signal. Hence, we may assume $T_0 = 0$. Later, we release this perfect synchronization assumption to model timing mismatch in the system.

First, we consider the linear MMSE estimator of $b_j^{(0)}$ given the sequence $a^{(0)}$

$$\hat{b}_j^{(0)} = \int_{-\infty}^{\infty} g_j^*(t) r(t)\, dt. \tag{8}$$

By the orthogonality principle [11], $g_j(t)$ is given by the solution of the following integral equation:

$$E_0\left[b_j^{(0)*} r(t)\right] = \int_{-\infty}^{\infty} E_0[r(t) r^*(s)] g_j(s)\, ds \tag{9}$$

where $E_0[\cdot]$ denotes the conditional expectation given $a^{(0)}$. We consider the form of solution, assuming it exists, defined by

$$g_j(t) = \int_{-\infty}^{\infty} \tilde{g}_j(s) h_j^{(0)}(t - s)\, ds \tag{10}$$

and let

$$\tilde{r}_j(t) = \int_{-\infty}^{\infty} r(s) h_j^{(0)*}(s - t)\, ds. \tag{11}$$

Then

$$\hat{b}_j^{(0)} = \int_{-\infty}^{\infty} \tilde{g}_j^*(t) \tilde{r}_j(t)\, dt \tag{12}$$

where $\tilde{g}_j(t)$ is the solution of

$$E_0\left[b_j^{(0)*} \tilde{r}_j(t)\right] = \int_{-\infty}^{\infty} E_0[\tilde{r}_j(t) \tilde{r}_j^*(s)] \tilde{g}_j(s)\, ds. \tag{13}$$

Physically, it means that we take observations after sequence-matched filtering (despreading).

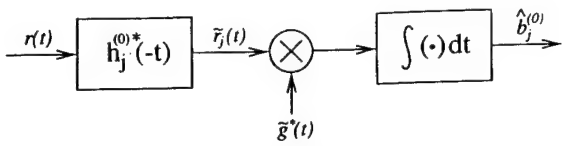


Fig. 1. Linear receiver for the $j$th data symbol.

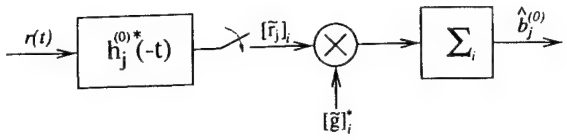


Fig. 2. Simplified linear receiver for the $j$th data symbol.

At the receiver, we assume the signature sequence of the desired user is available. Hence, $h_j^{(0)}(t)$ is known. From (13), we see that $\tilde{g}_j(s)$ changes with $j$. This means that we have to solve (13) each time for a new symbol. It is easy to see that the expectation [with respect to $a^{(0)}$] of each of the conditional expectations in (13) is not a function of $j$. In order to reduce the computational complexity, we average over all the desired user sequences[2] and consider the following linear estimator of $b_j^{(0)}$:

$$\hat{b}_j^{(0)} = \int_{-\infty}^{\infty} \tilde{g}^*(t)\tilde{r}_j(t)\,dt. \tag{14}$$

The filter $\tilde{g}(t)$ in (14) is the solution of

$$\tilde{\psi}(t) = \int_{-\infty}^{\infty} R_{\tilde{r}}(t, s)\tilde{g}(s)\,ds \tag{15}$$

where $\tilde{\psi}(t) = E[b_j^{(0)*}\tilde{r}_j(t)]$ and $R_{\tilde{r}}(t, s) = E[\tilde{r}_j(t)\tilde{r}_j^*(s)]$. The corresponding receiver is shown in Fig. 1. We notice that only the matched filter $h_j^{(0)*}(-t)$, which we know explicitly, changes every symbol period. Other parts of the receiver remain fixed. Of course, this receiver is suboptimal compared to the linear MMSE receiver described above.

Since $\tilde{g}(t)$ does not depend on $j$, we consider, without loss of generality, the detection of the symbol $b_0^{(0)}$ from this point onward. From (4) to (7) and (11), we obtain

$$\tilde{r}_0(t) = \tilde{y}(t) + \tilde{n}(t) \tag{16}$$

where $\tilde{n}(t) = \tilde{n}_I(t) + \tilde{n}_W(t)$ with the despread components indicated by the *tilde* symbol. We can easily evaluate the terms needed in order to solve (15)

$$\tilde{\psi}(t) = \sqrt{2P_0}T\hat{\psi}(t) \tag{17}$$

and

$$R_{\tilde{r}}(t, s) = R_{\tilde{y}}(t, s) + R_{\tilde{n}}(t, s) \tag{18}$$

where[3] $R_{\tilde{n}}(t, s) = R_{\tilde{n}_I}(t, s) + R_{\tilde{n}_W}(t, s)$

$$R_{\tilde{y}}(t, s) = \tilde{\psi}(t)\tilde{\psi}^*(s) + \frac{1}{N}\sum_{\substack{j=-\infty \\ j\neq 0}}^{\infty} \tilde{\psi}(t - jT_c)\tilde{\psi}^*(s - jT_c), \tag{19}$$

$$R_{\tilde{n}_I}(t, s) = \sum_{k=1}^{K} \frac{P_k}{NP_0} \sum_{j=-\infty}^{\infty} \tilde{\psi}(t - jT_c - T_k)\tilde{\psi}^*(s - jT_c - T_k) \tag{20}$$

and

$$R_{\tilde{n}_W}(t, s) = \frac{\sqrt{2}N_0}{\sqrt{P_0}}\,\hat{\psi}(t - s). \tag{21}$$

The function $\hat{\psi}(\cdot)$ is the autocorrelation of the chip waveform defined by

$$\hat{\psi}(t) = \frac{1}{T_c}\int_{-\infty}^{\infty} \psi(s)\psi^*(s - t)\,ds. \tag{22}$$

To satisfy the Nyquist criterion, we need to have $\hat{\psi}(0) = 1$ and $\hat{\psi}(jT_c) = 0$ for all $j \neq 0$.

Above, we have implicitly assumed that the sums indexed by $j$ in (19) and (20) converge. A sufficient condition for this is that $\int_{-\infty}^{\infty} |\hat{\psi}(t)|\,dt < \infty$, which we will assume throughout the rest of this paper. Therefore, when $N$ is large, we can neglect [7] the effect of the interchip interference terms (the sums indexed by $j$) in (19) and approximate $R_{\tilde{y}}(t, s)$ by $\tilde{\psi}(t)\tilde{\psi}^*(s)$. Also, it is obvious from (20) that we can assume $T_1, \cdots, T_K$ lie in the interval $[0, T_c)$, since $\tilde{n}_I(t)$ is cyclostationary with period $T_c$. With perfect knowledge of $\{T_1, \cdots, T_K\}$, we can solve the integral equation (15), provided a solution exists. We notice that the values of $\{\phi_0, \phi_1, \cdots, \phi_K\}$ do not affect the solution.[4]

However, we seldom have this knowledge beforehand in practice. Moreover, the number of interferers $K$ and $T_k$ may vary slowly in time. As a result, the continuous-time receiver described, though simple, is hardly of any practical interest. We observe that the matched filter part of the receiver is known. Hence, the major difficulty of implementing the receiver is to find $\tilde{g}(t)$, the solution of (15). As a first step to improve the practical applicability of the receiver, we impose two simplifications: observe the output of the matched filter for a finite duration and sample and weight the output instead of performing the continuous-time correlation. The simplified receiver is basically a special case of the one considered in [7], which is shown in Fig. 2.

More precisely, if we sample the output of the matched filter every $T_s$ seconds at $jT_s + T_0$ and let $[\tilde{\mathbf{g}}]_j = T_s\tilde{g}(jT_s + T_0)$, $[\mathbf{R}_{\tilde{\mathbf{r}}}]_{ij} = R_{\tilde{r}}(iT_s + T_0, jT_s + T_0)$, $[\tilde{\mathbf{r}}_0]_j = \tilde{r}_0(jT_s + T_0)$, and $[\tilde{\psi}]_j = \tilde{\psi}(jT_s + T_0)$, then (14) and (15) become

$$\hat{b}_0^{(0)} = \sum_j [\tilde{\mathbf{g}}]_j^*[\tilde{\mathbf{r}}_0]_j \tag{23}$$

and

$$[\tilde{\psi}]_i = \sum_j [\mathbf{R}_{\tilde{\mathbf{r}}}]_{ij}[\tilde{\mathbf{g}}]_j \tag{24}$$

[2]This approximation is similar to the single-chip filter in [5].

[3]For BPSK spreading, an extra term $\frac{1}{N}\sum_{\substack{j=-N+1 \\ j\neq 0}}^{N-1}((N - |j|)/N)\tilde{\psi}(t + jT_c)\tilde{\psi}^*(s - jT_c)$ should be added to the expression in (19).

[4]For QPSK spreading, the phase information has no effect on MAI cancellation. However, this is not true for the case of BPSK spreading, where we neglect the phase information and sacrifice a little performance gain for generality.

where the summations range over the finite number of samples taken.[5] Above, the offset $T_0$ is introduced to model the timing error in synchronizing the desired user signal. Usually, $T_0$ is small compared to $T_c$, but we do not know its value. Here, we assume that $T_0 \in [-T_c/2, T_c/2)$.[6] We develop an adaptive algorithm in Section VI to solve (24) without any knowledge of $\{T_0, T_1, \cdots, T_K\}$.

We note that (24) always has a unique solution, as the matrix $\mathbf{R}_{\tilde{n}}$ [the sample version of $R_{\tilde{n}}(t, s)$] is positive definite under the assumptions stated before. In fact, let $\mathbf{Q}_{\tilde{n}}$ be the inverse of $\mathbf{R}_{\tilde{n}}$. Then, by the matrix inversion lemma,[7]

$$[\tilde{\mathbf{g}}]_i = \frac{1}{1+\gamma} \sum_j [\mathbf{Q}_{\tilde{n}}]_{ij} \left[\tilde{\psi}\right]_j \tag{25}$$

where

$$\gamma = \sum_i \sum_j [\tilde{\psi}]_i^H [\mathbf{Q}_{\tilde{n}}]_{ij} \left[\tilde{\psi}\right]_j. \tag{26}$$

As mentioned in Section I, the MMSE receiver is closely related to the receivers in [4]–[6]. Here, we discuss the differences between them in detail. The major difference between [4], [5], and the above MMSE receiver is in the way in which the delays of the interferers are modeled. In [4] and [5], these delays are uniformly distributed random variables. In our development, they are treated as deterministic constants.[8] These two different models lead to many different interpretations and results. For example, the model in [4] and [5] implies that the MAI is stationary Gaussian. This is a reasonable approximation for the cases considered in [4] and [5], where there are a large number of equal-power users. However, this assumption is not accurate for the near–far situations (there are a few strong interferers) considered in this paper. By conditioning on the delays of the interferers, we know [12] that it is reasonable again to approximate the MAI (after the despreading) as Gaussian, with which MMSE and maximum SNR are reasonable optimization criteria. However, the MAI is cyclostationary, instead of stationary, now. The noise-whitening development in [4] cannot be applied directly, although a similar development can be obtained [6].

When there are a large number of interferers with equal powers, (20) approaches (17) in [5] by the law of large numbers. Loosely speaking, our model reduces to the one in [4] and [5] by averaging out the delay information, and our receiver reduces to the single-chip filter suggested in [5]. However, whether this averaging is a reasonable thing to do depends on the channel conditions. In fact, we will show that no MAI suppression is possible when all the interferers are chip-synchronous with the desired user. Hence, the noise-whitening receiver in [4] and [5] may degrade the SNR performance when there are only a few strong interferers. On the other hand, our model (delays are deterministic) is accurate for near–far cases. Based on this, we believe that our receiver is more suitable than the receiver in [4] and [5] in near–far situations.

The model assumed in [6] is a mixture of our model and the model in [4] and [5]. The locked users in [6] correspond to modeling the delays as deterministic constants, while the unlocked users [6] correspond to modeling the delays as uniform random variables. In this sense, our model can be viewed as a special case of the model in [6]. The approach employed in [6] is similar to that used in [4], namely maximizing the SNR and solving the corresponding integral equation. The powers and delays of the interferers are needed in order to solve the required integral equation. Although the results in [6] can be generalized for aperiodic sequences (periodic sequences are assumed), a different integral equation must be solved for every symbol and adaptive implementation is difficult. By sampling and vectorizing the output of the despreader per symbol as described above, the noise process, when averaged over all desired user signature sequences and viewed as a vector-valued process, becomes stationary, which is important for adaptive implementations. Our result can be viewed as a practical extension of the receiver in [6] for aperiodic sequences.

## IV. Performance Measure

To evaluate the effectiveness of the receiver under various conditions, we define a performance measure based on the average signal-to-noise ratio in the decision statistic at the output of the receiver

$$\text{SNR} \triangleq \frac{\left|\sum_j [\tilde{\psi}]_j^H [\tilde{\mathbf{g}}]_j\right|^2}{\sum_i \sum_j [\tilde{\mathbf{g}}]_i^H [\mathbf{R}_{\tilde{n}}]_{ij} [\tilde{\mathbf{g}}]_j} = \gamma. \tag{27}$$

It can be shown [7] that the solution of (24) maximizes the SNR defined above over all possible choices of $\tilde{\mathbf{g}} \neq \mathbf{0}$. Moreover, we can show (see Appendix A) that SNR $\leq \gamma_0$, where $\gamma_0 = P_0 T/N_0$ is exactly the SNR when there is no interferer in the perfectly synchronized ($T_0 = 0$) system.

The "near–far resistance" defined in [1] and [13] which measures the robustness of the receiver in a multiple-access environment under the periodic deterministic sequence assumption is not applicable in our case. Since we consider the average performance when we develop our receiver, it is reasonable to have a performance measure which indicates the "average robustness." In light of this, we define the "near–far efficiency" (NFE) as

$$\text{NFE} = \inf\{\text{SNR}/\gamma_0 \colon P_k \geq 0,\ k = 1, 2, \cdots, K\} \tag{28}$$

where SNR is defined in (27). We note that $0 \leq \text{NFE} \leq 1$. Moreover, samples of $r_0(t)$ exhibit Gaussian-like behavior when $N$ is large [12]. This also justifies the use of SNR.

We see that the SNR and NFE, defined above, are functions of $T_0, T_1, \cdots, T_K$. Sometimes, it is convenient to have performance measures that are independent of them. To do this,

[5] For convenience, we may index matrices with negative indexes.

[6] There can be several possible interpretations for this assumption. For example, it models the case in which we can only establish a coarse synchronization.

[7] Assuming all the required invertibilities, $(\mathbf{A} - \mathbf{BDC})^{-1} = \mathbf{A}^{-1} + \mathbf{A}^{-1}\mathbf{B}(\mathbf{D}^{-1} - \mathbf{CA}^{-1}\mathbf{B})^{-1}\mathbf{CA}^{-1}$.

[8] Equivalently, the development in Section III can be interpreted as conditioning on these delays.

we model the delays as uniform random variables on $[0, T_c)$[9] and define the "average signal-to-noise ratio" and "average near–far efficiency" as

$$\text{ASNR} = E_{T_0, T_1, \cdots, T_K}[\text{SNR}] \tag{29}$$

and

$$\text{ANFE} = E_{T_0, T_1, \cdots, T_K}[\text{NFE}] \tag{30}$$

where $E_{T_0, T_1, \cdots, T_K}[\cdot]$ denotes that expectation is with respect to $T_0, T_1, \cdots, T_K$.

The general expression of the SNR is too complex to give us any insight on the design of the receiver. Instead, we study in detail the simple system with two users, namely, a desired user and an interferer. It turns out that the expression for the least upper bound on the SNR for this case is clear and simple and can be used as a guide in designing the receiver.

First, define the function

$$\text{SNR}_\infty(T_1) = \gamma_0 \left[ 1 - \frac{\lambda_1}{1+\lambda_1} \sum_{l=-\infty}^{\infty} |\hat{\psi}(lT_c + T_1)|^2 \right] \tag{31}$$

where $\gamma_0 = P_0 T/N_0$ and $\lambda_1 = P_1 T/(N N_0)$. It is shown in Appendix A that $\text{SNR}_\infty$ is the least upper bound on the SNR achievable by any discrete-time receiver configuration described in Section III, even if the sampling times are not uniform. We note that $\text{SNR}_\infty$ is not a function of $T_0$. This means that the effect of the timing error can be neglected if we sample fine and long enough.[10] From (31), it is obvious the function defined as

$$\text{NFE}_\infty(T_1) = 1 - \sum_{l=-\infty}^{\infty} |\hat{\psi}(lT_c + T_1)|^2 \tag{32}$$

is the least upper bound on the NFE of any receiver under the single-interferer assumption. Similarly, we can see that

$$\text{ASNR}_\infty = \gamma_0 \left[ 1 - \frac{\lambda_1}{(1+\lambda_1)T_c} \int_{-\infty}^{\infty} \hat{\Psi}^2(f)\, df \right] \tag{33}$$

and

$$\text{ANFE}_\infty = 1 - \frac{1}{T_c} \int_{-\infty}^{\infty} \hat{\Psi}^2(f)\, df \tag{34}$$

are the least upper bounds on the ASNR and ANFE of any receiver under the single-interferer assumption. In (33) and (34), $\hat{\Psi}(f)$ is the Fourier transform of $\hat{\psi}(t)$.

Finally, we point out that the performance of the system will be worse if more and more interferers are added to the system. It can be shown, by augmenting the arguments in Appendix A, that (31)–(34) provide upper bounds on corresponding measures of any receiver under all system conditions in this paper.

[9]Here, we model the delays as random variables only to get simpler performance measures. The optimal filtering is still performed under the assumption of deterministic delays.

[10]This property is similar to the timing-error-resistance property of a fractionally spaced equalizer.

TABLE I
BANDWIDTHS (IN $1/T_c$ HZ) AND $\text{ANFE}_\infty$ OF DIFFERENT CHIP WAVEFORMS

| Chip waveform | (a) | (b) | (c) | (d) | (e) |
|---|---|---|---|---|---|
| 0.99-BW | 20.57 | 2.364 | 2.818 | 1.996 | 4.953 |
| Noise BW | 1 | 1.234 | 1.5 | 2 | 5 |
| Half-power BW | 0.8859 | 1.189 | 1.441 | 2 | 5 |
| $\text{ANFE}_\infty$ | 0.3333 | 0.4134 | 0.5189 | 0.5062 | 0.8010 |
| Bound on $\text{ANFE}_\infty$ (for 0.99-BW above) | 0.9524 | 0.5853 | 0.6522 | 0.5091 | 0.8021 |

## V. CHIP WAVEFORM SELECTION

From the previous section, we know that if we sample fine and long enough, the selection of the chip waveform is the only factor affecting the performance of the system that we are able to control. The effect of the chip waveform on the performance of the system can be large. However, it is generally difficult to evaluate this effect, as the dependence of the system performance on the chip waveform is usually very complicated. Since $\text{ASNR}_\infty$ and $\text{ANFE}_\infty$ provide upper bounds on the performance of any receiver and they depend on the chip waveform in a simple and clear fashion, we can use them to measure the effectiveness of a chip waveform.

In this section, we consider five sample chip waveforms and evaluate the performance of various receivers employing them. The five chip waveforms are: a) the rectangular pulse, b) the half-sine pulse, c) the time-domain raised-cosine pulse, d) the frequency-domain raised-cosine (2, 0.1) waveform, and e) the frequency-domain raised-cosine (5, 0.1) waveform (see Appendix B). We notice that a)–c) are time-limited, while d) and e) are band-limited. Their chip waveform functions are given [for d) and e), the autocorrelation functions of the chip waveforms are given instead], respectively, as

$$\psi_a(t) = p_{T_c}(t)$$
$$\psi_b(t) = \sqrt{2}\sin(\pi t/T_c) p_{T_c}(t)$$
$$\psi_c(t) = \sqrt{2/3}[1 + \cos(2\pi(t/T_c - 1/2))] p_{T_c}(t)$$
$$\hat{\psi}_d(t) = \frac{\sin(2\pi t/T_c)}{2\pi t/T_c} \frac{\cos(\pi t/10T_c)}{1 - t^2/25T_c^2}$$
$$\hat{\psi}_e(t) = \frac{\sin(5\pi t/T_c)}{5\pi t/T_c} \frac{\cos(\pi t/10T_c)}{1 - t^2/25T_c^2}$$

where $p_{T_c}(t) = 1$ for $0 \le t < T_c$, and $p_{T_c}(t) = 0$, otherwise.

The $\text{NFE}_\infty$'s of chip waveforms a)–e) are plotted in Fig. 3 as a function of $T_1$. Their $\text{ANFE}_\infty$'s are given in Table I. From Fig. 3, we see that there is no gain when $T_1 = 0$, i.e., when the desired user is chip-synchronous to the interferer. However, as the asynchrony between them increases, the NFE is larger than zero, which implies that the receiver is resistant to the near–far problem. On the average, we see that the frequency-domain raised-cosine waveform e) and the rectangular pulse a) give the largest and the smallest $\text{ANFE}_\infty$, respectively, among the five chip waveforms.

### A. Bandwidth Consideration

From (32), for any $\varepsilon > 0$, we can choose a chip waveform such that $\text{NFE}_\infty(T_1) = 1$ for all $T_1 \in [\varepsilon, T_c - \varepsilon]$. Hence,

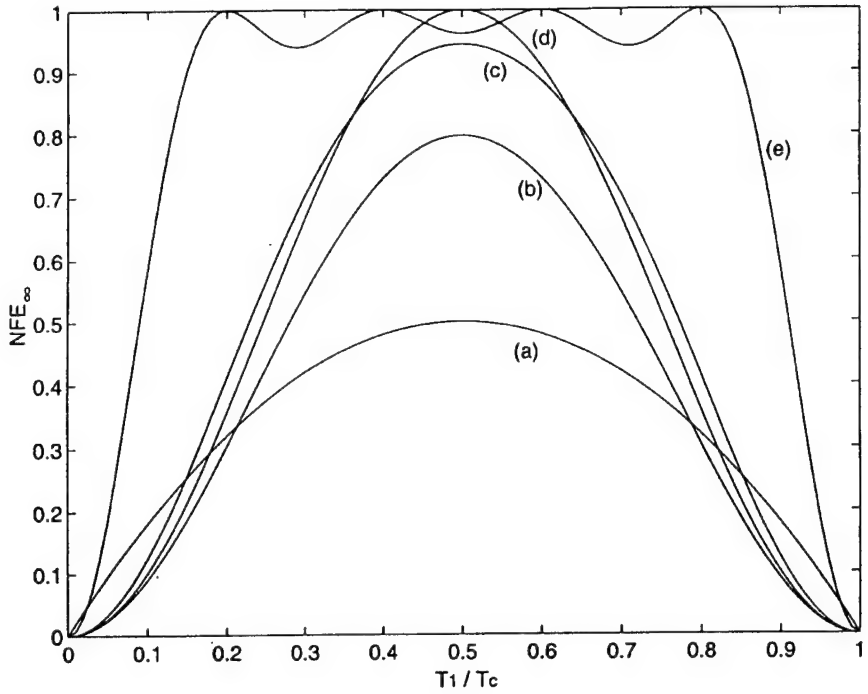


Fig. 3. $\text{NFE}_\infty$ versus $T_1$.

we can make $\text{ANFE}_\infty$ arbitrarily close to one by choosing suitable chip waveforms. This is very desirable in terms of MAI suppression. However, in order to make $\text{ANFE}_\infty$ smaller, we have to increase the system bandwidth, which is undesirable in terms of bandwidth efficiency. Since no notion of bandwidth is employed in defining $\text{ANFE}_\infty$ and $\text{ASNR}_\infty$, it is not very meaningful to directly compare chip waveforms using these two performance measures unless we restrict ourselves to a set of chip waveforms with equal bandwidths. To do so, we need to define the bandwidth of a DS-CDMA system. The bandwidth of the power spectral density of the communicating signal is usually taken as the bandwidth of a digital communication system. Based on the assumptions we made, it is not hard to see the power spectral density of the multiple-access signal is just a scaled version of $\hat{\Psi}(f)$. For a power spectral density which is not band-limited, there is no unique definition of bandwidth. In fact, there can be several different, but meaningful, definitions [15]. For our cases, Table I summarizes several different bandwidths of systems employing the five chip waveforms described above.

For simplicity, we pick the $\alpha$-fractional containment bandwidth ($\alpha$-BW) [15] as our working definition of bandwidth. We can derive a bound on $\text{ANFE}_\infty$ given the $\alpha$-BW of a system. Suppose the $\alpha$-BW of the system is $W_\alpha$, i.e., $\alpha$ fraction of all the signal power is contained inside $[-W_\alpha/2, W_\alpha/2]$. We have

$$\text{ANFE}_\infty \leq 1 - \frac{\alpha^2}{W_\alpha T_c}. \tag{35}$$

We note that the lowest possible value of $W_\alpha$ is $\alpha^2/T_c$, since there is no chip waveform with $W_\alpha < \alpha^2/T_c$ that satisfies the Nyquist criterion. The proof of (35) is given in Appendix B.

The bounds for the waveforms having the same 0.99-BW as each of the five sample chip waveforms are also given in Table I. We see that the $\text{ANFE}_\infty$'s of chip waveforms d) and e) are very close to their corresponding bounds. This implies that these chip waveforms are close to the optimal ones in the sets of legitimate chip waveforms with the given bandwidth limitations. On the other hand, the $\text{ANFE}_\infty$ of the rectangular pulse is much smaller than the bound in (35). Hence, the rectangular pulse is far from the optimal one in the corresponding set of chip waveforms. Optimization of $\text{ANFE}_\infty$ under the $\alpha$-BW constraint is difficult in general. However, under some special cases, we can employ the frequency-domain raised-cosine waveforms to achieve the bound in (35) as closely as desired. A detailed discussion of this is given in Appendix B.

We mention that we can improve the performance of a system by suitably choosing a chip waveform to increase the system bandwidth. A chip waveform with a larger bandwidth is usually more localized in time. With such a chip waveform, we can pack more chips into a symbol. It is natural to ask whether it is better to increase the number of chips per symbol (decrease the chip separation $T_c$) together with the bandwidth. We can employ the bound in (35) to answer this question when optimal chip waveforms are employed. From (35), we see that the $\text{ANFE}_\infty$ bound increases with the bandwidth-chip-separation product $W_\alpha T_c$. Any increase in the product $W_\alpha T_c$ due to the increased bandwidth will be offset by the decrease in the chip separation. Therefore, it is better to just simply increase the bandwidth while keeping the number of chips per symbol, $N$, fixed in near–far cases. We point out that there are two caveats to the interpretation above. First, $N$ has to be large for the argument to be valid. Hence, we cannot, say, reduce $N$ to one (no spreading) in order to get all the advantage from MAI cancellation. Second, the argument is valid only for near–far cases. When there are a large number of interferers

TABLE II
ASNR (IN dB) OF DIFFERENT SAMPLING SCHEMES

| Chip waveform | (a) | (b) | (c) | (d) | (e) |
|---|---|---|---|---|---|
| $\text{ASNR}_\infty$ | 15.335 | 16.240 | 17.201 | 17.096 | 19.050 |
| $T_s = T_c$, $[0, 0]$ | 2.9096 | 4.4554 | 7.4020 | 10.580 | 15.051 |
| $T_s = T_c$, $[-T_c, T_c]$ | 4.3126 | 5.3997 | 8.0678 | 10.586 | 15.054 |
| $T_s = T_c/2$, $[-T_c, T_c]$ | 13.653 | 15.846 | 16.598 | 16.187 | 17.067 |
| $T_s = T_c/4$, $[-T_c/2, T_c/2]$ | 14.169 | 16.207 | 17.191 | 16.703 | 18.120 |
| $T_s = T_c/4$, $[-T_c, T_c]$ | 14.692 | 16.215 | 17.197 | 16.898 | 18.522 |

with equal powers, it is shown in [4] that the performance only depends on the bandwidth. It does not matter whether we increase $N$ or not.

### B. Effect of Sampling

$\text{ASNR}_\infty$ and $\text{ANFE}_\infty$ provide upper bounds on the performance of a system. In practice, we cannot sample too finely or for too long. Therefore, the performance of the system will be poorer than that predicted by these two upper bounds. To give some indication on how large the degradation will be, we consider five different sampling schemes for systems with each of the five sample chip waveforms. Table II summarizes the ASNR of each of the sampling schemes for each of the chip waveforms. In Table II, the sampling schemes are identified by the values of $T_s$ and the observation intervals. To single out the effect of sampling, we consider a system with $N = 127$, a single interferer whose power is 20 dB above the desired user, and $\gamma_0 = 20$ dB. We also assume perfect synchronization is achieved, i.e., $T_0 = 0$.

The first row of Table II gives the ASNR for the conventional matched filter receiver. We observe that the ASNR improves greatly for chip waveforms a)–d), even if we just sample twice per chip. For chip waveforms b) and c), the ASNR approaches the $\text{ASNR}_\infty$ bound if we sample four times per chip and have an observation interval of $T_c$ seconds, which corresponds to just five samples.

### C. Effect of Timing Error

Since the functions $\text{SNR}_\infty$ and $\text{NFE}_\infty$ do not depend on $T_0$, we know that when we sample fine enough, the effect of timing error is minimal. However, when the sampling rate is not high, timing error can degrade the performance of the receiver significantly. To evaluate this effect, we reconsider the system in Section V-B, except that $T_0$ is modeled as a uniform random variable on $[-T_c/2, T_c/2)$. Table III shows the ASNR's for several different sampling schemes. Comparing the results with Table II, we see that chip waveforms b)–d) are relatively insensitive to timing error, whereas the effect of timing error is significant for chip waveforms a) and e).

### D. Conventional Matched Filter Receiver

It is interesting to consider the problem of chip waveform selection for the conventional matched filter receiver under the framework developed in Section IV. The SNR for the conventional matched filter receiver is given by

$$\text{SNR}_{mf}(T_1) = \frac{\gamma_0 |\hat{\psi}(T_0)|^2}{1 + \lambda_1 \sum_{l=-\infty}^{\infty} |\hat{\psi}(lT_c + T_1)|^2}. \tag{36}$$

It is obvious from (36) that the conventional matched filter receiver is sensitive to timing error in the system. Assuming $T_0 = 0$, we can obtain the ANFE of this receiver as

$$\text{ANFE}_{mf} = \frac{1}{T_c} \left| \left\{ T_1 \in [0, T_c) : \sum_{l=-\infty}^{\infty} |\hat{\psi}(lT_c + T_1)|^2 = 0 \right\} \right| \tag{37}$$

where $|\cdot|$ denotes the Lebesgue measure on $[0, T_c)$. It is shown in Appendix A that $\text{ANFE}_\infty \geq \text{ANFE}_{mf}$. Hence, we see that good (in terms of large ANFE) chip waveforms for the conventional matched filter receiver are also good for the MMSE receiver considered in Section III. However, the converse is not true, as we can see that all five sample chip waveforms give zero ANFE for the matched filter receiver. Effectively, the MMSE receiver acts to enlarge the set of chip waveforms which are robust in combating the near–far problem so that more practical waveforms, such as the five sample waveforms, can be used.

In [9] and [10], the problem of chip waveform selection for the matched filter receiver is also considered. In our notation, these references use

$$\text{STIR} = \frac{\gamma_0}{1 + \frac{\lambda_1}{T_c} \int_{-\infty}^{\infty} \hat{\Psi}^2(f)\, df} \tag{38}$$

as the performance measure. We get STIR from (36) if we set $T_0 = 0$ and average just the denominator over $T_1$. Roughly speaking, STIR can be treated as an approximation of $\text{ASNR}_{mf}$. Comparing (33) and (38), we see that both STIR and $\text{ASNR}_\infty$ depend on the same factor $\int_{-\infty}^{\infty} \hat{\Psi}^2(f)\, df$. As a result, chip waveforms which give large STIR also give large $\text{ASNR}_\infty$. However, STIR tends to zero as interfering power becomes very large, while $\text{ASNR}_\infty$ does not for most of practical chip waveforms. This, again, shows the advantage of the proposed receiver over the conventional matched filter receiver in terms of combating the near–far problem.

TABLE III
ASNR (IN dB) OF DIFFERENT SAMPLING SCHEMES WITH TIMING ERROR

| Chip waveform | (a) | (b) | (c) | (d) | (e) |
|---|---|---|---|---|---|
| $T_s = T_c$, $[-T_c, T_c]$ | 1.6441 | 2.9005 | 4.8503 | 7.4035 | 7.9935 |
| $T_s = T_c/2$, $[-T_c, T_c]$ | 11.297 | 15.312 | 15.697 | 15.7942 | 12.934 |
| $T_s = T_c/4$, $[-T_c/2, T_c/2]$ | 11.346 | 15.825 | 16.942 | 16.619 | 16.803 |
| $T_s = T_c/4$, $[-T_c, T_c]$ | 13.602 | 16.179 | 17.189 | 16.883 | 17.421 |

### E. Multiple Interferers

To indicate the performance of the receiver when there are multiple interferers in the system, we obtain the ASNR's of receivers with chip waveforms a) and d). Each interferer has

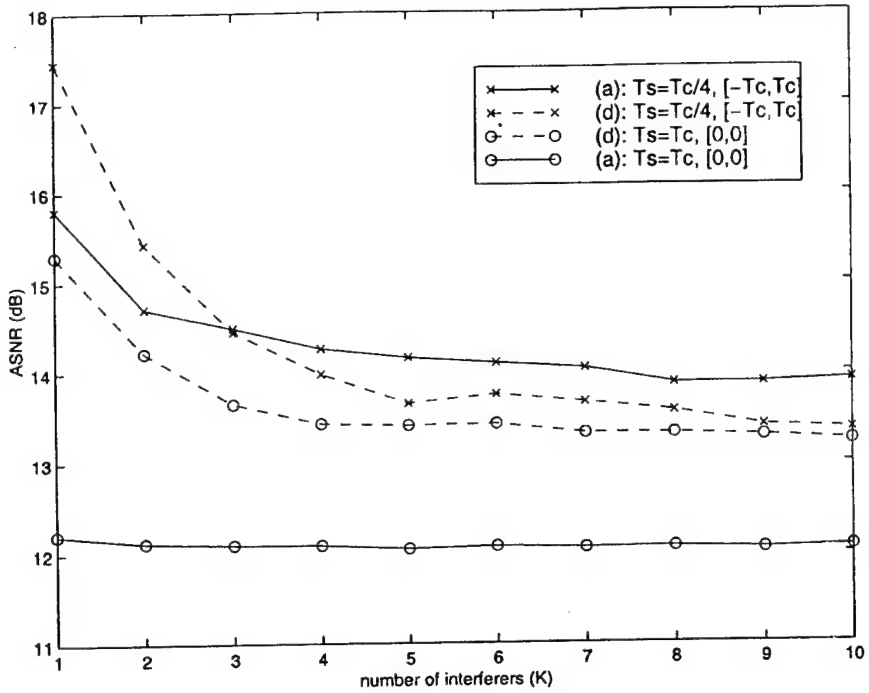


Fig. 4. ASNR versus number of interferers.

equal power, which adds up in such a way that the total interference power is 10 dB above the desired user power. All other system parameters are the same as those in Section V-B. The results shown in Fig. 4 indicate that the gain over the conventional matched filter reduces as the number of interferers increases.

We observe from Fig. 4 that the rectangular pulse a) outperforms chip waveform d) when there are a large number of equal-power interferers. This indicates that $\text{ANFE}_\infty$ is not a good measure of performance for this situation. It is mentioned in Section III that the MMSE receiver approaches the single-chip noise-whitening receiver in [5] when there are a large number of equal-power interferers. From [4], we know that the single-chip noise-whitening filter improves the SNR performance of a chip waveform to that of the "flat-spectrum" signal with the same bandwidth. When the noise-whitening filter is employed, the performance depends on the bandwidth only. Since the rectangular pulse a) has a larger bandwidth than chip waveform d), according to [4], the rectangular pulse should outperform chip waveform d) when there are a large number of interferers. However, the argument in [4] does not apply when there are only a few strong interferers (i.e., when MAI is best modeled by a cyclostationary process). In such cases, bandwidth alone is not sufficient and $\text{ANFE}_\infty$ becomes a better performance measure. From Table I, a) has a smaller $\text{ANFE}_\infty$ than d) and, hence, should have a poorer SNR performance when there are only a few interferers. This is readily observed in Fig. 4. Summarizing the discussion, our viewpoint in selecting the chip waveform differs from that of [4] and [5] in the sense that we focus on the near–far scenario, while [4] and [5] assume that there are a large number of equal-power interferers. As we see from above, the two different viewpoints lead to very different conclusions.

## VI. Adaptive Implementation

As mentioned in Section III, the MMSE receiver structure allows adaptive implementations. In this section, we can construct an LMS-type adaptive algorithm to solve (24).

Suppose, for the moment, we know the value of $T_0 = 0$. Hence, we can determine $\tilde{\psi}/\|\tilde{\psi}\|$, since it does not depend on $P_0$. For the detection of the $j$th symbol, we sample the despread received signal $\tilde{r}(t)$ every $T_s$ seconds as described in Section III to form the vector $\tilde{\mathbf{r}}_j$ of length, say, $M$. Then, the following algorithm can be used to solve (24).

Set $\alpha_0 = 0$ and for $j > 0$, get $\tilde{\mathbf{g}}_j$ by

$$\alpha_j = \lambda \alpha_{j-1} + \tilde{\mathbf{r}}_j^H \tilde{\mathbf{r}}_j \tag{39}$$

$$\tilde{\mathbf{g}}_j = \tilde{\mathbf{g}}_{j-1} + \mu \left( \frac{\tilde{\psi}}{\|\tilde{\psi}\|} - \frac{1-\lambda^j}{(1-\lambda)\alpha_j} (\tilde{\mathbf{r}}_j^H \tilde{\mathbf{g}}_{j-1}) \tilde{\mathbf{r}}_j \right) \tag{40}$$

where $\mu$ is the step size and $0 < \lambda < 1$ is chosen to smooth the average energy estimation of $\tilde{\mathbf{r}}_j$.

Strictly speaking, the solution given by this algorithm differs from the solution of (24) by a complex constant that has no effect on the SNR of the system. Because of the same reason, we do not need to know the phase of the desired user signal. In (39), we estimate the average energy of the vector $\tilde{\mathbf{r}}_j$. The update in (40) is the standard LMS update except that the observation vector $\tilde{\mathbf{r}}_j$ is normalized by its estimated average norm, i.e., the operation of a perfect automatic gain control (AGC) is performed. This normalization is necessary to avoid numerical instability. We note that the computational complexity of the algorithm is of the order of $M$ per iteration.

If we do not know the value of $T_0$, a standard strategy [14] is to hypothesize several different values of $T_0$ and use them to obtain different $\tilde{\psi}$ to run several applications of the adaptive algorithm above in parallel. We select the one that

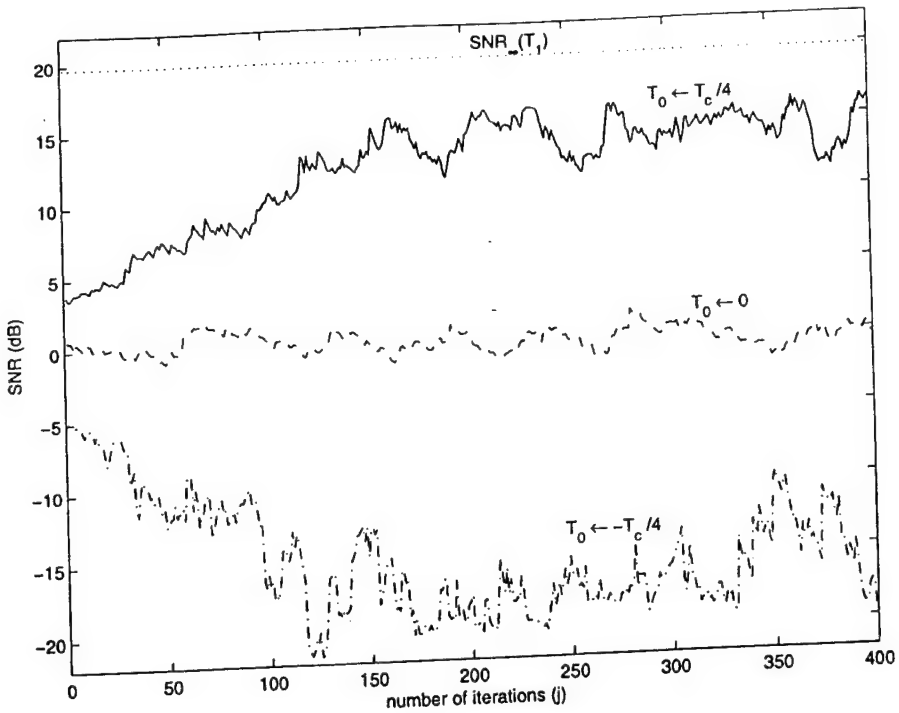


Fig. 5. SNR from a sample run of the adaptive algorithm.

maximizes the SNR. This requires us to estimate the SNR from the received signal. Again, due to the special form of $\mathbf{R}_{\tilde{\mathbf{r}}}$, we can have a very efficient way to estimate the SNR. After the sampling operation to get $\tilde{\mathbf{r}}_j$, we wait for several chip separations and sample the output of the matched filter $M$ times again to form another vector $\hat{\mathbf{r}}_j$. We point out that the time separation of $\tilde{\mathbf{r}}_j$ and $\hat{\mathbf{r}}_j$ must be an integral multiple of $T_c$, and large enough so that almost no desired user signal energy is contained in $\hat{\mathbf{r}}_j$. Then, the following measure gives a reasonable estimate of SNR + 1:

$$\sigma_j(T_0) = \frac{\sum_{i=1}^{j} \lambda^{j-i} |\tilde{\mathbf{g}}_i^H(T_0)\tilde{\mathbf{r}}_i|^2}{\sum_{i=1}^{j} \lambda^{j-i} |\tilde{\mathbf{g}}_i^H(T_0)\hat{\mathbf{r}}_i|^2}. \tag{41}$$

In (41), the dependence on $T_0$ is emphasized, and $0 < \lambda \leq 1$ is chosen to smooth out noise in the measure. Therefore, we can simply choose the one that maximizes $\sigma_j$ instead of the SNR. We note that $\sigma_j$ can be obtained recursively with complexity of order $M$ per iteration.

To demonstrate the algorithm, we consider the sample system in Section V-B with binary data and signature sequences, the time-domain raised-cosine pulse c) as the chip waveform $T_0 = T_c/4$, and $T_1 = T_c/2$. We sample twice per chip with the observation interval $[-T_c, T_c]$. We run three parallel applications of the adaptive algorithm hypothesizing $T_0 = -T_c/4$, 0 and $T_c/4$, respectively. The SNR and $\sigma_j$ for each of the applications resulting from a run of the algorithm are shown in Figs. 5 and 6, respectively. From Fig. 6, we see that the algorithm with hypothesis $T_0 = T_c/4$ gives the largest $\sigma_j$ after the algorithm settles down. According to the discussion above, we can deduce from this result that $T_0 = T_c/4$. Referring back to Fig. 5, we see that the algorithm with hypothesis $T_0 = T_c/4$ does converge to give a good SNR performance, while the algorithms with other hypotheses give much poorer SNR performances.

## VII. Conclusions

In this paper, based on the MMSE principle, we have developed a linear receiver capable of suppressing MAI for asynchronous DS-CDMA systems with aperiodic signature sequences. Relying only on the signature sequence and rough timing information of the desired user, we have developed an LMS-type adaptive algorithm to obtain the weights in the correlator. Moreover, we have obtained upper bounds on the performance of this receiver based on the special case of a single interferer. Using these upper bounds as performance measures, we have investigated some considerations, such as MAI suppression capability, bandwidth efficiency, and robustness, in selecting chip waveforms for DS-CDMA systems. We have found out that the criterion for selecting chip waveforms in the near–far scenario differs significantly from that for the case where there are a large number of equal-power interferers.

## Appendix A

In this Appendix, we show that (31) is the least upper bound on the SNR of any receiver described in Section III for the single-interferer channel.

First, we obtain the SNR of dyadically sampled systems with time-limited $\psi(t)$. Assume that $\psi(t)$ is time-limited to $[-L_1T_c, L_2T_c]$ with $(L_1 \geq 0, L_2 \geq 0)$. Then, $\hat{\psi}(t)$ is time-limited to $[-LT_c, LT_c]$ where $L = L_1 + L_2$. Consider the receiver which takes samples at $jT_s + T_0$ for $j = -(L+1)2^M, -(L+1)2^M + 1. \cdots, (L+1)2^M$, where $T_s = T_c/2^M$.

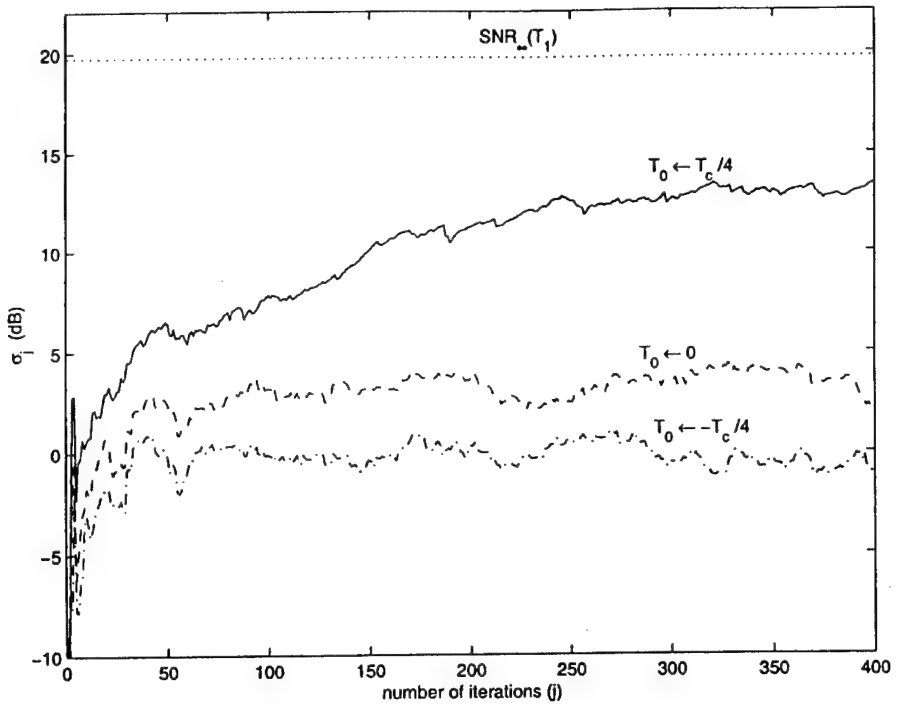


Fig. 6. $\sigma_j$ from a sample run of the adaptive algorithm.

We use the notation $\mathrm{SNR}_M$ to denote the SNR defined in (27) for this receiver. Then, we claim that, for $T_0 = l_0 T_s$ and $T_1 = l_1 T_s$, where $l_0 \in \{-2^{M-1}, -2^{M-1}+1, \cdots, 2^{M-1}-1\}$ and $l_1 \in \{0, 1, \cdots, 2^M - 1\}$

$$\mathrm{SNR}_M = \gamma_0 \left[1 - \frac{\lambda_1}{1+\lambda_1} \sum_{l=-L}^{L-1} \left|\hat{\psi}(lT_c + T_1)\right|^2\right]. \tag{42}$$

To show this, observe that since the chip waveform is time-limited, the summation indexed by $j$ in (20) has only a finite number of nonzero terms. Then, we can solve (24) recursively by the following result, which is based on repeat applications of the matrix inversion lemma: suppose $\mathbf{R}_0$ is a positive definite matrix $\mathbf{R}_l = \mathbf{R}_{l-1} + \xi_l \xi_l^H$ for $l = 1, 2, \cdots, P$, and $\mathbf{R} = \mathbf{R}_P + \eta\eta^H$. Then $\mathbf{R}_l$ for $l = 0, 1, \cdots, P$ and $\mathbf{R}$ are invertible. Write the inverse of $\mathbf{R}_l$ as $\mathbf{Q}_l$ where $l = 0, 1, \cdots, P$. Let $\mathbf{R}\mathbf{g} = \eta$ and $\gamma_l = \eta^H \mathbf{Q}_l \eta$. Then, for $l = 1, 2, \cdots, P$

$$\begin{aligned}
\mathbf{g}_l &= \mathbf{Q}_{l-1}\xi_l \\
\lambda_l &= \xi_l^H \mathbf{g}_l \\
\mathbf{Q}_l &= \mathbf{Q}_{l-1} - \frac{1}{1+\lambda_l}\mathbf{g}_l\mathbf{g}_l^H \\
\gamma_l &= \gamma_{l-1} - \frac{1}{1+\lambda_l}\left|\eta^H \mathbf{g}_l\right|^2.
\end{aligned}$$

Consider the dyadic receiver described above for $i, j = -(L+1)2^M, \cdots, (L+1)2^M$, $[\bar{\psi}]_i = [\overline{\psi}]_{i+l_0}$, $[\mathbf{R}_{\tilde{\mathbf{y}}}]_{ij} = [\overline{\psi}]_{i+l_0}[\overline{\psi}]^H_{j+l_0}$, $[\mathbf{R}_{\tilde{\mathbf{n}}\mathbf{w}}]_{ij} = (\sqrt{2}N_0/\sqrt{P_0})[\overline{\psi}]_{i-j}$, and

$$[\mathbf{R}_{\tilde{\mathbf{n}}_1}]_{ij} = \sum_{l=-2L-2}^{2L+1} \frac{P_1}{NP_0} [\overline{\psi}]_{i-l2^M-l_1+l_0} [\overline{\psi}]^*_{j-l2^M-l_1+l_0} \tag{43}$$

where $[\overline{\psi}]_i = \tilde{\psi}(iT_s)$.

To initialize the recursive process above, we set $[\mathbf{R}_0]_{ij} = [\mathbf{R}_{\tilde{\mathbf{n}}\mathbf{w}}]_{ij}$. Then, we have the following important equation:

$$\frac{\sqrt{P_0}}{\sqrt{2}N_0}\delta_{ij} = \sum_k [\mathbf{Q}_0]_{ik}[\overline{\psi}]_{k-j} \tag{44}$$

for $i, j = -(L+1)2^M, \cdots, (L+1)2^M$. By (44), we have $\gamma_0 = P_0 T/N_0$. Next, we arrange the terms in (43) as $\sum_{-2L-2}^{2L+1} = \sum_{-L}^{L-1} + \sum_{-2L-2}^{-L-1} + \sum_{L}^{2L+1}$ and apply the recursive procedure on them according to this ordering.

Again, by (44)

$$\begin{aligned}
[\mathbf{g}_1]_i &= \left(\sqrt{P_1/2N}/N_0\right)\delta_{i,\,-L2^M+l_1-l_0}, \\
\lambda_1 &= P_1 T/(NN_0), \\
\gamma_1 &= \gamma_0\left[1 - \frac{\lambda_1}{1+\lambda_1}\left|\hat{\psi}(-LT_c + T_1)\right|^2\right].
\end{aligned}$$

Inductively, we have

$$\begin{aligned}
[\mathbf{g}_{2L}]_i &= \left(\sqrt{P_1/2N}/N_0\right)\delta_{i,\,(L-1)2^M+l_1-l_0} \\
\lambda_{2L} &= P_1 T/(NN_0) \\
\gamma_{2L} &= \gamma_0\left[1 - \frac{\lambda_1}{1+\lambda_1}\sum_{l=-L}^{L-1}\left|\hat{\psi}(lT_c + T_1)\right|^2\right].
\end{aligned}$$

Now, consider the terms in the second and third summations. First

$$[\mathbf{g}_{2L+1}]_i = \sqrt{\frac{P_1}{NP_0}}\sum_j [\mathbf{Q}_0]_{ij}[\overline{\psi}]_{j+(2L+2)2^M-l_1+l_0}. \tag{45}$$

Due to the fact that $\mathbf{Q}_0$ is Hermitian and $\hat{\psi}(t)$ is time-limited to $[-LT_c, LT_c]$, it is easy to see from (44) and (45) that

$$\sum_j \left[\tilde{\psi}\right]_j^* [\mathbf{g}_{2L+1}]_j = 0$$

and hence $\gamma_{2L+1} = \gamma_{2L}$. Inductively, we can show that, for $l = 2L+1, 2L+2, \cdots, 4L+4$

$$\sum_j \left[\tilde{\psi}\right]_j^* [\mathbf{g}_l]_j = 0.$$

Therefore, we have $\gamma_{4L+4} = \gamma_{4L+3} = \cdots = \gamma_{2L+1} = \gamma_{2L}$. Finally, we see from (27) that $\mathrm{SNR} = \gamma_{4L+4}$ and, hence, (42) is established. It is also obvious that extending the observation interval further will not increase $\mathrm{SNR}_M$.

Next, we proceed to show the general case. In order to do that, we need the following obvious, but important, observation. Suppose, we have two receivers, say Receivers A and B. Both are constructed as in Section III, except that we allow the sampling times to be nonuniform. For fixed $T_0$ and $T_1$, let the SNR's, defined in (27), for them be $\mathrm{SNR}_A$ and $\mathrm{SNR}_B$, respectively. If the sampling times of Receiver B are a subset of those of Receiver A, then $\mathrm{SNR}_A \geq \mathrm{SNR}_B$ due to the fact that the SNR is always maximized in the construction of the receiver.

Moreover, it can be shown easily that $\hat{\psi}(t)$ is uniformly continuous on the real line. Let $t_1, t_2, \cdots, t_P$ be the sampling times of the receiver as in Section III. By the fact that $\hat{\psi}(t)$ is continuous and $\mathbf{R}_{\tilde{\mathbf{n}}\mathbf{w}}$ is positive definite under any sampling configuration, we find that the SNR, defined in (27), is a continuous function of $t_1, t_2, \cdots, t_P, T_0$, and $T_1$.

For the moment, continue to assume $\psi(t)$ is time-limited and reconsider the dyadic receivers described above. For fixed $T_0$ and $T_1$, $\mathrm{SNR}_M$ is an increasing sequence. From (42), $\mathrm{SNR}_M \leq \gamma_0$. Therefore, the sequence must have a limit. For $T_0/T_c$ and $T_1/T_c$ being dyadic rationals in $[-1/2, 1/2]$ and $[0, 1]$, respectively, this limit is given by (42). Otherwise, since dyadic rationals are dense in both $[-1/2, 1/2]$ and $[0, 1]$, and $\mathrm{SNR}_\infty$ and $\mathrm{SNR}_M$, for all $M$, are continuous functions of $T_0$ and $T_1$, $\mathrm{SNR}_M \leq \mathrm{SNR}_\infty$, for all $M$. But since $\mathrm{SNR}_M$, for all $M$, are bounded continuous functions of $T_0$ and $T_1$, $\lim_{M\to\infty} \mathrm{SNR}_M$ must also be continuous. This forces $\lim_{M\to\infty} \mathrm{SNR}_M = \mathrm{SNR}_\infty$ for all $T_0$ and $T_1$.

Now, let $\{t_1, t_2, \cdots, t_P\}$ be the set of sampling times of any receiver and $\mathrm{SNR}_0$ be the corresponding SNR. Due to the fact that the SNR is a continuous function of $t_1, t_2, \cdots, t_P$, there must be a receiver with sampling times $t_1', t_2', \cdots, t_P'$, which when divided by $T_c$ are dyadic rationals, whose SNR, namely SNR', is arbitrarily close to $\mathrm{SNR}_0$. Then, $\mathrm{SNR}' \leq \mathrm{SNR}_M \leq \mathrm{SNR}_\infty$, where $\mathrm{SNR}_M$ is the SNR of the dyadic receiver whose sampling time set contains $\{t_1', t_2', \cdots, t_P'\}$. This implies that $\mathrm{SNR}_0 \leq \mathrm{SNR}_\infty$.

Summarizing the above, we have established the least upper bound property of $\mathrm{SNR}_\infty$ when $\psi(t)$ is time-limited. To show this for the general case, let $\psi_L(t)$ be the $[-LT_c, LT_c]$ truncation of $\psi(t)$. Notice that we scale the energy of $\psi_L(t)$ so that it is equal to $T_c$. Then, it is easy to show that $\hat{\psi}_L(t)$ converges to $\hat{\psi}(t)$ uniformly. Moreover, if we let $\mathrm{SNR}_0$ be the SNR with $\psi(t)$ and $\mathrm{SNR}^L$ be the SNR with $\psi_L(t)$, $\lim_{L\to\infty} \mathrm{SNR}^L = \mathrm{SNR}_0$. But from the time-limited case, $\mathrm{SNR}^L \leq \mathrm{SNR}_\infty^L$, where $\mathrm{SNR}_\infty^L$ is given by (31) with $\hat{\psi}(t)$ replaced by $\hat{\psi}_L(t)$. It is also easy to show that $\lim_{L\to\infty} \mathrm{SNR}_\infty^L = \mathrm{SNR}_\infty$. Hence, by letting $L \to \infty$, we have $\mathrm{SNR}_0 \leq \mathrm{SNR}_\infty \leq \gamma_0$. On the other hand, the dyadic receiver gives SNR as close to $\mathrm{SNR}_\infty$ as desired when sampling rate increases.

## APPENDIX B

In this appendix, we discuss the achievability of the bound in (35).

Suppose the $\alpha$-BW of the system is $W_\alpha$. By the Schwartz inequality, $\int_{-W_\alpha/2}^{W_\alpha/2} \hat{\Psi}^2(f)\, df \geq \alpha^2/W_\alpha$. We can get (35) by putting this inequality into (34). Given the $\alpha$-BW, we note that equality in (35) is achieved when and only when $\hat{\Psi}(f)$ is constant on $[-W_\alpha/2, W_\alpha/2]$. There might not exist chip waveforms satisfying this condition and the Nyquist criterion simultaneously for all values of $\alpha$ and $W_\alpha$. Hence, the bound in (35) might not be always achieved and the optimization of $\mathrm{ANFE}_\infty$ is difficult in general.

However, in the special case when $\alpha = 1$ and $W_\alpha$ is slightly larger than any integral multiple of $1/T_c$, we can get as close to the bound as desired. Consider the frequency-domain raised-cosine $(n, \beta)$ chip waveform defined by $\hat{\Psi}(f)$ as shown in (46) at the bottom of the page where $0 < \beta \leq 1$ and $n$ is an integer. Note that this chip waveform satisfies the Nyquist criterion and is band-limited to $[-(n+\beta)/2T_c, (n+\beta)/2T_c]$. It is easy to see that $\mathrm{ANFE}_\infty = 1 - 1/n + \beta/4n^2$ and (35) gives $\mathrm{ANFE}_\infty \leq 1 - 1/(n+\beta)$. We achieve equality in (35) for $\beta = 0$ and any fixed $n$. Unfortunately, the autocorrelation function $\psi(t)$ of the frequency-domain raised-cosine $(n, 0)$ waveform does not satisfy the requirement that $\int_{-\infty}^{\infty} |\hat{\psi}(t)|\, dt < \infty$, which implies that it is not a legitimate chip waveform. Nevertheless, we can get as close to the bound as desired by choosing $\beta$ to be small enough. As a consequence, we can conclude that the frequency-domain raised-cosine $(n, \beta)$ waveform (for small $\beta$) is almost optimal under the constraint that the 1-BW of the system is limited to $(n+\beta)/T_c$.

## ACKNOWLEDGMENT

The authors thank M. Davis of LSI Logic, San Diego. CA, for his helpful comments.

$$\hat{\Psi}(f) = \begin{cases} \dfrac{T_c}{n}, & \text{if } 0 \leq |f| \leq \dfrac{n-\beta}{2T_c} \\ \dfrac{T_c}{2n}\left[1 + \cos\dfrac{\pi T_c}{\beta}\left(|f| - \dfrac{n-\beta}{2T_c}\right)\right], & \text{if } \dfrac{n-\beta}{2T_c} < |f| \leq \dfrac{n+\beta}{2T_c} \\ 0, & \text{otherwise} \end{cases} \tag{46}$$

## REFERENCES


[1] S. Verdú, "Multiuser detection," *Advances in Statistical Signal Processing*. Greenwich, CT: JAI Press, 1993, vol. 2, pp. 369–409.

[2] A. Duel-Hallen, J. Holtzman, and Z. Zvonar, "Multiuser detection for CDMA systems," *IEEE Personal Commun.*, vol. 2, pp. 46–58, Apr. 1995.

[3] TIA/EIA/IS-95 Interim Standard, "Mobile station-base station compatibility standard for dual mode wideband spread spectrum cellular system," Telecommunications Industry Association, Washington, DC, July 1993.

[4] A. Monk, M. Davis, L. B. Milstein, and C. W. Helstrom, "A noise-whitening approach to multiple-access noise rejection—Part I: Theory and background," *IEEE J. Select. Areas Commun.*, vol. 12, pp. 817–827, June 1994.

[5] M. Davis, A. Monk, and L. B. Milstein, "A noise-whitening approach to multiple-access noise rejection—Part II: Implementation issues," *IEEE J. Select. Areas Commun.*, vol. 14, pp. 1488–1499, Oct. 1996.

[6] Y. C. Yoon and H. Leib, "Matched filters with interference suppression capabilities for DS-CDMA," *IEEE J. Select. Areas Commun.*, vol. 14, pp. 1510–1521, Oct. 1996.

[7] T. F. Wong, T. M. Lok, J. S. Lehnert, and M. D. Zoltowski, "A linear receiver for direct-sequence spread-spectrum multiple-access systems with antenna arrays and blind adaptation," *IEEE Trans. Inform. Theory*, vol. 44, pp. 659–676, Mar. 1998.

[8] J. S. Lehnert, "Chip wavefore selection in offset quaternary direct-sequence spread-spectrum multiple-access communications," Coordinated Science Lab. Rep., Urbana, IL, Jan. 1981.

[9] A. J. Viterbi, "Very low rate convolutional codes for maximum theoretical performance of spread-spectrum multiple-access channels," *IEEE J. Select. Areas Commun.*, vol. 8, pp. 641–649, May 1990.

[10] J. Chaib and H. Leib, "Chip shaping and channel coding for CDMA," *European Trans. Telecommun. Related Technol.*, vol. 7, no. 2, pp. 133–143, Mar./Apr. 1996.

[11] H. V. Poor, *An Introduction to Signal Detection and Estimation*, 2nd ed. New York: Springer-Verlag, 1994.

[12] T. M. Lok and J. S. Lehnert, "An asymptotic analysis of DS/SSMA communication systems with general linear modulation and error control coding," *IEEE Trans. Inform. Theory*, vol. 44, pp. 870–881, Mar. 1998.

[13] R. Lupas and S. Verdú, "Near–far resistance of multiuser detectors in asynchronous channels," *IEEE Trans. Commun.*, vol. 38, pp. 496–508, Apr. 1990.

[14] U. Madhow, "Blind adaptive interference suppression for the near-far resistant acquisition and demodulation of direct-sequence CDMA signals," *IEEE Trans. Signal Processing*, vol. 45, pp. 124–136, Jan. 1997.

[15] F. Amoroso, "The bandwidth of digital data signals," *IEEE Commun. Mag.*, vol. 18, pp. 13–24, Nov. 1980.


**Tan F. Wong** received the B.Sc. degree (first class honors) in electronic engineering from the Chinese University of Hong Kong in 1991 and the M.S.E.E. and Ph.D. degrees in electrical and computer engineering from Purdue University, W. Lafayette, IN, in 1992 and 1997, respectively.

From July 1993 to June 1995, he was a Research Engineer working on the high-speed wireless networks project in the Department of Electronics at Macquarie University, Sydney, Australia. From August 1995 to October 1997, he was a Research and Teaching Assistant in the School of Electrical and Computer Engineering at Purdue University. From November 1997 to July 1998, he worked as a Post-Doctoral Research Associate at Purdue University. Currently, he is an Assistant Professor of electrical and computer engineering at the University of Florida, Gainesville. His research interests include spread-spectrum communication systems, multiuser communications, and wireless cellular networks.

**Tat M. Lok** received the B.Sc. degree in electronic engineering from the Chinese University of Hong Kong in 1991. He continued his education at Purdue University, West Lafayette, IN, and received the M.S.E.E. degree in electrical engineering and the Ph.D. degree in electrical and computer engineering in 1992 and 1995, respectively.

He had been a Research Assistant and a Post-doctoral Research Associate at Purdue University. Since 1996, he has been an Assistant Professor in the Department of Information Engineering, the Chinese University of Hong Kong. His research interests include code-division multiple-access systems, multiuser detection, adaptive antenna arrays, and communication theory.

**James S. Lehnert** received the B.S. (Highest Honors), M.S., and Ph.D. degrees in electrical engineering from the University of Illinois at Urbana-Champaign in 1978, 1981, and 1984, respectively.

From 1978 to 1984, he was a Research Assistant at the Coordinated Science Laboratory, University of Illinois, Urbana, IL. He was a University of Illinois Fellow from 1978 to 1979 and an IBM Pre-Doctoral Fellow from 1982 to 1984. He has held summer positions at Motorola Communications, Schaumburg, IL, in the Data Systems Research Laboratory, and Harris Corporation, Melbourne, FL, in the Advanced Technology Department. He is currently an Associate Professor of Electrical and Computer Engineering at Purdue University, West Lafayette, IN. He has served as Editor for Spread Spectrum for the IEEE TRANSACTIONS ON COMMUNICATIONS. His current research work is in communication and information theory with emphasis on spread-spectrum communications.

# Performance of a Type-II Hybrid ARQ Protocol in Slotted DS-SSMA Packet Radio Systems

Qian Zhang, Tan F. Wong, and James S. Lehnert, *Senior Member, IEEE*

***Abstract*—In this paper, the application of a type-II hybrid ARQ protocol in a slotted direct-sequence spread-spectrum multiple-access (DS-SSMA) packet radio system is investigated. Both the static performance and the dynamic performance of such a system are analyzed. In the physical layer, packet error and packet success probabilities are computed using the improved Gaussian approximation technique, which accounts for the bit-to-bit error dependence within a packet. In the data-link layer, two-dimensional Markov chains are employed to model the system dynamic. Based on this model, the performance of the type-II hybrid ARQ protocol is upper and lower bounded by considering, respectively, a superior scheme and an inferior scheme. Steady state throughput and delay performances of the two bounding schemes are obtained. Moreover, it is shown that for each fixed input load, there is an optimal retransmission probability under the finite user population assumption. Bounds on this optimal retransmission probability are also given.**

***Index Terms*—Automatic repeat request, code division multiaccess, Markov processes, networks, packet radio, spread spectrum communication.**

## I. Introduction

PURE automatic repeat request (ARQ), type-I hybrid ARQ [1], type-II hybrid ARQ [2], [3], and code combining [4]–[6] are data-link layer protocols, with increasing complexities, which try to provide error-free transmission for packet radio systems over noisy communication channels. Roughly speaking, because of the incorporation of forward error correcting capability into the feedback error control protocols, hybrid ARQ's and code combining give higher average system throughput than pure ARQ. On the other hand, since type-II hybrid ARQ and code combining adapt to changing channel conditions, they give lower average system delay than pure ARQ and type-I hybrid ARQ. Type-II hybrid ARQ has the potential to serve as a practical compromise between system performance and complexity. However, more detailed complexity and performance tradeoff analyses are needed to establish its usefulness.

Direct-sequence spread-spectrum (DS/SS) signaling [7], [8] is an effective physical layer modulation technique which allows multiple users to have simultaneous access to a common channel in a packet radio system. Due to the presence of the characteristic multiple-access interference (MAI) in the DS/SS signaling technique, packet error control protocols such as those mentioned above have to be applied in the data-link layer to ensure error-free transmission of packets when a feedback channel is available. Several researchers have proposed and analyzed the application of some of the feedback error control protocols to direct-sequence spread-spectrum multiple-access (DS-SSMA) systems. The application of pure ARQ to DS-SSMA systems is examined in [9]. DS-SSMA systems with type-I hybrid ARQ are examined in [8] and [10]. The use of code combining is investigated in [11] and [12].

The major difficulty in analyzing the feedback protocols described above is that the channel condition, in particular, the packet error probability, under the DS/SS signaling technique depends on the number of active transmitting users in the system. Hence, a reasonable analysis of such a system has to condition on the number of active users at a particular moment. In [11], the number of active transmitting users is assumed to be fixed. In [12], the numbers of active users at different time slots are assumed to be independent identically distributed Poisson random variables. Since the number of transmitting and retransmitting users at the current moment depends on the previous transmission events, the number of active transmitting users is actually a stochastic process with dependent time samples. As a result, the aforementioned traffic-dependent characteristic of a DS-SSMA channel is actually ignored in [11] and [12]. On the other hand, it is shown in [9] and [10] that system dynamics under the pure ARQ and type-I hybrid ARQ protocols can be modeled by time-homogeneous Markov chains, and hence, exact analyses of these two protocols can be obtained.

In this paper, we investigate the use of the type-II hybrid ARQ protocol (ARQ2) proposed in [3] to slotted DS-SSMA packet radio systems under the finite user population assumption. This protocol acts as a simple adaptive coding scheme to cope with the time-varying channel conditions of the DS-SSMA channel. Details of the DS-SSMA signaling technique and ARQ2 are given in Section II. By assuming the number of active transmitting users in the system to be fixed, we present several static system performance measures such as the packet error, undetectable error, and packet success probabilities in Section III. The improved Gaussian approximation technique

Paper approved by J. Chuang, the Editor for Wireless Networks of the IEEE Communications Society. Manuscript received June 10, 1997; revised April 16, 1998; August 7, 1998. This paper was presented in part at the IEEE Military Communications Conference (MILCOM'97), Monterey, CA, November 2–5, 1997.

Q. Zhang was with the School of Electrical and Computer Engineering, Purdue University, West Lafayette, IN 47907-1285 USA. He is now with Globespan Semiconductor, Inc., Red Bank, NJ 07701 USA (e-mail: jqzhang@globespan.net).

T. F. Wong was with the School of Electrical and Computer Engineering, Purdue University, West Lafayette, IN 47907-1285 USA. He is now with the Department of Electrical and Computer Engineering, University of Florida, Gainesville, FL 32611-6130 USA (e-mail: twong@ece.ufl.edu).

J. S. Lehnert is with the School of Electrical and Computer Engineering, Purdue University, West Lafayette, IN 47907-1285 USA (e-mail: lehnert@purdue.edu).

Publisher Item Identifier S 0090-6778(99)01930-3.

[7], which accounts for the bit-to-bit error dependence within a packet, is employed to obtain accurate results. In Section IV, we show that the system dynamic can be modeled by a multidimensional time-homogeneous Markov chain. This approach is similar to, but considerably more complex than, those in [9] and [10], where one-dimensional Markov chains are employed. Compared to [11] and [12], the traffic-dependent characteristic of the DS-SSMA channel is accurately modeled using this approach. Due to the complexity of the multidimensional model, an exact analysis of the system cannot be performed easily. Instead, we introduce an inferior scheme and a superior scheme, which bound the performance of ARQ2. Since both the inferior and superior schemes can be modeled by two-dimensional Markov chains, system performances can be obtained easily. In particular, we present the steady state throughput and delay performances of the bounding schemes. Moreover, we also show that for each fixed input load, there is a unique optimal retransmission probability in the sense of maximizing the throughput and minimizing the delay. Similar optimal retransmission probabilities are obtained for the pure ARQ and type-I hybrid ARQ protocols in [9] and [10], respectively. Finally, to demonstrate the performance of ARQ2, we present numerical results of the dynamic analysis of a sample system in Section V.

## II. System Model

In this section, we describe the DS-SSMA signaling technique and ARQ2 employed in the physical layer and the data-link layer of the system, respectively.

### A. Slotted DS-SSMA Packet Radio Network

We assume that DS-SSMA signaling, which provides the basis for the multiple access capability of the system, is employed as the digital modulation scheme in the physical layer. Without loss of generality, we assume that the transmitters and receivers in the DS-SSMA system work in pairs. Each transmitter-receiver pair uses an independent aperiodic random signature sequence, with spreading factor $N$ ($N$ chips per bit), to modulate data bits in the BPSK format. For simplicity, we ignore the presence of thermal noise and assume that possible bit errors are only caused by MAI from other active users in the system.

We model the system as a finite-user *slotted* packet radio network with packet size of $L$ bits. There are altogether $U$ users (active or not) in the system. The *slotted* transmission is interpreted in such a way that the transmissions of packets from different users are only approximately synchronous within a few chip durations.[1] This alleviates the difficulty in synchronizing the transmissions of packets from different users. We assume that both the spreading factor $N$ and the packet size $L$ are large as in any practical DS-SSMA system. Therefore, the system can be viewed as an asynchronous one on the chip level, while, on the packet level, it is a slotted system. Since such a system satisfies the requirements described in [7], the improved Gaussian approximation technique [7], which accounts for the bit-to-bit error dependence within a packet, can be employed to compute the packet error probability given the number of simultaneous active users in the system. We note [8] that since the improved Gaussian approximation gives accurate error probability estimates regardless of whether there are a large number of active users, our results are reliable under all load conditions.

[1] Guard times have to be added between adjacent slots to prevent inter-slot interference.

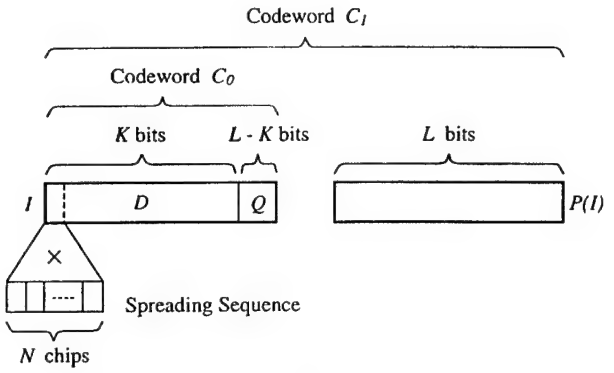


Fig. 1. Coding structure of the DS-SSMA system with the type-II hybrid ARQ protocol.

### B. Type-II Hybrid ARQ Protocol

We assume that there is an error-free feedback channel from the receiver back to the transmitter to convey all necessary control information, transmission errors are detected by the receiver, and the transmitter is immediately acknowledged after each packet transmission. We note that this assumption is valid for terrestrial radio communication systems in which the transmission delay over the link is much smaller than the packet duration. With the presence of the feedback channel, ARQ protocols can be employed to ensure error-free transmission of packets. In this paper, we suggest the application of the following type-II hybrid ARQ protocol [3] in the slotted DS-SSMA packet radio network.

Two block codes $C_0$ and $C_1$, where $C_0$ is an $(L, K)$ high-rate ($K$ is slightly smaller than $L$) error-detecting code and $C_1$ is an $(2L, L)$ half-rate invertible systematic code[2] with error-correcting capability $t_1$, which is designed for error correction only, are used. Transmission errors in a packet are detected by calculating the syndrome of code $C_0$. We assume that an idle user generates a new $K$-bit data block with probability $p_i$. $(L-K)$ parity bits based on $C_0$ are appended to the $K$-bit data block forming an $L$-bit data packet. We denote by $I = (D, Q)$ this $L$-bit data packet, which is a codeword in $C_0$, where $D$ is the $K$-bit data block and $Q$ is the corresponding $(L-K)$-bit parity block. An $L$-bit parity check packet, $P(I)$, of $I$ based on code $C_1$ in such a way that $(I, P(I))$ is a codeword of $C_1$ is constructed. The coding structure is shown in Fig. 1.

The data packet $I$ is first sent. The receiver calculates the syndrome of the received packet based on $C_0$. If the syndrome is zero, the transmission is assumed to be error-free and

[2] These codes are abundant, as it is shown in [1] that we can shorten any cyclic code with a suitable rate, for example, a BCH or a Reed–Solomon code, to obtain a half-rate invertible code without compromising the error correcting capability.

the transmitter is acknowledged. Otherwise, the received data packet is saved in a buffer and the transmitter is informed to restart the transmission. Upon a transmission failure, the transmitter will send the parity packet $P(I)$ with retransmission probability $p_b$ ($p_b$-persistent). The receiver, then, checks the syndrome of $P(I)$ (see [3] for details). If it is zero, the transmission is assumed to be successful and $P(I)$ is inverted to obtain $I$. Otherwise, $P(I)$, combined with the previously stored $I$, is decoded based on $C_1$. If the syndrome of the decoded packet $\tilde{I}$ is zero, the transmission is declared successful. Otherwise, $I$ will be replaced by $P(I)$ in the receiver buffer and the transmitter is informed to retransmit once again. The data packet $I$ and the parity check packet $P(I)$ are sent alternately in the way described above until the transmission is successful.

We assume that a backlogged user, who fails the transmission of the current packet, is prevented from generating new packets before successful retransmission of the current backlogged packet. After successful retransmission, the backlogged user will become an idle user again.

## III. Static Analysis

The channel characteristics of the DS-SSMA system depend on the number of active users in the channel at a particular moment. In this section, we study several static system performance measures, namely, the packet error probability, undetectable error probability, and the packet success probability, conditioned on the number of active users in the channel.

### A. Packet Error Probability

First, we derive the packet error probability. Based on the improved Gaussian method in [7], an accurate approximation of the packet error probability accounting for different channel conditions can be obtained. Let $P_e(i \mid k)$ be the probability of the event that $i$ errors occur in a packet given that there are $k$ active users transmitting in the same time slot. Then

$$P_e(i \mid k) = \int_0^\infty \binom{L}{i} \left[Q\left(\frac{N}{\sqrt{\psi}}\right)\right]^i \left[1 - Q\left(\frac{N}{\sqrt{\psi}}\right)\right]^{L-i} f_\Psi(\psi) d\psi \tag{1}$$

where $Q(\cdot) = 1 - \Phi(\cdot)$, with $\Phi(\cdot)$ representing the distribution function of a standard normal random variable. We note that the random variable $\Psi$ has the density function

$$f_\Psi(\psi) = \left(\frac{1}{2}\right)^{N-1} \sum_{j=0}^{N-1} \binom{N-1}{j} \left(\underbrace{f_{\Psi|j} * \cdots * f_{\Psi|j}}_{k-1}\right) \tag{2}$$

where $*$ denotes the convolution operator and

$$f_{\Psi|j}(\psi) = \frac{1}{2\pi\sqrt{(j+1/2)\psi}} \log\left|\frac{\sqrt{N-\psi}+\sqrt{j+1/2}}{\sqrt{N-\psi}-\sqrt{j+1/2}}\right|. \tag{3}$$

We note that, since the spreading sequences are aperiodic and independent, given the number of active users $k$ in a time slot, the packet error event of a user is conditionally independent of error events in other time slots and those of the other users in the same time slot.

### B. Undetectable Error Probability

Next, we consider the probability $P_{e,\mathrm{ARQ2}}$ that an erroneous data packet is delivered by ARQ2. We let $P_u$ be the probability that an erroneous received packet is undetected by the error-detecting code $C_0$. By the construction of $C_0$ and $C_1$, it can be shown [3] that $P_u$ is the same regardless of whether the received packet is a data packet or a parity packet. Suppose the number of active users is fixed to $k$, by combining the random coding argument in [1] and the improved Gaussian approximation in [7], for a suitably chosen $C_0$, we have

$$P_{u|k} \le 2^{-(L-K)}[1 - P_e(0 \mid k)] \le 2^{-(L-K)}. \tag{4}$$

We can also show that

$$P_{e,\mathrm{ARQ2}|k} \le \frac{2P_{u|k}}{P_{u|k} + P_e(0 \mid k)} \le \frac{2^{-(L-K)+1}}{P_e(0 \mid U)}. \tag{5}$$

Since the bounds in (4) and (5) do not depend on $k$ and $P_e(0 \mid U) > 0$, we can choose $C_0$ ($L - K$ large enough) to make both of the (unconditional) probabilities $P_u$ and $P_{e,\mathrm{ARQ2}}$ arbitrarily small. Therefore, from now on, we assume that $C_0$ is powerful enough to detect all errors in a packet and no erroneous data packet will be delivered by the ARQ2.

### C. Packet Success Probability

We give a simple demonstration of the improvement due to the adaptive coding capability of ARQ2. Here, we consider the 1-persistent retransmission policy and suppose that there is a mechanism to fix the number of active users in each time slot to be $k$, where $1 \le k \le U$. We look at one of the active users and let $P_s(t \mid k)$ be the probability of successful transmission in the $t$th slot for this user. Then, it is not hard to see that $P_s(0 \mid k) = P_e(0 \mid k)$ and for $t \ge 1$

$$P_s(t \mid k) = P_e(0 \mid k) + [1 - P_s(t-1 \mid k)]P_{C_1}(k), \tag{6}$$

where

$$P_{C_1}(k) = \sum_{\substack{m,n \ge 1 \\ m+n \le t_1}} P_e(m \mid k) P_e(n \mid k) < 1. \tag{7}$$

Solving (6), we have, for $t \ge 0$

$$P_s(t \mid k) = \frac{P_e(0 \mid k) + P_{C_1}(k) + [-P_{C_1}(k)]^{t+1}[1 - P_e(0 \mid k)]}{1 + P_{C_1}(k)}. \tag{8}$$

Hence, the stationary packet success probability is

$$P_s(k) \triangleq \lim_{t\to\infty} P_s(t \mid k) = \frac{P_e(0 \mid k) + P_{C_1}(k)}{1 + P_{C_1}(k)} \ge P_e(0 \mid k). \tag{9}$$

From (9), we see that when $P_e(0 \mid k)$ is small, the performance of the system is determined by the error correcting capability

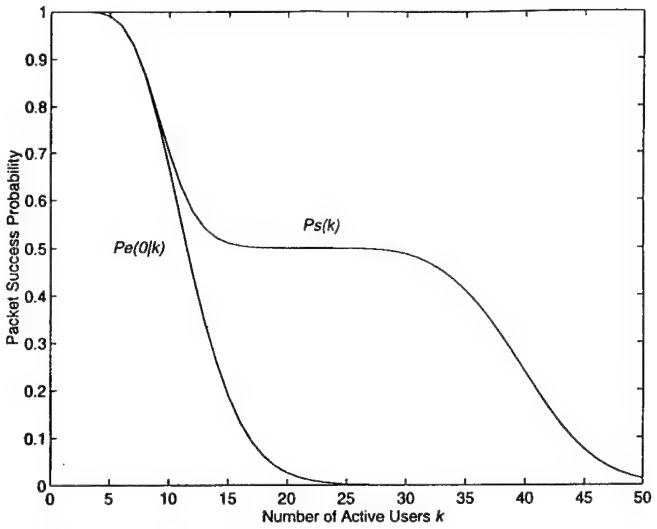


Fig. 2. Packet success probability.

of $C_1$. This can be much better than the pure ARQ protocol in which $P_s(k) = P_e(0 \mid k)$.

To demonstrate the advantage of ARQ2 over pure ARQ in the DS-SSMA system, we consider a sample system using the code $C_1$, adopted from [3], with $L = 500$ and $t_1 = 54$. The spreading factor $N$ is set to 31, and there are 50 users in the system, i.e., $U = 50$. Fig. 2 shows $P_e(0 \mid k)$ and $P_s(k)$ as functions of $k$. We see that ARQ2 provides a reasonably high packet success probability for a much larger range of $k$ than pure ARQ.

## IV. Dynamic Analysis

As mentioned in Section I, due to the traffic-dependent nature of the DS-SSMA channel, the number of active users in a time slot is a stochastic process with dependent time samples. The static analysis, as well as the analyses in [11] and [12], only give crude approximations to the real behaviors of the systems. In this section, we perform dynamic analyses taking the traffic-dependent characteristic of the DS-SSMA channel into account.

### A. Multidimensional Markov Model

Due to the statistical nature of the error and retransmission events, the number of active users $k$ varies from slot to slot. Since ARQ2 uses only the stored packet in the receiver buffer and the current received packet to perform decoding, the next state of the system is independent of all the previous activities given the current stored packets in all the receiver buffers. Moreover, by the construction of $C_0$ and $C_1$, the decoder sees the same statistical properties whether the current received packet is a data packet or a parity packet. Hence, the dynamic of the system can be modeled by a time-homogeneous[3] discrete-time Markov process. More precisely, we let $U_i(t)$, where $1 \le i \le t_1 - 1$, denote the number of users who fail the decoding in the $(t-1)$th slot with $i$ errors in each stored packet. Moreover, we use $U_0(t)$ to denote the number of idle users in the $t$th slot and $U_{t_1}(t)$ to denote the number of users who fail the decoding in the $(t-1)$th slot with each stored packet having at least $t_1$ errors. We note that there are $t_1 + 1$ groups, and the constraints $0 \le U_i \le U$ for $0 \le i \le t_1$ and $U_0 + U_1 + \cdots + U_{t_1} = U$ must be satisfied. We define the state vector as $\mathbf{X}(t) = (U_0(t), U_1(t), \cdots, U_{t_1-1}(t))$. Then, $\mathbf{X}(t)$ is a $t_1$-dimensional time-homogeneous Markov chain which gives a sufficient description of the dynamic of the system for the purposes in this paper. For example, we can evaluate the stationary distribution of the Markov chain $\mathbf{X}(t)$ and then obtain the steady state throughput and delay of the system. Unfortunately, the number of states in this model is of the order of $U^{t_1}$. In practice, both $t_1$ and $U$ are large, and the model becomes too complex for practical numerical computations.

[3]For a noninvertible code, we cannot use a time-homogeneous Markov chain to model the system dynamic. The reason is that for the case when the received parity check packet is error-free, we cannot invert it to obtain the data packet. However, this event can be neglected when there are a large number of active users transmitting (the system is operating near its capacity) since the chance of having an error-free received packet is low. As a result, for the operating region of interest, the time-homogeneous Markov model and the analysis in this paper are good approximations for a system employing a noninvertible code.

TABLE I
Error-Correction Capabilities of the Inferior and Superior Schemes

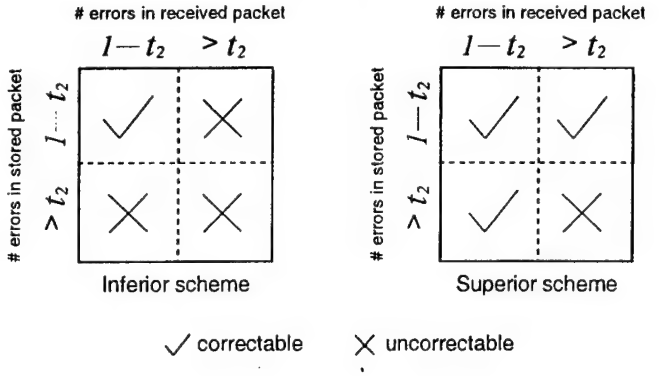


### B. Inferior and Superior Schemes

The $t_1$-dimensional Markov chain model in the previous section is too complex for practical values of $t_1$ and $U$. In this section, we introduce an inferior scheme and a superior scheme which bound the performance of ARQ2 described in Section II. We show that the system dynamics of each of the inferior and superior schemes can be modeled by a two-dimensional time-homogeneous Markov chain. As a result, the complexity of the analysis of them is much smaller than that required by the multidimensional model (order $U^2$ instead of order $U^{t_1}$). Both the inferior and superior schemes are based on ARQ2. They only differ in terms of their error correcting powers. Table I summarizes their error correcting capabilities. We recall that ARQ2 can correct up to a total of $t_1$ errors in the received packet and the previously stored packet. As shown in Table I, an error packet can be successfully decoded by the inferior scheme only when there are less than $t_2 = \lfloor t_1/2 \rfloor$ errors in each of the received packet and the previously stored packet. On the other hand, the superior scheme can give successful decoding unless there are more than $t_2$ errors in each of the received packet and the previously stored packet. It is obvious that the inferior scheme has a poorer error correcting capability than ARQ2, while the superior scheme has a stronger error correcting capability than ARQ2.

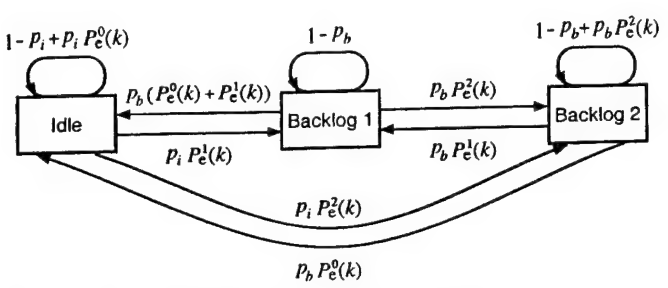


Fig. 3. State transition diagram for the inferior scheme.

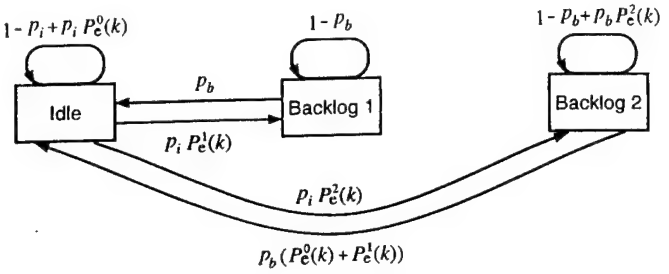


Fig. 4. State transition diagram for the superior scheme.

Therefore, the performance of ARQ2 is lower and upper bounded by the inferior and the superior schemes, respectively.

From the discussion in Section IV-A, the system dynamics of each of the two bounding schemes can be modeled by a time-homogeneous Markov chain. To analyze the dynamics of a user, it suffices to define three states of the user, namely, *Idle*, *Backlog1*, and *Backlog2*. The states *Idle*, *Backlog1*, and *Backlog2* correspond to the three events that the previous transmission is successful, that the previous transmission fails and the store packet has at most $t_2$ errors, and that the previous transmission fails and the store packet has more than $t_2$ errors, respectively. Based on Table I, it is easy to verify that every state transition event of a user is governed by the following set of rules.

1) In a time slot, a user must be in one of the three states.
2) A user in *Idle* transmits a new data packet with probability $p_i$ in the current time slot. If the transmission succeeds, the user will remain in *Idle* in the next time slot. Otherwise, it will go to either *Backlog1* or *Backlog2* depending on whether the received packet contains one to $t_2$ errors, or more than $t_2$ errors.
3) A user in *Backlog1* retransmits a packet (data or parity) with probability $p_b$ in the current slot. If the received packet is error-free or contains at most $t_2$ errors, then both the inferior and superior schemes will give successful decoding and the user will go back to *Idle*. Otherwise, the inferior scheme will give unsuccessful decoding and the user will go to *Backlog2*. On the other hand, the superior scheme will give successful decoding and the user will return to *Idle*.
4) A user in *Backlog2* retransmits a packet (data or parity) with probability $p_b$ in the current slot. If the received packet is error-free, i.e., the retransmission succeeds, then the user will return to *Idle*. If the received packet contains more than $t_2$ errors, then both the inferior and superior schemes will give unsuccessful decoding and the user will stay in *Backlog2*. Otherwise, the inferior scheme will give unsuccessful decoding and the user will go to *Backlog1*, while the superior scheme will give successful decoding and the user will go back to *Idle*.

The respective state transition diagrams describing this set of rules for the inferior and superior schemes are shown in Figs. 3 and 4. In the figures, $P_e^0(k)$, $P_e^1(k)$, and $P_e^2(k)$ are the probabilities that a received packet contains no error, one to $t_2$ errors, and more than $t_2$ errors conditioned on $k$ active users, respectively. It is obvious that

$$P_e^0(k) = P_e(0 \mid k) \tag{10}$$

$$P_e^1(k) = \sum_{i=1}^{t_2} P_e(i \mid k) \tag{11}$$

$$P_e^2(k) = \sum_{i=t_2+1}^{L} P_e(i \mid k) \tag{12}$$

where

$$P_e^0(k) + P_e^1(k) + P_e^2(k) = 1. \tag{13}$$

### C. Two-Dimensional Markov Model

With the classification in the previous section, the dynamic of the whole system can be modeled by a two-dimensional time-homogeneous Markov chain. Let $i(t)$ and $j(t)$ represent the total number of users in *Backlog1* and *Backlog2* in the $t$th slot, respectively. Hence, the total number of users in *Idle* is $U - i(t) - j(t)$. The state vector $\tilde{\mathbf{X}}(t) \triangleq (i(t), j(t))$ forms a two-dimensional Markov chain with state transition probabilities, for all $t \geq 0$,

$$P_\xi(i,j;k,l) \triangleq \Pr\{\tilde{\mathbf{X}}(t+1) = (k,l) \mid \tilde{\mathbf{X}}(t) = (i,j), \xi\} \tag{14}$$

where $\xi \in \{I, S\}$ indicates the inferior and superior schemes, respectively. We note that the state indexes $i$, $j$, $k$, and $l$ satisfy the constraints that $0 \leq i, j, k, l \leq U$, $i+j \leq U$, and $k+l \leq U$. The dependence of all the variables on the time $t$ is implicit in the notation above.

Suppose in the $t$th slot, $n$ out of the $U - i - j$ users in *Idle*, $i_1$ out of the $i$ users in *Backlog1*, and $j_1$ out of the $j$ users in *Backlog2* send packets to the channel. Hence, there are $n+i_1+j_1$ active users in the $t$th slot. Since the (re)transmission events are independent of each other and all other events given $i$ and $j$, the probability of the above event is

$$P(n, i_1, j_1 \mid i, j) = B(U - i - j, n, p_i) B(i, i_1, p_b) B(j, j_1, p_b) \tag{15}$$

where $B(\cdot,\cdot,\cdot)$ denotes the binomial distribution, i.e., for $0 \leq m \leq M$ and $0 \leq p \leq 1$

$$B(M, m, p) = \binom{M}{m} p^m (1-p)^{M-m}. \tag{16}$$

Then,

$$P_\xi(i,j;k,l) = \sum_{n=0}^{U-i-j} \sum_{i_1=0}^{i} \sum_{j_1=0}^{j} P_\xi(i,j;k,l \mid n,i_1,j_1) P(n,i_1,j_1 \mid i,j) \tag{17}$$

where $P_\xi(i,j;k,l \mid n,i_1,j_1)$ is the transition probability from state $(i,j)$ to state $(k,l)$ conditioned on $n$, $i_1$, and $j_1$. The detailed derivation of $P_\xi(i,j;k,l \mid n,i_1,j_1)$ for both the inferior and superior schemes is given in the Appendix.

We arrange the $(U+1)(U+2)/2$ states into the row vector

$$[(0,0),\cdots,(0,U),(1,0),\cdots,(1,U-1),\cdots,(U,0)]. \tag{18}$$

We can obtain the elements of the state transition matrix $\mathbf{P}_\xi$ according to the ordering in (18) by (17). Since the Markov chain $\tilde{\mathbf{X}}(t)$ is irreducible, a stationary distribution $\pi_\xi$ exists. According to the ordering in (18)

$$\pi_\xi = [\pi_\xi(0,0),\cdots,\pi_\xi(0,U),\cdots,\pi_\xi(U,0)] \tag{19}$$

where $\pi_\xi(i,j)$ is the stationary probability of state $(i,j)$. Moreover, $\pi_\xi$ can be found by solving the following set of equations:

$$\pi_\xi = \pi_\xi \mathbf{P}_\xi \tag{20}$$

$$\sum_{i=0}^{U} \sum_{j=0}^{U-i} \pi_\xi(i,j) = 1. \tag{21}$$

### D. System Throughput, Delay, and Traffic Intensity

From the stationary distribution obtained in the previous section, we can find out the average throughput of the system, which is defined as the steady state average number of successfully transmitted packets per slot, and the average delay of the system, which is defined as the average number of time slots required to successfully transmit a data packet when the system reaches its steady state.

First, the steady state average number of backlogged users in the system is

$$N_\xi = \sum_{i=0}^{U} \sum_{j=0}^{U-i} (i+j)\pi_\xi(i,j) \tag{22}$$

where $\xi \in \{I,S\}$ represents the inferior and superior schemes, respectively. We define the steady state backlog ratio as $\beta_\xi \triangleq N_\xi/U$, which measures the degree of congestion in the system. Also, the steady state average number of new data packets generated per slot is

$$\begin{aligned}\Lambda_\xi &= \sum_{i=0}^{U} \sum_{j=0}^{U-i} E\{n \mid i,j\}\pi_\xi(i,j) \\ &= \sum_{i=0}^{U} \sum_{j=0}^{U-i} p_i(U-i-j)\pi_\xi(i,j) \\ &= p_i U(1-\beta_\xi).\end{aligned} \tag{23}$$

With the time dependent notations in Section IV-C, we have, for $t \geq 0$

$$i(t+1) + j(t+1) = i(t) + j(t) + n(t) - s(t) \tag{24}$$

where $s(t)$ is the number of successfully (re)transmitted packets in the $t$th slot. Taking expectations in (24) and noting that, for each $\xi \in \{I,S\}$

$$\begin{aligned}\lim_{t\to\infty} E[i(t)+j(t)] &= N_\xi \\ \lim_{t\to\infty} E[n(t)] &= \Lambda_\xi \\ \lim_{t\to\infty} E[s(t)] &= S_\xi\end{aligned}$$

we see that the average throughput is

$$S_\xi = \Lambda_\xi = p_i U(1-\beta_\xi). \tag{25}$$

Therefore, we can apply Little's theorem [13] to obtain the steady state average delay of the system

$$D_\xi = 1 + \frac{N_\xi}{\Lambda_\xi} = 1 + \frac{\beta_\xi}{p_i(1-\beta_\xi)}. \tag{26}$$

Also, we can obtain the average traffic intensity, which is defined as the steady state average number of active transmitting users (packets) in a slot

$$T_\xi = p_b U \beta_\xi + S_\xi. \tag{27}$$

### E. Optimal Retransmission Probability

Our objective is to maximize the system throughput and minimize the system delay. Suppose the packet generation probability $p_i$ is fixed, by eliminating $\beta_\xi$ from (25) and (26), we get

$$(p_i D_\xi + 1 - p_i) S_\xi = p_i U. \tag{28}$$

Since (28) holds for all values of $p_b$ ranging from zero to one, maximizing the throughput $S_\xi$ implies minimizing the delay $D_\xi$ simultaneously. Moreover, from (25) and (26), we see that the maximization of $S_\xi$ and minimization of $D_\xi$ is equivalent to the minimization of the backlog ratio $\beta_\xi$. It is easy to see from the previous two sections that for both the inferior and superior schemes, $\beta_\xi$ is a bounded rational function of $p_b$. Hence, $\beta_\xi$ must attain its minimum value for $p_b \in [0,1]$, and this minimum value can only be attained at a finite number of different values of $p_b$. On the other hand, once $\beta_\xi$ passes its minimum value, increasing the retransmission probability $p_b$ will only cause more congestion, and hence, increase in $\beta_\xi$. This simple physical observation indicates that $\beta_\xi$ attains its minimum at a unique value of $p_b$. In summary, for every fixed $p_i$, there is a unique optimal retransmission probability, denoted by $p^*_{b,\xi}$, in the sense of maximizing the system throughput and minimizing the system delay simultaneously under both the inferior and superior schemes.

Applying a similar argument to the multidimensional Markov model of the adaptive coding scheme in Section IV-A,

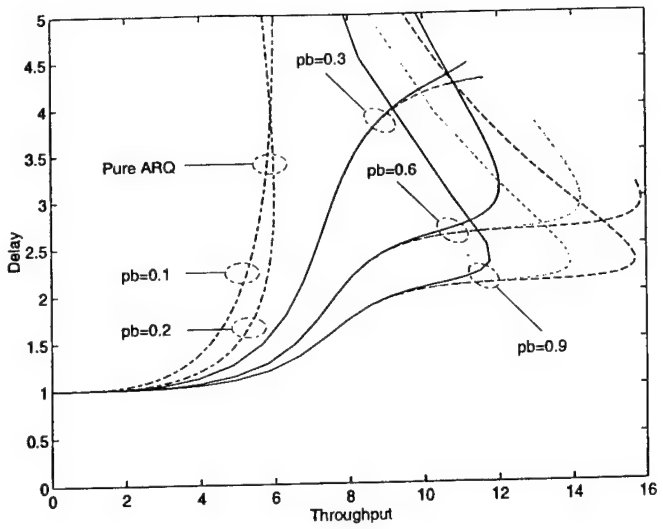


Fig. 5. Delay-throughput characteristic.

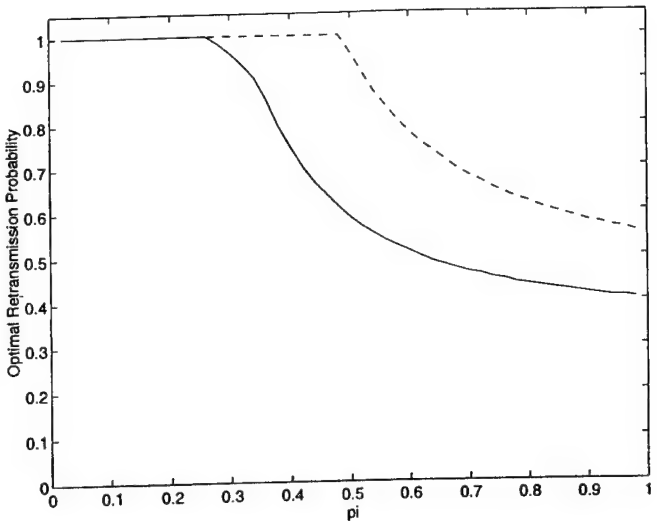


Fig. 6. Optimal retransmission probability.

we can also show that for every fixed $p_i$, there is a unique optimal retransmission probability, denoted by $p_b^*$, for ARQ2. Moreover, by simple physical arguments as above, $p_b^*$ is bounded between $p_{b,I}^*$ and $p_{b,S}^*$.

## V. Numerical Results

In this section, we present numerical results of the dynamic analysis in Section IV for the sample system described in Section III-C. We recall that the system parameters for the sample system are: $U = 50$, $L = 500$, $t_1 = 54$, and $N = 31$. In the figures below, we use solid lines and broken lines to show analytical results obtained from Section IV for the inferior and superior schemes, respectively. Moreover, results obtained from Monte Carlo simulations for ARQ2 are shown by dotted lines. Our main objective here is to illustrate the kind of information which can be obtained by the analysis described in Section IV. Following the procedures given below, it is trivial to investigate the effects of different parameters, such as $N$, $U$, and $t_1$, on the performance of the system.

### A. Delay-Throughput Characteristic

Fig. 5 shows the delay-throughput characteristic of the system for three different values of $p_b$, namely, $p_b = 0.3$, 0.6, and 0.9. Each curve is the delay-throughput locus with $p_i$ varying from zero to one. In the same figure, the delay-throughput characteristic of a system with the pure ARQ protocol [14] is also shown for comparison. We see from the delay-throughput characteristic of the inferior scheme in Fig. 5 that with a suitable choice of $p_b$ and a slight increase in delay, we can at least double the throughput by using ARQ2 instead of pure ARQ. For $p_b = 0.6$ and 0.9, for both the superior and inferior schemes, the system reaches its capacity (the turning points at the delay-throughput loci) before $p_i$ reaches one. Beyond those turning points, an increase in $p_i$ causes more congestion, and hence, decreases the throughput and increases the delay. However, for $p_b = 0.3$, the system never reaches its capacity. We can see from the figure that before the system reaches its capacity, the inferior and superior schemes closely bound the actual performance of ARQ2. Beyond that, the bounds are not as tight.

### B. Optimal Retransmission

The respective optimal retransmission probabilities $p_{b,I}^*$ and $p_{b,S}^*$ for the inferior and superior schemes derived in Section IV-E are obtained and plotted as functions of $p_i$ in Fig. 6. We observe from the figure that when $p_i$ is smaller than a critical value determined by $t_1$ and $U$ (0.28 and 0.49 for the inferior and superior schemes, respectively, in the sample system), the optimal $p_b$ is one. This means that when the system is lightly loaded, we should always retransmit any failed packet immediately. Beyond this critical $p_i$, the system becomes congested. In order to maximize the throughput and minimize the delay, we should reduce $p_b$. We note that the optimal $p_b$ for the sample system is always larger than 0.4. This agrees with the observation from Fig. 5 that the system never reaches its capacity for $p_b = 0.3$.

The optimal traffic intensity, maximum throughput, and minimum delay corresponding to the optimal retransmission probability obtained above for each of the bounding schemes are plotted in Figs. 7, 8, and 9, respectively. From Fig. 7, we see that when $p_i$ increases beyond the critical value, in order to achieve the maximum throughput, we have to decrease $p_b$ to the extent that the traffic intensity is kept to a specific constant level determined by $t_1$ and $U$ (about 27 and 34 for the inferior and superior schemes, respectively, in the sample system). By cross-checking with Fig. 2, we observe that these two values lie in the range such that $P_s(k)$ is about 0.5. Roughly speaking, in order to achieve maximum throughput, when $p_i$ is larger than some critical value, we have to choose $p_b$ to maintain (on the average) a certain constant number of active transmitting users on the channel so that the packet success probability is about 0.5.

From Fig. 8, we see that the maximum throughput level after $p_i$ passes the critical value. This indicates that the system reaches its capacity. Further increase in $p_i$ will not increase the maximum throughput. Intuitively, the minimum delay can

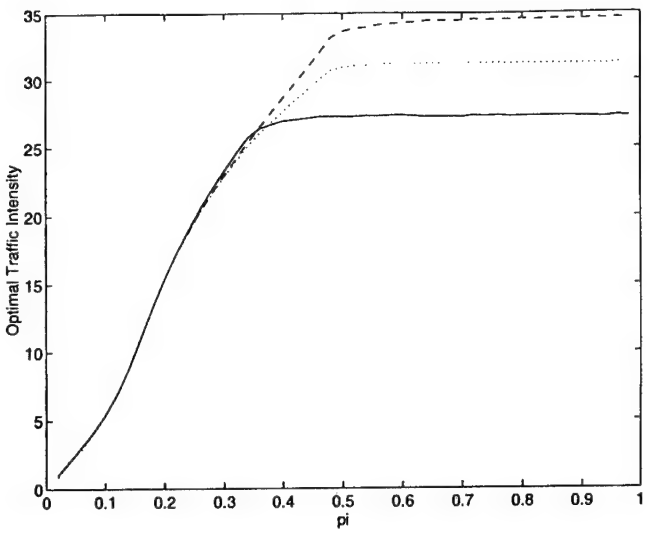


Fig. 7. Optimal traffic intensity.

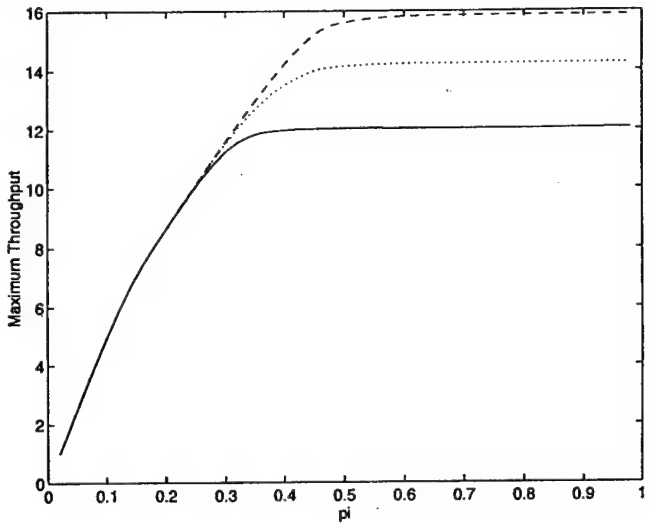


Fig. 8. Maximum system throughput.

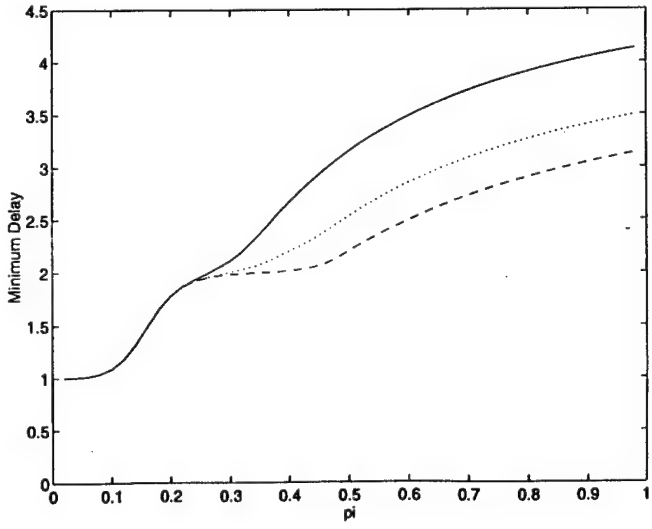


Fig. 9. Minimum system delay.

be divided into two components, namely, the delay due to retransmission because of packet error and the waiting time due to the random retransmission policy. When $p_i$ is below but near the critical value, the optimal $p_b$ is one, and the packet success probability is about 0.5 as discussed above. On the average, we need to transmit a packet twice and the waiting time is zero since $p_b = 1$. So, the minimum delay is about two slots. When $p_i$ passes the critical value, we decrease $p_b$ in order to maintain the packet success probability at 0.5. We still need to transmit a packet twice, but the waiting time increases since $p_b$ decreases. So, the minimum delay increases with $p_i$.

We estimate $p_b^*$ by $\hat{p}_b^* = (p_{b,I}^* + p_{b,S}^*)/2$ and perform Monte Carlo simulations to find the traffic intensity, throughput, and delay for ARQ2 by using $\hat{p}_b^*$. The results are also plotted in Figs. 7–9. From the figures, we see that these results lie between those of the superior and inferior schemes and exhibit similar behaviors. This indicates that $\hat{p}_b^*$ is a good estimate of the real $p_b^*$.

In a practical system, we have to use transmitter buffers in the transmitters. From the discussion above, for the sample system, the transmitter buffers should be designed to give $p_i \approx 0.5$. We should select the optimal $\hat{p}_b^*$ corresponding to this $p_i$. Then, we get a throughput of 14 packets per slot and a delay of 2.5 slots, which are the optimal values for the sample system.

## VI. Conclusion

In this paper, we have applied the type-II hybrid ARQ protocol in a slotted DS-SSMA packet radio system. Using the improved Gaussian approximation technique, we have performed static analysis on such a system to obtain the packet error and packet success probabilities. Moreover, we have employed two-dimensional Markov chains to analyze the dynamic behavior of the system. Based on this model, we have upper and lower bounded the performance of the type-II hybrid ARQ protocol by considering the superior scheme and the inferior scheme, respectively. We have obtained the steady state throughput and delay performances and the optimal retransmission probabilities of the two bounding schemes. Using the sample system as an example, we have shown how to derive the design criteria for the transmitter buffers in order to achieve the system capacity with minimum delay.

Finally, we point out the exact dynamic analysis described in Section IV is generally too complex to perform a stability analysis of the system. In [15], the stability of the system is analyzed based on the equilibrium point analysis (EPA) technique, which provides an approximation to the dynamic of the system. Moreover, extensions of the dynamic analysis to code combining are not trivial because we can no longer model the system dynamic by a time-homogeneous Markov chain. Approximation techniques, such as EPA, are probably needed.

## Appendix

In this appendix, we derive $P_\xi(i,j;k,l \mid n,i_1,j_1)$ in (17) for both the inferior and superior schemes.

Suppose $i$, $j$, $i_1$, $j_1$, and $n$ are all given. From the set of rules described in Section IV-B, the state transitions of a user under the inferior and superior schemes are governed by three packet error events, namely, the received packet contains no error, one to $t_2$ errors, and more than $t_2$ errors. Since there are $n+i_1+j_1$ active users, the probabilities of these three events are $P_e^0(n+i_1+j_1)$, $P_e^1(n+i_1+j_1)$, and $P_e^2(n+i_1+j_1)$, respectively. Let $P_0(n_1,n_2 \mid n,i_1,j_1)$ be the probability that out of those $n$ packets sent by users in *Idle*, $n_1$ of them have one to $t_2$ errors and $n_2$ of them have more than $t_2$ errors. Since the error events from different users are independent given $n+i_1+j_1$,

$$P_0(n_1,n_2 \mid n,i_1,j_1) = \frac{n!}{(n-n_1-n_2)!n_1!n_2!} \cdot \left[P_e^0(n+i_1+j_1)\right]^{(n-n_1-n_2)} \cdot \left[P_e^1(n+i_1+j_1)\right]^{n_1} \cdot \left[P_e^2(n+i_1+j_1)\right]^{n_2} \quad (29)$$

where $0 \le n_1, n_2 \le n$, and $n_1+n_2 \le n$. Let $P_1(k_1 \mid n,i_1,j_1)$ be the probability that out of those $i_1$ packets retransmitted by the users in *Backlog1*, $k_1$ of them have at most $t_2$ errors. Then

$$P_1(k_1 \mid n,i_1,j_1) = B\big(i_1,k_1,P_e^0(n+i_1+j_1) + P_e^1(n+i_1+j_1)\big) \quad (30)$$

where $0 \le k_1 \le i_1$. Let $P_2(l_1 \mid n,i_1,j_1)$ be the probability that out of those $j_1$ packets retransmitted by the users in *Backlog2*, $l_1$ of them have at most $t_2$ errors. Then

$$P_2(l_1 \mid n,i_1,j_1) = B\big(j_1,l_1,P_e^0(n+i_1+j_1) + P_e^1(n+i_1+j_1)\big) \quad (31)$$

where $0 \le l_1 \le j_1$. Note that the three events with probabilities $P_0(\cdot)$, $P_1(\cdot)$, and $P_2(\cdot)$ above are independent.

From the discussion above, $n_1$, $n_2$, $k_1$, and $l_1$ completely characterize a state transition of the system. First, we consider the superior scheme. Given $n_1$, $n_2$, $k_1$, and $l_1$ in a time slot, the system will enter state $(k,l)$ in the next slot, where

$$k = n_1 + (i-i_1) \quad (32)$$

$$l = n_2 + (j-j_1) + (j_1-l_1). \quad (33)$$

Summing over all the events leading into state $(k,l)$, we get, for

$$i-i_1 \le k \le n+(i-i_1),$$
$$j-j_1 \le l \le n+(i-i_1)+j-k,$$

$$P_S(i,j;k,l \mid n,i_1,j_1) = \sum_{n_2} P_0(k-(i-i_1),n_2 \mid n,i_1,j_1) \times P_2(n_2+j-l \mid n,i_1,j_1) \quad (34)$$

where the summation ranges over

$$\max(0,l-j) \le n_2 \le \min(l-(j-j_1),n+(i-i_1)-k).$$

Otherwise, $P_S(i,j;k,l \mid n,i_1,j_1) = 0$.

Similarly, for the inferior system, given $n_1$, $n_2$, $k_1$, and $l_1$, the system will enter state $(k,l)$ in the next slot, where

$$k = n_1 + (i-i_1) + l_1 \quad (35)$$

$$l = n_2 + (j-j_1) + (j_1-l_1) + (i_1-k_1). \quad (36)$$

Hence, we get, for

$$i-i_1 \le k \le n+(i-i_1)+j_1,$$
$$\max(j-j_1,(i-i_1)+j-k) \le l \le n+i+j-k,$$

$$P_I(i,j;k,l \mid n,i_1,j_1) = \sum_{n_1}\sum_{n_2} P_0(n_1,n_2 \mid n,i_1,j_1) P_2(k-(i-i_1) - n_1 \mid n,i_1,j_1) \cdot P_1((n_1+n_2)+(i+j) - (k+1) \mid n,i_1,j_1) \quad (37)$$

where the summations range over

$$\max(0,k-(i-i_1)-j_1) \le n_1 \le \min(n,k-(i-i_1),k+l-(i-i_1)-j),$$
$$\max(0,(k+l)-(i+j)-n_1) \le n_2 \le \min(n,k+l-(i-i_1)-j)-n_1.$$

Otherwise, $P_I(i,j;k,l \mid n,i_1,j_1) = 0$.

## REFERENCES


[1] S. Lin and D. J. Costello Jr., *Error Control Coding: Fundamentals and Applications*. Englewood Cliffs, NJ: Prentice-Hall, 1983.

[2] S. Lin and P. S. Yu, "A hybrid ARQ scheme with parity retransmission for error control of satellite channels," *IEEE Trans. Commun.*, vol. 30, pp. 1701–1719, July 1982.

[3] Y. M. Wang and S. Lin, "A modified selective-repeat type-II hybrid ARQ system and its performance analysis," *IEEE Trans. Commun.*, vol. COM-31, pp. 593–608, May 1983.

[4] D. Chase, "Code combining—A maximum-likelihood decoding approach for combining an arbitrary number of noisy packets," *IEEE Trans. Commun.*, vol. COM-33, pp. 385–393, May 1985.

[5] S. Kallel and D. Haccoun, "Sequential decoding with ARQ and code combining: A robust hybrid FEC/ARQ system," *IEEE Trans. Commun.*, vol. 36, pp. 773–780, July 1988.

[6] S. Kallel, "Analysis of a type II hybrid ARQ scheme with code combining," *IEEE Trans. Commun.*, vol. 38, pp. 1133–1137, Aug. 1990.

[7] R. K. Morrow Jr. and J. S. Lehnert, "Bit-to-bit error dependence in slotted DS/SSMA packet systems with random signature sequences," *IEEE Trans. Commun.*, vol. 37, pp. 1052–1061, Oct. 1989.

[8] ——, "Packet throughput in slotted ALOHA DS/SSMA radio systems with random signature sequences," *IEEE Trans. Commun.*, vol. 40, pp. 1223–1230, July 1992.

[9] D. Raychaudhuri, "Performance analysis of random access packet-switched code division multiple access systems," *IEEE Trans. Commun.*, vol. COM-29, pp. 895–901, June 1981.

[10] J. M. Hanratty and G. L. Stüber, "Performance analysis of hybrid ARQ protocols in a slotted direct-sequence code-division multiple-access network: Jamming analysis," *IEEE J. Select. Area Commun.*, vol. 8, pp. 562–579, May 1990.

[11] S. Souissi and S. B. Wicker, "A diversity combining DS/CDMA system with convolutional encoding and Viterbi decoding," *IEEE Trans. Veh. Technol.*, vol. 44, pp. 304–312, May 1995.

[12] A. M. Y. Bigloo, T. A. Gulliver, and V. K. Bhargava, "Maximum likelihood decoding and code combining for DS/SSMA slotted ALOHA," *IEEE Trans. Commun.*, vol. 45, pp. 1602–1612, Dec. 1997.

[13] D. Bertsekas and R. Gallager, *Data Networks*, 2nd ed. Englewood Cliffs, NJ: Prentice-Hall, 1992.

[14] P. W. de Graaf and J. S. Lehnert, "Performance comparison of a slotted ALOHA DS/SSMA network and a multi-channel narrowband slotted ALOHA network," in *IEEE MILCOM*, vol. 2, 1994, pp. 574–578.

[15] Q. Zhang, T. F. Wong, and J. S. Lehnert, "Stability of a type-II hybrid ARQ protocol for slotted DS-SSMA packet radio systems," in *Proc. IEEE INFOCOM'98*, San Francisco, CA, Apr. 1998, vol. 3, pp. 1301–1308.

**Qian Zhang** was born on July 16, 1964, in Beijing, China. He received the B.S. degree from Tsinghua University, China, in 1986 and the M.S. degree from Peking University, China, in 1989. He received the M.S.E.E. degree from the University of Central Florida, Orlando, FL, in 1991, and the Ph.D. degree in electrical and computer engineering from Purdue University, West Lafayette, IN, in 1998.

From 1992 to 1994, he was a Research Engineer and a Project Engineer working at PTR Technology, Inc., Palm Bay, FL, and at Ampro Corporation, Melbourne, FL, respectively. His work included hardware design and software programming for a radio transmitter geolocation system and for a big screen projection television system. From 1994 to May 1998, he was a Ph.D. student and a Research Assistant in the School of Electrical and Computer Engineering at Purdue University. In May 1998, he joined Globespan Semiconductor, Inc., Red Bank, NJ, to develop xDSL modem chipsets for high-speed digital communications over telephone lines. His current research interests and work responsibilities include CDMA systems, adaptive coding, diversity techniques, wireless cellular networks, discrete multi-tone modulation, equalization, xDSL modems, and the development of cable modems.

**Tan F. Wong** received the B.Sc. degree (1st class honors) in electronic engineering from the Chinese University of Hong Kong in 1991 and the M.S.E.E. and Ph.D. degrees in electrical and computer engineering from Purdue University, West Lafayette, IN, in 1992 and 1997, respectively.

From July 1993 to June 1995, he was a Research Engineer working on the high-speed wireless networks project in the Department of Electronics at Macquarie University, Sydney, Australia. From Aug. 1995 to Oct. 1997, he was a Research and Teaching Assistant in the School of Electrical and Computer Engineering at Purdue University. From November 1997 to July 1998, he worked as a Post-Doctoral Research Associate at Purdue University. Currently, he is an Assistant Professor of electrical and computer engineering at the University of Florida, Gainesville. His research interests include spread-spectrum communication systems, multiuser communications, and wireless cellular networks.

**James S. Lehnert** (S'83–M'84–SM'95) received the B.S. (highest Honors), M.S., and Ph.D. degrees in electrical engineering from the University of Illinois at Urbana-Champaign in 1978, 1981, and 1984, respectively.

From 1978 to 1984, he was a Research Assistant at the Coordinated Science Laboratory, University of Illinois, Urbana, Illinois. He has held summer positions at Motorola Communications, Schaumburg, IL, in the Data Systems Research Laboratory, and Harris Corporation, Melbourne, FL, in the Advanced Technology Department. He is currently an Associate Professor of Electrical and Computer Engineering at Purdue University, West Lafayette, IN. He has served as Editor for Spread Spectrum for the IEEE TRANSACTIONS ON COMMUNICATIONS. His current research work is in communication and information theory with emphasis on spread-spectrum communications.

Dr. Lehnert was a University of Illinois Fellow from 1978 to 1979 and an IBM Pre-Doctoral Fellow from 1982 to 1984.

*International Journal of Wireless Information Networks, Vol. 5, No. 3, 1998*

# Buffered Type-II Hybrid ARQ Protocol for DS-SSMA Packet Radio Systems

**Qian Zhang,[1] Tan F. Wong,[1] and James S. Lehnert[1,2]**

The performance and stability of a slotted direct-sequence spread-spectrum multiple-access (DS-SSMA) packet radio network employing the type-II hybrid automatic-repeat-request (ARQ) protocol with finite-length transmitter buffers are considered. The equilibrium point analysis (EPA) technique is employed to analyze the system stability and to approximately compute the system throughput, delay, and packet rejection probability. It is found that the system exhibits bistable behavior in some situations. Issues of system design, such as the required length of the transmitter buffers and the desirable region of operation based on a predetermined performance requirement for packet rejection, are also investigated.

**KEY WORDS:** Automatic repeat request; code division multiple access; equilibrium point analysis; packet radio network; spread-spectrum communication.

## 1. INTRODUCTION

It is shown in [1, 2] that the type-II hybrid automatic-repeat-request (ARQ) protocol effectively increases the system capacity of a direct-sequence spread-spectrum multiple-access (DS-SSMA) packet radio network. The complexity of the type-II hybrid ARQ protocol is quite reasonable. Apart from capacity and complexity, another important issue affecting the performance of the protocol is system stability, which is not considered in [1, 2]. Moreover, it is assumed in [1, 2] that a user is prevented from generating any new packets until the transmission of the current packet succeeds. In practice, data sources are usually continuous. Hence, transmitter buffers are needed to hold the incoming packets from the data sources. The assumption of [1, 2] is equivalent to assuming the transmitter buffer of a user can hold only one packet. It is obvious that this restriction is not practical since using a buffer of length 1 will reject too many packets attempting to enter the transmitter buffer. The goal of this paper is to investigate the performance and stability of a DS-SSMA packet radio network employing the type-II hybrid ARQ protocol with finite-length transmitter buffers.

Although we know [1, 2] that the system dynamics can be modeled exactly by a multidimensional Markov chain, this model is too complex to allow us to study the system performance and stability. In this paper, we employ the equilibrium point analysis (EPA) technique [3–5] to approximately compute the system performance and analyze the system stability. Approximate system throughput, delay, and packet rejection probability are obtained via EPA. The accuracy of the EPA approximations is checked by comparing the results given by EPA against the results obtained from Monte Carlo simulations.

A key result obtained in EPA of the system is that the system stability can be described in terms of the number of stable (defined in Section 3.5) equilibrium points. Like some ALOHA systems [6, 7], we observe that the system exhibits bistable behavior, i.e., there are two stable equilibrium points in some situations. When the system is bistable, it oscillates between the two stable equilibrium points, one of which corresponds to a sys-

[1]School of Electrical and Computer Engineering, Purdue University.
[2]Correspondence should be directed to James S. Lehnert, School of Electrical and Computer Engineering, Purdue University, West Lafayette, IN 47907-1285; e-mail: lehnert@purdue.edu.
[3]Department of Electrical and Computer Engineering, University of Florida.



1068-9605/98/0700-0203$15.00/0 

tem state of high throughput (low packet rejection probability) and the other of which corresponds to a system state of low throughput (high packet rejection probability). In this case, the overall system performance is a weighted average of the performances at the "good" and "bad" equilibrium points. In designing a DS-SSMA network, the oscillation between equilibrium points should be avoided. Using the results given by the EPA technique, we are able to set up a procedure to determine the required length of the transmitter buffers so that the packet rejection probability is smaller than a predetermined threshold. After choosing the transmitter buffer length, we can also determine a desirable region of operation for the DS-SSMA network.

In Section 2, we describe the DS-SSMA network employing the type-II hybrid ARQ protocol. In Section 3, we perform EPA on the system by solving the equilibrium system equations and obtain the system throughput, delay, and packet rejection probability. We also provide simulation results to check the EPA approximations. The system stability is investigated by considering the nature of the equilibrium points obtained by EPA. In Section 4, we develop a procedure to choose the required length of the transmitter buffers and establish a desirable region of operation for the DS-SSMA network. Finally, we conclude this paper in Section 5.

## 2. SYSTEM DESCRIPTION

In this section, we describe the DS-SSMA radio network and the type-II hybrid ARQ protocol. We model the system as a finite-user *slotted* packet radio network with a packet size of $L$ bits. We assume that direct-sequence spread-spectrum signaling is employed as the digital modulation scheme in the physical layer. Without loss of generality, we assume that the transmitters and receivers in the DS-SSMA system work in pairs. There are $U$ transmitter-receiver pairs (active or not), which are referred to as *users*, in the system. Each of them uses an independent aperiodic random signature sequence, with spreading factor $N$ ($N$ chips per bit), to modulate data bits in the BPSK format. For simplicity, we ignore the presence of thermal noise and assume that possible bit errors are only caused by interference from other active users in the system. Moreover, we assume that the received power of each interfering signal is the same as that of the desired user signal.

We assume that there is an error-free feedback channel from the receiver back to the transmitter to convey all necessary control information, transmission errors are detected by the receiver, and the transmitter is immediately acknowledged after each packet transmission. Therefore, the application of the following type-II hybrid ARQ protocol [8] in the slotted DS-SSMA packet radio network is possible.

Two block codes, $C_0$ and $C_1$, are used. The code $C_0$ is a $(L, K)$ high-rate error-detecting code, and the code $C_1$, designed for error correction only, is a $(2L, L)$ half-rate invertible systematic code with error-correcting capability $t_1$. Any transmission error in a packet will be detected by calculating the syndrome of code $C_0$. We assume that each data source delivers a new $K$-bit data block to the corresponding transmitter with probability $p_i$ at the beginning of each slot. There is a packet buffer of length $M$ in the transmitter. If the buffer is not full, the data block will be added to the buffer. Otherwise, the data block will be dropped. Meanwhile, $(L - K)$ parity bits based on $C_0$ are appended to the $K$-bit data block at the head of the buffer forming an $L$-bit data packet. We denote by $I = (D, Q)$ this $L$-bit data packet, which is a codeword in $C_0$, where $D$ is the $K$-bit data block and $Q$ is the corresponding $(L - K)$-bit parity block. An $L$-bit parity check packet, $P(I)$, of $I$ based on code $C_1$ in such a way that $(I, P(I))$ is a codeword of $C_1$ is constructed. The coding structure [8] is shown in Fig. 1.

The data packet $I$ is first sent. If the transmission is error-free, it is completed. Otherwise, the received data packet is saved in a receiver buffer, and the transmitter is informed to restart the transmission. Upon a transmission failure, the transmitter will send the parity packet $P(I)$. If the transmission is successful, $P(I)$ is inverted to obtain $I$. Otherwise, $P(I)$, combined with the previously stored $I$, is decoded based on $C_1$. If the decoding is suc-

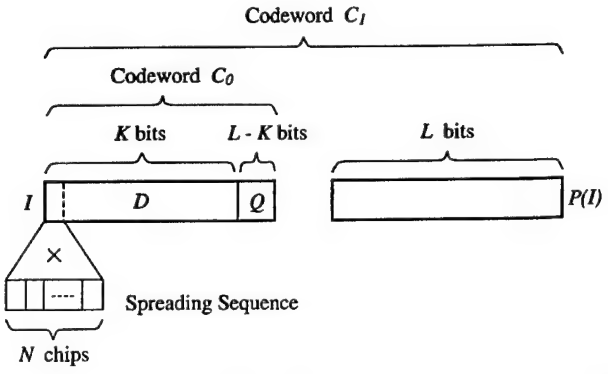


**Fig. 1.** Coding structure of the DS-SSMA system with the type-II hybrid ARQ protocol.

cessful (i.e., the total number of errors in $I$ and $P(I)$ is at most $t_1$), the transmission is completed. Otherwise, $I$ is replaced by $P(I)$ in the receiver buffer, and the transmitter is informed to retransmit once again. The data packet $I$ and the parity check packet $P(I)$ are sent alternately in the way described above until the transmission is successful. After a successful transmission has been acknowledged at the end of a time slot, the data block at the head of the transmitter buffer is removed.

It is shown in [2] that the performance of the DS-SSMA network is mainly determined by its traffic intensity since the DS-SSMA signaling technique is interference limited. We need to maintain a certain level of traffic intensity in the network in order to achieve its maximum capacity. We employ, as the simplest way to control the network traffic, the following scheme to direct the (re)transmissions of data and parity packets in the type-II hybrid ARQ protocol described above. We perform a simple form of channel load sensing by using the length of the transmitter buffer as an indicator. If a newly arrived data block enters an empty buffer, it will be sent instantly (neglecting the processing time required to calculate the parity bits). Other than that, all (re)transmissions take place in a slot with probability $p_b$. Intuitively, this transmission scheme can be understood as follows. When the transmitter buffers are empty, the network traffic is probably low, i.e., there is a high chance that the transmission will be successful. Hence, the newly arrived packet should be sent immediately to reduce the delay. On the other hand, a failed transmission and a filled transmitter buffer both indicate that the network may be congested. Hence, it is reasonable to set the (re)transmission probability to $p_b$ to limit the traffic intensity.

## 3. EQUILIBRIUM POINT ANALYSIS

First, we assume that the system changes states at each slot boundary and observation is made at the beginning of each slot, just before any data block arrives. We say that a user is in state $S_i$, for $i = 1, \ldots, M$, when the transmission succeeds in the previous slot and there are $i$ data blocks in the transmitter buffer. A user is in state $E_{i,j}$, for $i = 1, \ldots, M$ and $j = 1, \ldots, t_1 - 1$, when the transmission fails in the previous slot, the stored packet in the receiver buffer has $j$ errors, and the transmitter buffer contains $i$ data blocks. Similarly, a user is in state $E_{i,t_1}$ when the transmission fails in the previous slot, the stored packet in the receiver buffer has at least $t_1$ errors, and the transmitter buffer contains $i$ data blocks. Moreover, a user is in state *Idle* when its transmitter buffer is empty. Fig. 2 shows all the possible states for a user in the system.

We let $R_{i,j}$ be the number of users in $E_{i,j}$, for $1 \le i \le M$ and $1 \le j \le t_1$, $R_i$ be the number of users in $S_i$, for $1 \le i \le M$, and $R_I$ be the number of users in *Idle*. We note that the following constraint is satisfied:

$$R_I + \sum_{i=1}^{M} \left( R_i + \sum_{j=1}^{t_1} R_{i,j} \right) = U \tag{1}$$

where $0 \le R_i, R_{i,j} \le U$, for $1 \le i \le M$ and $1 \le j \le t_1$, and $0 \le R_I \le U$. Then the vector $\mathbf{X}(t) = [R_I, R_1, R_{1,1}, \ldots, R_{1,t_1}, \ldots, R_M, R_{M,1}, \ldots, R_{M,t_1-1}]$, for $t \ge 1$, forms a time-homogeneous Markov chain that models the dynamics of the system. Unfortunately, this $M(t_1+1)$-dimensional Markov chain is too complex to allow exact analysis. As an alternative, we employ the EPA technique [3–5] to approximately compute the system performance and analyze the system stability.

In EPA, it is assumed that the system is at equilibrium, i.e., the expected number of users leaving a given state is exactly equal to the expected number of users entering the same state. We assume that the system operates about the equilibrium point instead of in a manner that is randomly distributed according to the stationary distribution of the Markov chain. Then we approximate the steady-state (average) system performance by the performance at the equilibrium point. We note that it is possible for a system to have multiple equilibrium points. In this case, the system stays around one equilibrium point for a random amount of time, then moves and stays in the vicinity of another equilibrium point, and so on. It is this kind of oscillating behavior that allows us to describe the stability of the system.

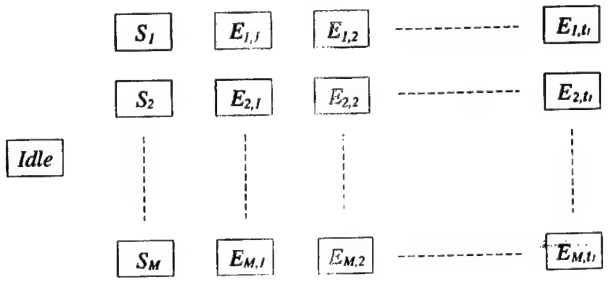


**Fig. 2.** States of a user in the DS-SSMA system.

### 3.1. Equilibrium-State Transitions of a User

We let $r_I$, $r_1$, $r_{1,1}, \ldots, r_{M,t_1}$ be the values of $R_I$, $R_1, R_{1,1}, \ldots, R_{M,t_1}$ at an equilibrium point, respectively. We note that all of the values can be nonnegative real numbers, but

$$r_I + \sum_{i=1}^{M} \left( r_i + \sum_{j=1}^{t_1} r_{i,j} \right) = U \tag{2}$$

We approximate the system dynamics about the equilibrium point by assuming that each user resides in *Idle* independently with probability $r_I/U$. Then the total number of users in *Idle* is binomial distributed with mean $r_I$. Next, we focus on one of the users in the system. The behavior of this user can be modeled by the Markov chain with states *Idle*, $S_1$, $E_{1,1}, \ldots, E_{M,t_1}$. To obtain the state transition probabilities of the Markov chain, we need to know, for $k = 0, \ldots, U-1$, the probability, $P_k$, that there are $k$ interferers transmitting in the same slot. Given that a user is transmitting and there are $n$ other users in *Idle*, each of these $n$ users transmits a packet in the same slot with the same probability $p_i$. At the same time, there are $U-1-n$ users (in other states) who transmit packets with probability $p_b$. By the law of total probability, we see that, for $k = 0, \ldots, U-1$.

$$P_k = \sum_{n=0}^{U-1} \sum_{l=\max(0,k+n-U+1)}^{\min(n,k)} \cdot B(n,l,p_i)B(U-1-n,k-l,p_b)B(U-1,n,r_I/U) \tag{3}$$

where $B(\cdot,\cdot,\cdot)$ denotes the binomial distribution, i.e., for $0 \le j \le J$ and $0 \le p \le 1$,

$$B(J,j,p) = \binom{J}{j} p^j (1-p)^{J-j} \tag{4}$$

Next, we let $P(j)$, for $j = 0, \ldots, t_1 - 1$, be the probability that there are $j$ errors in the received packet given that the user does transmit a packet in the current slot. Moreover, we use $P(t_1)$ to denote the probability that there are at least $t_1$ errors in the received packet under the same condition. It is easy to see that, for $j = 0, \ldots, t_1$,

$$P(j) = \sum_{k=0}^{U-1} P_e(j|k+1)P_k \tag{5}$$

where $P_e(j|k)$ is the conditional probability of the event that there are $j$ errors (when $j = t_1$, it means at least $t_1$ errors) in the received packet given that there are $k$ simultaneously active users in the system. We note that $P_e(j|k)$ can be obtained by the improved Gaussian approximation technique [9, 10], which accounts for the bit-to-bit error dependence within a packet. The detailed derivation of $P_e(j|k)$ can be found in [9].

In this section, we consider the case where the buffer length $M \ge 2$. The case for $M = 1$ will be considered separately in Section 3.3. We divide the $M(t_1 + 1) + 1$ states into seven groups,[1] namely, $\{Idle\}$, $\{S_1\}$, $\{E_{1,1} \ldots, E_{1,t_1}\}$, $\{S_M\}$, $\{E_{M,1} \ldots, E_{M,t_1}\}$, $\{S_i\}$, and $\{E_{i,1}, \ldots, E_{i,t_1}\}$, for $2 \le i \le M-1$. States in different groups behave differently, and states in the same group behave similarly. With this classification, it is easy to obtain the state transition probabilities. Fig. 3 shows the state transition diagrams of a user with state transitions involving a sample state in each of the seven

[1]When $M = 2$, we have only five groups: $\{Idle\}$, $\{S_1\}$, $\{E_{1,1} \ldots, E_{1,t_1}\}$, $\{S_2\}$, and $\{E_{2,1} \ldots, E_{2,t_1}\}$.

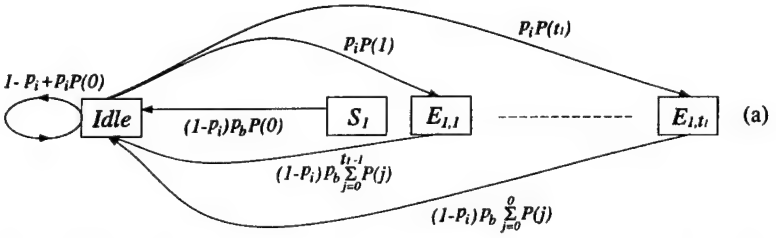


**Fig. 3.** State transition diagrams of a user when $M \ge 2$: (a) *Idle;* (b) $S_1$ and $E_{1,j}$, for $1 \le j \le t_1$; (c) $S_M$ and $E_{M,j}$ for $1 \le j \le t_1$; (d) $S_i$, for $2 \le i \le M-1 (M \ge 3)$; (e) $E_{i,j}$, for $2 \le i \le M-1$ and $1 \le j \le t_1 (M \ge 3)$.

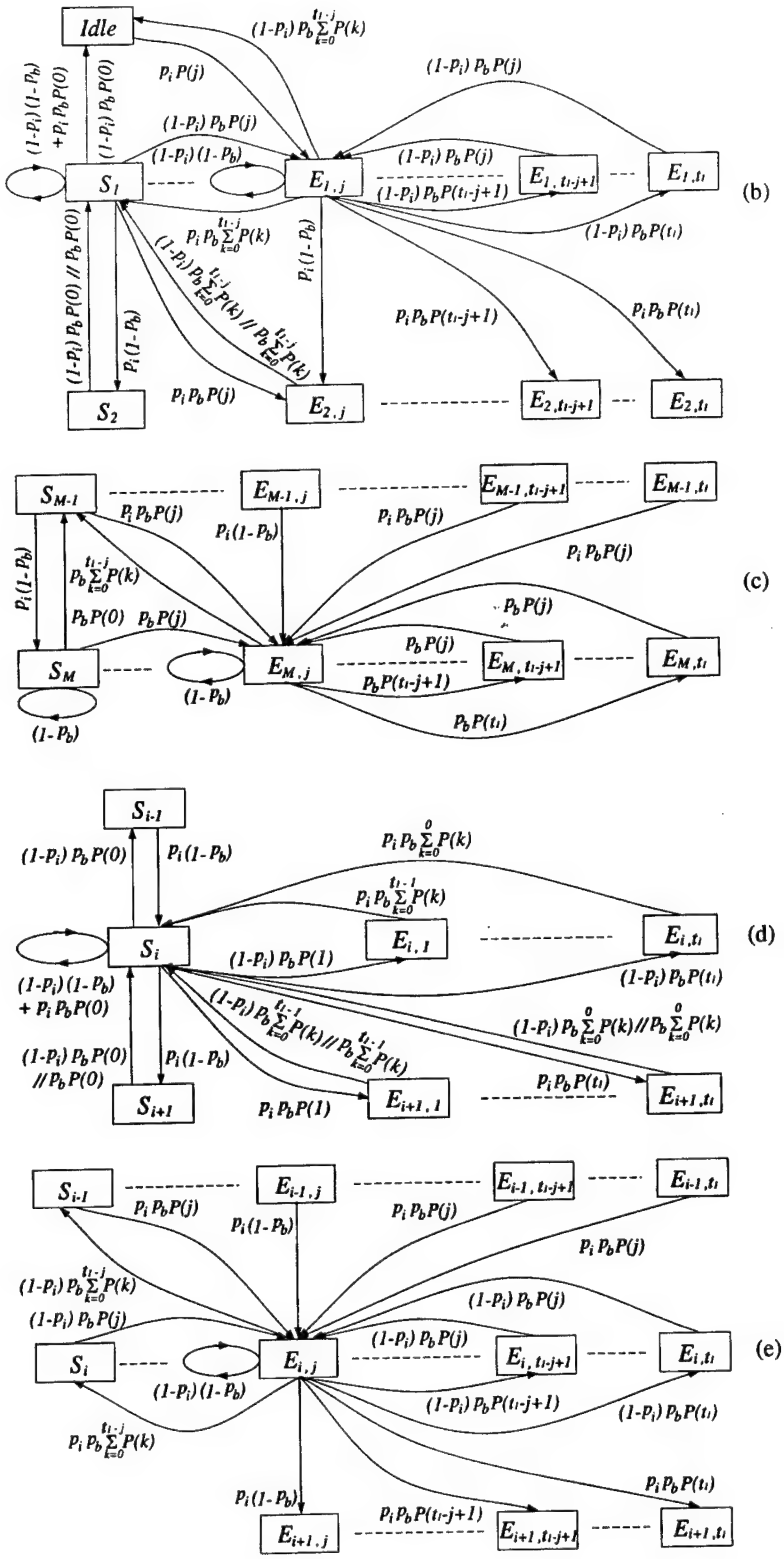


**Fig. 3.** (*Continued*)

groups. In Fig. 3, most of the transitions are self-explanatory. However, special attention should be given to those transitions involving $E_{i,j}$ in Figs. 3b, 3c, and 3e. For clarity, only the cases for $t_1 - j + 1 > j$ are shown in these three figures. For $t_1 - j + 1 \le j$, the transition probability of each of the vertical transitions and self-loops involving $E_{i,j}$ is the sum of two terms shown in the figures: one from the state indexed by the subscript $j$ and the other from the state indexed by the subscript $t_1 - j' + 1$, where $t_1 - j' + 1 = j$. Moreover, we use the notation $x||y$ in Fig. 3b to represent the different transition probabilities $x$ and $y$ for the cases where $M \ge 3$ and $M = 2$, respectively. The same notation is also used in Fig. 3d to represent the different transition probabilities for the cases where $i \ne M - 1$ and $i = M - 1$, respectively.

### 3.2. Equilibrium Equations

Again, we consider the case where $M \ge 2$ in this section. At equilibrium, the expected inflow to each of the system states, *Idle*, $S_1$, $E_{1,1}, \ldots, E_{M,t_1}$, is identical to the expected outflow from it. Using vector notation, we let

$$\mathbf{r} = [r_I, r_1, \mathbf{r}_1, \ldots, r_i, \mathbf{r}_i, \ldots, r_M, \mathbf{r}_M] \tag{6}$$

where, for $1 \le i \le M$,

$$\mathbf{r}_i = [r_{i,1}, \ldots, r_{i,t_1}] \tag{7}$$

Furthermore, we define three row vectors with $t_1$ elements:

$$\mathbf{P} = \left[ \sum_{j=0}^{t_1-1} P(j), \sum_{j=0}^{t_1-2} P(j), \ldots, P(0) \right] \tag{8}$$

$$\mathbf{P}(j) = [0, \ldots, 0, \underbrace{P(j), \ldots, P(j)}_{j \text{ terms}}] \tag{9}$$

$$\mathbf{h}(j) = [0, \ldots, 0, \underbrace{1}_{j\text{-th term}}, 0, \ldots, 0] \tag{10}$$

From Fig. 3a, it is easy to see that the expected inflow to and the expected outflow from *Idle* are, respectively, given by $\mathbf{ra}_I$ and $r_I$, where

$$\mathbf{a}_I = [1 - p_i(1 - P(0)), (1 - p_i)p_b P(0), (1 - p_i)p_b \mathbf{P}, 0, \ldots, 0]^T \tag{11}$$

From Fig. 3b, the expected inflow to and the expected outflow from $S_1$ are, respectively, given by $\mathbf{ra}_1$ and $r_1$, where

$$\mathbf{a}_1 = [0, (1 - p_i)(1 - p_b) + p_i p_b P(0), p_i p_b \mathbf{P}, \{(1 - p_i)p_b || p_b\}P(0), \{(1 - p_i)p_b || p_b\}\mathbf{P}, 0, \ldots, 0]^T \tag{12}$$

From Fig. 3b, the expected inflow to and the expected outflow from $E_{1,j}$, for $1 \le j \le t_1$, are, respectively, given by $\mathbf{ra}_{1,j}$ and $r_{1,j}$, where

$$\mathbf{a}_{1,j} = [p_i P(j), (1 - p_i)p_b P(j), (1 - p_i)p_b \mathbf{P}(j) + (1 - p_i)(1 - p_b)\mathbf{h}(j), 0, \ldots, 0]^T \tag{13}$$

From Fig. 3c, the expected inflow to and the expected outflow from $S_M$ are, respectively, given by $\mathbf{ra}_M$ and $r_M$, where

$$\mathbf{a}_M = [\underbrace{0, \ldots, 0,}_{(M-2)(t_1+1)+1 \text{ terms}} p_i(1 - p_b), \underbrace{0, \ldots, 0,}_{t_1 \text{ terms}} 1 - p_b, \underbrace{0, \ldots, 0}_{t_1 \text{ terms}}]^T \tag{14}$$

From Fig. 3c, the expected inflow to and the expected outflow from $E_{M,j}$, for $1 \le j \le t_1$, are, respectively, given by $\mathbf{ra}_{M,j}$ and $r_{M,j}$, where

$$\mathbf{a}_{M,j} = [\underbrace{0, \ldots, 0,}_{(M-2)(t_1+1)+1 \text{ terms}} p_i p_b P(j), p_i p_b \mathbf{P}(j) + p_i(1 - p_b)\mathbf{h}(j), p_b P(j), p_b \mathbf{P}(j) + (1 - p_b)\mathbf{h}(j)]^T \tag{15}$$

From Fig. 3d, when $M \ge 3$, the expected inflow to and the expected outflow from $S_i$, for $2 \le i \le M - 1$, are, respectively, given by $\mathbf{ra}_i$ and $r_i$, where

$$\mathbf{a}_i = [\underbrace{0, \ldots, 0,}_{(i-2)(t_1+1)+1 \text{ terms}} p_i(1 - p_b), \underbrace{0, \ldots, 0,}_{t_1 \text{ terms}} (1 - p_i)(1 - p_b) + p_i p_b P(0), p_i p_b \mathbf{P}, \{(1 - p_i)p_b || p_b\}P(0) \{(1 - p_i)p_b || p_b\}\mathbf{P}, 0, \ldots, 0]^T \tag{16}$$

From Fig. 3e, when $M \ge 3$, the expected inflow to and the expected outflow from $E_{i,j}$, for $2 \le i \le M - 1$ and

$1 \le j \le t_1$, are, respectively, given by $\mathbf{ra}_{i,j}$ and $r_{i,j}$, where

$$\mathbf{a}_{i,j} = [\underbrace{0, \ldots, 0,}_{(i-2)(t_1+1)+1 \text{ terms}} p_i p_b P(j), p_i p_b \mathbf{P}(j) + p_i(1-p_b)\mathbf{h}(j), (1-p_i)p_b P(j), (1-p_i)p_b \mathbf{P}(j) + (1-p_i)(1-p_b)\mathbf{h}(j), 0, \ldots, 0]^T \quad (17)$$

By rewriting Eq. (6) and equating inflows to outflows, we have the following set of equilibrium equations in matrix form:

$$\mathbf{r}[\mathbf{A}, \mathbf{q}] = [\mathbf{r}, U] \quad (18)$$

where $\mathbf{A} = [\mathbf{a}_I, \mathbf{a}_1, \mathbf{a}_{1,j}, \ldots, \mathbf{a}_i, \mathbf{a}_{i,j}, \ldots, \mathbf{a}_M, \mathbf{a}_{M,j}]$ and $\mathbf{q}$ is an all-ones column vector with $M(t_1+1)+1$ elements.[2] If all the elements of a solution vector, $\mathbf{r}$, of the equilibrium equations in (18) lie in $[0, U]$, then $\mathbf{r}$ defines an *equilibrium point* about which the system is assumed to operate.

First, the existence of at least one equilibrium point is guaranteed by the following proposition, whose proof can be found in the Appendix:

**Proposition 1:** The set of equilibrium equations in (18) has an odd number of solutions, and all elements of every solution lie in $(0, U)$.

Next, we proceed to find all the equilibrium points. We note that the first $M(t_1 + 1) + 1$ equations in (18) are linearly dependent. Hence, we can remove, say, the $(M(t_1 + 1) + 1)$-th equation without affecting the solutions of the original set of equations. Since all elements of $\mathbf{A}$ are functions of $r_I$, it is simpler to solve (18) by first expressing $\tilde{\mathbf{r}} = [r_1, \mathbf{r}_1, \ldots, r_M, \mathbf{r}_M]$ in terms of $r_I$. This can be done by further deleting the first equation in (18) and solving the resulting system of linear equations in terms of $r_I$. Then we obtain the solutions of (18) by substituting $r_1, \mathbf{r}_1, \ldots, r_M, \mathbf{r}_M$ into the first equation to solve for $r_I$.

More precisely, consider the following set of linear equations obtained by removing the first and the $(M(t_1 + 1) + 1)$-th equations in (18):

$$[r_I, \tilde{\mathbf{r}}][\mathbf{B}, \mathbf{q}] = \mathbf{b} \quad (19)$$

where $\mathbf{b} = [\underbrace{0, \ldots, 0,}_{M(t_1+1)-1 \text{ terms}} U]$ and $\mathbf{B}$ is obtained by deleting the first and the last columns of the matrix $\mathbf{A} - \mathbf{I}$. Now, we partition the $M(t_1 + 1) + 1$-by-$M(t_1 + 1)$ matrix $[\mathbf{B}, \mathbf{q}]$ into the form:

$$[\mathbf{B}, \mathbf{q}] = \begin{bmatrix} \mathbf{c} \\ \mathbf{C} \end{bmatrix} \quad (20)$$

where $\mathbf{c}$ is a row vector of $M(t_1 + 1)$ elements and $\mathbf{C}$ is a square matrix of size $M(t_1 + 1)$. Then the solution of Eq. (19) is

$$\tilde{\mathbf{r}} = (\mathbf{b} - r_I \mathbf{c})\mathbf{C}^{-1} \quad (21)$$

We note that we have assumed the fact that $\mathbf{C}$ is invertible in Eq. (21). This is guaranteed by the following proposition, whose proof is given in the Appendix:

**Proposition 2:** The square matrix $\mathbf{C}$ is invertible for each $r_I$ in $[0, U]$.

Next, we define

$$F_I = r_I - \mathbf{ra}_I \quad (22)$$

Physically, $F_I$ represents the expected *net* outflow from *Idle* at equilibrium. We note from Eqs. (21) and (22) that $F_I$ is a function of $r_I$ only. To indicate this dependence, we use the notation $F_I(r_I)$. Finally, we make use of the first equation in (18), which is equivalent to

$$F_I(r_I) = 0 \quad (23)$$

So, if Eq. (23) has a solution in $[0, U]$, then the whole set of equilibrium equations has a legitimate solution when all the $r_1, \mathbf{r}_1, \ldots, r_M, \mathbf{r}_M$ obtained by Eq. (21) lie in the same interval. By Proposition 1, this is guaranteed.

As a summary, we can find the equilibrium point(s) of the system by the following algorithm:

1. Construct $\mathbf{A}$ as a function of $r_I$ in $[0, U]$ using Eqs. (11)–(17).
2. Find the zero(s) of $F_I(r_I)$ in $[0, U]$ using Eqs. (21) and (22).
3. Obtain $r_1, \mathbf{r}_1, \ldots, r_M, \mathbf{r}_M$ by Eq. (21) for each zero.

[2] In the rest of this paper, we will use the same notation $\mathbf{q}$ to denote the all-ones column vectors of different sizes.

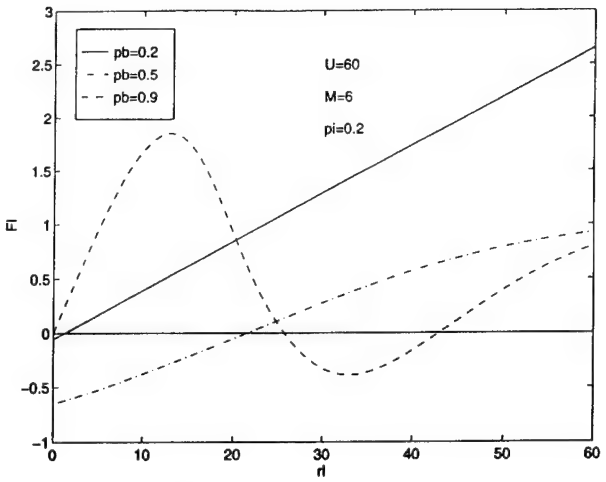


**Fig. 4.** $F_I$ as a function of $r_I$.

4. Each solution $\{r_I, r_1, \mathbf{r}_1, \ldots, r_M, \mathbf{r}_M\}$ gives an equilibrium point.

For example,[3] we consider the sample coding structure [2] when $N = 31$, $L = 500$, and $t_1 = 54$. In Fig. 4, we plot $F_I$ as a function of $r_I$ for different values of $p_b$ by fixing $U = 60$, $M = 6$, and $p_i = 0.2$. We observe that $F_I$ has a single zero for $p_b = 0.2$ and 0.5. When $p_b$ increases to 0.9, $F_I$ has three zeros. We note that each of these zeros corresponds to an equilibrium point of the system. Hence, we conclude that for some values of $p_i$ and $p_b$, the system can have multiple equilibrium points.

[3]For this and all the following numerical examples, we employ the same sample coding structure.

### 3.3. $M = 1$ Case

When $M = 1$, since the buffer can hold only one packet, any newly arrived packet will only see either an empty buffer or a full buffer filled by the packet that fails in the previous transmission. Hence, a user will never enter the state $S_1$, and it makes no difference if we remove $S_1$ from the Markov chain model of a user. Figs. 5a and 5b show the resulting state transition diagrams of a user with state transitions involving *Idle* and $\{E_{1,1}, \ldots, E_{1,t_1}\}$, respectively. By removing $S_1$, the resulting Markov chain becomes irreducible. Thus, Propositions 1 and 2 still hold with appropriate modifications, and the procedure for finding the equilibrium points of the system is the same as before.

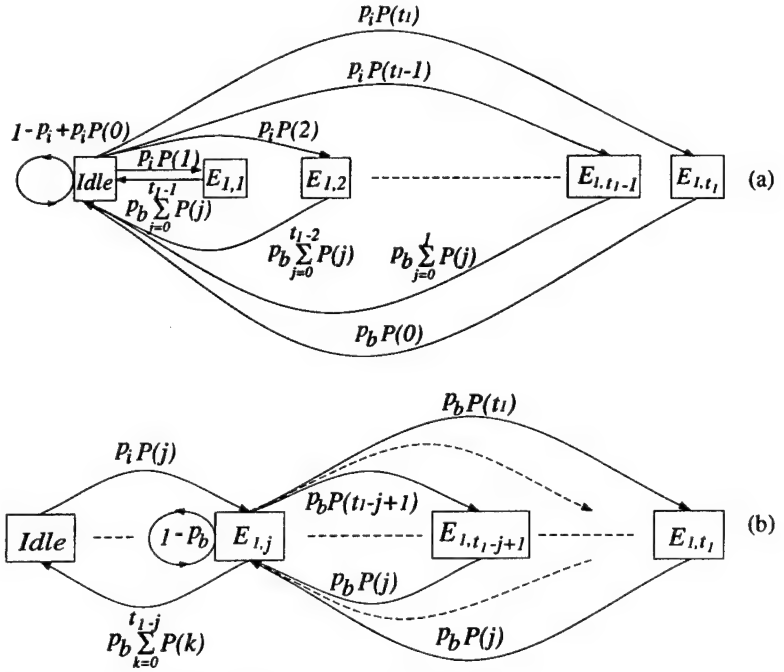


**Fig. 5.** State transition diagrams of a user when $M = 1$: (a) *Idle;* (b) $E_{1,j}$, for $1 \le j \le t_1$.

### 3.4. Equilibrium Throughput, Delay, and Packet Rejection Probability

After an equilibrium point of the system has been obtained by the method described in the previous section, we can calculate the system throughput, delay, and packet rejection probability at this equilibrium point. The system throughput, $S$, is defined as the average number of successfully transmitted packets per slot. Since a user will go to *Idle* or $S_i$ in the next slot when a (re)transmission of the user occurs and succeeds, it is easy to see from Fig. 3 that

$$S = p_i P(0) r_I + \sum_{i=1}^{M} \left\{ p_b P(0) r_i + \sum_{j=1}^{t_1} \left[ p_b \sum_{k=0}^{t_1 - j} P(k) \right] r_{i,j} \right\} \tag{24}$$

We use $\Lambda$ to denote the average number of packets accepted by the system (the transmitter buffers) per slot. Since a user in any states except $S_M$, $E_{M,1}, \ldots, E_{M,t_1}$ can accept an arriving packet to its transmitter buffer, we have

$$\Lambda = p_i \left[ r_I + \sum_{i=1}^{M-1} \left( r_i + \sum_{j=1}^{t_1} r_{i,j} \right) \right] \tag{25}$$

By adding together the equilibrium equations in (18) of the states with the same number of packets in the transmitter buffer and substituting the resulting $M$ equations recursively, we can show that

$$S = \Lambda \tag{26}$$

Physically, Eq. (26) means that the average number of packets accepted to the system is equal to the system throughput. This relationship is intuitive since the system does not act as a sink to packets.

At equilibrium, the average number of packets waiting in the system, $W$, is

$$W = \sum_{i=1}^{M} \left[ i \left( r_i + \sum_{j=1}^{t_1} r_{i,j} \right) \right] \tag{27}$$

The system delay, $D$, is defined as the average number of time slots required to successfully transmit a data packet after it is admitted to the transmitter buffer. Because of Eq. (26), we can apply Little's theorem [11] to obtain the system delay:

$$D = 1 + \frac{W}{\Lambda} = 1 + \frac{W}{S} \tag{28}$$

The packet rejection probability, $P_{rej}$, is defined as the probability of the event that a packet generated by a data source is rejected from entering the transmitter buffer of the corresponding user. As mentioned above, an arriving packet is rejected from entering the transmitter buffer of a user only when the user is in one of the states $S_M$, $E_{M,1}, \ldots, E_{M,t_1}$. Hence,

$$P_{rej} = \frac{1}{U} \left( r_M + \sum_{j=1}^{t_1} r_{M,j} \right) \tag{29}$$

Combining Eqs. (2), (25), (26), and (29), we obtain the following equation relating $S$ and $P_{rej}$:

$$\frac{S}{U} + p_i P_{rej} = p_i \tag{30}$$

To verify the EPA technique, we perform Monte Carlo simulations to obtain estimates of the system throughput, delay, and packet rejection probability and use these estimates to check the validity of the EPA results. Figs. 6a–c show the system throughput, delay, and packet rejection probability as functions of $p_b$, respectively, for the system with $U = 60$ and $p_i = 0.2$. Depending on the value of $M$, the system has a single equilibrium point when $p_b$ is small. However, the system has three equilibrium points when $p_b$ is large (see Fig. 4). When there are three equilibrium points, we show, in Fig. 6, the EPA results for the two stable equilibrium points (defined in Section 3.5). We see that the stimulation and EPA results match very well when there is a single equilibrium point. When there are three equilibrium points, the simulation results fall between the EPA results of the stable equilibrium points. An interesting observation is that except for the case of $M = 1$, the simulation results are closer to the equilibrium point with low throughput (high packet rejection probability) when $p_b$ is large. As expected, a longer transmitter buffer helps to reduce $P_{rej}$.

Next, we consider the case with $U = 60$ and $p_i = 0.4$. Figures 7a–c show the corresponding throughput, delay, and packet rejection probability curves, respectively. We note that the system has only one equilibrium point when

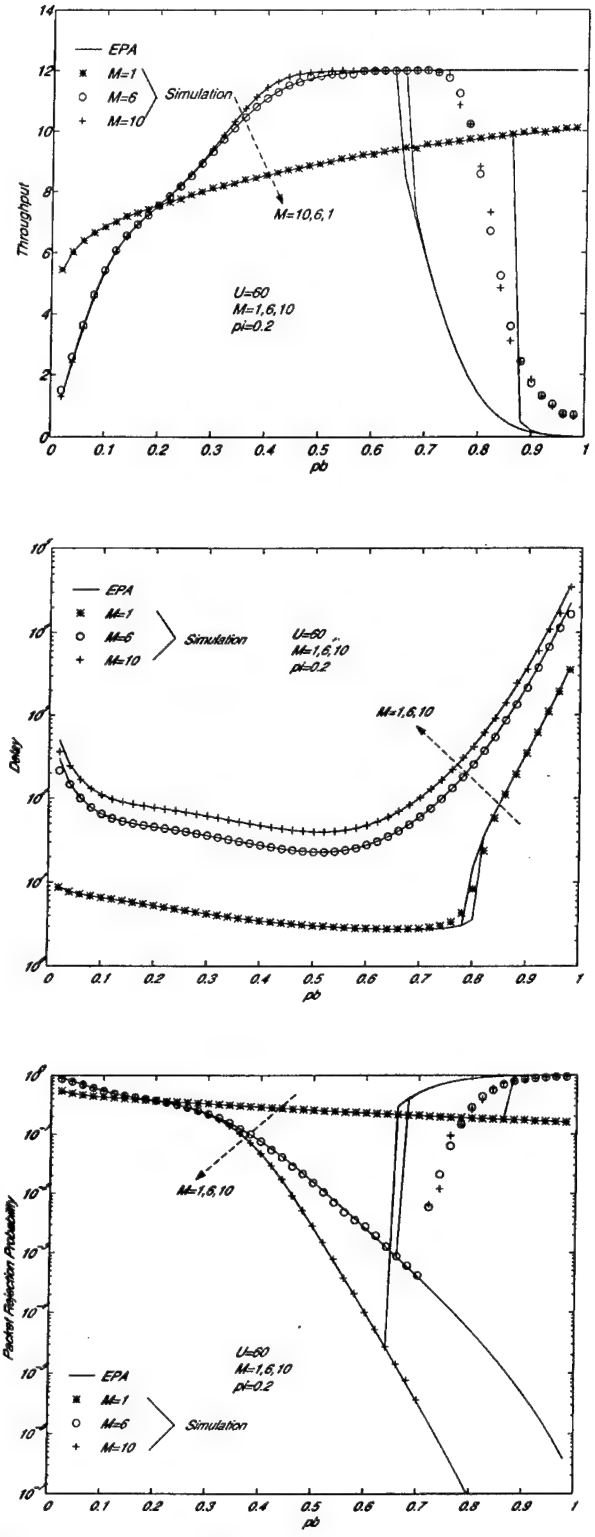


**Fig. 6.** Equilibrium throughput, delay, and packet rejection probability ($p_i$ = 0.2): (a) throughput; (b) delay; (c) packet rejection probability.

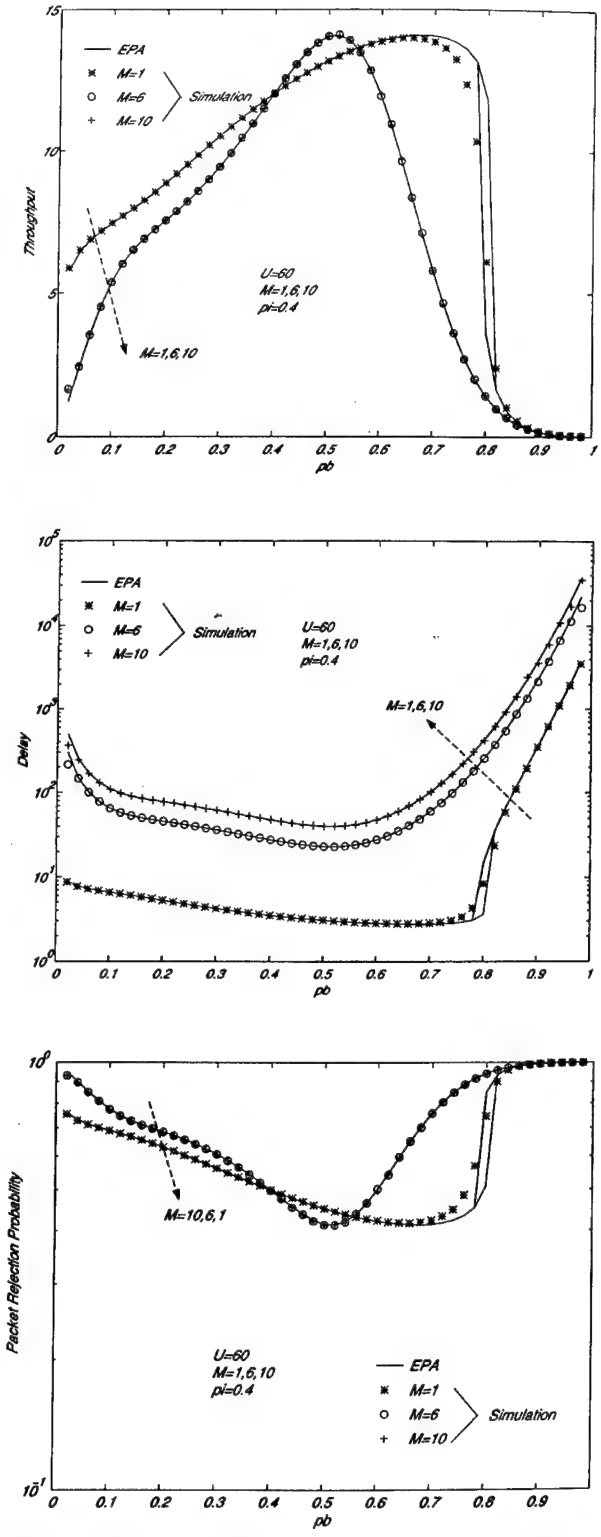


**Fig. 7.** Equilibrium throughput, delay, and packet rejection probability ($p_i$ = 0.4): (a) throughput; (b) delay; (c) packet rejection probability.

$M$ = 6 and 10. From the figures, we see that the simulation results also match the EPA results well in this case. Although the maximum throughput achieved in this case is larger than that in the case where $p_i$ = 0.2, the packet rejection probability is very high even when $M$ is large. This indicates that the system cannot handle an input rate of $p_i$ = 0.4. Moreover, this result also indicates that the maximum system throughput alone may not be a good measure of the system performance. More detailed discussion on the capacity of the system will be given in Section 4.

We conclude from Figs. 6 and 7 that the EPA technique can provide accurate approximations of the system throughput, delay, and packet rejection probability when there is a single equilibrium point, i.e., when we can assume that the system operates in the vicinity of the equilibrium point. When there are multiple equilibrium points, the system behavior is more complex (see Section 3.5).

### 3.5. System Stability

It is demonstrated in the previous section that the system can have multiple equilibrium points. Roughly speaking, the system oscillates among some equilibrium points in this case. The existence of these oscillations determines the stability behavior of the system.

First, we classify the equilibrium points according to stability:

**Definition 1:** An equilibrium point $\{r_I, r_1, r_{1,1}, \ldots, r_{M,t_1}\}$ is stable if $F_I'(r_I)$, the derivative of $F_I$ at $r_I$, is positive. Otherwise, it is unstable.

Physically, this definition is based on the following observation. If $F_I'(r_I) > 0$, $F_I$ increases (decreases) as $r_I$ increases (decreases) slightly from the equilibrium value. We note that $F_I$ represents the expected net outflow from *Idle*. When $F_I$ increases (decreases), more (less) users are going to leave *Idle*, and, hence, $r_I$ decreases (increases). This regulatory effect keeps the system at the equilibrium point. Therefore, the equilibrium point is stable. On the contrary, if $F_I'(r_I) < 0$, an increase (decrease) in $r_I$ will cause a further increase (decrease) in $r_I$ itself. Hence, upon a slight statistical fluctuation, the system will leave the equilibrium point in this case, i.e., this equilibrium point is unstable.

From Fig. 4, we see that for the cases of $p_b$ = 0.2 and 0.5, the single equilibrium points are stable. On the other hand, for $p_b$ = 0.9, the middle equilibrium point is unstable and the boundary ones are stable. The physical interpretation above indicates that a system with a single stable equilibrium point (e.g., $U$ = 60, $M$ = 6, $p_i$ = 0.2, $p_b$ = 0.5) stays in the vicinity of the equilibrium point. In this case, we say the system is *stable*. For the system with two stable equilibrium points (e.g., $U$ = 60, $M$ = 6, $p_i$ = 0.2, $p_b$ = 0.9), oscillation occurs between those points with stays of random durations. In this case, we say the system is *bistable*. Figs. 8a and 8b show the time trajectories of $r_I$ obtained in a simulation run for the two sample systems. The results in the figures verify the system dynamics predicted by the EPA technique.

For the bistable system shown in Fig. 8b, one of the two stable equilibrium points ("good") corresponds to a high system throughput and a low packet rejection probability, whereas the other one ("bad") corresponds to a low system throughput and a high packet rejection prob-

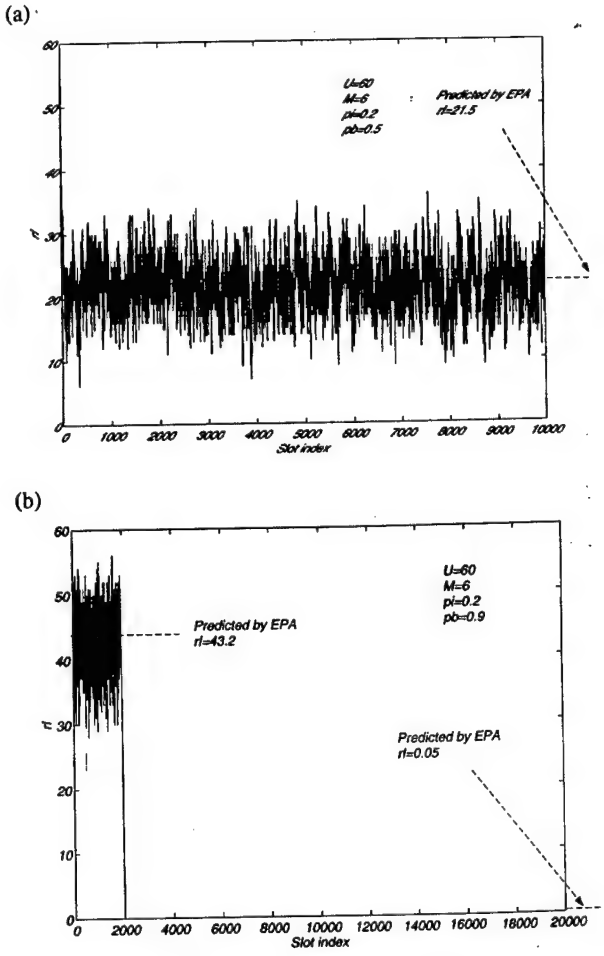


Fig. 8. Time trajectories of $r_I$: (a) stable system; (b) bistable system.

ability (cf. Fig. 6). Since the bistable system oscillates between the two stable equilibrium points, the actual system throughput (packet rejection probability) should be a weighted average of the throughputs (packet rejection probabilities) at the two stable equilibrium points. The simulation result shown in Fig. 8b seems to indicate that the system spends much more time about the "bad" equilibrium point than the "good" one, i.e., the actual system throughput (packet rejection probability) is close to that at the "bad" equilibrium point. In fact, we observe from extensive simulations that for $M \geq 4$ and some large $p_b$, once the bistable system enters the vicinity of the "bad" equilibrium point, it is extremely unlikely that it will leave it. Intuitively, this phenomenon can be explained by the fact that for large $M$ and $p_b$, once the transmitter buffers are full, they act as continuous packet sources. As a result, the air interface becomes very congested. Since the DS-SSMA technique is interference limited, it is unlikely that most of the transmissions succeed. Hence, the transmitter buffers do not clear up and the system stays at the "bad" equilibrium point. This explains why the simulation results for large $M$ in Fig. 6 are close to the "bad" equilibrium points when the system is bistable. In summary, we should avoid operating in the region where the system is bistable.

## 4. SYSTEM DESIGN

In this section, we consider some issues affecting the design of a DS-SSMA system with the type-II hybrid ARQ protocol. We assume that the total number of users in the system is fixed to $U$. In practice, $U$ may represent the maximum number of users allowed in the system. We also fix the error correcting capability of $C_1$ to $t_1$ based on complexity considerations. The system design criterion we consider is that the packet rejection probability should always be smaller than a predetermined threshold $P^*_{rej}$ under all allowable input loads $p_i$. In practice, this threshold can be set to the maximum acceptable packet rejection probability.

### 4.1. Transmitter Buffer-Length Selection

First, we develop a procedure to select the transmitter buffer length $M$ to satisfy the packet rejection criterion, namely $P_{rej} \leq P^*_{rej}$. From the discussion in Section 3.5, we know that it is undesirable to operate when the system is bistable. Hence, we only consider the stable region of operation, i.e., those values of $p_i$, $p_b$, a $M$ for which the system is stable. From the numeric results in Section 3.4, we observe that the packet reje tion criterion is not satisfied for all values of $p_i$, $p_b$, a $M$. This leads us to make the following definition of t maximum admissible input load $p^*_i(M)$ for each $M$:

**Definition 2:** Let $\mathcal{A}_{p_i,M} = \{p_b \in (0,1]: r_I(p_i,p_b,M)$ the only solution of $F_I(r_I) = 0$ in $[0, U]$ and $F'_I(r_I) > 0$ be the set of $p_b$ such that the system is stable for fixed $p_i$ and $M$. For each buffer length $M$, define the maximu admissible input load $p^*_i(M)$ as

$$p^*_i(M) = \inf\{p_i \in [0,1]: P_{rej}(p_i,p_b,M) > P^*_{rej}, \text{for all } p_b \in \mathcal{A}_{p_i,M}\} \quad (3$$

If the set in Eq. (31) is empty, we set $p^*_{rei}(M) = 1$.

The above definition means that for a fixed $M$, if $p_i$ $p^*_{rej}(M)$ we can always choose a $p_b$ such that $P_{rej} \leq P^*_{re}$

Figure 9 shows the plot of $p^*_i(M)$ against $M$ for di ferent values of $P^*_{rej}$. We observe that $p^*_i(M)$ levels o when $M$ is large. This implies that the length of the tran mitter buffer (if it is large enough) does not affect max mum admissible input load. Intuitively, since the tran mitter buffer is only used to prevent packet rejectio once its length is large enough that the packet rejectio criterion is satisfied, further increase in its length has n effect on the system capacity, which is basically dete mined by the coding capability $t_1$. More precisely, w can define the capacity of the system as follows:

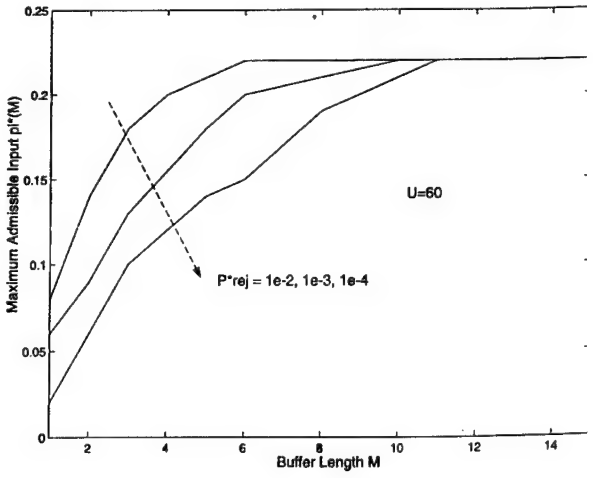


Fig. 9. $p^*_i(M)$ as a function of $M$.

**Definition 3:** Given $U$ and $t_1$, the capacity of the system is defined as

$$S^* = \liminf_{P^*_{rej} \downarrow 0} \{\sup_{M \geq 1} p_i^*(M)U\} \tag{32}$$

For the sample coding structure considered, $S^* \approx 13.2$. This is the maximum average number of packets per slot that the system can handle given $U = 60$ and $t_1 = 54$.

Based on the development above, we can construct the following procedure to select the transmitter buffer length:

1. Given $U$ and $t_1$, specify the maximum input load $L_I$ (packets per slot). If $L_I \geq S^*$, increase $t_1$ to make $L_I < S^*$.
2. Choose a desirable $P^*_{rej}$ and find the minimum $M$ such that $p_i^*(M) > L_I/U$.
3. Set transmitter buffer length to this $M$.

For example, for the packet rejection threshold $P^*_{rej} = 10^{-3}$ and a load $L_I = 12$ packet per slot, $M = 6$ is enough.

### 4.2. Desirable Region of Operation

After choosing the length of the transmitter buffer, we can determine the region of operation within which the packet rejection criterion is satisfied. In other words, for each $p_i \leq L_I/U$, we determine the range of $p_b$ such that $P_{rej} \leq P^*_{rej}$. As discussed in Section 3.5, we should avoid operating in the bistable region. Hence, we limit the desirable region of operation to be a subset of the stable region. Then it is easy to see that the desirable region of operation can be defined as follows:

**Definition 4:** Given $U$, $t_1$, and $M$, the desirable region of operation is defined as

$$\mathcal{D}_M = \{(p_i, p_b): p_i \in [0, L_I/U], p_b \in \mathcal{A}_{p_i,M}, \text{ and } P_{rej}(p_i, p_b, M) \leq P^*_{rej}\} \tag{33}$$

We note that in Eq. (33), $L_I/U < p_i^*(M)$ because of the buffer length selection procedure described in the previous section. Hence, $\mathcal{D}_M$ is nonempty.

Figure 10 shows the desirable region of operation when $L_I = 12$ packets per slot. To satisfy the packet rejection criterion, we have to operate inside this region. As shown in the previous section, we know that $M = 6$ is enough for $U = 60$ and $P^*_{rej} = 10^{-3}$. The shape of the region follows the intuition that we can have more choices of $p_b$ when the load $p_i$ is small.

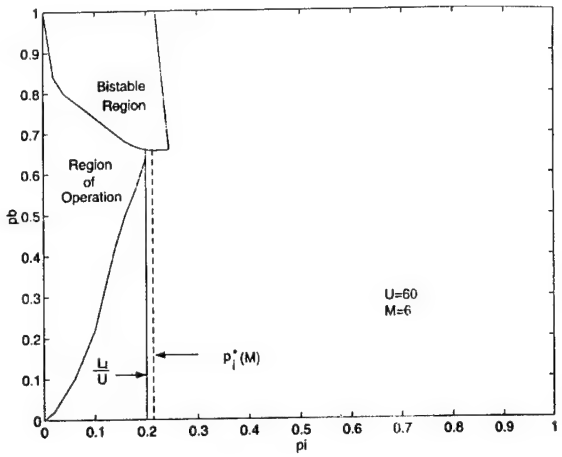


**Fig. 10.** Desirable region of operation.

After constructing the desirable region of operation, we can have two strategies of choosing $p_b$ depending on whether we know (can estimate) the instantaneous value of $p_i$. If we do know the instantaneous value of $p_i$, we can choose the value of $p_b$ that maximizes the throughput or minimizes the delay for this $p_i$ by using curves similar to those shown in Figs. 6 and 7. Otherwise, we need to choose a fixed value of $p_b$ so that the packet rejection criterion is satisfied for all $p_i \leq L_I/U$. For example, we can choose $p_b = 0.65$ by consulting Fig. 10.

## 5. CONCLUSIONS

In this paper, we have employed the EPA technique to study the slotted DS-SSMA packet radio network employing the type-II hybrid ARQ protocol with finite-length transmitter buffers. We have analyzed the system stability under various operating conditions and computed the system throughput, delay, and packet rejection probability. We have also performed computer simulations to verify the results given by EPA. We have observed that the system exhibits bistable behavior in some situations, which we should avoid in designing the system. Moreover, we have given a procedure to determine the required length of the transmitter buffers and the desirable region of operation based on a predetermined performance requirement for packet rejection.

## APPENDIX

In this Appendix, we prove Propositions 1 and 2. To this end, we need the following theorem concerning an irreducible Markov chain from [12]:

**Theorem 1:** Let $\mathbf{P}$ be the state transition matrix of an irreducible aperiodic Markov chain with finitely many states. Then there is a unique solution, $\pi$, satisfying

$$\pi[\mathbf{P}, \mathbf{q}] = [\pi, 1] \tag{34}$$

This solution $\pi$ represents the stationary distribution of the Markov chain and each element of $\pi$ lies in (0, 1).

First, for each fixed $r_I$ in $[0, U]$, we see that the matrix $\mathbf{A}$ represents the state transition matrix of an irreducible aperiodic Markov chain with states $\{Idle, S_1, E_{1,1}, \ldots, E_{M,t_1}\}$. Hence, by Theorem 1, for each $r_I$ in $[0, U]$, the corresponding Markov chain has the stationary distribution $\pi(r_I)$. Comparing Eqs. (18) and (34), we observe that $U\pi(r_I)$ is a solution to Eq. (18) if $\pi_1(r_I) = r_I/U$, where $\pi_1$ is the first element of the vector $\pi$. Now, we consider the function $f(r_I) \triangleq \pi_1(r_I) - r_I/U$. It is easy to see that $f(r_I)$ is a continuous function in $[0, U]$ as each element of $\mathbf{A}$ is a continuous function in $[0, U]$. Moreover, by Theorem 1, since $\pi_1(r_I)$ lies in (0,1) for all $r_I \in [0, U]$, we have $f(0) > 0$ and $f(U) < 0$. Hence, $f(r_I) = 0$ has an odd number of solutions in $(0, U)$, and so does Eq. (18). This proves Proposition 1.

Next, for each fixed $r_I$ in $[0, U]$, we modify the Markov chain above by deleting the state *Idle* and passing the original transitions going into *Idle* to $E_{M,t_1}$. It is easy to see that the resulting Markov chain ($M(t_1 + 1)$ states) is still irreducible and aperiodic. Let the state transition matrix of the resulting Markov chain be $\hat{\mathbf{A}}$. Again, by Theorem 1, this modified Markov chain has a unique positive stationary distribution, $\hat{\pi}$, i.e., there is a unique $\hat{\pi}$ such that

$$\hat{\pi}[\hat{\mathbf{A}} - \mathbf{I}, \mathbf{q}] = [\underbrace{0, \ldots, 0,}_{M(t_1+1)\text{ terms}} 1] \tag{35}$$

Hence, the rank of the matrix $[\hat{\mathbf{A}} - \mathbf{I}, \mathbf{q}]$ must be $M(t_1 + 1)$. Moreover, as for the original Markov chain, the last column of the matrix $\hat{\mathbf{A}} - \mathbf{I}$ can be written as a linear combination of the other columns. So, the rank of $\hat{\mathbf{A}} - \mathbf{I}$ must be $M(t_1 + 1) - 1$. But we observe that the $M(t_1 + 1)$-by-$M(t_1 + 1)$ matrix $\mathbf{C}$ can be obtained by removing the $(M(t_1 + 1))$-th column from $[\hat{\mathbf{A}} - \mathbf{I}, \mathbf{q}]$. Therefore, the rank of $\mathbf{C}$ is $M(t_1 + 1)$, i.e., it is invertible. This proves Proposition 2.

## REFERENCES


1. Q. Zhang, T. F. Wong, and J. S. Lehnert, Adaptive coding for s ted DS-SSMA packet radio systems, *Proceedings of IEEE M COM'97*, Monterey, California, Vol. 1, pp. 291–295, Nov. 19
2. Q. Zhang, T. F. Wong, and J. S. Lehnert, Performance of a typ hybrid ARQ protocol in slotted DS-SSMA packet radio syste *IEE Transactions on Communications*, to appear.
3. S. Tasaka, Stability and performance of the R-ALOHA pac broadcast system, *IEEE Transactions on Comput.*, Vol. 32, 1 8, pp. 717–726, Aug. 1983.
4. S. Nanda, D. J. Goodman, and U. Timor, Performance of PRM A packet voice protocol for cellular systems, *IEEE Transacti on Vehicular Technology*, Vol. 40, No. 3, pp. 584–598, Aug. 19
5. L. Tan and Q. T. Zhang, A reservation random-access pro col for voice/data integrated spread-spectrum multiple-access s tems, *IEEE Journal of Selected Area Communications*, Vol. No. 9, pp. 1717–1727, Dec. 1996.
6. A. B. Carleial and M. E. Hellman, Bistable behavior of ALOH type system, *IEEE Transactions on Communications*, Vol. 23, 1 4, pp. 401–409, Apr. 1975.
7. L. Kleinrock and S. Lam, Packet switching in a multiaccess bro cast channel: Performance evaluation. *IEEE Transactions on Co munications*, Vol. 23, No. 4, pp. 410–423, Apr. 1975.
8. Y. M. Wang and S. Lin, A modified selective-repeat type-II hyb ARQ system and its performance analysis, *IEEE Transactions Communications*, Vol. 31, No. 5, pp. 593–608, May 1983.
9. R. K. Morrow Jr. and J. S. Lehnert, Bit-to-bit error dep dence in slotted DS/SSMA packet systems with random signat sequences, *IEEE Transactions on Communications*, Vol. 37, 1 10, pp. 1052–1061, Oct. 1989.
10. R. K. Morrow Jr. and J. S. Lehnert, Packet throughput in sl ted ALOHA DS/SSMA radio systems with random signature quences, *IEEE Transactions on Communications*, Vol. 40, No. pp. 1223–1230, July 1992.
11. D. Bertsekas and R. Gallager, *Data Networks*, 2nd ed., Prenti Hall, 1992.
12. E. Cinlar, *Introduction to Stochastic Processes*, Prentice-H 1975.


**Qian Zhang** received the B.S. degree from Tsinghua Universi China, in 1986, the M.S. degree from Peking University, China, 1989, the M.S.E.E. degree from University of Central Florida, Orlan in 1991, and the Ph.D. degree from Purdue University, West Lafayet Indiana, in 1998, all in electrical engineering. From 1992 to 1994, was a research engineer and a project engineer working in PTR Tec nology Inc., Palm Bay, Florida, and Ampro Corp., Melbourne, Flori

respectively. His work included hardware design and software programming for radio transmitter geolocationing systems and big-screen projection unit systems. From 1994 to 1998, he was a Ph.D. student and a research assistant in the School of Electrical and Computer Engineering at Purdue University. His current research interests include CDMA systems, adaptive coding, diversity techniques, and wireless cellular networks.

**Tan F. Wong** received the B.Sc. degree (1st class honors) in electronic engineering from the Chinese University of Hong Kong in 1991, and the M.S.E.E. and Ph.D. degrees in electrical engineering from Purdue University in 1992 and 1997, respectively. From 1993 to 1995, he was a research engineer working on the high-speed wireless networks project in the Department of Electronics at Macquire University, Sydney, Australia. From 1995 to 1998, he served as a research assistant and a postdoctoral research associate in the School of Electrical and Computer Engineering at Purdue University. He is currently an Assistant Professor of Electrical and Computer Engineering at the University of Florida. His research interests include spread-spectrum communication systems, multiuser communications, and wireless cellular networks.

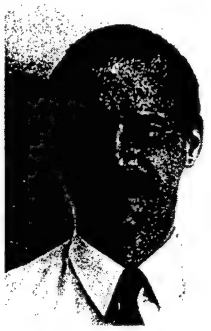

**James S. Lehnert** received the B.S. (highest honors), M.S., and Ph.D. degrees in electrical engineering from the University of Illinois at Urbana–Champaign in 1978, 1981, and 1984, respectively. From 1978 to 1984, he was a research assistant at the Coordinated Science Laboratory, University of Illinois, Urbana. Dr. Lehnert was a University of Illinois Fellow from 1978 to 1979 and an IBM Predoctoral Fellow from 1982 to 1984. He has held summer positions at Motorola Communications, Schaumburg, Illinois, in the Data Systems Research Laboratory, and Harris Corporation, Melbourne, Florida, in the Advanced Technology Department. He is currently an Associate Professor of Electrical Engineering at Purdue University, West Lafayette, Indiana. Dr. Lehnert has served as Editor for Spread Spectrum for the *IEEE Transactions on Communications*. His current research work is in communication and information theory with emphasis on spread-spectrum communications.

# Blind Adaptive Signal Reception for MC-CDMA Systems in Rayleigh Fading Channels

Tat M. Lok, *Member, IEEE*, Tan F. Wong, and James S. Lehnert, *Senior Member, IEEE*

***Abstract*—In this paper, we consider signal reception in multicarrier code-division multiple-access (MC-CDMA) systems. A blind adaptive algorithm is proposed to determine a weight vector which optimally combines the desired signal contributions from different carriers while suppressing noise and interference. No knowledge of the channel conditions (fading coefficients, signature sequences and timing of interferers, statistics of other noises, etc.) nor any training sequence is required. The performance is examined for Rayleigh fading channels. Results show that the proposed algorithm performs well and is robust to the near–far problem. Hence, the results show that MC-CDMA systems are attractive candidates for future CDMA systems.**

***Index Terms*—Adaptive signal detection, code-division multiple access, fading channels, interference suppression, multicarrier modulation.**

## I. Introduction

RECENTLY, different multicarrier code-division multiple-access (MC-CDMA) systems [1] have been proposed and investigated. With the possibility of efficient fast Fourier transform (FFT) implementations [2], MC-CDMA systems can be of practical interest. In one of these systems, direct-sequence (DS) spreading is employed together with multicarrier modulation [3] to derive the benefits of both techniques. The maximal ratio combiner (MRC) is adopted to counteract fading and narrow-band interference. However, the use of the MRC requires the estimation of each fading coefficient associated with each carrier. When interference, especially multiple-access interference (MAI), and noise other than additive white Gaussian noise (AWGN) are also present, not only does it become more difficult to estimate the fading coefficients, but the statistics of the interference and the noise also have to be estimated for optimal reception. Explicit estimation of these quantities can be inefficient and might not be able to adapt quickly to changes in channel conditions.

Paper approved by U. Mitra, the Editor for Spread-Spectrum/Equalization for the IEEE Communications Society. Manuscript received August 19, 1997; revised March 3, 1998 and August 14, 1998. This paper is based upon work supported in part by The Chinese University of Hong Kong Research Committee and in part by the Army Research Office under Grant DAAH04-95-1-0246. This paper was presented in part at the IEEE Military Communications Conference (MILCOM'98), Boston, MA, October 18–21, 1998.

T. M. Lok is with the Department of Information Engineering, Chinese University of Hong Kong, Shatin, Hong Kong.

T. F. Wong is with the Department of Electrical and Computer Engineering, University of Florida, Gainesville, FL 32611-6130 USA.

J. S. Lehnert is with the Department of Electrical and Computer Engineering, Purdue University, West Lafayette, IN 47907-1285 USA (e-mail: lehnert@purdue.edu).

Publisher Item Identifier S 0090-6778(99)02173-X.

In [4] and [5], a blind adaptive receiver has been proposed for DS systems. Here, we propose a blind adaptive algorithm for the MC-CDMA systems defined in [3] for fading channels. The algorithm determines a weight vector which optimally combines the contributions from different carriers. The desired signal contributions are constructively combined, while noise and interference are suppressed. No knowledge of the fading coefficients, the signature sequences and the timing of the interferers, the statistics of other noise, etc., is assumed, and no training sequence is required. The proposed algorithm yields a weight vector that maximizes the signal-to-noise ratio (SNR) and in general performs better than the MRC. Under some channel conditions when the MRC is optimal, the proposed algorithm reduces to maximal ratio combining. In these cases, the noise and interference across different carriers are uncorrelated. However, this property does not hold generally. Channels with the near–far problem provide common counterexamples in which interference contributions in different channels are correlated and the MRC fails to achieve MAI cancellation. Different methods [6], [7] with different levels of complexity have been proposed to tackle the near–far problem in DS systems. With multicarrier modulation, the proposed algorithm can exploit the correlation between the received signals across different carriers to cancel MAI and, hence, alleviate the near–far problem. This property distinguishes MC-CDMA systems from DS systems. The simplicity of the proposed algorithm used with MC-CDMA results in an attractive system. The algorithm is presented in Section III, and its performance is discussed in Section IV.

Antenna arrays are shown [4], [5], [8] to be effective in boosting received signal energy and suppressing interference in DS spread-spectrum communication systems. In some cases, it may be desirable to use antenna arrays in MC-CDMA systems. It turns out that the proposed algorithm for MC-CDMA signal reception can be readily generalized to incorporate the use of antenna arrays. The directions of arrival of different carriers of the signals are not required to be known *a priori*. The proposed scheme implicitly determines the directions of arrival, the fading coefficients, and the noise statistics to yield the optimal weight vector. This generalization is contained in Section V.

In Section VI, we present numerical examples to verify various results in the paper. Conclusions are drawn in Section VII.

## II. System Model

In this section, we describe the model of the MC-CDMA system. We assume that there are $K$ simultaneous users, which use the same $M$ carriers in the system.

The $k$th user, for $1 \le k \le K$, is provided with a random signature sequence $a^{(k)}$ given by

$$a^{(k)} = (\cdots, a_0^{(k)}, a_1^{(k)}, \cdots, a_{N-1}^{(k)}, \cdots) \tag{1}$$

where the elements $a_i^{(k)}$ are modeled as independent and identically distributed (i.i.d.) random variables such that $\Pr(a_i^{(k)} = -1) = \Pr(a_i^{(k)} = 1) = 1/2$. The same signature sequence $a^{(k)}$ is used to modulate each of the $M$ carriers of the $k$th user.

The $k$th transmitter, for $1 \le k \le K$, generates a stream of data symbols $b^{(k)}$, given by

$$b^{(k)} = (\cdots, b_0^{(k)}, b_1^{(k)}, b_2^{(k)}, \cdots). \tag{2}$$

The data symbols $b_j^{(k)}$ are random variables with $E[|b_j^{(k)}|^2] = 1$. Each data symbol is multiplied by $N$ chips of the signature sequence.

The $k$th transmitted signal can be expressed as the real part of the complex signal given by

$$\sum_{m=1}^{M} \sqrt{2P_k} c_m^{(k)} \left\{ \sum_{i=-\infty}^{\infty} b_{\lfloor i/N \rfloor}^{(k)} a_i^{(k)} \psi(t - iT_c) \right\} e^{j\omega_m t}. \tag{3}$$

The parameter $P_k$ is the power for each carrier of the $k$th transmitted signal, $\omega_m$ is the frequency of the $m$th carrier, and the parameters $c_m^{(k)}$ can be used as a code across the $M$ carriers of the $k$th transmitter, or can be chosen to condition the peak-to-average power ratio of the $k$th transmitted signal [9]. For simplicity, we assume that $|c_m^{(k)}|^2 = 1$. We assume that the chip waveform $\psi(t)$ is bandlimited and the carrier frequencies are well separated so that adjacent frequency bands do not interfere with each other. We also assume that $\psi(t)$ is normalized so that $\int_{-\infty}^{\infty} |\psi(t)|^2 \, dt = T_c$. The parameter $T_c$ is the delay between consecutive chips. Since each data symbol is multiplied by $N$ chips on a carrier, the symbol interval is $NT_c$.

Without loss of generality, we consider the signal from the first transmitter as the desired signal and the signals from all other transmitters as interfering signals throughout the paper.

We now describe the channel model. We assume that the channel is a frequency selective fading channel. By suitably choosing $M$ and the bandwidth of $\psi(t)$ [3], we can assume that each carrier undergoes independent frequency nonselective slow Rayleigh fading. We also assume the presence of other noise sources that are independent of the user signals, namely, AWGN with power spectral density $N_0$ and wide-sense stationary narrow-band interference.

The received signal in complex analytic form is given by

$$\begin{aligned} r(t) = \sum_{k=1}^{K} \sum_{m=1}^{M} & \sqrt{2P_k} c_m^{(k)} \\ & \cdot \left\{ \sum_{i=-\infty}^{\infty} b_{\lfloor i/N \rfloor}^{(k)} a_i^{(k)} \psi(t - T_k - iT_c) \right\} \\ & \cdot e^{j\omega_m (t - T_k)} \alpha_{k,m} + n(t) \end{aligned} \tag{4}$$

where $\alpha_{k,m}$ accounts for the overall effects of phase shift and fading for the $m$th carrier of the $k$th user, $T_k$ represents the delay of the $k$th user signal,[1] and $n(t)$ represents other noise. We model $\alpha_{k,m}$, for $k = 1, \cdots, K$ and $m = 1, \cdots, M$, as i.i.d. zero-mean complex Gaussian random variables so that the amplitude of each carrier is Rayleigh distributed. We assume that synchronization has been achieved with the first transmitted signal. Therefore, the delay of the first transmitted signal $T_1$ can be taken to be zero.

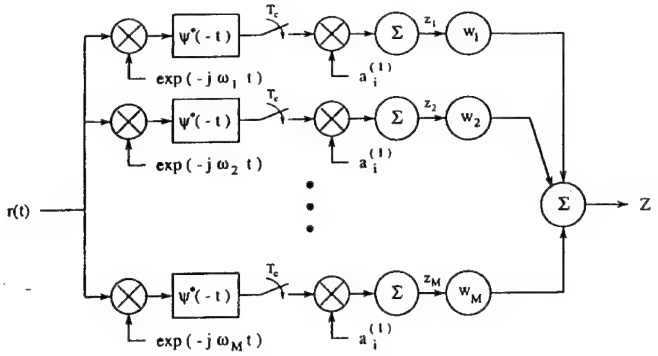


Fig. 1. Receiver for the first user in the MC-CDMA system.

We consider the receiver shown in Fig. 1. It consists of $M$ branches. Each branch consists of a correlator and an appropriate weight, and is responsible for the demodulation of one carrier. The correlator on the $m$th branch consists of a chip-matched filter and a combiner that combines the contributions from different chips according to the signature sequence of the first transmitter. We assume that the chip waveform and the chip-matched filter are chosen to satisfy the Nyquist criterion so that there is no inter-chip interference. The weight vector $\mathbf{w} = [w_1, w_2, \cdots, w_m]^T$, whose value is determined in the following section, is an $M$-dimensional vector that optimally combines the contributions from the $M$ branches to give the decision statistic.

## III. Weight Vector Determination

We consider symbol-by-symbol detection. Without loss of generality, we consider the detection of the symbol $b_0^{(1)}$. The output of the correlator on the $m$th branch, due to the first transmitted signal, is given by

$$s_m = b_0^{(1)} \sqrt{2P_1} N T_c c_m^{(1)} \alpha_{1,m}. \tag{5}$$

We define an $M$-dimensional vector $\mathbf{s} = [s_1 \; s_2 \; \cdots \; s_M]^T$. The output of the correlator on the $m$th branch, due to the $k$th transmitted signal, for $k \ge 1$, is given by

$$\begin{aligned} i_{k,m} = & \sqrt{2P_k} c_m^{(k)} e^{-j\omega_m T_k} \alpha_{k,m} \\ & \cdot \sum_{i=0}^{N-1} \sum_{\lambda=-\infty}^{\infty} b_{\lfloor \lambda/N \rfloor}^{(k)} a_i^{(1)} a_\lambda^{(k)} \hat{\psi}((i-\lambda)T_c - T_k) \end{aligned} \tag{6}$$

where the function $\hat{\psi}(\cdot)$ is the output of the chip waveform through the chip-matched filter, i.e., $\hat{\psi}(t) = \int_{-\infty}^{\infty} \psi(s)\psi^*(s - t)\, ds$. We also define the $M$-dimensional vectors $\mathbf{i}_k = [i_{k,1} \; i_{k,2} \; \cdots \; i_{k,M}]^T$. We denote the output of the correlator

[1] Although an asynchronous system is being considered, the method works equally well with synchronous systems and serves to extend the number of users to beyond $N$ in synchronous systems.

on the $m$th branch due to other noise by $n_m$, and similarly define an $M$-dimensional vector $\mathbf{n} = [n_1 \ n_2 \ \cdots \ n_M]^T$. The overall output of the correlators, in vector form, is given by

$$\mathbf{z} = \mathbf{s} + \mathbf{n} + \sum_{k=2}^{K} \mathbf{i}_k. \tag{7}$$

By the assumption that other noise contributions are independent of the user signals, $\mathbf{n}$ is uncorrelated with $\mathbf{s}$ and $\mathbf{i}_k$ for all $k$. Moreover, it is easy to check that the vectors $\mathbf{i}_k$ are uncorrelated for different $k$ and are uncorrelated with $\mathbf{s}$. Therefore, the noise and interference correlation matrix is given by

$$\mathbf{R_{ni}} = E_\alpha\left[\mathbf{n}\mathbf{n}^H + \sum_{k=2}^{K} \mathbf{i}_k\mathbf{i}_k^H\right] \tag{8}$$

and the overall output correlation matrix is given by

$$\mathbf{R_z} = E_\alpha[\mathbf{z}\mathbf{z}^H] = E_\alpha[\mathbf{s}\mathbf{s}^H] + \mathbf{R_{ni}} \tag{9}$$

where $E_\alpha[\cdot]$ denotes the conditional expectation given $\alpha_{k,m}$, for $k = 1, \cdots, K$ and $m = 1, \cdots, M$, and the superscript $H$ denotes the Hermitian (conjugate transpose) operation.

The decision statistic for the symbol $b_0^{(1)}$ is given by $Z = \mathbf{w}^H\mathbf{z}$. We assume that the channel coefficients $\alpha_{k,m}$ and $T_k$ vary slowly so that they effectively remain constant within the time interval used to determine an appropriate weight vector.

One way to determine a weight vector is the approach of maximal ratio combining [3], [10]. Each component of the weight vector is determined separately by

$$w_m = \frac{E_\alpha[b_0^{(1)*} z_m]}{\mathrm{var}_\alpha[b_0^{(1)*} z_m]} = \frac{\sqrt{2P_1}NT_c c_m^{(1)}\alpha_{1,m}}{[\mathbf{R_{ni}}]_{mm}} \tag{10}$$

where the superscript $*$ denotes complex conjugation, $\mathrm{var}_\alpha[\cdot]$ denotes the conditional variance given $\alpha_{k,m}$ for all $k$ and $m$, $z_m$ is the $m$th component of $\mathbf{z}$, and $[\mathbf{R_{ni}}]_{mm}$ is the $m$th diagonal component of the correlation matrix $\mathbf{R_{ni}}$. We note that the constant gain $\sqrt{2P_1}NT_c$ can be omitted without affecting the performance of the MRC. The MRC is optimal in the sense of maximizing the SNR when noise and interference across different carriers are uncorrelated, for example, when only AWGN is present. In order to obtain the MRC, the channel coefficients $\alpha_{k,m}$ have to be estimated. The estimation of these coefficients becomes more difficult when MAI is also present. Actually, since MAI across different carriers are correlated, the MRC is not optimal.

In this paper, we determine the optimal weight vector that maximizes the SNR defined by

$$\mathrm{SNR} = \frac{E_\alpha[|\mathbf{w}^H\mathbf{s}|^2]}{E_\alpha\left[\left|\mathbf{w}^H\left(\mathbf{n} + \sum_{k=2}^{K}\mathbf{i}_k\right)\right|^2\right]}. \tag{11}$$

Equivalently, we find the weight vector that maximizes

$$\mathrm{SNR} + 1 = \frac{E_\alpha[|\mathbf{w}^H\mathbf{z}|^2]}{E_\alpha\left[\left|\mathbf{w}^H\left(\mathbf{n} + \sum_{k=2}^{K}\mathbf{i}_k\right)\right|^2\right]} = \frac{\mathbf{w}^H\mathbf{R_z}\mathbf{w}}{\mathbf{w}^H\mathbf{R_{ni}}\mathbf{w}}. \tag{12}$$

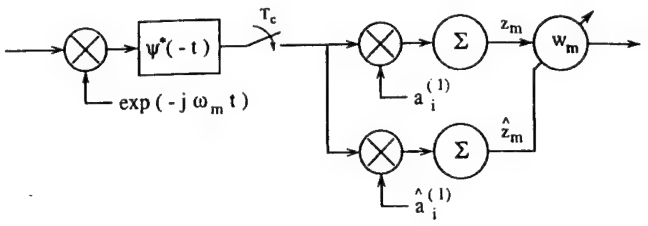


Fig. 2. The $m$th branch of the receiver for weight vector determination.

It can be shown [11] that the optimal weight vector that maximizes the last expression in (12), and hence the SNR, is given by the generalized eigenvector associated with the largest eigenvalue of the matrix pencil $(\mathbf{R_z}, \mathbf{R_{ni}})$. The matrix $\mathbf{R_z}$ can be easily estimated from the outputs $\mathbf{z}$ of the correlators. It remains to estimate $\mathbf{R_{ni}}$.

Due to the special structure of the spread-spectrum signals, it is possible to remove the desired signal component while maintaining the same statistics of the noises and interference. To estimate $\mathbf{R_{ni}}$, we pass the outputs of the chip-matched filter on each branch through another combiner, as shown in Fig. 2. On the $m$th branch, the sequence $(\hat{a}_0^{(1)}, \hat{a}_1^{(1)}, \cdots, \hat{a}_{N-1}^{(1)})$ is chosen to be orthogonal to the sequence $(a_0^{(1)}, a_1^{(1)}, \cdots, a_{N-1}^{(1)})$. For example, $N$ is chosen to be even, and

$$\hat{a}_i^{(1)} = \begin{cases} a_i^{(1)}, & \text{for } 0 \le i < \dfrac{N}{2} \\ -a_i^{(1)}, & \text{for } \dfrac{N}{2} \le i \le N-1. \end{cases} \tag{13}$$

Then, at the output of the second combiner on each branch, the first user signal component is nullified. On the other hand, it is straightforward to check that the (second-order) statistics of the outputs due to other transmitted signals and noise are the same as those of the first combiner. In particular, if the overall output from these second combiners is denoted by $\hat{\mathbf{z}}$, then the corresponding correlation matrix is given by

$$\mathbf{R}_{\hat{\mathbf{z}}} = E_\alpha[\hat{\mathbf{z}}\hat{\mathbf{z}}^H] = \mathbf{R_{ni}}. \tag{14}$$

Therefore, $\mathbf{R_{ni}}$ can be estimated from $\hat{\mathbf{z}}$ and, hence, the optimal weight vector can be determined.

In [5], it is shown that the generalized eigenvector associated with the largest eigenvalue of a matrix pencil of the form given by $(\mathbf{R_z}, \mathbf{R}_{\hat{\mathbf{z}}})$ can also be found by a constrained stochastic gradient algorithm similar to the least mean squares (LMS) algorithm but without a training sequence. The computational complexity of this blind adaptive algorithm is of the order $M$ per iteration, which is much smaller than the calculation of the generalized eigenvectors. In the notation of this paper, the algorithm can be expressed as follows. For each symbol interval, we obtain the vectors $\mathbf{z}$ and $\hat{\mathbf{z}}$ at the outputs of the $2M$ combiners. For the $j$th symbol interval, we denote them by $\mathbf{z}(j)$ and $\hat{\mathbf{z}}(j)$, respectively. We denote the weight vector in the $j$th symbol interval by $\mathbf{w}(j)$ and update $\mathbf{w}(j)$ for each $j$ according to the following rule:

For $j > 0$, get $\mathbf{w}(j)$ by

$$\mathbf{w}(j) = C(j)\{\mathbf{w}(j-1) + \mu[\mathbf{z}(j)^H\mathbf{w}(j-1)] \cdot [(\hat{\mathbf{z}}(j)^H\hat{\mathbf{z}}(j))\mathbf{z}(j) - (\hat{\mathbf{z}}(j)^H\mathbf{z}(j))\hat{\mathbf{z}}(j)]\} \tag{15}$$

where $C(j)$ is chosen to stabilize the algorithm and $\mu$ is the adaptation step size that controls the speed of convergence. Details concerning the stabilization constant $C(j)$, the adaptation step size $\mu$, and the initialization of the algorithm can be found in [4] and [5]. This blind adaptive algorithm has been shown to be effective for DS systems.

## IV. Performance

When the channel is only corrupted by AWGN and uncorrelated narrow-band interference without MAI, it can be readily shown that the noise and interference components across the $M$ carriers are uncorrelated, and, hence, the MRC gives the optimal weight vector. Under these conditions, it is straightforward to check that the proposed algorithm reduces to the MRC. However, the noise and interference components are not always uncorrelated, especially when the near–far problem exists. In this section, we examine the performance of the MC-CDMA system with the proposed algorithm in situations with the near–far problem. It turns out that the proposed algorithm exploits the high dimensional space and the correlation between the received samples provided by multicarrier modulation to cancel MAI and, hence, handles the near–far problem in a very effective way.

For convenience, we define, for $k = 1, \cdots, K$, the vectors $\mathbf{d}_k = [d_{k,1} \quad d_{k,2} \quad \cdots \quad d_{k,M}]^T$ by

$$d_{k,m} = c_m^{(k)} e^{-j\omega_m T_k} \alpha_{k,m} \tag{16}$$

for $m = 1, \cdots, M$. Notice that since $\alpha_{k,m}$, for $k = 1, \cdots, K$ and $m = 1, \cdots, M$, are i.i.d. zero-mean complex Gaussian random variables, so are $d_{k,m}$. It is shown in [12] that the generalized eigenvector associated with the largest generalized eigenvalue of the matrix pencil $(\mathbf{R}_z, \mathbf{R}_{\hat{z}})$, i.e., the optimal weight vector maximizing the SNR defined in (11), is given by

$$\mathbf{w}_* = \mathbf{R}_{\mathrm{ni}}^{-1}\mathbf{d}_1. \tag{17}$$

### A. Single Interferer

It is instructive to consider the case of $K = 2$, i.e., when there is only a single strong interferer. Then, the noise and interference correlation matrix is given by

$$\mathbf{R}_{\mathrm{ni}} = N_0 N T_c \mathbf{I} + \beta_2 \mathbf{d}_2 \mathbf{d}_2^H \tag{18}$$

where

$$\beta_k = 2P_k N \sum_{\lambda=-\infty}^{\infty} |\hat{\psi}(\lambda T_c - T_k)|^2. \tag{19}$$

The optimal weight vector is given by

$$\mathbf{w}_* = \mathbf{R}_{\mathrm{ni}}^{-1}\mathbf{d}_1 = \frac{1}{N_0 N T_c}\left(\mathbf{d}_1 - \frac{\beta_2 \mathbf{d}_2^H \mathbf{d}_1}{N_0 N T_c + \beta_2 |\mathbf{d}_2|^2}\mathbf{d}_2\right) \tag{20}$$

and the resulting SNR is given by

$$\mathrm{SNR}_* = \frac{2P_1 N T_c}{N_0}\left(|\mathbf{d}_1|^2 - \frac{\beta_2 |\mathbf{d}_2^H \mathbf{d}_1|^2}{N_0 N T_c + \beta_2 |\mathbf{d}_2|^2}\right). \tag{21}$$

We note that, if $\mathbf{d}_1$ and $\mathbf{d}_2$ are orthogonal, then the optimal weight vector annihilates the contribution of the interferer without any penalty in SNR.

Geometrically, the contributions of the users are represented by the vectors $\mathbf{d}_1$ and $\mathbf{d}_2$ in an $M$-dimensional space. If the vectors are perpendicular, then the optimal weight vector is $\mathbf{d}_1$. It collects energies from all carriers of the first user while rejecting energies from the second user by destructive interference. In general, $\mathbf{d}_1$ and $\mathbf{d}_2$ are not always perpendicular. However, as shown below, in a high dimensional space, it is likely that they are nearly perpendicular.

In a Rayleigh fading channel, $d_{k,m}$, for $k = 1, 2$, and $m = 1, \cdots, M$, are i.i.d. complex Gaussian random variables with zero mean and unit variance. We also assume that $T_2$ is uniformly distributed on $[0, T_c)$. We define an outage probability $P_o$ as the probability that the SNR of the first user suffers more than 3 dB of loss due to the interference from the second user. From (21), the outage probability is given by

$$\begin{aligned} P_o &= \Pr\left(\frac{|\mathbf{d}_1|^2}{2} \le \frac{\beta_2 |\mathbf{d}_1^H \mathbf{d}_2|^2}{N_0 N T_c + \beta_2 |\mathbf{d}_2|^2}\right) \\ &\le \Pr\left(\frac{|\mathbf{d}_1|^2}{2} \le \frac{|\mathbf{d}_1^H \mathbf{d}_2|^2}{|\mathbf{d}_2|^2}\right). \end{aligned} \tag{22}$$

The bound on the outage probability is the probability that the vectors make an angle between 0 and 45° (or between 135° and 180°). We note that the bound remains valid no matter how large the power of the second transmitted signal becomes.

Conditioned on $\mathbf{d}_1$, we perform a unitary transformation so that $\mathbf{d}_1$ is transformed into $\mathbf{d}_1' = [|\mathbf{d}_1|, 0, \cdots, 0]^T$, and $\mathbf{d}_2$ is transformed into some vector $\mathbf{d}_2'$. The components of $\mathbf{d}_2'$ remain i.i.d. complex Gaussian random variables with zero mean and unit variance. Hence, the conditional outage probability is bounded by

$$\begin{aligned} P_{o|\mathbf{d}_1} &\le \Pr\left(\sum_{m=1}^{M} |d_{2,m}'|^2 \le 2|d_{2,1}'|^2\right) \\ &= \Pr\left(\sum_{m=2}^{M} |d_{2,m}'|^2 \le |d_{2,1}'|^2\right) \end{aligned} \tag{23}$$

where $d_{2,m}'$ is the $m$th component of $\mathbf{d}_2'$. The random variables $X = \sum_{m=2}^{M} |d_{2,m}'|^2$ and $Y = |d_{2,1}'|^2$ are independent and are chi-square distributed with degrees of freedom equal to $2(M-1)$ and 2, respectively. Their probability density functions are

$$f_X(x) = \frac{1}{\Gamma(M-1)} x^{M-2} e^{-x}, \quad \text{for } x \ge 0 \tag{24}$$

and

$$f_Y(y) = e^{-y}, \quad \text{for } y \ge 0 \tag{25}$$

where $\Gamma(\cdot)$ is the gamma function. By direct integration and using the definition of the gamma function, the conditional outage probability is found to be bounded by

$$P_{o|\mathbf{d}_1} \le \Pr(X \le Y) = \frac{1}{2^{M-1}}. \tag{26}$$

Since the result does not depend on the vector $\mathbf{d}_1$, the unconditional outage probability $P_o$ is also bounded by $1/2^{M-1}$.

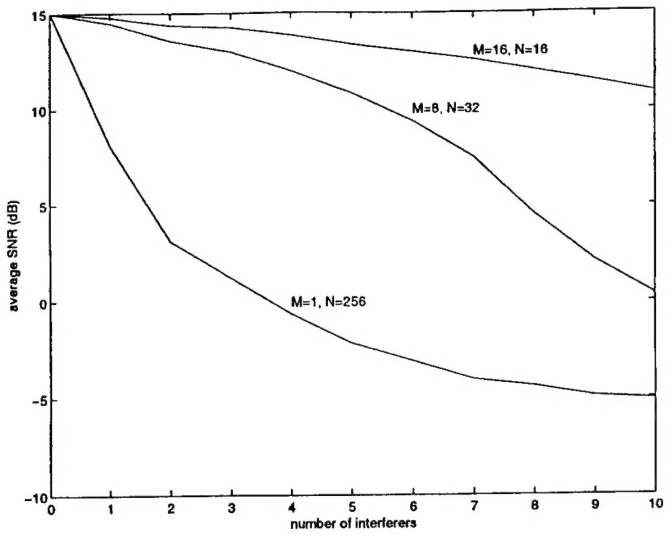


Fig. 3. Average optimal SNR with multiple interferers.

We can see from (26) that the outage probability drops at least exponentially with the number of carriers. For example, with eight carriers the outage probability is bounded by $7.81\times10^{-3}$.

### B. Multiple Interferers

When there are more interferers in the system, the SNR can still be found. Since the expression for the SNR for the case with multiple interferers is considerably more complex than (21), it is omitted here. Instead, we plot the "average" optimal SNR as a function of the number of interferers in Fig. 3 to demonstrate the performance of the proposed algorithm. The average is taken over 500 realizations. In each realization, the fading coefficients for different users are randomly generated, and the resulting SNR is analytically determined under the random signature sequence model. The power of each interferer is 20 dB above the desired user power, and the average signal-to-thermal-noise ratio (STNR $= 2P_1MNT_c/N_o$) is 15 dB. The SNR performances for three different numbers of carriers, namely, $M = 1$, 8, and 16, are shown. In each case, we adjust $N$ to give $MN = 256$ so that the bandwidth of the system is kept constant.

From Fig. 3, we see that multicarrier systems together with the proposed algorithm cancel MAI when there are a moderate number of strong interferers in the system. For a fixed value of $M$, the MAI canceling capability decreases as the number of interferers increases.

## V. Incorporation of Antenna Arrays

We note from [3] and Section II that, given the coherence bandwidth of a fading channel and a limit on the system bandwidth, the number of carriers $M$ cannot be arbitrarily large. Although it is shown in (26) that the outage probability decreases exponentially with $M$, for some fading channels, the MAI canceling capability of the multicarrier system is still inadequate. It is shown in [4] and [5] that MAI cancellation can be achieved in a single-carrier DS-CDMA system with a linear phase antenna array, where spatial diversity of the users is exploited. The idea can also be applied to multicarrier systems to enhance their MAI canceling capability. Actually, the approach in Section III can be readily generalized to incorporate the use of antenna arrays. Suppose that an antenna array of $D$ elements is used for signal reception. Then, the received signal in (4) becomes

$$\mathbf{r}(t) = \sum_{k=1}^{K}\sum_{m=1}^{M}\sqrt{2P_k}c_m^{(k)} \cdot\left\{\sum_{i=-\infty}^{\infty} b_{\lfloor i/N\rfloor}^{(k)}a_i^{(k)}\psi(t-T_k-iT_c)\right\} \cdot e^{j\omega_m(t-T_k)}\alpha_{k,m}\tilde{\mathbf{d}}_{k,m} + \mathbf{n}(t) \tag{27}$$

where $\tilde{\mathbf{d}}_{k,m}$ is a $D$-dimensional vector that accounts for the direction of arrival of the $m$th carrier of the $k$th user. The received vector $\mathbf{r}(t)$ becomes $D$-dimensional, as does the noise contribution $\mathbf{n}(t)$.

The output of each correlator becomes $D$-dimensional. Therefore, on the $m$th branch, the desired signal component $\mathbf{s}_m$, the interference from the $k$th transmitter $\mathbf{i}_{k,m}$, and other noise contributions $\mathbf{n}_m$ are all $D$-dimensional vectors. We can concatenate the $D$-dimensional vectors $\mathbf{s}_m$ in the $M$ different branches to obtain an $MD$-dimensional desired signal vector $\mathbf{s}$. Similarly, we can obtain the $MD$-dimensional noise vector $\mathbf{n}$ and the $MD$-dimensional interference vectors $\mathbf{i}_k$. Therefore, we obtain (7) with all the vectors becoming $MD$-dimensional. Moreover, $\mathbf{s}$, $\mathbf{n}$, and $\mathbf{i}_k$, for all $k$, remain uncorrelated. The optimal vector $\mathbf{w}_* = [\mathbf{w}_{1,*}^T, \mathbf{w}_{2,*}^T, \cdots, \mathbf{w}_{M,*}^T]^T$, which is now $MD$-dimensional, can be obtained in exactly the same way as before.

As in Section V, it is illustrative to examine the outage probability of the multicarrier system with an antenna array under the assumption of a single interferer. For simplicity, we assume that the angles of arrival and the array response vectors of the desired transmitted signal (or the interfering signal) are the same for all carriers. We assume a linear array of $D$ isotropic elements, which are separated by a half wavelength, is being used. We assume that the bandwidth of the system is much smaller than the carrier frequency, and, thus, by using the same linear array, the array response vectors for all carriers are approximately given by

$$\tilde{\mathbf{d}}_{k,m} = \tilde{\mathbf{d}}_k = \left[1, e^{j\pi\sin\theta_k}, \cdots, e^{j(D-1)\pi\sin\theta_k}\right]^T \tag{28}$$

for $k = 1$ and 2, and $m = 1, \cdots, M$. These are the array responses due to the desired transmitted signal and the interfering signal, respectively. In (28), $\theta_1$ and $\theta_2$, which are modeled by two uniform random variables on $[-\pi, \pi)$, are the incident angles of the two signals.

Similar to (21), the optimal SNR in this case is

$$\widetilde{\mathrm{SNR}}_* = \frac{2P_1NT_c}{N_0}\left(|\mathcal{D}_1|^2 - \frac{\beta_2|\mathcal{D}_1^H\mathcal{D}_2|^2}{N_0NT_c+\beta_2|\mathcal{D}_2|^2}\right) \tag{29}$$

where $\mathcal{D}_1 = \mathbf{d}_1 \otimes \tilde{\mathbf{d}}_1$, $\mathcal{D}_2 = \mathbf{d}_2 \otimes \tilde{\mathbf{d}}_2$, and $\otimes$ denotes the Kronecker product.

We again consider the outage probability $\tilde{P}_o$ of the multicarrier system with the linear array as the probability that the

interfering signal causes $\widetilde{\mathrm{SNR}}_*$ to drop by 3 dB. Similar to the steps in Section IV, from (29), we have

$$\tilde{P}_o \le \Pr\left(\frac{|\mathcal{D}_1|^2}{2} \le \frac{|\mathcal{D}_1^H \mathcal{D}_2|^2}{|\mathcal{D}_2|^2}\right). \tag{30}$$

Conditioned on $\mathbf{d}_1$ and $\phi = \sin\theta_1 - \sin\theta_2$, we let $\mathbf{U}$ be the unitary transformation considered in Section IV-A. Then, the unitary transformation defined by $\mathcal{U} = \mathbf{U} \otimes \mathbf{I}_{D\times D}$ transforms $\mathcal{D}_1$ to $[|\mathbf{d}_1|\tilde{\mathbf{d}}_1^T, 0, \cdots, 0]^T$ and $\mathcal{D}_2$ to $\mathbf{d}_2' \otimes \tilde{\mathbf{d}}_2$. Using this transformation, we have

$$\tilde{P}_{o|\mathbf{d}_1,\phi} \le \Pr\left(\sum_{m=2}^{M} |d_{2,m}'|^2 \le [2g_D(\phi) - 1]|d_{2,1}'|^2 | \mathbf{d}_1, \phi\right) \tag{31}$$

where

$$0 \le g_D(\phi) = \left[\frac{\sin(D\pi\phi/2)}{D\sin(\pi\phi/2)}\right]^2 \le 1. \tag{32}$$

Again, by the fact that the random variables $\sum_{m=2}^{M} |d_{2,m}'|^2$ and $|d_{2,1}'|^2$ are independent chi-square distributed, it is easy to show that

$$\tilde{P}_{o|\phi} \le \begin{cases} 0, & \text{if } 0 \le g_D(\phi) \le 1/2 \\ \left[1 - \dfrac{1}{2g_D(\phi)}\right]^{M-1}, & \text{if } 1/2 < g_D(\phi) \le 1. \end{cases} \tag{33}$$

Finally, we have

$$\tilde{P}_o \le \int_{\{\phi:\, 1/2 < g_D(\phi) \le 1\}} \left[1 - \frac{1}{2g_D(\phi)}\right]^{M-1} f_\Phi(\phi)\, d\phi \tag{34}$$

where $f_\Phi(\phi)$ is the density function of $\phi$, given by

$$f_\Phi(\phi) = \begin{cases} \dfrac{4}{\pi^2(2+|\phi|)} K\left(\dfrac{2-|\phi|}{2+|\phi|}\right), & \text{if } 0 < |\phi| < 2 \\ 0, & \text{otherwise.} \end{cases} \tag{35}$$

In the above, $K(x) = \int_0^{\pi/2} du/\sqrt{1 - x^2 \sin^2 u}$, for $|x| < 1$, is the complete elliptic integral of the first kind [13].

For $M = 8$ and $D = 5$, we obtain $\tilde{P}_o \le 7.83 \times 10^{-4}$, which is about 10 times smaller than the bound on $P_o$ obtained in Section V-A. Since both of the bounds in (26) and (34) are tight when the interferer power is strong, we see that the incorporation of an antenna array in the multicarrier system does help in enhancing its MAI canceling capability. In addition to enhancing the MAI canceling capability, the multi-element array also provides an additional antenna gain of $D$, which can be obtained easily by the proposed combining algorithm.

## VI. Numerical Examples

In this section, we investigate the performance of the proposed multicarrier scheme under different channel conditions by Monte Carlo simulations. Throughout this section, the STNR is fixed at 15 dB. Moderate values of $N = 32$ and $M = 8$ are used. The chip waveform employed is the raised-cosine waveform with a roll-off factor of 0.1 [10], i.e.,

$$\hat{\psi}(t) = \frac{\sin(\pi t/T_c)}{\pi t/T_c} \frac{\cos(\pi t/10T_c)}{1 - t^2/25T_c^2}. \tag{36}$$

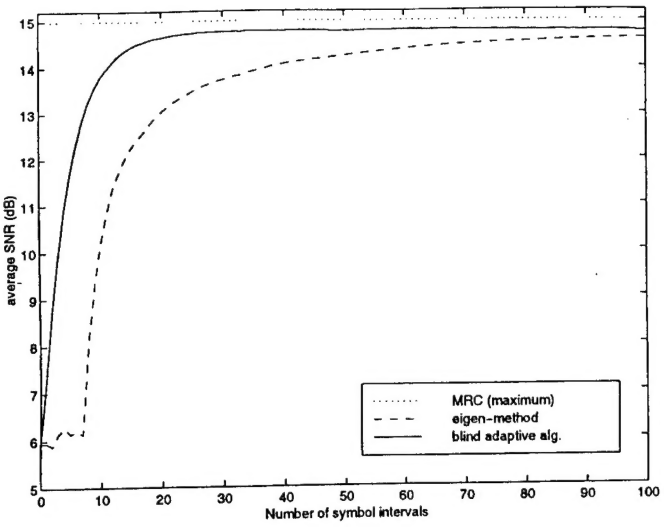


Fig. 4. Performance under fading channels.

All curves shown are the results of averaging over 500 realizations. We use dotted lines, broken lines, solid lines, and dash–dotted lines to show the SNR's obtained by the MRC, the eigen analysis method, the blind adaptive algorithm, and the maximum achievable SNR in (11), respectively.

First, we consider the simple case of a fading channel with AWGN only, i.e., no multiple-access interference or narrow-band interference. The results are shown in Fig. 4. In this case, the optimal weight vector is the MRC determined by the fading coefficients. As expected, the obtained SNR is about 15 dB. Without any knowledge of the fading coefficients, both the eigen analysis method and the blind adaptive algorithm can give SNR's very close to the 15-dB limit. In this simple case, we can choose the adaptation rate of the blind adaptive algorithm to be faster than the eigen method by adjusting $\mu$ in (16). It can be seen that the weight vector adapts quickly and the SNR climbs to within 0.5 dB of the optimal value in less than 20 symbol intervals.

Next, we consider the case where, in addition to AWGN, the fading channel is also contaminated by narrow-band interference occupying one of the frequency bands of the multicarrier signals. The power of the narrow-band interference is taken to be 20 dB stronger than the total power from all carriers of the desired signal. Thus, the power of the narrow-band interference is about 29 dB above the power of the desired signal in that frequency band. The results of the simulation are shown in Fig. 5. In this case, the optimal weight vector is, again, the MRC determined by the fading coefficients, the location, and the power of the narrow-band interference. The maximum achievable SNR is slightly below 15 dB, which shows that narrow-band interference can be effectively suppressed with suitable choices of weight vectors. When the required knowledge of the channel and the interference is not available, we need to employ either the eigen method or the blind adaptive algorithm to obtain the optimal weight vector. In this case, we choose the adaptation rate of the blind adaptive algorithm to be similar to that of the eigen method. It can be seen that the SNR's climb to about 2 dB from the optimal value

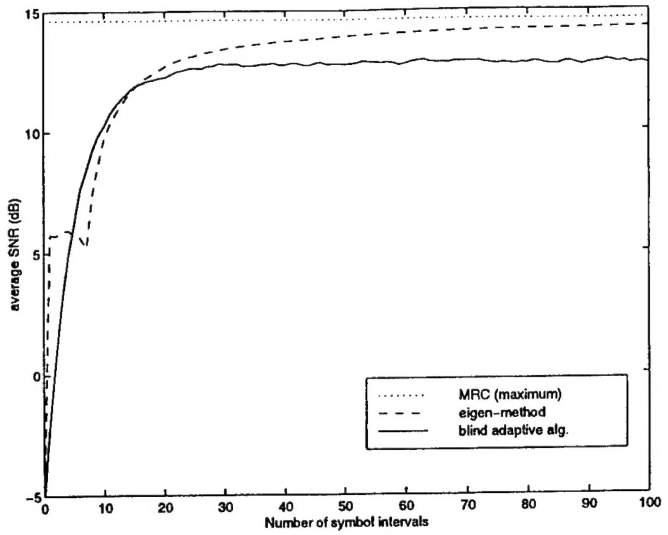


Fig. 5. Performance under fading channels with narrow-band interference.

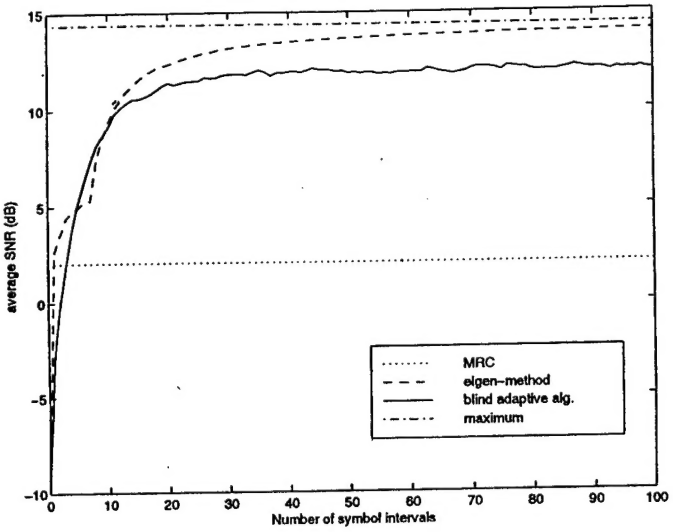


Fig. 6. Performance under fading channels with a strong interferer.

in about 20 symbol intervals. While the eigen method can attain an SNR level very close to the optimal value, the SNR obtained by the blind adaptive algorithm is 2 dB below the optimal value. The loss in performance of the blind adaptive algorithm is due to its stochastic nature and can be traded off with its convergence speed.

It is well known that DS spreading allows multiple users to share the same communication channel when the powers of all users are comparable. However, the performance degrades under imperfect power control. We consider the worst case scenario where the near–far problem exists. Fig. 6 shows the case where there is an interferer with power 40 dB stronger than that of the desired user. We see that the optimal SNR is slightly less than 15 dB. This implies that the interfering signal can be effectively cancelled. However, the SNR obtained by the MRC is about 2 dB, which is far from optimal. For comparison, we choose the adaptation rate of the blind adaptive algorithm to be similar to that of the eigen method. Again, the eigen method can attain an SNR level very close to

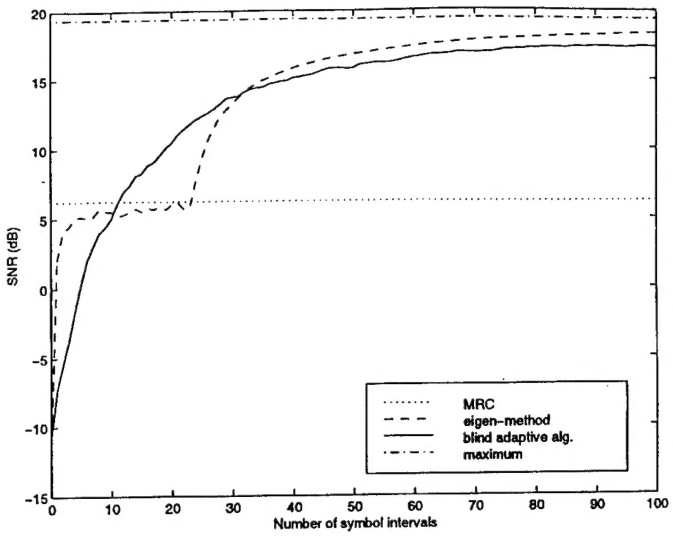


Fig. 7. Performance using an antenna array under fading channels with a strong interferer.

the optimal value, but the SNR obtained by the blind adaptive algorithm is 3 dB below the optimal value. Nevertheless, by using either one of the methods, we can get an SNR of at least 11 dB in about 20 symbol durations.

Finally, we consider the case of a single interferer, where a linear antenna array of three elements is used. The simulation results are shown in Fig. 7. In this case, the adaptation rates of both of the eigen method and the blind adaptive algorithm are slower because of the large numbers of weights. Otherwise, the results are similar to the previous case, except for an additional 5-dB gain due to the antenna array.

## VII. Conclusions

We have considered a signal reception scheme in MC-CDMA systems. We have shown for communication over fading channels that, by suitably combining the received signals on all the carriers, the proposed receiver can combine the desired signal contributions from different carriers constructively, while canceling noise and MCI. Moreover, we have proposed a blind adaptive algorithm to determine an optimal weight vector, which is used to combine the received signals from different carriers optimally. The approach can be generalized to incorporate the use of antenna arrays in MC-CDMA systems. Simulations show that the proposed algorithm performs very well under different channel conditions including situations with the near–far problem. Thus, MC-CDMA systems with the proposed algorithm are attractive candidates for future CDMA systems.

## References

[1] S. Hara and R. Prasad, "Overview of multicarrier CDMA," *IEEE Commun. Mag.*, pp. 126–133, Dec. 1997.

[2] J. A. C. Bingham, "Multicarrier modulation for data transmission: An idea whose time has come," *IEEE Commun. Mag.*, pp. 5–14, May 1990.

[3] S. Kondo and L. B. Milstein, "Performance of multicarrier DS CDMA systems," *IEEE Trans. Commun.*, vol. 44, pp. 238–246, Feb. 1996.

[4] T. F. Wong, T. M. Lok, J. S. Lehnert, and M. D. Zoltowski, "Spread-spectrum signaling techniques with antenna arrays and blind adaptation," in *Proc. IEEE MILCOM'96*, 1996, vol. 1, pp. 194–198.

[5] ——, "A linear receiver for direct-sequence spread-spectrum multiple-access systems with antenna arrays and blind adaptation," *IEEE Trans. Inform. Theory*, vol. 44, pp. 659–676, Mar. 1998.
[6] S. Verdú, "Multiuser detection," in *Advances in Statistical Signal Processing*. Greenwich, CT: JAI Press, 1993, vol. 2, pp. 369–409.
[7] A. Duel-Hallen, J. Holtzman, and Z. Zvonar, "Multiuser detection for CDMA systems," *IEEE Personal Commun. Mag*, vol. 2, pp. 46–58, Apr. 1995.
[8] A. F. Naguib, A. Paulraj, and T. Kailath, "Capacity improvement with base-station antenna array in cellular CDMA," *IEEE Trans. Veh. Technol.*, vol. 43, pp. 691–698, Aug. 1994.
[9] B. M. Popovic, "Synthesis of power efficient multitone signals with flat amplitude spectrum," *IEEE Trans. Commun.*, vol. 39, pp. 1031–1033, July 1991.
[10] J. G. Proakis, *Digital Communications*, 3rd ed. New York: McGraw-Hill, 1995.
[11] F. R. Gantmacher, *The Theory of Matrices*, vol. I. Chelsea, NY: Chelsea Publishing, 1960.
[12] S. Haykin, *Adaptive Filter Theory*, 2nd ed. Englewood Cliffs, NJ: Prentice Hall, 1991.
[13] F. Bowman, *Introduction to Elliptic Functions with Applications*. New York: Dover, 1961.

**Tat M. Lok** (S'95–M'95) received the B.Sc. degree in electronic engineering from the Chinese University of Hong Kong, Shatin, in 1991 and the M.S.E.E. degree in electrical engineering and the Ph.D. degree in electrical and computer engineering from Purdue University, West Lafayette, IN, in 1992 and 1995, respectively.

He was a Research Assistant and a post-doctoral Research Associate at Purdue University. Since 1996, he has been an Assistant Professor in the Department of Information Engineering, The Chinese University of Hong Kong. His research interests include code-division multiple-access systems, multiuser detection, adaptive antenna arrays, and communication theory.

**Tan F. Wong** received the B.Sc. degree (first class honors) in electronic engineering from the Chinese University of Hong Kong, Shatin, in 1991, and the M.S.E.E. and Ph.D. degrees in electrical and computer engineering from Purdue University, West Lafayette, IN, in 1992 and 1997, respectively.

From July 1993 to June 1995, he was a Research Engineer working on the high-speed wireless networks project in the Department of Electronics at Macquarie University, Sydney, Australia. From August 1995 to October 1997, he was a Research and Teaching Assistant in the School of Electrical and Computer Engineering, Purdue University. From November 1997 to July 1998, he worked as a post-doctoral Research Associate at Purdue University. Currently, he is an Assistant Professor of Electrical and Computer Engineering at the University of Florida, Gainsville. His research interests include spread-spectrum communication systems, multiuser communications, and wireless cellular networks.

**James S. Lehnert** (S'83–M'84–SM'95) received the B.S. (with highest honors), M.S., and Ph.D. degrees in electrical engineering from the University of Illinois at Urbana-Champaign in 1978, 1981, and 1984, respectively.

From 1978 to 1984, he was a Research Assistant at the Coordinated Science Laboratory, University of Illinois, Urbana. He was a University of Illinois Fellow from 1978 to 1979 and an IBM predoctoral Fellow from 1982 to 1984. He has held summer positions at Motorola Communications, Schaumburg, IL, in the Data Systems Research Laboratory, and Harris Corporation, Melbourne, FL, in the Advanced Technology Department. He is currently an Associate Professor of Electrical and Computer Engineering at Purdue University, West Lafayette, IN. His current research work is in communication and information theory with emphasis on spread-spectrum communications.

Dr. Lehnert has served as Editor for Spread Spectrum for the IEEE TRANSACTIONS ON COMMUNICATIONS.